Dissertation

submitted to the

Combined Faculty of Natural Sciences and Mathematics

of the Ruperto Carola University Heidelberg, Germany

for the degree of

Doctor of Natural Sciences

Presented by

Katharina Zirngibl, M.Sc. Biology

born in: Erlangen, 10.10.1987

Oral examination: 04.12.2018

Adaptability of metabolic networks in evolution and disease

Referees Prof. Dr. Robert Russell
Dr. Lars Steinmetz

There are 114.101 small molecule metabolites currently annotated in the Human Metabolome Database, which are highly connected amongst each other, with a few metabolites exhibiting an estimated number of more than 103 connections. Redundancy and plasticity are essential features of metabolic networks enabling cells to respond to fluctuating environments, presence of toxic molecules, or genetic perturbations like mutations. These system-level properties are inevitably linked to all aspects of biological systems ensuring cell viability by enabling processes like adaption and differentiation. To this end, the ability to interrogate molecular changes at omics level has opened new opportunities to study the cell at its different layers from the epigenome and transcriptome to its proteome and metabolome. In this thesis, I tackled the question how redundancy and plasticity shape adaptation in metabolic networks in evolutionary and disease contexts. I utilize a multi-omics approach to study comprehensively the metabolic state of a cell and its regulation at the transcriptional and proteomic level. One of the challenges with multi-omics approaches is the integration and interpretation of multi-layered data sets. To approach this challenge, I use genome scale metabolic models as a knowledge-based scaffold to overlay omics data and thereby to enable biological interpretation beyond statistical correlation. This integrative methodology has been applied to two different projects, namely the evolutionary adaptation towards a nutrient source in yeast and the metabolic adaptations following disease progression. For the latter, I also curated a current human genome-scale metabolic model and made it more suitable for flux predictions. In the yeast case study, I investigate the metabolic network adaptations enabling yeast to grow on an alternative carbon source – glycerol. I could show that network redundancy is one of the key features of fast adaptation of the yeast metabolic network to the new nutrient environment. Genomics, transcriptomics, proteomics, metabolomics and metabolic modeling together revealed a shift of the organism's redox-balance under glycerol consumption as a driving force of adaption, which can be linked to the causal mutation in the enzyme Kgd1. On the other hand, the limitations of metabolic network adaptation also became apparent since all evolved and adapted strains exhibited metabolic trade-offs in other environmental conditions than the adaptation niche. Either an impaired diauxic shift (as in the case of the glycerol mutant) or an increased sensitivity towards osmotic stress (caused by mutations in the HOG pathway) was coupled with efficient use of glycerol. In the second project, the molecular phenotype of regressed breast cancer cells was studied to identify what differentiates these cells from healthy breast tissue and to characterize the potential source of tumor recurrence. Using a breast cancer mouse model with inducible oncogenes, transcriptomics together with an extensive set of different types of metabolomics (targeted and untargeted metabolomics, lipidomics and flux-omics) could show that regressed cancer cells, albeit their apparently normal morphology, possess a highly altered molecular phenotype with an oncogenic memory. While in cancer redundancy and plasticity enable the adaptation towards a proliferative state, in regressed cells, on the contrary, prolonged oncogenic signaling leads to a loss of metabolic network regulation and the entering of an irreversible metabolic state. This state appears to be insensitive to adaptation mechanisms as transcripts and metabolites reciprocally enhance each other to maintain the tumor-like metabolic phenotype. In conclusion, this work demonstrates how genome scale metabolic models can help identifying functional mechanisms from complex and multi-layered omics data. Appropriate genome scale metabolic models combined with metabolite measurements have proven particularly useful in this context. The comprehensive understanding of all integrated aspects of a cell's physiology is a challenging endeavor and the results of this thesis might stimulate further research towards this goal.

Mehr als 114,101 verschiedene sogenannte „small molecule“ Metabolite sind in der Metabolom Datenbank annotiert. Diese Metabolite korrelieren stark miteinander, einige besitzen dabei mehr als 103 Verbindungen zu anderen Metaboliten. Redundanz und Plastizität sind entscheidende Merkmale von metabolischen Netzwerken damit sich Zellen auf eine sich verändernde Umwelt, die Anwesenheit von toxischen Molekülen oder genetische Störungen anpassen können. Diese komplexen Eigenschaften sind verbunden mit allen Aspekten eines biologischen Systems um das überleben der Zellen durch Prozesse wie Adaption oder Differenzierung zu sichern. Die Fähigkeit Veränderungen in Zellen auf ihren verschiedenen Ebenen, von Epigenom, Transkriptom über Proteom und Metabolom, auf molekularer Ebene durch „omics“ Daten zu erfassen hat hierbei neue Möglichkeiten eröffnet. In dieser Arbeit habe ich mich mit der Frage auseinandergesetzt, wie Redundanz und Plastizität die Anpassung von metabolischen Netzwerken im Kontext der Evolution oder Erkrankung beeinflussen. Mithilfe eines „multi-omic“ Ansatzes habe ich umfassend den metabolischen Status einer Zelle und ihrer Regulation auf Transkriptions- und Proteom-Ebene analysiert. Eine der Schwierigkeiten bei „multi-omics“ Ansätzen ist die Integration und Interpretation von vielschichtigen Datensätzen. Um dies zu bewältigen habe ich genomweite metabolische Modelle verwendet, die ein wissensbasiertes Gerüst für die Integration von „omics“ bieten und dadurch eine biologische Interpretation über die statistische Korrelation hinaus zu ermöglichen. Diese Methodik wurde auf zwei unabhängige Projekte angewendet: 1) die evolutionäre Anpassung an eine Nahrungsquelle in Hefe und 2) die metabolische Anpassung bei fortschreitender Erkrankung. Für das letztere Project habe ich ein genomweites metabolisches Modell der menschlichen Zelle für die verbesserte Nutzung von metabolischen Fluxen überarbeitet. , iso dass es besser geeignet. In der Hefe-Studie wurde die Anpassung des metabolischen Netzwerks von Hefezellen an eine alternative Kohlenstoffquelle – Glycerol – untersucht. Ich konnte zeigen, dass Netzwerk Redundanz eines der Schlüsselmerkmale der schnell adaptierenden Hefezellen auf die Umweltveränderung ist. Untersuchungen auf genomischer, transkriptomischer, proteomischer und metabolomischer Ebene zusammen mit metabolischem Modeling zeigten eine Verschiebung des Redox-Gleichgewichts in der Zelle unter Wachstum mit Glycerol als treibende Kraft der Adaption, welche verbunden war mit der Mutation des Enzyms Kgd1. In dieser Analyse konnten die Einschränkungen der metabolischen Netzwerkadaption gezeigt werden, da alle evolvierten und adaptierten Hefe-Stämme metabolische Ausgleiche in anderen Umweltbedingungen als in der Adaptionsnische aufzeigten. Entweder die Unfähigkeit den „diauxic shifts“ durchzuführen (im Falle des Glycerol Mutanten) oder eine erhöhte Sensitivität in Richtung des osmotischen Stresses (ausgelöst durch Mutationen im HOG-Signalweg) waren gekoppelt an die effiziente Nutzung von Glycerol in der Hefe-Zelle. Im zweiten Projekt wurde der molekulare Phänotyp von regredierenden Brustkrebszellen analysiert um die Unterschiede dieser Zelle zum gesunden Brustgewebe und eine potentielle Quelle für Tumorrezidive zu identifizieren. In einem Mausmodell für Brustkrebs mit induzierbaren Onkogenen wurde mithilfe von Transkriptom- und Metabolom-Analysen (gerichtete und ungerichtete Metabolomics, Lipidomics und Fluxomics) gezeigt, dass regredierte Krebszellen, obwohl ihre Morphologie normal erschien, einen stark veränderten Phänotyp mit onkogenem Gedächtnis aufwiesen. Während Redundanz und Plastizität in der Krebszelle die Adaption an eine erhöhte Proliferation ermöglichen, führte in regredierten Zellen eine Fortführung der onkogenen Signalgebung zu einem Verlust der metabolischen Netzwerkregulation und dem Eintritt in einen irreversiblen metabolischen Status. Dieser Status erschien unveränderlich durch Adaptionsmechanismen da sich Transkripte und Metabolite gegenseitig erhöhen und so dazu beitragen den Tumor-ähnlichen Phänotyp zu erhalten. Zusammenfassend hat diese Arbeit gezeigt wie genomweite metabolische Modelle angewendet werden können um funktionelle Mechanismen

in komplexen und vielschichtigen „omics“ Daten zu identifizieren. Passende Modelle zusammen mit Metabolitmessungen haben sich als besonders geeignet in diesem Zusammenhang erwiesen. Das umfangreiche Verständnis aller integrierten Prozesse in der Physiologie der Zelle ist ein komplexes Unterfangen und die Ergebnisse dieser Arbeit regen hoffentlich weitere Forschung zum Erreichen dieses Ziels an.

ACKNOWLEDGEMENTS

My first thank you goes to **Dr. Kiran Raosaheb Patil**.Without you this journey would probably not have been possible. Thank you for accepting me as part of your group, and for your continuous support, patience, motivation, immense knowledge and creative mind. Your guidance helped throughout this thesis.
To my thesis advisory committee members, **Dr. Lars Steinmetz**, **Prof. Dr. Rob Russell**, **Prof. Dr. Ursulla Klingmueller**, **Dr. Judith Zaugg**, for accepting without hesitating to be part of my defense committee. I consider myself extremely lucky to have group leaders of your scientific expertise judging my work.
To **Dr. Lars Steinmetz**, **Prof. Dr. Rob Russell**, **Dr. Wolfgang Huber**, **Dr. Martin Beck**, for providing regular encouragement, critiques and feedbacks during the course of my PhD.
To my lab members, thank you for your constant support, helpfulness. **Eva-Maria Geissen**, thanks for your delicious birthday cakes ! **Dimitrios Konstantinidis**, the tireless good mood of our group. A special thanks goes to **Natalia Paula Gabrielli Lopez**, **Vinita Periwal**, **Filipa Pereira** and **Sergej Andrejev**.
Paula Jouhten, you are an examplary scientist and I'm honoured to have learned so much from you. **Tomas Strucko**, you came as a co-worker and left as a very good friend.
Martin Jechlinger, **Ksenija**. Working with you so closely gave me the feeling of being in an independent group. Together, we have acomplished milestones in the field of breast cancer and this thesis would certainly not be the same without you. This observation goes for **Ashna** as well. Thank you for always looking at life with a different perspective.
To the **EMBL core facilities**, in particular to the proteome and genome core facilities, a big thank you. Without you there would be no data to analyse and I would not be writing this thesis.
To **Bernd Klaus**, your statistical expertise and pedagogy trully are unequal. Thank you for all the help you've brought me.
Last but not least, I don't know what my time at EMBL would have been without the **bike and running club**. Thanks for that one in a life time ride to Grenoble and the countless runs through the woods !

Und nun der Dank an all die Menschen, die mich auf dem Weg zu meinem Doktor und während meines Doktors begleitet haben. Der erste, riesengroße Dank geht an meine Familie. An meine **Eltern**, dafür, dass sie mir die unerschütterliche Sicherheit geben, immer und bei allem was ich tue, voll auf Ihre Unterstützung und ihren Glauben an mich zählen zu können – auch und gerade dann, wenn ich meine Grenzen erreiche. Ihre Liebe und ihre Vorbild werden mich immer begleiten, welche Wege auch immer ich noch bestreiten werde. An meine Brüder **Florian** und **Klemens** und meine Schwester **Sophie** für all ihre Besuche, die ausufernden Spieleabende, die Nächte im Vetters, die gegenseitige Stütze und einfach dafür, dass sie mir alle so nah sind. An meine Tante **Elfi**, deren unaufdringliche, umso großzügigere und herzliche Art,

für andere da zu sein mir immer ein Vorbild ist und an meine Tante **Eva** für ihre riesige Energie und Herzlichkeit. Ich danke aus vollem Herzen **Samy**, die unverrückbare Säule in meinem Leben, mit dem ich mich ohne zu zögern jeder möglichen und noch lieber den scheinbar völlig unmöglichen Herausforderungen stellen kann. Die Liste dessen, wofür ich ihm dankbar bin ist wahrscheinlich länger als die Strecken, die wir gemeinsam auf Rädern, Füßen, Händen und Brettern zurückgelegt haben. Deshalb danke ich ihm schlicht dafür, dass er mir das beste Gegenstück ist, das ich mir wünschen kann. Ich danke ebenso **Samys Eltern** und seiner **Schwester**, die mich so herzlich willkommen geheißen haben in ihrer Familie. Danke für das große Verständnis dafür, dass wir viel zu wenig Zeit hatten während meiner Arbeit und dafür, dass sie es geschafft haben, die wenige gemeinsame Zeit mit viel Lachen, Charme und wunderbaren Essen zu füllen. Und ich verspreche, nach der Verteidigung auch endlich meinen Teil zu unserer sprachlichen Annäherung zu tun :) Mein Dank geht außerdem **Julia B.** für viel zu viel! Für ihre Freundschaft, für unzähligen Ratschläge, für ihre riesige Verlässlichkeit, dafür, dass man sie um alles bitten kann und noch viel mehr dafür, dass sie nie lang fackelt, sondern einfach anpackt, wenn Not am Mann ist. Achja und nicht zu vergessen, die vielen gemütlichen Weststadtmarktbesuche und gemeinsamen Erlebnisse :) An **Julia S.** ebenso für ihre Freundschaft, für ihre Verrücktheit, für ihre Empathie, die vielen wundervollen Gespräche, die geteilte Kaffeeleidenschaft, ihr famoses Essen und dafür, dass sie immer und bei allem dabei ist, ganz egal, was man ihr vorschlägt. An **Emiliano**, der mich seit meinem ersten Tag in Heidelberg vor 7 Jahren begleitet hat und der mir ein beständiger Freund und Begleiter in allen Lebenslagen ist. Ich danke ihm dafür, dass er mir mit seiner erfrischenden Perspektive auf die Welt neue Inspiration gibt. An **Mechthild** und **Almuth** für die geteilte Begeisterung an sportlichen Herausforderungen, die einfach Spaß macht und sich nicht an irgendwelche Konventionen halten muss. Danke für all die gemeinsamen Abende, die gemeinsame Chemie und für Gespräche, die niemand beenden will, trotz unweigerlichem Schlafmangel. Und natürlich für die nachträglichen Geburtstagsglückwünsche eine Woche zu früh ;) An **Isa**, meine älteste Freundin, dafür, dass ich sie und sie mich durch so viele wichtige Lebensabschnitte begleitet hat und dafür, dass sie einen unerschöpflichen Vorrat an Verständnis hat. Ich weiß, dass ich immer auf dich zählen kann. Und genauso wichtig, ein großes Dankeschön an mein Patenkind **Elias**, für diese neue Rolle als Patentante und dafür, dass ich mit ihm endlich wieder mit herrlich verspielten, ständig überraschten Kinderaugen auf die Dinge blicken kann. An **Sara**, die ich zwar erst in der Endphase meines Doktors richtig kennengerlernt habe, die aber mit ihrem ungeschlagenen Optimismus und ihrer Lebensfreude jede Zeit davor aufgeholt hat. An **Susi**, deren geteilte Liebe zum Triathlon mich durch so viele Wettkämpfe getragen hat und mit deren Begleitung ich immer weiter gewachsen bin. Und nicht zu vergessen, unser traditioneller Nikolauslauf - das ungeschlagene Highlight der sportlichen Vorweihnachtszeit. An **Thomas** für all die Ratschläge und Vorbilder zur Doktorarbeit, die französische selbstgemachte Salami, unser Skibergsteigen, die musikalischen Hochgenüsse der George Brassens Cover und den Rush der letzten Nacht vor Abgabe der Diss ! An **Malte**, mit dem man fast besser fränkisches Bier trinken kann als mit Franken selbst und mindestens genauso gut mit dem Mountainbike durch den Wald jagen kann.

TABLE OF CONTENTS

List of Tables

List of Figures

Chapter 1

Introduction

1.1 Redundancy and plasticity in metabolic networks

Redundancy and plasticity are key features of metabolic networks, which equip an organism with an enhanced robustness towards fluctuating environments or the loss of components of this network (e.g. through mutations in enzyme coding genes) and thus, ensure the cells viability [65]. The characteristics of plasticity and redundancy have often been studied in the context of synthetic lethal pairs [60] [67] [65] and are depicted in Figure 1.1. In this context functional plasticity is defined as the ability to reorganize metabolic fluxes after a loss of a reaction while the environmental conditions remain stable. Functional redundancy, on the contrary, is defined as the simultaneous flux of compensatory reactions in a stable environment [65].

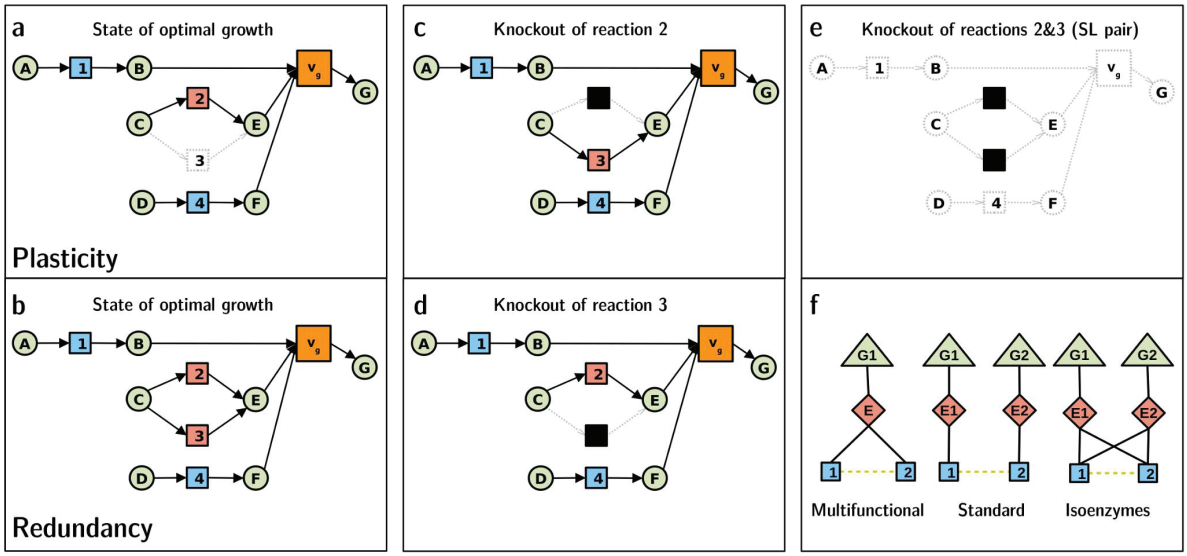

FIGURE 1.1. Schematic representation of plasticity and redundancy in metabolic networks. Metabolites are represented by circles and reactions by squares. Colored reactions with black arrows represent active reactions, whereas grey discontinuous lines are used for inactive reactions and metabolites and black for knockouts of reactions. The biomass production reaction is represented as a larger square with an associated flux vg. When it turns to inactive, meaning that it has no associated flux, the organism is not able to grow. (a) Illustration of metabolic network plasticity (reaction 2 active and reaction 3 inactive). Reaction 2 and 4 show metabolic plasticity when (b) Illustration of metabolic network redundancy (both reactions 2 and 3 active). (c) Final configuration after knockout of reaction 2 in (a) or (b). (d) Final configuration after knockout of reaction 3 in (a) or (b). In both cases (c) and (d) the organism is still able to grow due to the basic features of redundancy and plasticity in the network. (e) The simultaneous knockout of reaction 2 and 3 in (a) or (b) leads to a loss of viability. (f) Different possible organization of genes, enzymes and reactions enabling plasticity or redundancy. *This figure and the text in this legend have been reproduced from Güell et al. (2014) with permission [65].*

The structure of metabolic networks in prokaryotes and eukaryotes has been estimated to possess a high degree of redundancy and plasticity compared to random networks [60]. This is further illustrated by the generally low number of essential genes [163] [62] [94] [194]. However the extent of both, plasticity and redundancy, might depend on the environmental conditions [60] [67]. Furthermore, it has been shown that metabolic key reactions possess a higher redundancy than expected by random or than seen in less important reactions [60].

1.2 Constraint-based modeling on genome scale provides a framework to predict biological capabilities

The prediction of a biological phenotype has been a long desired outstanding goal, e.g. the inference of a morphological phenotype from its genetic make-up. In regard to the metabolic status of a cell this goal has come closer than in other areas of biology. Metabolism is constituted of biochemical reactions assembled in a complex network (Figure 1.2a). Genome scale metabolic models build a knowledge-based reconstruction of the entirety of these reactions known from an organism, which is assembled in a mathematical matrix (O'Brian 2015). The mathematical matrix is an abstract representation of the reactions in the form of stoichiometric coefficients of its participating metabolites and allows the calculation of flux distributions in the network (Figure 1.2b). In this matrix, negative values indicate consumed metabolites whereas positive values indicate produced metabolites and the fluxes are calculated under the steady state assumption that all metabolites that are produced in the network have to be consumed in a mass balanced manner [133]. One special reaction in the model constitutes the biomass reaction that formulates the metabolic demands of a cell under growth (e.g. ATP, amino acids, nucleotides). These cellular requirements for growth are imposed on the model in the form of a biomass objective function (Figure 1.2d). The representation of the mathematical matrix maintains the genetic basis of an organism as well as the physiochemical laws of its environment by imposing constraints. The imposition of physiochemical constraints to limit the computable phenotypes is a fundamental concept of Constraint-based modeling and analysis (COBRA) approaches [102]. With these constraints the principally indefinite number of solutions shrink to a so called "solution space", which limits the solutions to biologically feasible regions (Figure 1.2c). With linear programing a flux distribution that maximizes or minimizes the objective function within the solution space is identified (Figure 1.2e) [20]. Metabolic modeling approaches can be improved by improving the imposed constraints to more physiologically relevant or by extending the mathematical structure to regulatory elements acting on metabolism and including gene-regulatory information [190].

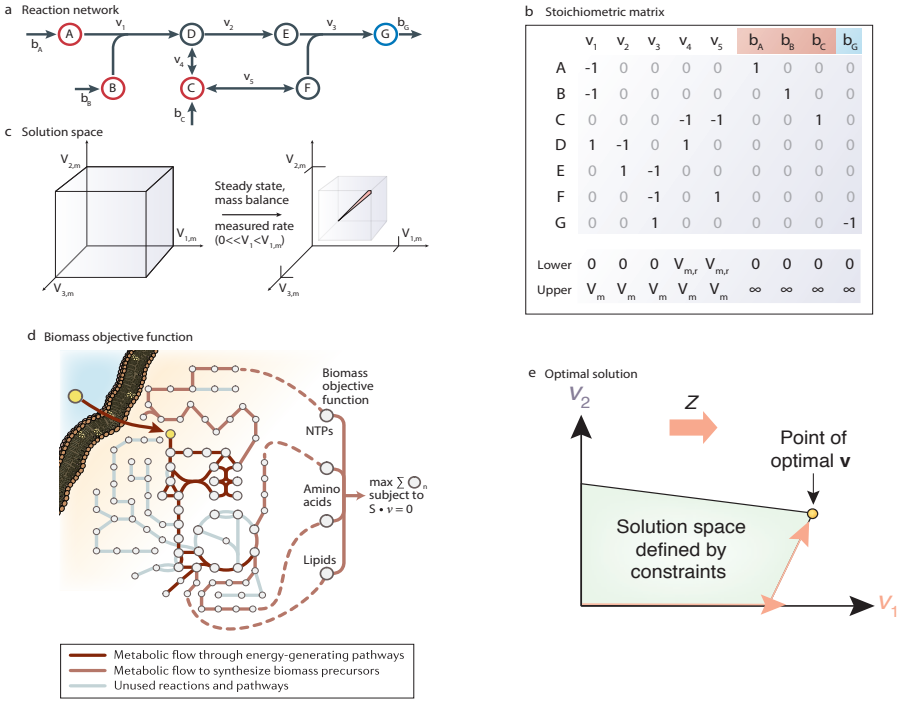

	v_1	v_2	v_3	v_4	v_5	b_A	b_B	b_C	b_G
A	-1	0	0	0	0	1	0	0	0
B	-1	0	0	0	0	0	1	0	0
C	0	0	0	-1	-1	0	0	1	0
D	1	-1	0	1	0	0	0	0	0
E	0	1	-1	0	0	0	0	0	0
F	0	0	-1	0	1	0	0	0	0
G	0	0	1	0	0	0	0	0	-1
Lower	0	0	0	$V_{m,r}$	$V_{m,r}$	0	0	0	0
Upper	V_m	V_m	V_m	V_m	V_m	∞	∞	∞	∞

FIGURE 1.2. Fundamentals of genome-scale metabolic modeling. The constraint-based reconstruction and anaylsis (COBRA) approach is based on three primary fundamental concepts: network constraints (parts a–c), objective functions (part d) and the association of reactions with the genome (a) A complex mixture of molecules (red) can react to yield end products (blue). In the model, metabolites enter the system through boundary pseudo reactions. (b) The stoichiometry of this reaction network is described mathematically in a stoichiometric matrix, with each column representing the stoichiometry of a reaction. Negative and positive values represent reactants and products, respectively. Reaction flux is limited by thermodynamics and catalytic capacities described by upper and lower bounds on the flux for each reaction. Vm = velocity of the forward enzyme-catalyzed reactions, Vm,r = velocity of the forward and reverse enzyme-catalyzed reactions. (c) Reaction constraints result in a 'solution space' that contains all feasible flux distributions. Additional constraints reduce the space of feasible flux distributions as shown in the pink line. (d) The biomass objective function describes an evolutionary pressure for growth, and describes the metabolic demands for the basic metabolite building blocks for all cellular components. (e) Linear programing is used to identify a flux distribution that maximizes or minimizes the objective function within the space of allowable fluxes (green region) defined by the constraints imposed by the mass balance equations and reaction bounds. The thick brown arrow indicates the direction of increasing objective function (Z). As the optimal solution point lies as far in this direction as possible, the thin brown arrows depict the process of linear programming, which identifies an optimal point at an edge or corner of the solution space. *This figure and the text in this legend have been adapted from Lewis et al. (2012) [102] and Orth et al. (2010) [133].*

1.3 Omics data integration with genome-scale models of metabolism

The development of new technologies permitting the probing of an organism at various cellular layers (genome, transcriptome, proteome, metabolome) at high throughput have enable us to study the physiology of cells in health and disease in greater depth [68]. The cellular layers are highly connected and the inherent complexity of biological systems manifests itself in multiple layers of regulation (Figure 1.3).

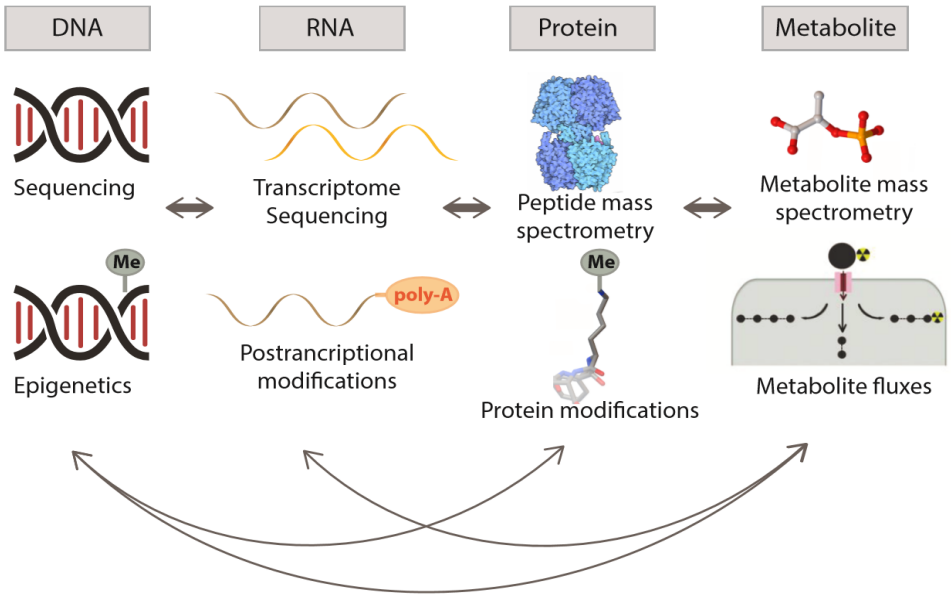

FIGURE 1.3. Overview of the different layers of a cells physiology and the corresponding omics technologies for measurement. Although classically perceived as a linear path, all different layers of a cell's physiology are interconnected. Each layer possesses various modifications, from which only the most commonly studied ones are depicted. Additionally the omics technology with which the respective layer of the cell can be measured is specified.

To address the challenge of integrating these complex omics data sets two main approaches have emerged, a statistical approach analyzing commonalities amongst the data sets and a modeling approach, using first principle models as a scaffold for interpretation [68] [8] [77] (Vivek-Ananth) [89] [131]. Analyzing the data by statistical means (e.g. correlations) is a statistical approach for omics convergence. However, confounders as well as a non-linearity of the regulation make it difficult to trace back a phenotype to its genomic origin it. Contrasting the trends of different omics layers with modeling approaches can offer a systematic way of addressing this difficulty. Metabolic models are particularly well suited for this task due to their comprehensiveness and the key role metabolism plays in various biological processes. Furthermore, metabolomics constitute a specific characteristic amongst the different types of omics in terms of their interpretability. Changes in metabolite abundances do not reveal anything about the underlying flux changes. Fluxomics would offer a better approach in this regard, but are often not available, because they are technically challenging and also not so suitable for the assessment of pathways outside central carbon metabolism. Instead, metabolic modeling can help tunneling the most probable effect of metabolite concentration changes by limiting the degrees of freedom in the metabolic network. Figure 1.4 summarizes the three main approaches by which constraint based metabolic modeling can be utilized for omics data integration. All three mentioned approaches have been utilized within the different projects of this thesis. These examples illustrate how omics data integrated with genome-scale metabolic models can not only explain complex gene expression dynamics but also help in predicting metabolic phenotype changes for experimental validation or for intervention.

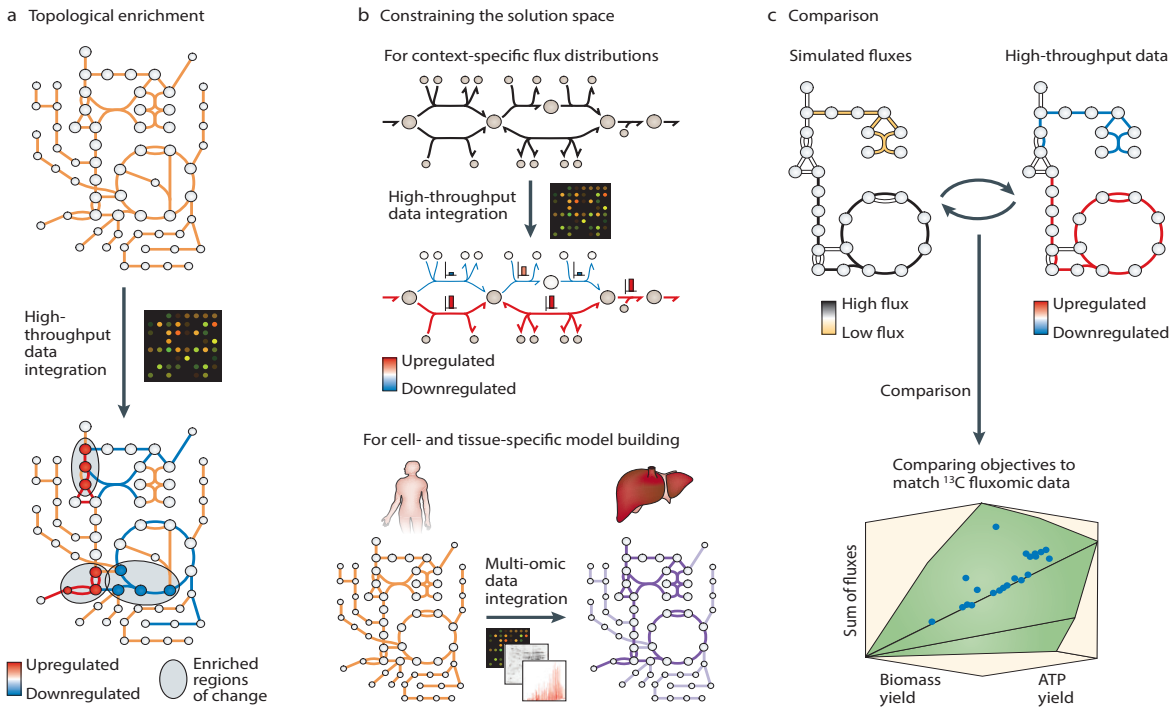

FIGURE 1.4. The multiple uses of high-throughput data in constraint-based models. Constraint-based modeling can be used to interpret and augment omics data sets by using an underlying cellular network that has been biochemically validated. Metabolites are represented by circles. (a) Similarly to pathway enrichment analysis and interaction networks, high-throughput data can be integrated with the metabolic network topology to determine enriched regions and even significantly perturbed metabolites (b) Omics data add an additional layer of constraints for reaction fluxes. Expression data can be integrated to determine context-specific flux distributions (pathway shown in red), which increases the fidelity of the data (represented as bars) as well as the accuracy of flux predictions (upper panel). In addition, omics data can be used to build cell- and tissue-specific models of human metabolism by removing unexpressed reactions (shown as uncolored reactions) from the global human metabolic network (lower panel). Differences in these networks can be exploited to learn unique features of each network. (c) Constraint-based analysis predictions can be compared and validated against fluxomics data. *This figure and the text in the legend have been reproduced from Bordbar et al. (2014) with permission [20]*

1.4 Thesis outline

In this thesis two contexts of metabolic network adaptability are being analyzed. In Chapter 1, I introduce the general characteristics of metabolic networks, genome scale metabolic modeling as a tool to study metabolic network fluxes and different approaches to use models for the integration of multi-omics data. The first project (Chapter 2) on glycerol adaptation in yeast was initiated in collaboration with Dr. Tomas Strucko, currently at the Technical University of Denmark (DTU). The question on what enables yeast to grow on glycerol as the sole carbon source, is tackled with an evolutionary approach. The genomic basis of the adaptive solution of yeast after evolution to utilize glycerol is revealed by a combined approach of classical yeast engineering, omics data analysis and genome scale metabolic modeling. My contribution to this project is to find genomic determinants of this adaptation and to assess these alterations functionally with a comprehensive study of re-engineered cells harboring these mutations at the different levels of genes, transcripts, proteins and metabolites. The second project (Chapter 4) is conducted together with the group of Dr. Martin Jechlinger from the EMBL Heidelberg, who developed an inducible breast cancer mouse model. This mouse model is used to study minimal residual disease in an aggressive form of breast cancer with a high rate of recurrence. I specifically investigate the molecular phenotype of regressed cells in comparison to their healthy counterparts by analyzing and integrating their transcriptional and metabolic alterations. For the integration I make specifically use of a hybrid approach of genome scale metabolic modeling tailored by transcriptional data to predict fluxes in the context of the observed metabolic alterations. Therefore, I curate in Chapter 3 a currently available genome scale metabolic model to be more suitable for flux analysis. In Chapter 5, I conclude the implications of my findings in the context of adaptation and how general features of metabolic networks such as redundancy and plasticity shape adaptation in the context of evolution and disease.

CHAPTER 2

GENETIC ADAPTATION TO CHANGES IN CARBON SOURCE

Summary

In this part I investigate the ability of an "isolated" metabolic network of a unicellular eukaryotic organism to adapt towards varying nutritional environments, specifically changes in C-sources. This case study reveals genetic determinants underlying glycerol catabolism and the associated fitness trade-offs. Mechanistically, the redox balance is shown as a core driving force on the rewiring of metabolic network and C-source usability. The study demonstrates the flexibility and complexity of the metabolic phenotype towards external stimuli and addresses the still largely undiscovered genotype-phenotype linkage in metabolic network regulation. The project further exemplifies how metabolic modeling can provide a knowledge-based scaffold and help interpreting multi-layered data, viz., the genome sequence, transcripts, proteins and metabolites, and thereby connect the evolved genotype to the observed phenotype. Metabolic modeling thus contributes to the field of large-scale data integration by providing a novel and comprehensive analytical approach aiming at mechanistic understanding of the genotype-phenotype relation at the level of metabolism.

*I had the pleasure to collaborate with highly motivated and talented people whose contribution fruited the project immensely, first of all Dr. Tomas Strucko from the Technical University of Denmark (DTU) in Denmark. He conducted majority of the experimental work, namely the laboratory evolution experiments, physiological characterization of evolved strains, strain crossing and reengineering as well as the omics experiments. The latter was performed with the help of Dr. Filipa Pereira from EMBL Heidelberg. The sequencing and proteomics experiments were conducted at the EMBL Core Facilities (EMBL, Heidelberg). Eleni Kafkia, also from EMBL Heidelberg, collected and analyzed all the metabolomics data. Dr. Paula Jouhten from the VTT Technical Research Centre of Finland, who also developed the switchPheno algorithm, modeled the growth on different carbon sources. I performed the complete computational analysis, including the genome sequencing analysis, genomic variant analysis, transcriptome analysis, as well as the integration of the sequencing data, modeling results and results from all the omic layers. The results of this project are published in (Strucko, **Zirngibl** et al., Metab. Eng. 2018) [178].*

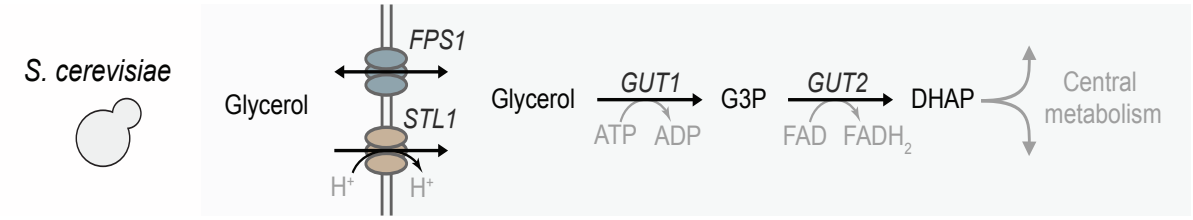

FIGURE 2.1. Glycerol catabolism pathway of *S. cerevisiae*. STL1 – glycerol/H^+ symporter, FPS1 – aquaglyceroporin, *GUT1* – glycerol kinase, GUT2 – FAD^+-dependent glycerol 3-phosphate dehydrogenase, DHAP – dihydroxyacetone phosphate. This figure and the text in this legend have been reproduced from Strucko et al. (2018) with permission [178].

2.1 Introduction

2.1.1 Most *Saccharomyces cerevisiae* strains lack the ability to grow on glycerol as the sole C-source

The natural capability of yeast to utilize glycerol as the sole carbon source varies greatly between different species as well as strains within the same species [181] [92]. Considering that glycerol is a ubiquitous organic compound in nature, this is somewhat surprising, especially for natural isolates, but may be related to an evolutionary trade-off between glycerol consumption and strong Crabtree driven sugar consumption [92]. The spectrum of glycerol utilization ranges from almost comparable growth rates to glucose to very poorly or no growth at all, as in the case of most laboratory strains of the model yeast *Saccharomyces cerevisiae* [181] [120] [92]. However, even the non-growing *S. cerevisiae* contain the necessary genes for glycerol catabolism, namely STL1, FPS1, *GUT1* and GUT2, and thus should in principle be able to uptake and metabolize glycerol (Figure 2-1) [92]. In parts, the differences in growth rate levels could be attributed to varying efficiencies in glycerol uptake owing to the expression of different transport systems [59] [92] [98]. But even under efficient glycerol uptake the catabolism efficiency of glycerol varies greatly between different yeasts. Even more intriguing from a regulatory network point of view is the fact that if supplemented with amino acids, all *S. cerevisiae* stains are able to grow on glycerol, even if somewhat slowly [181].

Several mutations have been identified to either facilitate or enable growth on glycerol, such as the combination of mutations in the genes *GUT1*[1], *UBR2* and *SSK1* by Swinnen [181] or only *UBR2* and *GUT1* by Ho [74]. Different *GUT1* alleles have shown to possess higher enzymatic activities and thereby influencing the observed growth rate. However, except for the obvious mutation in the gene *GUT1*, coding for a glycerol transporter, all of the identified mutations so far lacked functional or mechanistic insights.

2.1.2 Adaptive laboratory evolution leads to novel traits as a result of natural selection

The process of adaptation to a given selection pressure can be systematically studied in laboratory settings in the form of adaptive laboratory evolution (ALE) experiments. ALE is an experimental procedure in which an evolutionary pressure is selectively applied to a population of cells or organisms to develop a certain trait of interest. The selective pressure is exerted via the environment to which the population is subjected to for a prolonged time. During the course of the experiment, mutations randomly arise and are fixed in the population by natural selection in case they are beneficial. Over time, a new population with different traits and an overall increased fitness evolves. ALE experiments are typically performed with microorganisms since they are easy to cultivate, have large population sizes, small genome sizes and are possessing short generation times [96] [97] [122].
Applications of this approach are very broad and include industrial and basic science applications. In the industrial sector, ALE helps, for example, to achieve untargeted strain design/optimization for biotechnological goals such as heterologous protein and compound production, product formation, substrate utilization, stress resistance and growth temperature or inhibitor tolerance [157] [156] [25] [95] [75] [26] [164] [155] [10]. ALE is particularly useful in areas where genetic manipulation is either forbidden[2] or where rational design becomes difficult because of a lack of mechanistic and functional understanding of the genetic determinents [96] [195] [148]. ALE has also proven to be a powerful method in research contexts to increase scientific understanding of the basic mechanisms of molecular evolution [40], the dynamics of the evolutionary processes [122] or the adaptive changes during perturbations occurring from a reference state to another [183] [30]. The latter helps answering questions of complex genotype-phenotype linkages, such as antibiotic resistances, including the complexity of the regulatory circuits of a system or deciphering the entirety of the physiological response [82] [27].
Of paramount importance for an ALE experiment to be applied successfully is the choice of the environmental conditions imposing an evolutionary selection pressure on the organisms, such that the desired trait gets selected for [96]. In microbial laboratory evolution, this typically requires

[1] encodes a glycerol kinase
[2] e.g. food applications

coupling the desired trait with growth[3], which is not always trivial and might not be achievable for all traits [195]. Several attempts have been made to define the environment exhibiting the right evolutionary pressure in a more rational and systematic manner. For instance, the EvolveX algorithm developed by Jouhten et al., makes use of the yeast genome scale metabolic model to predict the right evolution media to evolve the over production of a certain metabolite [140]. To circumvent the limitation of growth coupling of a desired trait to become targetable by ALE, Jouhten P. developed the idea of the phenoSwitch algorithm in which the original evolution niche gets separated from the final target niche [140]. In that way an organism is first evolved in a predicted growth-coupled evolution environment, in which the flux distributions evolve in such a way that once the organism gets moved to the target environment, the desired trait, which doesn't have to be growth coupled at that point, is necessarily exploited. This approach is specifically useful for short-term applications, in which the evolved organism's trait doesn't need to be stable over evolutionary relevant time, such as e.g. food batch production.
Other important variables that influence the type, diversity, variability and possibly trade-offs of the phenotypic adaptation of the evolution experiment include the strength and the alterations of the selection pressure[4], the population size, the passage size[5], the mutation rate and finally the time scale of the evolution experiment, which in turn also depends on the previous parameters [195] [97] [40]. In regards to the length of the ALE experiment it is important to note that the fitness increase as a function of the total number of generations passed is not linear and is usually fastest at the beginning of the experiment [40]. The mutation rate can be enhanced via, e.g., chemical mutagens, using mutants deficient in DNA repair or utilizing transposon-based mutagenesis. A higher mutation rate increases the genetic diversity within the evolving population and the adaptation can be accelerated [195] [40]. Clearly, higher mutation rates can only be beneficial to a certain extent as it also results in a higher genetic load, which can lead to undesired side-effects such as decreased stress resistance or a loss of viability [40]. Another strategy to shorten the adaptation time or to push it in a predetermined direction is to start the culture from a library of mutants [122]. Depending on the choice of all the parameters in an ALE experiment, complex population structures may arise resulting from clonal interference where multiple lineages with different independent beneficial mutations are coexisting in a population and are competing for fixation [195] [122] [40]. But depending on the time point when the ALE experiment is stopped, some of the adaptive mutations present earlier in evolution also might already been lost [195].

[3] i.e., exponential growth rate, biomass yield, stationary phase fitness, or lag phase duration
[4] including the growth phase of the passages
[5] only in serially passaged batch cultures

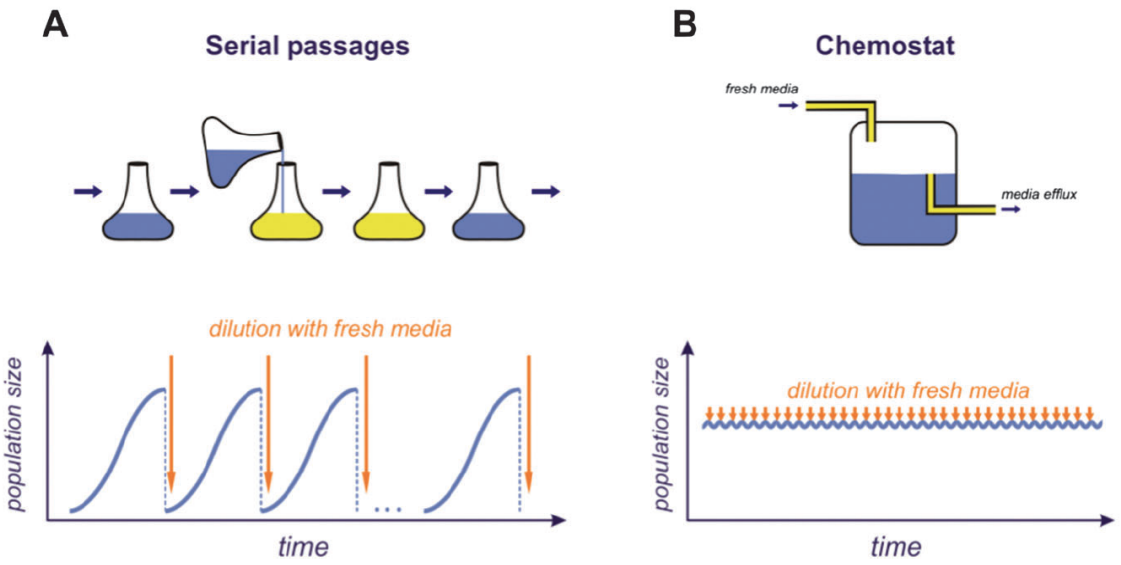

FIGURE 2.2. Methods used for studying microbial evolution *in vivo*. The most common techniques used to maintain control over environmental conditions and microbial growth rates for prolonged times are: (a) serial passages and (b) chemostat cultivations. In a chemostat it is possible to continuously monitor and control the growth conditions at a desired level; however, this approach requires a complex experimental setup. When a large number of strains need to be evolved in parallel, serial passages are frequently used to increase the feasibility of an experiment. In the latter case, microbial cultures are periodically diluted with fresh media to limit the microbial concentration and supply the growing populations with new nutrients. Inevitably, some of the environmental parameters fluctuate between the passages (e.g. the nutrient concentration and pH) but other parameters like the temperature and oxygen concentration can be kept constant. Figure and figure legend have been reproduced from Mozhayskiy & Tagkopoulos (2013) with permission [122].

On the technical front, there are two basic methods of ALE experiments, serial batch cultures and continuous chemostats cultivation. Both types of cultivation methods differ in handling and their capabilities to constitute the environment. This imposes different characteristics on some of the above-mentioned parameters, such as the type and alteration of the selection pressure [122] [195]. In batch cultures, the cells are typically grown in shake flasks or multi-well plates and propagated to a subsequent batch culture once they reach a certain OD or growth phase (Figure 2-2a) [40]. Batch cultures have the advantage of being relatively easy to set up and carry out, but the environmental conditions, population densities, nutrient supply and growth rates or growth phases fluctuate along the experimental course. This creates a more complex selection pressure and thus a more complex fitness landscape, which might lead to a conflicting phenotypic outcome [96] [40] [122]. An extreme example of this is the case when cells are only passaged after they

have reached the stationary phase [97]. There not only the growth rate but also the ability to maintain viability and restart growth after stationary phase contribute to the fitness.
Furthermore, batch cultures are more susceptible to genetic drift since random sampling during the transfers imposes bottlenecks on the developed mutations to be carried over [195] [122]. The passage size is therefore a crucial parameter in batch cultures, determining the variability and rate of evolution [96] [122]. Recent attempts have been made to model and predict the optimal passage size for a given experiment [96].
In contrast to the batch cultivation, chemostats are continuous culture systems that do not require transfers and can allow for a more precise control with minimal fluctuation of the environmental conditions, growth rate and population densities (Figure 2-2b). They can therefore selectively apply one defined selection pressure, as for example keeping the cells always in exponential growth phase, which would make fitness equivalent with growth rate [96] [195] [40]. Thus, homogeneous populations are more frequently observed in chemostats than in serial passages [32]. On the negative side, the cells evolved in chemostats may lose other traits such as tolerance to pH or osmotic stress that are important for industrial application.

2.1.3 An integrated approach of reverse engineering, multi-omics analysis and metabolic modeling to mechanistically understand adaptation to glycerol

To functionally understand the basis of glycerol catabolism in yeast, we first performed parallel ALE experiments using the *S. cerevisiae* CEN.PK113-7D strain to evolve the ability to use glycerol as the sole carbon source in minimal media (Figure 2-3a). Given the genetic existence of a glycerol catabolism pathway in yeast, ALE experiments are particularly suited for evolving yeasts to efficiently grow on glycerol. Previous studies have already demonstrated that *S. cerevisiae* strains could acquire the ability to utilize glycerol in minimal media by using ALE. Using serial batch cultivations growth rates $\mu_{\max}$ of about 0.2 h-1 were reached [120] [74]. However, none of the studies mechanistically linked the evolved phenotype to its genetic determinants explained the underlying mechanisms of the evolved phenotype and its genetic determinants.

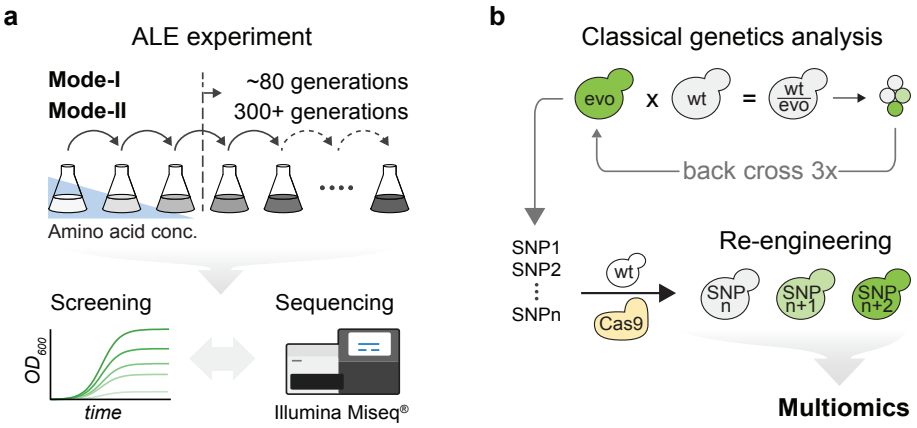

FIGURE 2.3. Outline of the experimental approach to understand the metabolic phenotype under glycerol consumption in yeast. (a) Laboratory adaptive evolution of *S. cerevisiae* for growth on glycerol combined with phenotypic screening and sequencing. (b) Workflow for genomic strain analysis and identification of the causal mutations. Re-engineering with CRISPR/Cas9. This figure and the text in this legend have been adapted from Strucko et al. (2018) [178].

In addition to the wild-type (WT) strain, a second strain having a NADH oxidase introduced *NOX* gene from *Streptococcus pneumoniae* encoding for cytosolic water forming NADH oxidase *NOX* was used for evolution. The *NOX* mutant was chosen as it was previously hypothesized that unbalanced levels of intracellular NADH hamper glycerol catabolism in minimal media [120]. The evolutionary selection pressure was exerted by growing the strains on 1% glycerol and gradually decreasing the supplementation of amino acids[6]. The evolution experiments were conducted in two modes, which resulted in slightly different evolutionary pressures by having the transfer at different growth phases: mode-I, short-term[7], and mode-II, long-term[8]. In mode-I, two *NOX* based replicates were used, whereas in mode-II five parallel lineages of each WT and *NOX* were evolved. Phenotypic characterization under different conditions was performed to review the evolved glycerol growth phenotypes and identify potential trade-offs. As it is generally observed that adaptation rates are highest in the early stages [196] [16], we also characterized the intermediate lineages from mode-I. Subsequently whole genome sequencing of the parental strains, all final evolved lineages as well as intermediate lineages from mode-I was performed to identify genetic changes that were introduced in the final population during the course of the ALE experiment (Figure 2-3a).

Determining the genetic changes that enable the fitness increase amongst the multiple mutations that evolved strains harbor can be a time-consuming and complex process. We used two strategies to facilitate the discovery process: i) comparing mutations of the evolved strains/lineages with

[6] which help yeast assimilate glycerol but also provide carbon
[7] up to 80 generations, manual transfers during late stationary growth phase
[8] >300 generations, automated transfers during early exponential growth phase

those of the parental strains, and ii) identifying gene regions or pathways in which mutations occur more frequently across the independent replicate experiments. Furthermore, to narrow down on a set of causal mutations underlying a glycerol growth phenotype, a strain isolate of one of the successfully evolved endpoint lineages was crossed back with a wild type strain until the number of mutations were substantially reduced while still retaining the parental growth phenotype on glycerol (Figure 2-3b). The selected remaining candidate mutations[9] were then reengineered one by one into the WT strain. Finally, to understand the functional relationships between the identified mutations and the metabolic phenotype as well as to gain mechanistic insights into the metabolic pathway regulation under glycerol, the functional impact of the mutations was analyzed with an integrated approach of transcriptomics, proteomics and metabolomics profiling and genome-scale constrained based modeling.

2.2 Materials and Methods

Material and methods have been published in [178]. The text has been adapted from the publication.

2.2.1 Strains and cultivation media

Escherichia coli DH5α strain was used for maintenance and amplification of cloned plasmids, and was propagated in 2xYT medium (Sigma) supplemented with 100 mg/L of Ampicillin (Sigma). *S. cerevisiae* strains used in this study were prototrophic laboratory haploid strains CEN.PK113-1A and CEN.PK113-7D, and industrially relevant diploid strains L.1528 and CLIB382 (Table A.2). For maintenance and genetic transformation of yeast strains a yeast extract peptone dextrose (YPD) medium containing 10 g/L of yeast extract, 20 g/L of peptone and 20 g/L of glucose was used. Solid YPD medium was prepared by addition of 20 g/L of agar prior autoclavation. For selection of yeast strains with dominant markers NatMX, KanMX or HphMX, YPD medium was supplemented (after autoclavation) by 100 mg/L of nourseothricin (ClonNat, Werner BioAgents), 200 mg/L of G418 disulfate salt (Sigma) or 200 mg/L hygromycin B (Sigma), respectively. For high osmotic stress sensitivity assays, the YPD medium was supplemented with potassium chloride to a final concentration of 0.5 moles/L. Plates with sporulation (SPO) medium were prepared as described elsewhere [172].

Adaptive laboratory evolution and strain characterization was done in a well-defined mineral (M) media described by [189] containing 5 g/L (NH4)2SO4, 3 g/L KH2PO4, 0.75 g/L Mg2SO4, 1.5 mL/L trace metal solution and 1.5 mL/L vitamins solution. The composition of the trace metal solution is 3 g/L FeSO4.7H2O, 4.5 g/L ZnSO4.7H2O, 4.5 g/L CaCl2.6H2O, 0.84 g/L MnCl2.2H2O, 0.3 g/L CoCl2.6H2O, 0.3 g/L CuSO4.5H2O, 0.4 g/L NaMoO4.2H2O, 1 g/L H3BO3, 0.1 g/L KI and 15 g/L Na2EDTA.2H2O. The vitamin solution includes 50 mg/L d-biotin, 200 mg/L para-amino

[9] selection guided by the comparative genomic analysis

benzoic acid, 1.0 g/L nicotinic acid, 1.0 g/L Ca-pantothenate, 1.0 g/L pyridoxine-HCl, 1.0 g/L thiamine-HCl and 25 mg/L minositol. The carbon source in the M medium was either 10 mL/L of glycerol or 30 g/L of glucose resulting in MG or MD media, respectively. The pH was adjusted with KOH/H2SO4 to 4.2 for the MG and to 6.5 for the MD medium. For the initial stage of the adaptive laboratory evolution MG medium was additionally supplemented with 1.92 g/L of Y1501 amino acid mix (Sigma) and was denoted as MG+ medium. For small-scale cultivations, the media was filter-sterilized by a bottle-top (0.45 μm pore size) filter (VWR). For the 1L batch fermentation experiments medium was heat-sterilized, sterile vitamin solution and glycerol were added after medium cooled down to 30°C .

2.2.2 Molecular cloning

All DNA fragments that constituted genetic elements[10] or plasmids backbone sequences were amplified by PCR using PfuX7 [127] polymerase with specific primers (Table A.1). The TEF1 promoter sequence was amplified from the pSP-GM1 [139] plasmid, and the *NOX* gene from genomic DNA (gDNA) of *Streptococcus pneumoniae* SV1. Integrative plasmid pTS1 targeting the specific chromosomal site X-3 (described earlier [121]) was assembled by the uracil-specfic excision reagent (USER^{TM} following well established protocols [61]. Specifically, the TEF1 promoter and the *NOX* was USER-cloned into AsiSI/Nb.BsmI linearized pCfB2223 ([176]) plasmid backbone resulting in pTS1. The construction of plasmids harboring single guide RNAs (gRNAs) expression cassette targeting specific genetic loci were constructed as follows. Unique linear fragments were obtained by PCR amplifying the pCfB2311 ([176]) plasmid backbone with the generic 5‘-phosphorylated primer (TS109) in combination with the specific primer for each genetic target (Table A.1). Thereafter, each fragment was independently circularized via blunt end ligation by T4 ligase (Thermo Fisher Scientific) according to the manufacturer’ s recommendations. The construction of pTS83 vector encoding three gRNAs cassettes was assembled by USER-cloning as described previously [81]. In short, three gRNA cassettes targeting *GUT1*, *UBC13* and *KGD1* loci were independently amplified from plasmids pTS53, pTS56 and pTS70, respectively. Subsequently, the resulting PCR fragments were USER cloned into AsiSI/Nb.BsmI linearized pTAJAK71 [81] vector. All genetic constructs were validated using Mix2Seq sequencing (Eurofins Genomics). All used and constructed plasmids are listed in Table A.32.

2.2.3 Yeast genetic transformation

All genetic modifications of *S. cerevisiae* laboratory and industrial strains were done using well described (Lithium acetate, PEG and ssDNA) transformation protocol (Gietz and Schiestl, 2007). Routinely, 200-500 ng of plasmid DNA and 0.5-1 μg of linear DNA was used per transformation. For CRISPR/Cas9 genome editing purpose, 2.5 mM of 90-bp long dsOligo was used as a repair

[10] i.e., promoters, open reading frames (ORFs) and terminators

template. For industrial *S. cerevisiae* strains the amount of 90-bp dsOligo was doubled. All transformants were selected on YPD medium plates supplemented accordingly with appropriate selection drug/s. Finally, single colonies were streak-purified on a selection medium prior further analyses and subsequent genetic manipulations.

2.2.4 Adaptive laboratory evolution

Two starting *S. cerevisiae* strains, the WT CEN.PK113-7D and the TS29 *NOX* strain expressing water forming NADH oxidase from *S. pneumoniae* were used in adaptive laboratory evolution (ALE) experiments. Moreover, ALE was done in two modes - I) manual ALE and II) using automated robotic set-up. The mode-I ALE was performed in 500 mL shake flasks with 50 mL of medium using only the *NOX* expressing strain. Prior to ALE, two cultures of *NOX* strain were preconditioned by 72 hours cultivation in MG+ medium at 30°C and constant agitation at 250 rpm. Subsequently, cultures were re-inoculated into the 50:50 of MG+ and MG media mix and cultivated until the stationary growth phase was reached. Thereafter, ALE was done exclusively in the MG medium by serial transfer of yeast cultures into fresh medium at late-exponential/stationary growth phase. The fresh cultures were inoculated to a starting OD600 0.1 to 0.3. The ALE experiment lasted for up to 80 cumulative generations in MG media. Cryostocks of the intermediate cultures were prepared at regular intervals. For the mode-II ALE experiment, two strains WT and *NOX* were pre-cultured in two separate 500 mL shake flasks with 50 mL of MG+ medium. Five replicates with 15 mL of MG+ medium were inoculated to a starting OD600 of 0.3 per strain. The tubes were cultured at 30°C with constant agitation at 1000 rpm. A total of 900 μ of culture was serially passaged to fresh medium during early-exponential phase. The OD600 was automatically measured at regular intervals to assess cultures growth state. The growth medium composition was gradually changed from the MG+ to the MG medium[11] during the ALE experiment. The last 300+ generations were evolved purely in the MG medium. Cryostocks of the intermediate cultures were prepared at regular intervals, however, only the final ALE lineages were used in further analyses. All growth curves are plotted using R language using 'loess' method based on two biological replicates.

2.2.5 Characterization of growth in microtiter scale

All evolved and re-engineered yeast strains were characterized in microtiter scale setting using the Growth Profiler 1152 systems (Enzyscreen). An overnight pre-culture was prepared by inoculating each strain into a well of 24-deep well plate (Porvair Sciences) filled with 3 mL of YPD medium and incubating at 30°C with 300 rpm shaking. Next day, the plate with the pre-culture was spun-down at 2200 g for 5 min and resuspended in 3 mL of MG medium. 200 μL aliquots of resuspended pre-culture was transferred to a volume of fresh MG medium in order to reach

[11] mixing from 100:0 to 0:100

a pre-inoculum suspension of OD600 4.5. Finally, 50 μL of each pre-inoculum was inoculated into a separate well of Krystal 24-well clear bottom white microplate (Porvair Sciences) prefilled with 700 μL per well of MG media and incubated for minimum of 80 hours at 30°C with 225 rpm shaking. Cell growth[12] was monitored by scanning the bottom of the plates in 30 min intervals. G-value was converted to an OD600 equivalent by using a spline fitted calibration curve using the data from Bergdahl et al. (unpublished data). For growth characterization in MD medium the procedure was done exactly as described above. Growth rates were estimated by calculating the maximum slope values of best linear fit on log-transformed OD values[13]. All growth curves are plotted using R language using 'loess' method based on two biological replicates.

2.2.6 Spot assays

To assess osmo-sensitivity, yeast cells were inoculated in 3 mL of YPD medium and grown overnight at 30°C with constant shaking 250 rpm. Next day, 100 μ aliquots of each culture were resuspended in sterile MiliQ water to OD600 = 2, and 3 μL of 10-fold dilution series were plated on YPD plates with and without KCl. Plates were incubated at 30°C for 3 days and cell growth was monitored once a day.

2.2.7 Classical genetics techniques

Classical genetic techniques were done according to standard protocols [172] with slight modifications. In brief, diploids were generated by combining two medium sized single colonies of the haploid strains with opposite mating type in 200 μL of sterile water in a 1.5 mL Eppendorf tube and vortexing them vigorously. Thereafter, 10 μL of the suspension was plated onto YPD plate and incubated for 4 6 hours at 30°C. The cell mix was then scraped out from the YPD plate and resuspended in 400 μ of sterile water. 10 μL of the suspension is plated on YPD plate and formed zygotes were isolated using spore dissection microscope. The ploidy and mating type was confirmed by multiplex colony PCR on MAT locus [78] using the primers MAT_R, MATα_F and MAT_F. The sporulation was induced by plating diploid cells on SPO plates and incubating at 30°C for up to 6 days depending on sporulation efficiency. After confirming the presence of tetrads on SPO plates a small portion of biomass with spores was resuspended in 50 μ of (2.5 mg/mL) sterile Glucanex^{R} (Thermo Fisher Scientific) solution and digested for up to 15 min at approx. 25°C. The reaction was stopped by adding 450 μ of sterile MilliQ water and up to 5 μ of the resulting suspension was carefully transferred to a dissection plate. Tetrads were dissected using Axio Scope.A1(Carl Zeiss) microscope equipped with dissection platform. Plates with dissected spores were incubated at 30°C for 2 days at 30°C.

[12] green color intensity, G-value
[13] minimum of 10 data points

2.2.8 Re-engineering mutations found in evolved strains

In order to re-engineer the mutations of interest in the wild type strains the CRISPR-Cas9 techniques [81] [176] optimized for the *S. cerevisiae* were used. For each modification, a specific gRNA sequence (Table A.1) targeting the Cas9 nuclease to the appropriate genetic locus was designed. The quality and specificity of gRNA was assessed using a CRISPRdirect online tool developed by Naito et al. [124]. In order to repair a DNA double strand break introduced by Cas9 repair templates (90-bp dsOligo flanking 45 bp upstream and downstream of the specific cut site) were designed for each locus of interest. Each repair template contained a specific mutation and a silent mutation that would disturb (NGG) PAM site motive (Table A.1). First, the two laboratory strains CEN.PK113-7D and CEN.PK113-1A were transformed (as described above) with the Cas9 expressing plasmid pCfB2312 resulting in strains 7D_Cas9 and 1A_Cas9, respectively. Yeast transformants were selected on YPD+G418 plates. Subsequently, the Cas9 expressing strains were individually transformed with different single gRNA expressing plasmids (Table A.32) and resulting cells were selected on YPD+G418+CloNat. To confirm that the gene editing was successful routinely 5 colonies per edit were tested. A 500 bp long DNA fragment flanking the locus of an edit was amplified by colony-PCR using OneTaq^{R} 2X Master Mix (New England Biolabs) with specific primers (Table A.1), column purified using NucleoSpin^{R} kit (MACHEREY-NAGEL) and sent for sequencing (Eurofins Genomics). Each engineered strain harboring a correct genetic edit was streaked on YPD+G418 plates and incubated for 2-3 days at 30°C. Subsequently, yeast strains were replica-plated on YPD+G418+CloNat and YPD+G418 media in order to select for the mutants that have lost gRNA expressing plasmid. Next, yeast cells with a single genetic edit (without the corresponding gRNA plasmid) were transformed with a new gRNA expressing plasmid targeting a different locus. Subsequently, gRNA plasmids were "kicked out" from the correct strains harboring a double genetic edit. The transformation cycle was repeated for generation of the strains containing triple gene mutations (Table A.2).

2.2.9 Controlled batch fermentation

The evolved lineage ALE2 and re-engineered strains TS154(R-GU), TS170(R-GK) and TS177(R-GKU) from YPD plate were inoculated to 0.5 L shake flasks with 100 mL of MG (pH 4.2). Pre-cultures were incubated in an orbital shaker set to 200 rpm at 30°C until late-exponential phase (OD600 5 7). Cell suspension was up-concentrated by centrifugation and resuspension in fresh MG medium and used for inoculation. Batch cultivations were performed under aerobic conditions in one liter Sartorius fermenters equipped with continuous data acquisition (Braun Biotech International). Each fermenter was inoculated to an initial OD600 of 0.2. Cell culture aeration was ensured by constant airflow of 1.5 v.v.m. (80 L/h) and stirring speed of 1000 rpm. The temperature was maintained at 30°C during the fermentation and pH (4.2) level was controlled by automatic addition of 2M NaOH solution. The exhaust gas composition was constantly monitored by off gas analyzer 1311 Fast response triple gas (Innova) combined with Mass Spectrometer

Prima Pro Process MS (ThermoFisher Scientific). The batch cultures were sampled in regular intervals for estimation of OD600, cell dry weight (CDW) and extracellular metabolites. Samples for transcriptomic, proteomics and intracellular metabolomics were taken at the early-exponential growth state (OD600 2 5). All experiments were done in triplicates except for the strain TS154 (R-GU), which was done in duplicate.

2.2.10 Cell dry weight sampling

The biomass concentration was determined by measuring CDW as previously described [106] using polyethersulfone filters with a pore size of 0.45 μm Montamil^{R} (Membrane Solutions, LLC). The filters were pre-dried in a microwave oven at 150 W for 20 min and weighted on analytical scales. 5 mL of cultivation broth was filtered and then washed with three volumes of distilled water. Thereafter, the filters with biomass were dried in the microwave oven at 150 W for 20 min and cooled down in a desiccator for a minimum of 2 hours. The filters with dried biomass were weighed in order to determine the CDW.

2.2.11 Genomic DNA sample preparation

Genomic DNA of *S. cerevisiae* strains was isolated using a ZR Fungal/Bacterial DNA MiniPrep^{TM} kit (Zymoresearch). DNA was extracted following the manufacturer's recommendations, except that yeast cells were disrupted by five cycles of 1 min vortex and 1 min on ice. The quality and the concentration of extracted DNA was assessed with the spectrophotometer NanoPhotometer^{R} P-Class (IMPLEN). 150 bp pair-end DNA libraries were prepared using TruSeq Nano DNA HT Library Prep Kit and sequenced using Miseq^{TM} platform (Illumina).

2.2.12 RNA-seq sample preparation

All RNA samples were prepared as follows, 10 mL of fermentation broth was sprayed into 50 mL Falcon^{R} tube filled with ice and immediately centrifuged at 10000 x g for 5 min at 4°C. After centrifugation supernatant was discarded and cell pellet was frozen by placing the tube into dry-ice bath. Tubes with frozen biomass were kept at -80°C until extraction. Total RNA of each sample was isolated using RNAeasy kit (Qiagen) by following manufacturer's protocol. Briefly, 594 μL of RLT buffer plus 6 μL of β-mercaptoethanol were added to the Falcon^{R} tube containing the frozen cell pellet and let it unfreeze on ice. Cell suspension was transferred to an ice-cold FastPrep Cap tube containing 600 μL of glass beads (400 nm acid washed, Sigma). Cells were disrupted using FastPrep (2 cycles with the following conditions: 10 seconds at speed 6, 15 seconds on ice). Cell lysate was transferred to a new tube and centrifuged 2 min at full speed in microcentrifuge (Eppendorf). Supernatant was careful mixed with 1 volume of 70 % HPLC-grade ethanol. Sample was transferred to an RNAeasy column and washed according to the manufacturer's instructions. RNA was then eluted with 60 μL of RNase-free water. Eluted sample

was digested with Turbo DNAse (Invitrogen Ambion) accordingly to manufacture instructions followed by RNA clean-up (RNAeasy kit, Qiagen). The RNA library was prepared using the Illumina TruSeq Stranded mRNA LT sample prep kit starting with 500 ng of total RNA, following manufactures instructions using Beckman Biomek FX Laboratory automation station. Samples were sequenced using Hiseq2000 instruments in the 50 bp single read mode and loaded 8 pM onto the flow cell at the Genomics Core Facility of EMBL (Heidelberg, Germany).

2.2.13 Analysis of genomic variants

The bioinformatics pipeline for sequencing read analysis to identify mutations included the following steps. All sequencing reads were passed through quality control with FastQC [6] (version 0.11.3), followed by adapter trimming using cutadapt [117] (version 1.9.1) with default options. Subsequent quality trimming and filtering was performed with FaQCs (Lo and Chain, 2014) (version 1.34) using default parameters. Since the sequencing data were of good quality and aligners are already able to do soft-clipping[14] the impact of the quality control process steps on the alignment quality and the final variant calling results was neglectable. Bowtie2 (version 2.0.2) was used for sequence read alignment to the *S. cerevisiae* CEN.PK113-7D [125] or S288C (R64-2-1_20150113) [44] reference genome using the following parameters: –very-sensitive-local -I 180 -X 1000 –score-min G,70,8. Picard Tools (version 1.129) (http://broadinstitute.github.io/picard/) were used for file formatting and the removal of read duplicates. The genome-wide detection of single- and multi-nucleotide variants (SNVs and MNVs) was performed with the GATK HaplotypeCaller [119] (version 3.3.0) using default settings except for the ploidy, which was set to 5 in order to also detect variants that might be only present in a fraction of the lineages. Post-processing and manual filtering of the raw VCF (Variant Call Format) files was conducted according to the GATK Best Practices [38] recommendations, which included a minimum variant calling quality of 900 (Figure A.1 and Figure A.2). In addition, while analyzing the tetrad genomes, only the variants with a 2:2 segregation pattern were kept. Intermediate sized structural variants (SVs) were investigated with delly2 following the workflow for somatic SV calling [152] (version 0.7.2). Large SVs were investigated by read-depth analysis summarizing all high-quality aligned reads in consecutive genomic windows of 1 kb across the genome and then using Circular Binary Segmentation. All samples had an average mapped coverage of at least 40 reads. Mutations of interest were confirmed by Sanger sequencing 500 bp long fragments of the loci of interest obtained by PCR with specific primers.

2.2.14 Differential expression analysis

The quality of the raw RNA sequencing reads was assessed using FastQC [6] (version 0.11.3). Prior to the alignment, adapter trimming was performed using cutadapt [117] (version 1.9.1) with

[14] removing adapters

default options providing the standard lllumina TrueSeq Index adapters. Subsequent quality trimming and filtering was performed with FaQCs (Lo and Chain, 2014) (version 1.34) using the following parameters: -q 20 -min_L 25 -n 5 -discard 1. The total reads per sample after trimming and filtering ranged from 17.5 to 27 million. The sequencing reads were aligned to the reference genome of *S. cerevisiae* CEN.PK113-7D [125]. using tophat2 [90] (version 2.0.10) with the following parameter: -G -T -x 20 -M –microexon-search –no-coverage-search –no-novel-juncs -a 6. Only reads with unique mappings were considered for differential expression analysis. Gene level count tables were obtained using the count script of the HTSeq [4] python library (version 0.6.1p1.) with default options. All reads mapped in total to about 5400 genes. This was followed by statistical analysis using the Bioconductor package DESeq2 ([109]) (version 1.12.4). Size-factor based normalization to control for batch effects and inter-sample variability and dispersion estimation were conducted using package defaults. The differential expression analysis was again performed with the package defaults, which include multiple testing correction, independent filtering and cooks cutoff (Anders and Huber, 2010) for outlier detection. Raw P-values ("orig_") as returned by DESeq2 were used as input to fdrtool [177] (version 1.2.15) in order to compute q-values[15] ("re.estimated_"). Genes with FDR < 0.1 were considered as significantly differentially expressed. Biostatistical analyses were conducted using R V.3.3.1 (R Development Core Team).

2.2.15 Proteomics sample preparation and data analysis

For proteomics analysis 10 mL of fermentation broth was transferred into ice-cold 15 mL Falcon^{R} and immediately centrifuged at 10000 x g for 2 min at 4°C. After centrifugation supernatant was discarded and cell pellet was washed once with PBS buffer. Pellet was frozen by placing the tube into dry-ice bath. Frozen samples were kept at -80°Cuntil extraction. Cell pellets were lysed using 0.1 % RapiGest in 100 mM ammonium bicarbonate. Three cycles of sonication (Cell disruptor, Sonifier, Branson) were applied to the lysate (1 cycle: 15 seconds sonication, 15 seconds on ice), followed by 15 min bead beating using Precellys Lysing Kit (KT0361-1-004.2). Cell lysate was transferred into a new tube after centrifugation (5 min, 5000 x g) and incubated at 80°C for 15 min. Benzonase (25U, Merck) was added to the lysate for 30 min at 37°C. Cysteines were reduced using dithiothreitol (56°C, 30 min, 10 mM). The sample was cooled to 24°C and alkylated with iodacetamide (room temperature, in the dark, 30 min, 10 mM). Proteins were TCA precipitated, TCA pellet was washed by acetone and dried. The proteins were digested in 50 mM HEPES (pH 8.5) using LysC (Wako) with an enzyme to protein ration 1:50 at 37°C for 4 hours, followed by trypsin (Promega) with an enzyme to protein ratio 1:50 at 37°C overnight. TMT10plex^{TM} Isobaric Label Reagent (ThermoFisher) was added to the samples according the manufacturer's instructions. Labeled peptides were cleaned up using OASIS^{R} HLB μElution Plate (Waters). Offline high pH reverse phase fractionation was performed using an Agilent 1200 Infinity high-performance liquid chromatography (HPLC) system, equipped with a Gemini

[15] false discovery rates (FDRs)

C18 column (3 μm, 110 Å, 100 x 1.0 mm, Phenomenex). The solvent system consisted of 20 mM ammonium formate (pH 10.0) as mobile phase A and 100 % acetonitrile as mobile phase B.

2.2.16 Peptide analysis by LC-MS/MS

Peptides were separated using the UltiMate 3000 RSLC nano LC system (Dionex) fitted with a trapping cartridge (μ-Precolumn C18 PepMap 100, 5 μm, 300 μm i.d. x 5 mm, 100 Å and an analytical column (Acclaim PepMap 100 75 μm x 50 cm C18, 3 μm, 100 Å. The outlet of the analytical column was coupled directly to a QExactive plus (Thermo) using the proxeon nanoflow source in positive ion mode. Solvent A was water, 0.1 % formic acid and solvent B was acetonitrile, 0.1 % formic acid. Trapping time was 6 min with a constant flow of solvent A at 30 μ/min onto the trapping column. Peptides were eluted via the analytical column a constant flow of 0.3 μ/min. During the elution step, the percentage of solvent B increased in a linear fashion from 2 % to 4 % B in 4 min, from 4 % to 8 % in 2 min, then 8 % to 28 % for a further 96 min, and finally from 28 % to 40 % in another 10 min. Column cleaning at 80 % B followed, lasting 3 min, before returning to initial conditions for the re-equilibration, lasting 10 min. The peptides were introduced into the mass spectrometer (QExactive plus, ThermoFisher) via a Pico-Tip Emitter 360 μm OD x 20 μm ID; 10 μm tip (New Objective) and a spray voltage of 2.3 kV was applied. The capillary temperature was set at 320°C. Full scan MS spectra with mass range 350-1400 m/z were acquired in profile mode in the FT with resolution of 70,000. The filling time was set at maximum of 100 ms with a limitation of 3x106 ions. DDA was performed with the resolution of the Orbitrap set to 35000, with a fill time of 120 ms and a limitation of 2x105 ions. Normalized collision energy of 32 was used. A loop count of 10 with count 1 was used and a minimum AGC trigger of 2e2 was set. Dynamic exclusion time of 30 seconds was applied. The peptide match algorithm was set to 'preferred' and charge exclusion 'unassigned', charge states 1, 5 - 8 were excluded. Isolation window was set to 1.0 m/z and 100 m/z set as the fixed first mass. MS/MS data was acquired in profile mode.

2.2.17 Metabolomics sample preparation and analysis

For intracellular metabolomics analysis, cells were harvested using a fast filtration protocol properly adapted from ([90]). Briefly, 5 mL of culture were sampled at mid-exponential growth phase and were vacuum-filtered through nylon membrane filters (0.45 μm, WhatmanTM), followed by three rapid washing steps with 5 mL of PBS to ensure no contamination from extracellular metabolites. The polar metabolites were extracted by adding the cell-containing filter in 5 mL of cold (-20 oC) HPLC-grade methanol (Biosolve Chimie, France)/MilliQ water (1:1, v/v) and incubating for 1 h at -20 oC. The mixture of metabolites and cell debris was centrifuged at 10000 rpm and 0 oC for 10 min, and the supernatants were collected and dried with speed-vac. The dried metabolites were derivatized to their (MeOx)TMS-derivatives through reaction with 100 μL of 20 mg/mL methoxyamine hydrochloride (Alfa Aesar, UK) solution in pyridine (Sigma-Aldrich)

for 90 min at 40 oC, followed by reaction with 200 μL N-methyl-trimethylsilyl-trifluoroacetamide (MSTFA) (Alfa Aesar, UK) for 10 hours at room temperature, as justified in (Kanani and Klapa, 2007). The metabolic profile of each sample was measured thrice using a Shimadzu TQ8040 GC-(triple quadrupole) MS system (Shimadzu Corp.). The gas chromatograph was equipped with a 30 m x 0.25 mm x 0.25 μm DB-50MS capillary column (Phenomenex, USA). The detector was operated both in scan mode recording in the range of 50-600 m/z, as well as in MRM mode for the mentioned metabolites. The metabolite quantification was carried out by calculating the peak areas of the identified marker ions of each metabolite (Table A.3). For glucose, the smaller of the two derivative peaks was used for quantification. Samples for quantification of extracellular metabolites were prepared by filtering (0.20 μm Phenex-RC, Phenomenex) 1.5 mL of fermentation broth into glass vials and stored at -20°C until further analyses. Glycerol and several metabolites of the central carbon metabolism were analyzed by high performance liquid chromatography (HPLC system, Waters) equipped with Rezex ROA-Organic Acid column (Phenomenex). The column temperature was set to 65°C and elution was done by sulfuric acid 0.5 mM with constant flow-rate 0.5 mL/min. Metabolites were detected by RI differential refractometer (Waters) and PDA detector (Waters) at 210 nm wavelength.

2.2.18 Genome scale metabolic modeling

Metabolic reactions that likely become re-regulated during adaptive evolution of *S. cerevisiae* for glycerol utilization were identified using model simulations and the in house developed switchPheno algorithm. Specifically, the switchPheno algorithm uses a mixed-integer linear programming routine to identify a minimum number of reactions, in the genome-scale metabolic model of *S. cerevisiae* (iFF708 [54]), that have to be re-regulated to achieve optimal glycerol utilization. As a reference metabolic state for re-regulation we used the distribution of fluxes during respiratory growth on glucose. A set of minimum number of reactions were then identified whose (absolute) flux have to change for optimal glycerol utilization by >25 % beyond the (absolute) flux range extremes [113] ($\pm$ 0.001 mmol/(g CDW h) when 6 C-moles of carbon source were converted to biomass) under the reference metabolic state (Table A.4). Equal C-molar conversion of carbon source to biomass was considered in the reference metabolic state and glycerol utilization. All the simulations were performed with Matlab R2015a v. 8.5.0 using IBM ILOG CPLEX v. 12.6.1 functions 'cplexlp' and 'cplexmilp'.

2.3 Results and Discussion

2.3.1 Phenotypic characterization of the evolved lineages of *S. cerevisiae* growing on glycerol minimal media

While the growth performances in terms of growth rates and residual glycerol levels were similar between the evolved WT and *NOX* lineages of mode-II[16], the *NOX* lineages reached higher final ODs (Figure 2-4a, b, d). Both strains resulted in lineages with maximum growth rates on minimal glycerol medium (mean μmax $\approx$ 0.22) (Figure 2-4b). Interestingly, the adaptation rates of the *NOX* lineage were faster and whereas all of the *NOX* lineages evolved to grow on glycerol only two of the WT based lineages did (Figure 2-4a, c). While there were only minor differences in the final growth performance between the lineages of the two starting strains, the variation of the evolution mode resulted in different growth phenotypes. The manually evolved lineages[17] possess slightly higher final ODs and higher total glycerol consumption, thus seem to be able to use low concentrations of glycerol more efficiently (Figure 2-4a, d). Indeed, when being transferred only at the stationary phase better glycerol exhaustion is expected to be beneficial. On the contrary, the mode-I lineages do not grow as fast as the ALE lineages with lower maximum growth rates on minimal medium (mean μmax $\approx$ 0.16) (Figure 2-4a, b). Being constantly transferred in early exponential phase puts evolution pressure on the growth rate, thus it is not surprising that the final evolved ALE lineages are growing faster. Characterizing intermediate lineages of mode-I, the lineage 2 showed faster adaption with bigger increases in growth performance at early stages than the lineage 1 (Figure 2-4e). The growth phenotype of the final lineage was reached after around 58 generations in mode-I lineage 1 and after around 51 generations in mode-I lineage 2. The best performing isolate was ALE7 from mode-II with μmax = 0.229 $\pm$ 0.002 (Table A.5 Table A.6). Notably, the evolved lineages show on average a four-fold faster growth rate in minimal medium compared to the parental strains in a rich medium containing amino acids.

[16] automated transfer at early exponential phase
[17] mode-I, stationary phase transfers

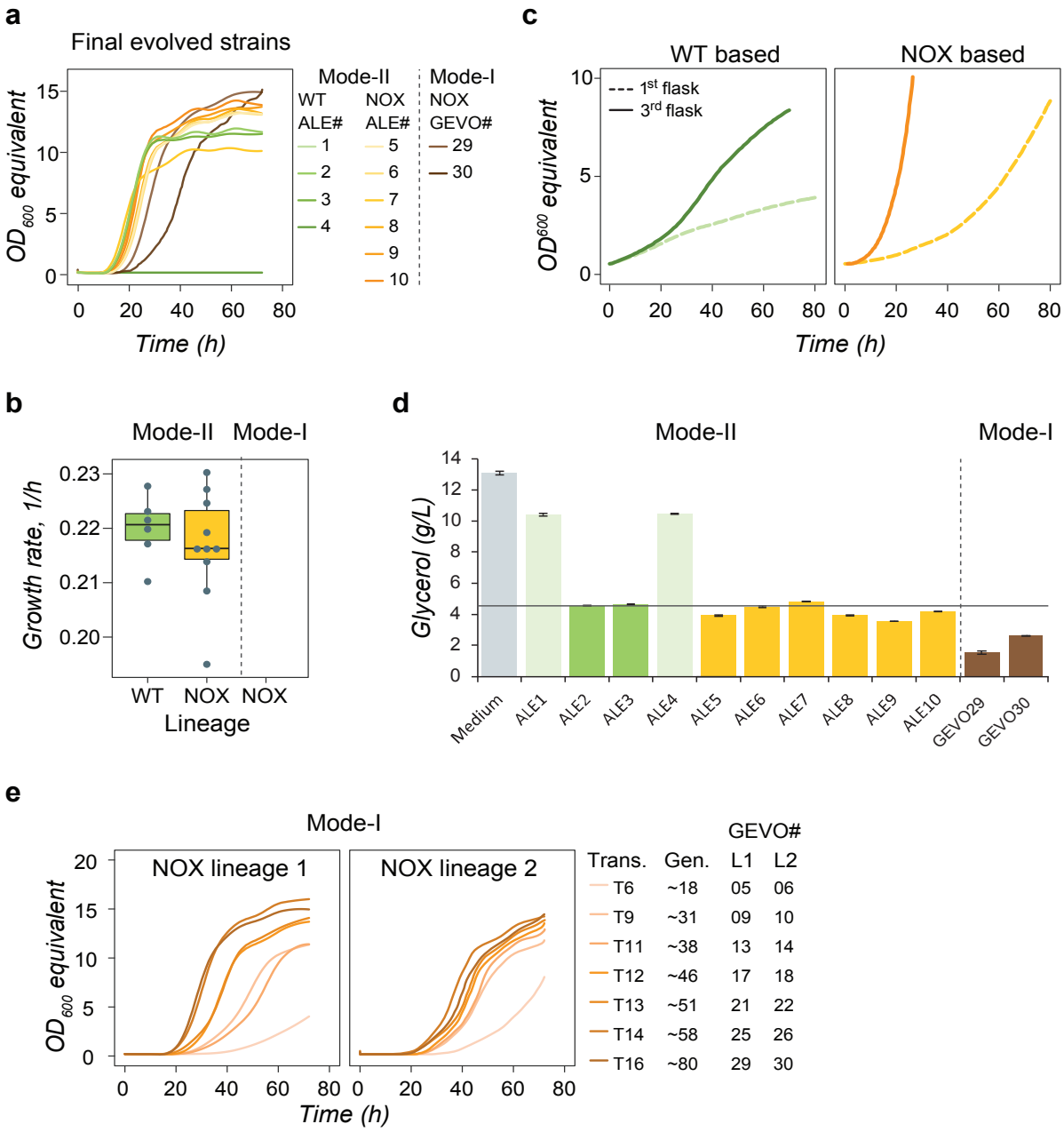

FIGURE 2.4. Growth characteristics of intermediate and final evolved lineages. (a) Growth curves of the evolved *NOX* lineage I from mode-I and the *NOX* and WT lineages from mode-II. (b) Boxplots of maximum growth rates of all evolved lineages. (c) Growth profiles of WT and *NOX* strains in MG+ medium supplemented with amino acids in the initial flasks and after two passages. (d) Color bars represent residual glycerol concentration in MG after 72h of cultivation of all final evolved lineages. Error bars represent standard deviations of two replicates. Note, that ALE1 and ALE4 didn't evolve to grow on MG medium. (e) Growth characteristics of intermediate and final evolved mode-I lineages. Growth rates are estimated based on two biological replicates. This figure and the text in this legend have been adapted from Strucko et al. (2018) [178].

2.3.2 Genomic characterization of the evolved lineages of *S. cerevisiae*

2.3.2.1 Single- and multi-nucleotide variants

The sequencing results revealed 93 unique mutations across the seventeen evolved lineages (Table A.7). The vast majority of the mutations were single nucleotide insertions and SNVs (>95%), whereas only a few were single or double nucleotide deletions and multi-nucleotide variants (Figure 2-5a). The relative high percentage of small indels in comparison to SNVs of 53 percent might hint at a too relaxed post-variant-calling filtering process as other studies analyzing the nature of spontaneously arising mutations observed ratios of only up to maximally 3 percent [207] [126]. About one third (34) of the unique mutations hit coding regions (Table A.7), which is much less than the annotated percentage of coding regions in the genome (75%) that got evenly hit in comparable mutation accumulation (MA) experiments [207] [36] [126]. Considering only SNVs, this ratio increases to expected 72%, which underlines the hypothesis that a too relaxed filtering procedure resulted in a high number of false positive indel calls. Since insertions constitute the vast majority of the identified small indels, they were excluded from the following analysis. Interestingly, almost all of the mutations in coding regions cause amino acid substitutions (Figure 2-5a), whereas in random spontaneous mutation spectra only 75% of all changes should be non-synonymous. In studies without a selective pressure this distribution is typically achieved [126]. Thus, the observed mutations in coding regions seem highly affected by selection/subjected to selection. Various categories of genes were affected by the SNPs ranging from metabolic genes to regulatory and signaling genes. Interestingly, three genes were found mutated in more than one evolved lineages (Figure 2-5a). The glycerol kinase encoding gene *GUT1* was the most frequently mutated gene with independent mutations in five lineages, followed by HOG1 with mutations in four, and PBS2 with mutations in two lineages. The two latter genes are both coding for key proteins of the high-osmolarity glycerol (HOG) pathway and are exclusively found in all the lineages harboring the *NOX* gene. On average 6.5 ± 5.7 new mutations evolved across all final end point lineages growing on glycerol. The huge standard deviation is owned to two outlier lineages harboring about four and a half times more mutations than the rest of the lineages (Figure 2-5b). Interestingly, these are the only two lineages, which do not have any HOG pathway related mutation (Table A.7). The two final GEVO lineages have about one mutation less on average than the ALE lineages of the same strain background, which is most probably owned to the difference in length of evolution (80 vs. 300 generations) (Figure 2-5c). The mutation rate of the SNVs is estimated to be 2.26 ± 1.5 x 10^{-9} per base per generation, which is higher than previously reported, but expectable since these experiments were performed under no selection pressure (Lynch 2008; 3.3 (SE = 0.8) x 10^{-10}). In the case of [126] (2.9 x 10^{-10}) and [207] (1.67 ± 0.04 x 10^{-10}) they additionally analyzed diploid yeasts, which (especially in their vegetative state) are thought to be genomically more stable than other ploidys. Interestingly, the Mode-II evolved *NOX* lineages had a lower mutation rate (1.18 ± 0.13 x 10^{-9} per base and generation) than the Mode-I evolved *NOX* lineages (3.62 ± 0.73 x 10^{-9} per base and generation),

suggesting a possibly higher evolution pressure in the latter (Figure 2-5d).

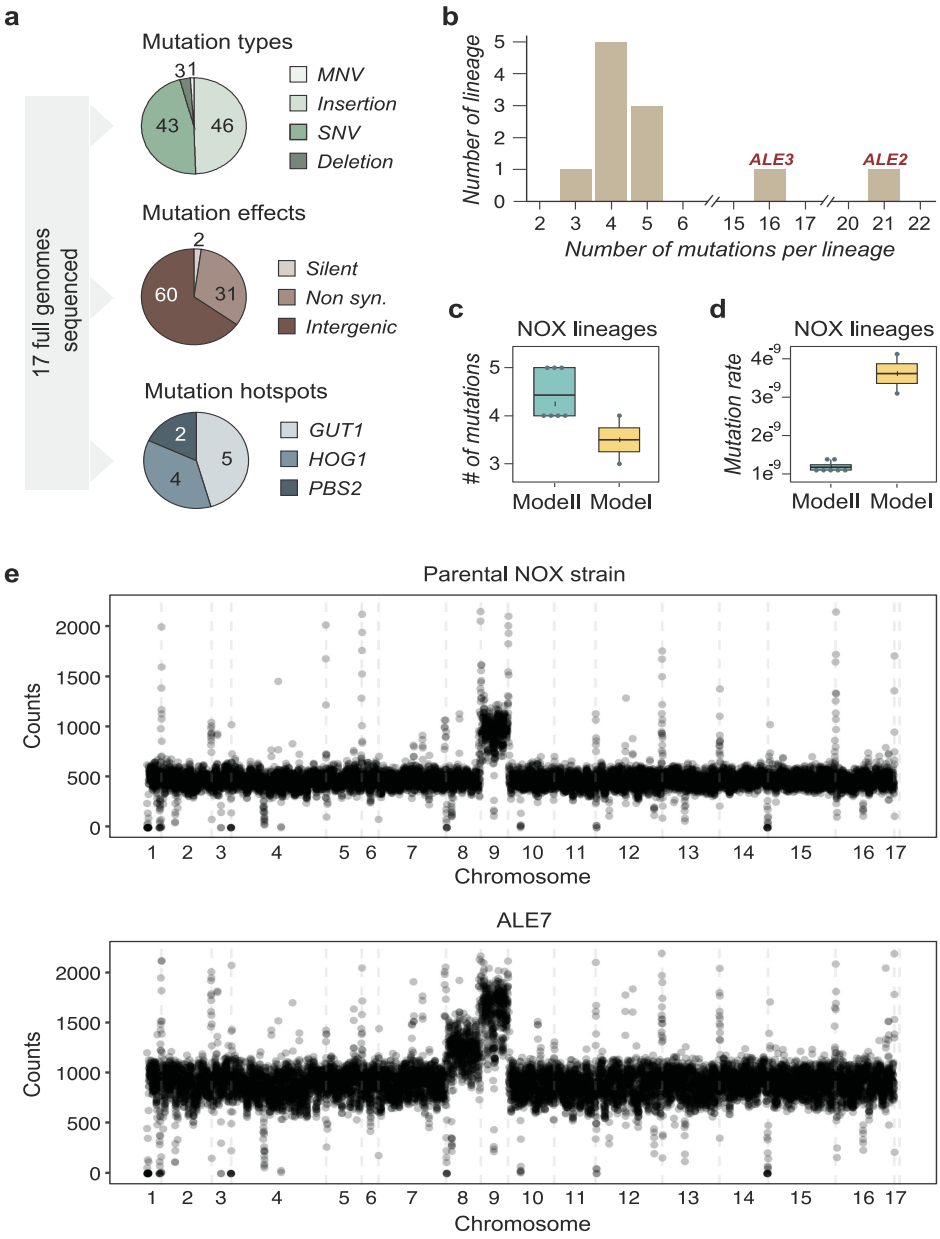

FIGURE 2.5. Genomic characterization of intermediate and final evolved lineages. (a) Mutations found by sequencing of all evolved lineages summarized by mutation types, mutation effects and mutation hotspots. HOG1: Mitogen-activated protein kinase of the HOG pathway, PBS2: MAP kinase kinase of the HOG signaling pathway. (b) Distribution of number of evolved mutations of all evolved final end point lineages growing on MG. (c, d) Comparison of (c) number of mutations and (d) evolution rates in *NOX* lineages between the two evolution modes. The mode-I lineages evolved for about 80 generation, whereas the mode-II lineages evolved for about 300 generations. (e) Sequencing reads of the *NOX* parental strain and the mode-II evolved *NOX* lineage ALE7 aligned to the *S. cerevisiae* S288C reference genome and summarized in 1 kb windows. Part (a) of this figure and the corresponding legend text have been adapted from Strucko et al. (2018) [178].

2.3.2.2 Structural variants

Among all evolved lineages, one copy number variation (CNV) evolved, namely a copy number gain of chromosome 8 in ALE7 (Figure 2-5e). The lower final growth OD of ALE7 in comparison with the other *NOX* based lineages could possibly be attributed to the evolved chromosome duplication in chromosome 8 (Figure 2-4a). Interestingly, the gene *GUT1* is located on chromosome 8 and ALE7 is one of the few lineages without a detected mutation in this gene. Mutations in this gene are also the only mutations, which were found on chromosome 8. The predicted copy number gain is one copy and only possible under the assumption that the original copy number of the chromosome was two. Since CEN.PK is a haploid strain, this observation makes it likely, that already the parental *NOX* strain is diploid for chromosome 8. Additionally, the parental *NOX* strain has a copy number gain of chromosome 9, which is predicted to be double the copy number of the rest of the genome. Thus, the WT and *NOX* lineages (considering the integrated *NOX* gene) did not entirely have the same genetic base to start from. Possibly, during the integration procedure of the *NOX* gene a genome duplication with a copy number variation had taken place in the *NOX* strain. No intermediate sized structural variants (300bp – 10kb) were found in any of the evolved lineages. Small structural variants (10bp – 300bp) are difficult to detect with short-read data. It has previously been shown that the ploidy[18] of the evolving lineages as well as the length of the laboratory evolution (max. 300 generations) make structural variants generally unlikely to occur [169] [207] [99] [126]. As a side note, the sequencing also uncovered that a mixing between the automatically evolved lineages has occurred at some point of the experiment and therefore not all mode-II evolved lineages are completely independent experiments. Analyzing the duplicated chromosome 9 in all the *NOX* lineages as well as reads aligning to the *NOX* gene, the WT lineage 5 (ALE 5) has been overtaken by one of the *NOX* lineages (Figure A.3-A.5). The same is true for a strain evolved in parallel for an independent experiment, which sequence was then added to the results (ALE 11). Considering the distribution of the identified SNPS among the evolved lineages it is furthermore highly likely that ALE6, ALE8 and ALE11 were intermixed at some point of the experiment as they show many overlapping SNVs (Figure 2-6). Also, ALE5 and ALE9 got probably mixed as well as ALE2, which has a huge overlap with ALE3. Thus finally, we have only 7 independently evolved strains growing on glycerol. Interestingly, the mode-I *NOX* lineage 1 clusters relatively closely with the ALE lineages of mode-II. Since these were evolved in physically separated experiments, either identical mutations occurred by chance or, more likely, some background mutations of the parental *NOX* strain were undetected in the variant calling process of the parental strain.

[18] haploid

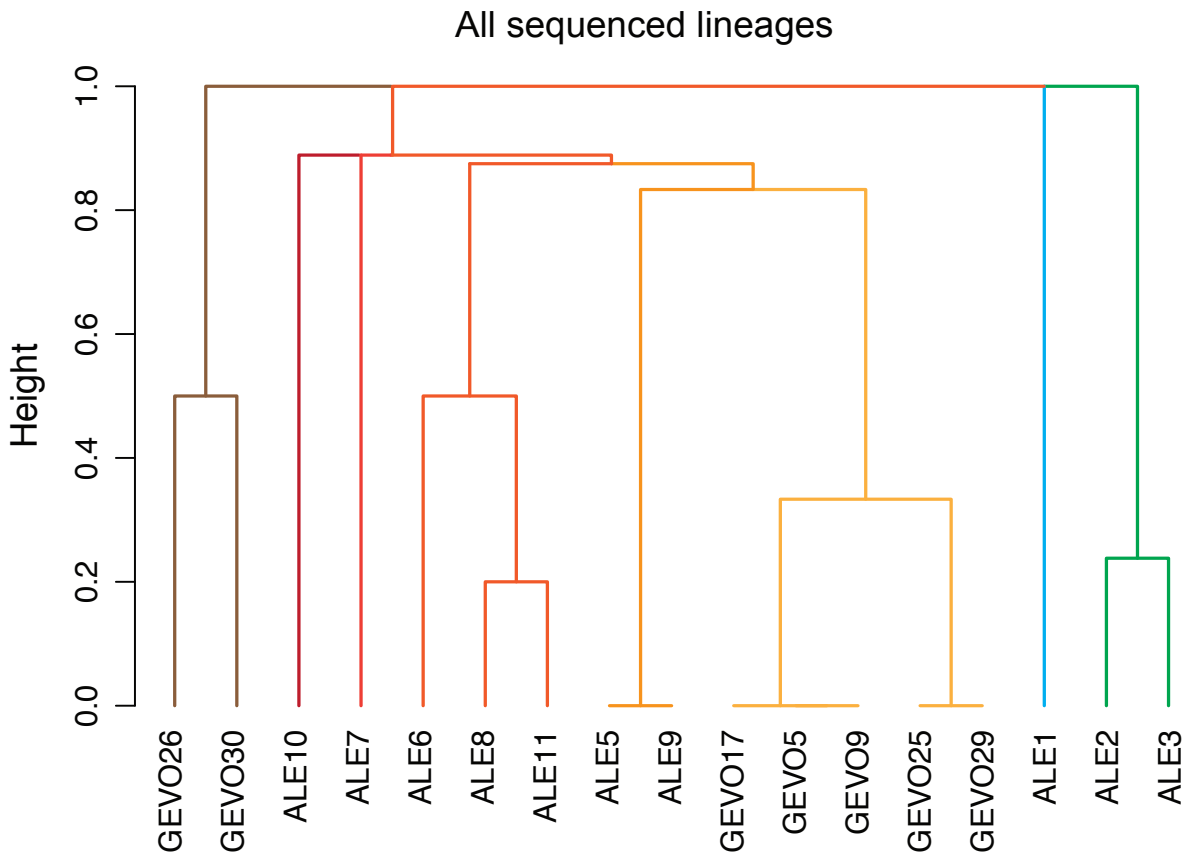

FIGURE 2.6. Hierarchical clustering of all sequenced evolved lineages based on newly evolved SNVs, MNV and deletions. Note that ALE4 didn't evolve to grow on glycerol and couldn't be recovered for sequencing.

2.3.3 Mutations in the HOG pathway and *GUT1* enable growth on glycerol while introducing an osmo-sensitive trade-off phenotype

To identify functional mutations for glycerol utilization from our evolution experiment, first, mutations in the three most frequently mutated genes were further analyzed. *GUT1* has a known function in the glycerol uptake pathway and was shown to facilitate glycerol utilization previously (Figure 2-1). However, solely introducing this mutation wasn't sufficient for growth on glycerol [181] [74]. The dominance of mutations in HOG pathway genes is striking, making it also a good candidate mutation for efficient growth on glycerol. Furthermore, the HOG pathway has been previously implicated in glycerol utilization (Kvitek and Sherlock, 2013). Although we could experimentally demonstrate the positive effect of these mutations by reintroducing them in the wild-type strain, the full phenotype of the endpoint mode-I lineages could not be entirely recapitulated (Figure 2-7a and Figure A.6). As previously observed, neither of the reintroduced *GUT1* mutations is sufficient for growth on glycerol. Nevertheless, a clear positive interaction

between *GUT1* and PBS2 or HOG1 was observed (Figure 2-7a and Figure A.6). Since the HOG pathway mutations only evolved in the *NOX* lineages, two candidate mutations in combination with a *GUT1* mutation were additionally reintroduced in the *NOX* strain. The growth phenotype achieved with the reintroduced double mutations was independent of the background strain (Figure A.7). Interestingly, the HOG pathway and *GUT1* mutations seem to evolve irrespective of the evolution mode. The differences in the growth characteristics between the mode-I and mode-II lineages could be due to additional individual sets of mutations affecting additional genes or due to the specific mutations in the genes of the HOG pathway or *GUT1*. Whether the higher final growth ODs and the faster adaptation rates of the *NOX* in comparison to the WT lineages are due to HOG pathway mutations, due to additional mutations, due to the genomic background of the *NOX* strain or due to the *NOX* gene itself remains unclear. Finally, if *NOX* lineages are more likely to evolve a HOG pathway related solution or if evolving a HOG pathway solution is more likely than other solutions in general can't be assessed since only one independent WT lineage evolved the ability to grow on glycerol.

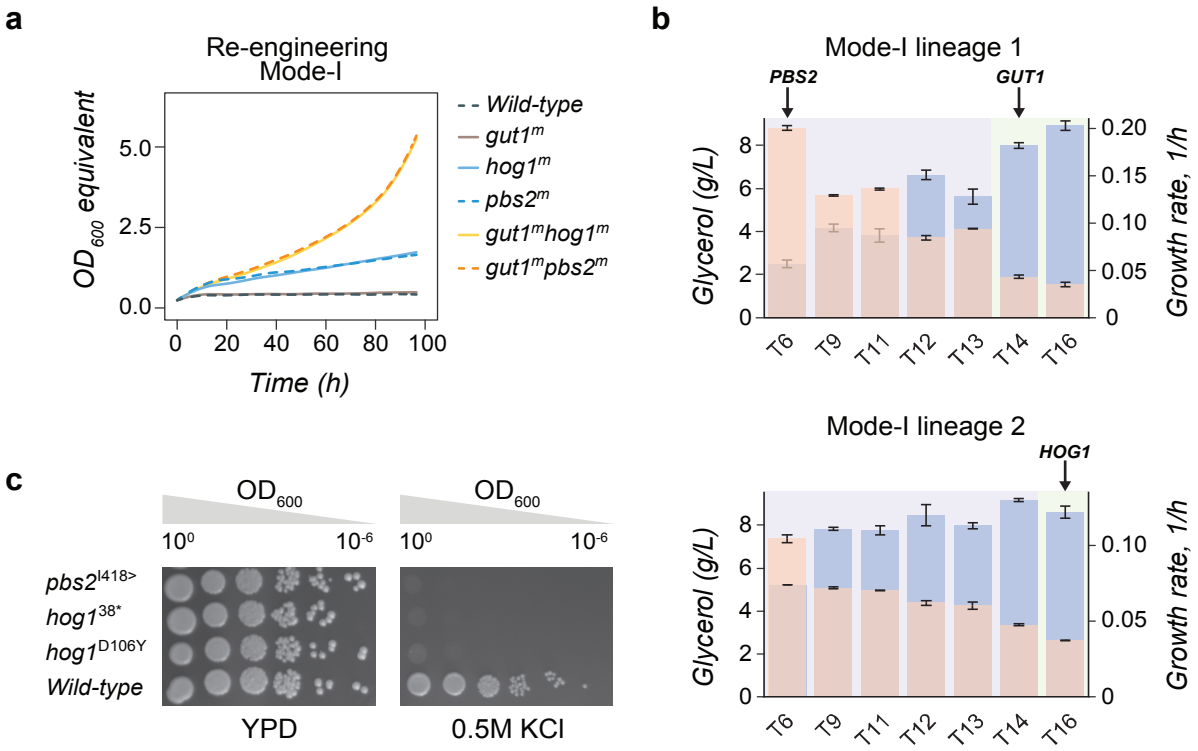

FIGURE 2.7. Investigating causal mutations of the *NOX* lineages and their phenotypic signatures. (a) Re-engineering of the glycerol phenotype achieved in the *NOX* strain-based evolution experiments. (b) Glycerol consumption and growth rates of intermediate lineages of the mode-I experiments. Time point of evolution of HOG pathway and *GUT1* mutations is indicated. (c) Spot assay experiment confirming the osmo-sensitive trade-off phenotypes of WT strains carrying single point mutations in HOG1 or PBS2 identified in the evolved *NOX* lineages. Part (a) and (c) of this figure and the corresponding legend text have been reproduced from Strucko et al. (2018) with permission [178].

(Kvitek and Sherlock, 2013) have reported that the major signaling pathways, including HOG, of *S. cerevisiae* were affected earliest during laboratory evolution. This is in partial agreement with the sequencing results of the intermediate samples of the mode-I lineage 1 experiment, where the PBS2 gene mutated as early as after five passages of the adaptation process (Figure 2-7b). In the mode-I lineage 2, the HOG1 mutation was only detected in the sample taken after 15 passages. Unfortunately, we only sequenced two samples from this lineage, so the sample size is not meaningful for any further conclusions. The *GUT1* mutation arises very late during the course of the experiment for mode-I lineage 1. Additionally, it is found in the lineage ALE6 but not in its related lineages ALE8 and ALE11, which support the observation that it evolves later during evolution. This is in line with the fact that contrary to the HOG pathway mutations, a *GUT1*

related mutation was detected in most, but not all evolved *NOX* lineages (Table A.7). Through testing the identified HOG pathway mutations for their functional impact, we individually assessed the osmo-sensitivity of several variants of HOG1 and PBS2 that were re-engineered into the wild-type CEN.PK. In all tested cases, a single nucleotide substitution in the genes led to an osmo-sensitive phenotype suggesting a loss-of-function mutation (Figure 2-7c) [161] [21]. Exclusively, the HOG pathway related mutations caused an osmo-sensitive phenotype as only those lineages displayed elevated sensitivity to osmotic stress (Figure A.8).

2.3.4 A joint approach of classical yeast genetics and inverse metabolic engineering identifies causal mutations beyond the HOG pathway

2.3.4.1 Three SNPs, in the genes *GUT1*, *KGD1* and *UBC13*, are additive causal mutations restoring the evolved growth phenotype

To further identify causal mutations underlying the evolved growth phenotype other than the HOG pathway, the endpoint lineage ALE2 evolved from the parental CEN.PK113-7D WT strain in mode-II was chosen. This lineage did not exhibit increased sensitivity towards osmotic stress and had a final growth on glycerol of μmax = 0.220 ± 0.004. Starting with 21 candidate SNPs[19] the ALE2 lineages was crossed back with a wild type strain (Figure 2-3b). Six tetrads of this backcross were characterized in MG medium and showed a pronounced growth phenotype heterogeneity segregating in a non-Mendelian manner[20] (Figure A.9). Three tetrads of the first generation were sequenced to follow the segregation pattern of the mutations and compare them against the growth phenotypes. We identified three additional mutations in these tetrads, which were not found before, probably because only a small subpopulation in the ALE2 lineage harbored them (Table A.8). Tetrad 2A and 2D appear to be very interesting cases since they have a relatively similar growth profile yet almost a perfect split between the mutations (Figure A.9 and Table A.8). The growth traits in combination with the mutation segregation pattern raised a diverse and convoluted picture, supporting the complex nature of the glycerol utilization phenotype. The crossing procedure was thus subsequently repeated two more times with spores exhibiting the growth phenotype of the ALE2 lineages (Figure 2-8a). The number of candidate causal SNPs could be ultimately reduced to one intergenic mutation and four mutations in ORFs. Two of these mutations were hitting the metabolic genes, *GUT1* encoding a glycerol kinase and *KGD1* encoding a subunit of the alpha-ket oglutarate dehydrogenase complex, while the other two were affecting genes coding for globally acting signaling/regulatory proteins, viz., *UBC13* encoding an E2 ubiquitin-conjugating enzyme and INO80 encoding a nucleosome spacing factor (Figure 2-8b and Table A.8).

[19] including 12 non-synonymous mutations in coding regions
[20] not a 2:2 segregation

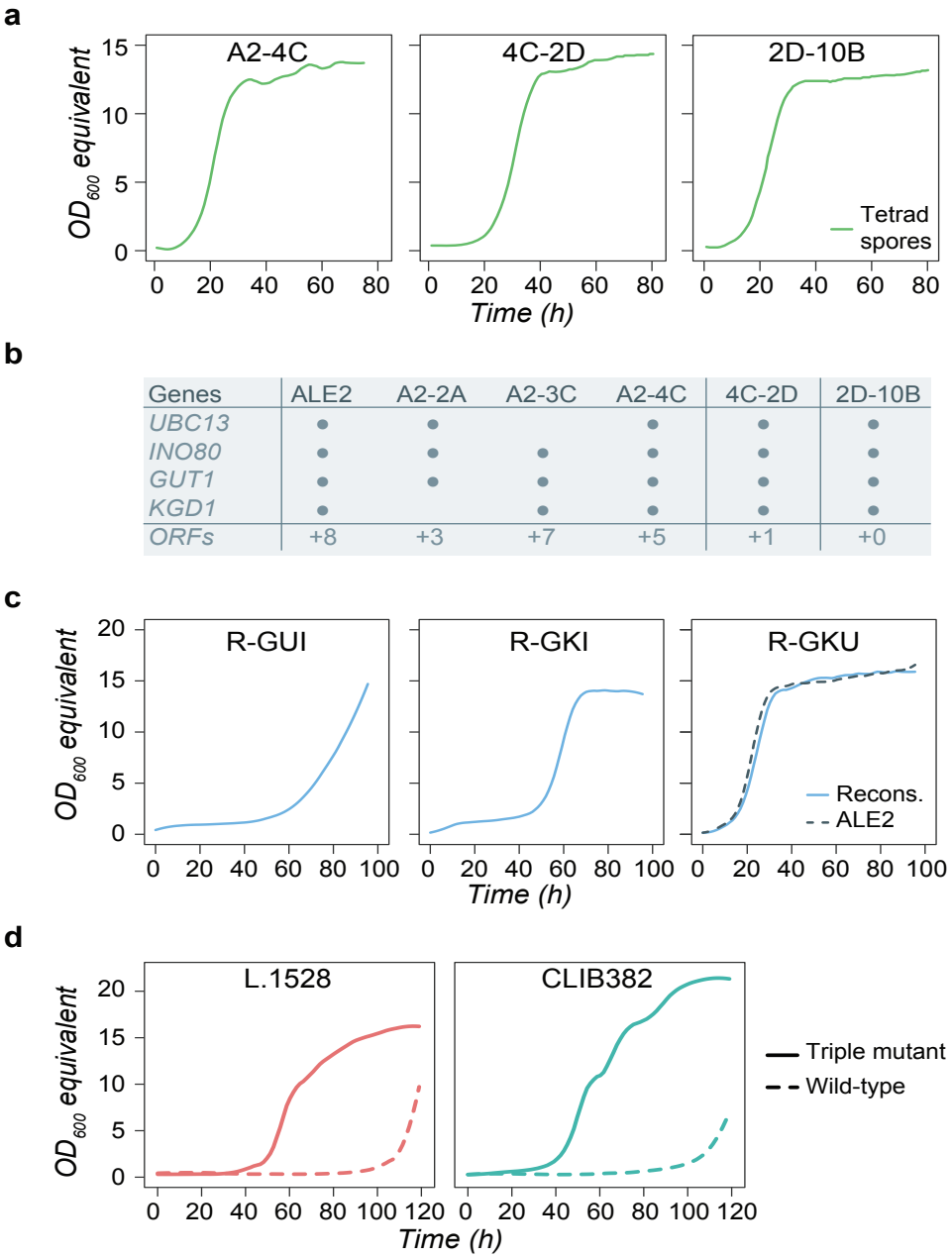

FIGURE 2.8. Investigating causal mutations in the WT lineage ALE2. (a) Growth curves observed in tetrad analysis. Strain names correspond to the names in panel b. (b) Mutation mapping during backcross experiment. (c) Growth curves observed in the reengineering of combination of narrowed down triple mutants. R-GUI (*GUT1*, *UBC13* and INO8), R-GKI (*GUT1*, *KGD1* and INO80) and R-GKU (*GUT1*, *KGD1*) and *UBC13*. (d) Growth phenotypes of the two industrially relevant *S. cerevisiae* isolates L.1528 (wine yeast from Chile) and CLIB382 (a beer yeast from Ireland) with and without reengineered triple mutations (*GUT1*, *KGD1* and *UBC13* identified in ALE2. Growth curves represent two biological replicates. This figure and the corresponding legend text have been adapted from Strucko et al. (2018) [178].

These SNPs were reengineered one by one in a WT CEN.PK113-7D strain. While engineering only one mutation at a time resulted in no growth on minimal 1% glycerol media, most of the double combinations of mutations showed a synergistic growth improvement that was yet short of the ALE2 growth performance (Figure A.10 and Figure A.11). Interestingly, a range of growth traits appeared in different double or triple mutants, hinting at a composite quality of the mutations (Figure A.10) . Notably, combining the three mutations found in the two metabolic genes *GUT1* and *KGD1* and the signaling gene *UBC13* (R-GKU strain) restored the full growth phenotype of ALE2 (Figure 2-8c and Figure A.11) . Thus, the three SNPs in the genes *GUT1* (E572Q), *KGD1* (A990D) and *UBC13* (R70fs) were identified as additive causal mutations underlying the evolved ability to grow on minimal glycerol medium. Interestingly, tetrad 4A had only one of the causal mutations of full growth phenotype (*UBC13* and still was able to grow slightly as opposed to the *UBC13* mutation alone (Figure A.10) . Possibly, this tetrads combination of mutations involving *UBC13* and resulting in an inferior glycerol phenotype might have evolved early in evolution.

2.3.4.2 Identified causal mutations are generally applicable in yeast

Finally, we tested if the three identified causal mutations are of more generic nature and thus would be causative beyond the laboratory CEN.PK strain. Introducing them in two industrial strains from different geographic locations, a wine yeast L.1528 from Chile and a beer yeast CLIB382 from Ireland, substantially improved their growth on glycerol (Figure 2-8d). This demonstrates the importance of the *GUT1*, *KGD1* and *UBC13* modulations for glycerol utilization also in industrial yeasts.

2.3.5 Functional assessment of the causal mutations using multi-omics analysis and metabolic modeling

To understand the functional relationships between the identified SNPs and their manifestation on the level of metabolism, the functional impact of each mutation was analyzed. The SNP found in the gene encoding the glycerol kinase Gut1 directly affects the glycerol metabolism. Gut1 phosphorylates glycerol to glycerol-3-phospate as the initial step of glycerol catabolism (Figure 2-1). This gene has previously been proven to be indispensable for the utilization of glycerol as its deletion completely abolishes growth [181]. Furthermore, *GUT1* was found mutated at several positions leading to amino acid changes when a yeast isolate, which was naturally able to grow on glycerol, was compared to a laboratory yeast showing no growth [181]. The *GUT1* variant found in the ALE2 lineage has a single amino acid residue change (E572Q), which is within 12 amino acids distance from the ATP binding site and exchanges a negatively charged with a neutral amino acid. Taking its essential role in the glycerol uptake pathway and the fact that its combination with either the *KGD1* or the *UBC13* mutation has a beneficial effect on the growth phenotype, it is most likely that the SNP in *GUT1* is acting as a gain-of-function mutation

increasing the efficiency of glycerol catabolism (Figure A.10) .
While the SNP in *GUT1* has an obvious connection to the glycerol metabolism the functional relationship of the SNPs in the genes encoding the proteins Kgd1 and Ubc13 was not clear from their known functions and have not previously been reported in the context of glycerol utilization. To elucidate their implications, transcriptomics and proteomics profiles of the two reconstructed double mutants R-GK (*GUT1*, *KGD1* and R-GU (*GUT1*, *UBC13* as well as the triple mutant R-GKU and the ALE2 lineage grown on minimal glycerol media in well-controlled reactors were analyzed.

2.3.5.1 Triple mutant R-GKU captures the majority of the induced transcriptional and proteomic changes of the evolved lineage ALE2

Comparing the ALE2 lineage with the R-GKU triple mutant, 271 genes were found differentially expressed (Figure 2-9a and Table A.9). However, this translated only into three proteins having different levels (Figure 2-9a and Table A.12). Two out of these, Ste3 and Bar1, are proteins involved in mating. The differences in these genes as well as most of the transcriptional changes can be explained (using GO term enrichment) by the opposite mating types of the ALE2 and the WT strain (Table A.13). Together with the observed similar growth physiology, the few differences on transcriptional or proteomic level between the R-GKU strain and the ALE2 lineage further validated that the three mutations constitute the major genetic contributors of efficient glycerol utilization.

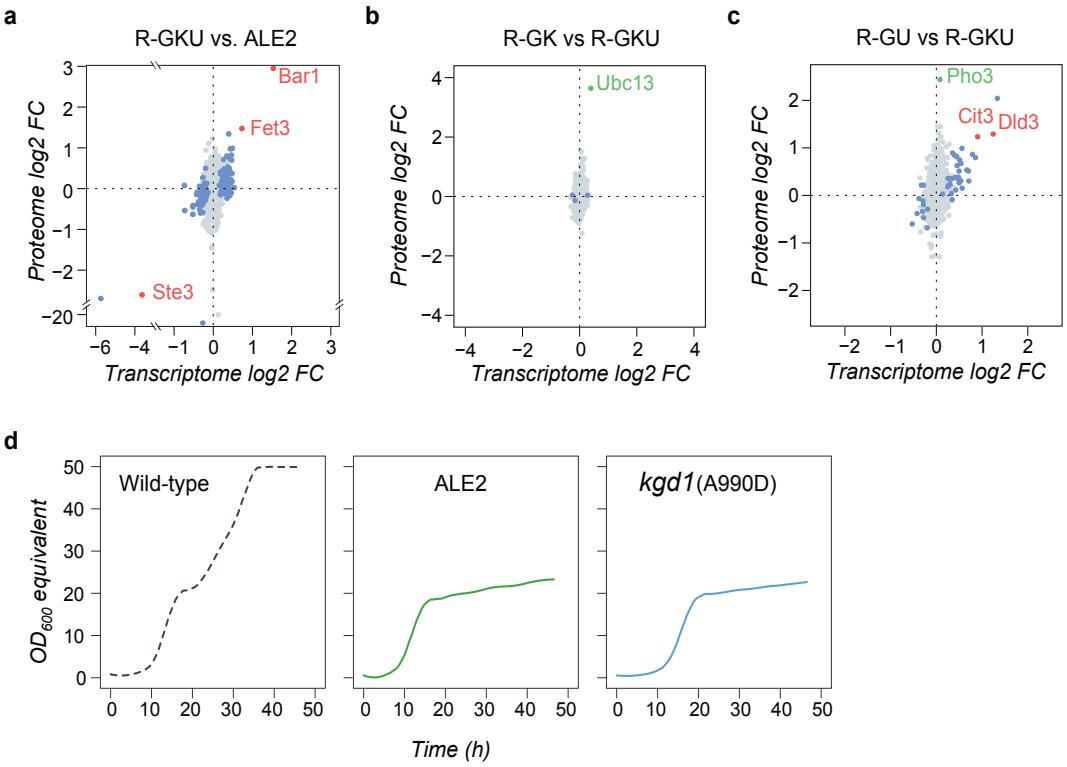

FIGURE 2.9. Functional assessment of the causal mutations for glycerol catabolism. (a, b, c) Log2 fold changes (log2FC) of expression and translation of genes from the union of transcriptomic and proteomic data of (a) R-GKU vs. ALE2 (b) R-GK vs. R-GKU and c) R-GU vs. R-GKU. Blue dots depict only significantly changed transcripts ($p_{adj} < 0.1$), green – only significantly changed levels of proteins ($p_{adj} < 0.1$), and red – significantly altered levels in both protein and transcript ($p_{adj} < 0.1$). (d) Growth curves of the ALE2 lineage and reengineered *KGD1* mutant on glucose minimal medium. The absence of the diauxic shift in the *KGD1* mutant confirms the loss-of-function mutation leading to a trade-off phenotype lacking the respiratory metabolism. This figure and the corresponding legend text have been reproduced from Strucko et al. (2018) with permission [178]. Parts (a)-(c) have been originally done and written by myself.

2.3.5.2 *UBC13* mutation acts through mechanisms other than transcriptional or proteomic level changes

UBC13 encodes an E2 ubiquitin-conjugating enzyme, which is involved in the error-free DNA post-replication repair pathway [49]. The *UBC13* variant likely results in loss-of-function as the 476ΔG mutation caused a translation frame shift with a premature stop codon after the 71st amino acid (Figure A.25). The variant thus lacks its well-described functional regions [5]. However, the binding side with its interaction partner Mms2 possibly remains intact [28]. Considering its involvement in the DNA repair pathway and its relatively broad action of synthesizing K63

ubiquitin chains a loss-of-function mutation in this gene would be expected to affect a broad group of proteins.
However, transcriptomics and proteomics comparison of the R-GK with the R-GKU strain revealed no broad effect of the *UBC13* mutation (Figure 2-9b, Table A.10 and Table A.12). Only Ubc13 protein levels itself was strongly decreased in the triple mutant, which supports the hypothesis that its translation is indeed impaired. This could also explain the considerably higher number of mutations that accumulated in the ALE2 lineage as it is known that the ΔUbc13 mutant has an increased mutation rate [24]. Possibly decreased rates of Ubc13 protein ubiquitylation might be involved in glycerol utilization and a signaling function aside from protein degradation might explain the lack of transcriptional and proteomic effects in our results. It is known for example that several nutrient permeases are targeted for endocytosis by K63 ubiquitin chains [49]. Furthermore, two recent studies showed that a truncated version of the E3 ubiquitin-protein ligase Ubr2 in conjunction with other mutations increased growth on glycerol [74] [180]. But it is important to note, that the mode of action of Ubc13 and Ubr2 are thought to be different and, thus, different mechanisms might be at play in these two cases [49]. Nevertheless, these studies, together with the beneficial role of the *UBC13* variant in the glycerol growth phenotype in our study, point to a yet undiscovered function of Ubc13 in glycerol catabolism, possibly carried out via protein ubiquitylation

2.3.5.3 *KGD1* mutation adjusts redox cofactor utilization by decoupling oxidative phosphorylation from TCA cycle

The third causal mutation is an A990D substitution in the gene *KGD1* coding for the α-ketoglutarate dehydrogenase complex of the tricarboxylic acid cycle (TCA cycle). This substitution causes a loss of the enzymatic activity as the reengineered strain with the *KGD1* mutation fully resembles the ΔKgd1 phenotype with impaired diauxic shift[21] [154] (Figure 2-9d). Comparing the R-GKU with R-GU strains, again only two out of 96 differentially expressed genes show an effect at the protein level (Figure 2-9c, Table A.11 and Table A.12). It appears that both affected enzymes are connected to the activity of the TCA cycle, namely Cit3[22] and Dld3[23]. To investigate why an inactivity of Kgd1 would increase the metabolism of glycerol and to explain the observed decreased levels of Cit3 and Dld3, we modeled growth on glycerol using a genome-scale metabolic model of *S. cerevisiae* [54]. Specifically, we used an in house developed switchPheno algorithm that identifies the minimum number of fluxes that must be re-regulated for a given change in phenotype. In this case, the wild type phenotype is corresponding to optimal growth on glucose and is changed to optimal growth on glycerol. This algorithm might be of particular value for imitating solutions found in evolutionary short-term experiments since the network structure

[21] no growth on ethanol
[22] citrate synthase, an initial TCA cycle enzyme
[23] 2-hydroxyglutarate transhydrogenase, acting on the Kgd1 substrate α-ketoglutarate

that remains constant could be assumed to evolve slowly for novel connections and the shortest pathway solutions will be naturally selected for.

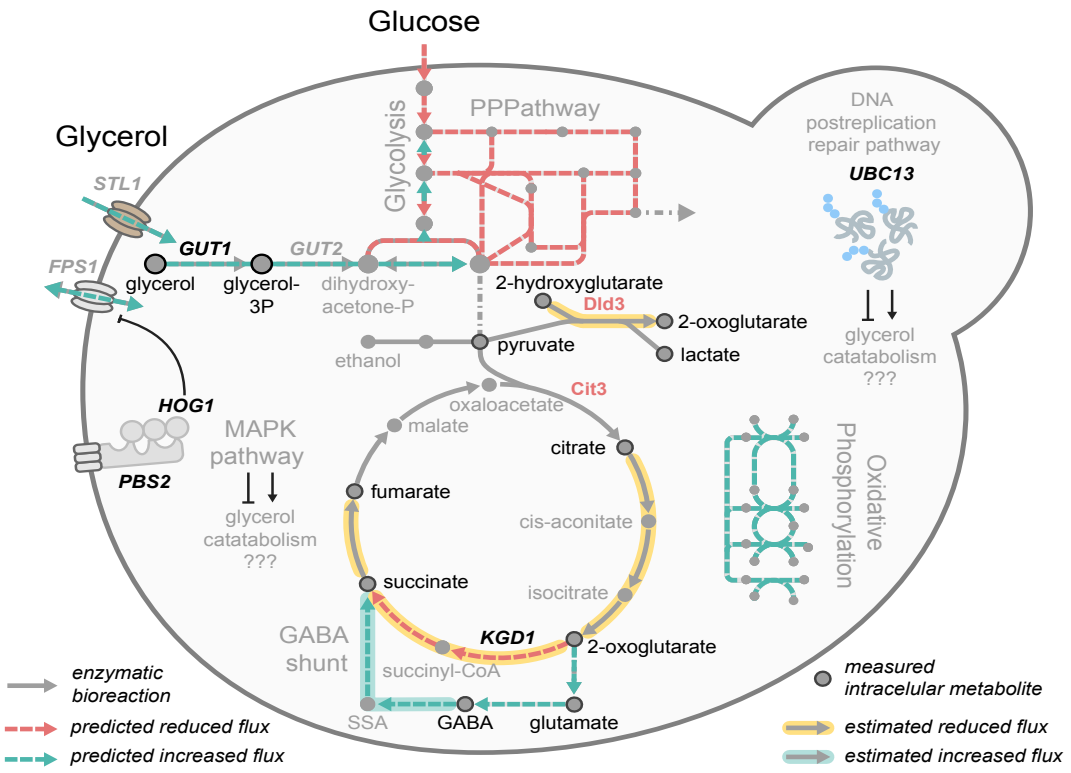

FIGURE 2.10. Pathway schema of *S. cerevisiae* 's central carbon depicting the causal mutations and their metabolic consequences. Fluxes predicted up-regulated and down-regulated when carbon source is shifted from glucose to glycerol (by the switchPheno algorithm) are represented in colored dashed arrows. Highlighted arrows depict observed flux changes estimated by comparing measured metabolite ratios in the *KGD1*ALE2 (R-GKU) vs. *KGD1*WT (R-GU) mutants grown in MG medium. GABA: Γ-aminobutyric acid, SSA: succinate semialdehyde. This figure and the corresponding legend text have been reproduced from Strucko et al. (2018) with permission [178].

The switchPheno algorithm expectedly predicted the required up-regulation of the glycerol uptake pathway with a down regulation of the upper part of glycolysis at the same time (Figure 2-10). Interestingly, optimal growth on glycerol also required a re-regulation of the TCA cycle flux after the 2-oxoglutarate branching point, namely a down-regulation of the flux going through the reaction catalyzed by Kgd1. Simultaneously the flux through the oxidative phosphorylation was up regulated, fed by an increased flux through the GABA shunt, bypassing TCA cycle (Figure 2-10). This implies a decoupling of the relative activities of the TCA cycle and the oxidative phosphorylation. The ability of the *KGD1* mutants to metabolize glycerol combined with their simultaneous impairment of the diauxic shift proves that this is indeed the case. This is due to the fact that the metabolization of glycerol needs oxidative phosphorylation, while the ethanol utilization during the diauxic shift would require the activity of the full TCA cycle. Glycerol

carbons are more reduced than glucose or ethanol carbons and yield more NADH per C-mole when metabolized. Thus, lower relative TCA cycle activity might be required to produce less NADH and oxidative phosphorylation is required to regenerate NAD+. The GABA shunt on the contrary could enhance glycerol utilization by generating NADPH[24] instead of NADH[25]. Concomitantly, the model predicts a decreased flux through the NADP+ utilizing pentose phosphate pathway (PPP). Supportively, when the GABA shunt is active[26] a pathway intermediate has been suggested to trigger the repression of DLD3 [107]. Lastly, the modeled metabolic flux alterations were supported by changes observed in the TCA cycle metabolites (Figure 2-10 and Table A.14). The identified *KGD1* loss-of-function mutation thus reveals a novel and non-intuitive link between the TCA cycle operation and glycerol metabolism.

2.4 Conclusions and future directions

This chapter demonstrates the versatility of yeast's metabolic network to adapt to changes in the nutritional environment. The ability to grow on glycerol as the sole carbon source was acquired within 80 to 300 generations, depending of the mode of adaptive evolution. Only three point mutations were necessary to rewire the metabolic network flux and change the phenotypic outcome as drastically as from no growth at all to efficient growth on glycerol. Furthermore, two different strategies [27] of the adapted yeast lineages were identified to rewire the metabolic network. Both included a mutation in a gene with broad and systemic regulatory reach, which is typically observed in adaptive evolution [32]. Interestingly, both strategies achieved the same maximum growth rate exemplifying the redundancy of the cellular metabolic network regulation. However, both adaptation strategies were accompanied by metabolic fitness trade-offs regarding other nutrient sources or environments. The lineages displayed either sensitivity towards osmotic stress as a cause of the impairment of the HOG signaling pathway or the lack of respiratory metabolism because of a lack-of-function mutation in the enzyme Kgd1. These trade-offs offer an explanation to why yeast isolates show sub-optimal or no capacity for glycerol metabolism. From an evolutionary standpoint, these would heavily compromise S. cerevisiae survival strategies, since growth in high glucose concentration environments as well as the subsequent utilization of ethanol are essential in its natural habitats [85] [206]. In a broader perspective, these results show how the metabolic capability of a species can remain latent, and how it can be uncovered through laboratory evolution.

Studying the lineage harboring the KGD1 mutation more deeply reveals that efficient growth on glycerol as sole carbon source is a complex trait requiring synergistic interactions between, in this case, three genes, including genes in metabolic pathways and regulatory processes.

[24] in succinate semialdehyde dehydrogenase reaction
[25] in α-ketoglutarate dehydrogenase reaction
[26] i.e. used for L-glutamate degradation
[27] possibly favored by different genetic backgrounds

Besides verifying the known target GUT1, our study was able to identify two novel non-intuitive mutations in the context of glycerol utilization, namely KGD1 and UBC13. This novel link exemplifies our limited understanding of metabolic network interplay and its function, regulation and requirements. Analyzing the functional implications of the KGD1 mutation in greater depth revealed redirection of fluxes in the central carbon metabolism. Namely an up-regulation of the oxidative phosphorylation combined with the concomitant down regulation of TCA cycle flux and the likely up-regulation of the GABA shunt as predicted by modeling. As glycerol has a higher reduction state than glucose, it probably requires a different wiring of NAD+ utilizing pathways and a change in the network redox flux balance in order to be metabolized. Metabolic modeling has thus proven to be a useful tool for the interpretation as well as integration of multi-omics data as it could explain the novel and non-intuitive link between the TCA cycle operation and glycerol metabolism.

CHAPTER 3

HUMAN GENOME-SCALE METABOLIC MODEL FOR FLUX BALANCE ANALYSIS

Summary

In the third part of this thesis I present the results of an improved version of a human genome-scale metabolic model (GEMM) for constrained based modeling techniques. Unlike model organisms like yeast, for which genome-scale models have been developed and optimized for various applications including constrained based modeling for more than a decade, genome-scale models for human cells are relatively new in their application. A review of the currently available genome-scale metabolic models for human revealed a lack of models with robust predictive capability of basic metabolic phenotypes, such as lactate secretion under hypoxic growth conditions. To overcome this limitation, we revised the available human genome-scale metabolic model HMR2 to make phenotype predictions matching more closely the available experimental data. The major changes encompass the introduction of a "mitochondrial intra-membrane" space (adapted from Swainston 2016) to improve the prediction of respiratory ATP synthesis, the revision of reactions from the beta-oxidation pathway and auxiliary enzymes and the introduction of an ATP maintenance cost. Furthermore, atomically unbalanced reactions were removed, the directionality of reactions was constraint where infeasible, exchange reactions were revised and new reactions were added. Lastly, the uptake and release constraints for metabolites were adapted to closely mimic the environment present in a human cell culture system. In addition, we revised the gene-reaction associations to make the model also more suitable for integrating transcriptomics and proteomics data. As a benchmark we compared the revised model's predictions with the available metabolic phenotypic data as well as data from a gene essentiality study of human cell cultures. The resulting model provides a valuable resource for constraint based metabolic modeling of human cells and tissues.

*This revised human model is an essential part of this thesis, as it will be used for omics data integration in chapter IV. In this project I worked together with Dr. Paula Jouhten (currently at VTT Technical Research Centre of Finland Ltd), with whom I shared the revision work, the phenotypic flux predictions and the major part of the benchmark procedure. I also collaborated with Sergej Andrejev from EMBL Heidelberg, who assisted me with the calculation of the model's predicted essential genes. I am first author of the manuscript (currently in preparation) and contribute to all aspects of the publication (**Katharina Zirngibl**, Paula Jouhten, Sergej Andrejev, Kiran Raosaheb Patil, Human metabolic model for flux balance analysis, Manuscript in preparation.).*

3.1 Introduction

3.1.1 Genome-scale metabolic network reconstructions

GEMMs belong to the family of COBRA approach and allow the usage of these modeling techniques at the genome scale (see General Introduction chapter for more details about COBRA) [130]. Conceptually, a GEMM comprises the sum of all known biochemical reactions of an organism of interest (reactome) assembled in a network, which is employable for computation [102]. Besides the individual reactions, their substrates, products, stoichiometric coefficients and reversibility, the biochemical network reconstructions can include additional information, such as the compartment of the reactions or the genes coding for the enzymes associated with the reactions, so called gene-protein-reaction (GPR) associations [130] [11]. Thus, a genome-scale reconstruction can also be viewed as the knowledge bases for the systemized genome-scale assembly of cellular metabolism and other disparate information about an organism of interest. In order to be usable by constraint-based simulation methods, such as FBA, a genome-scale reconstruction must be converted into a computational model. This is achieved by converting the network topology of metabolic reactions into a chemically accurate mathematical representation. More specifically a numerical matrix is created in which each reaction is represented by the stoichiometric coefficients of its participating metabolites (Figure 3-1) [102]. Furthermore, each reaction can be assigned to constraints, which are mathematically represented either in the form of reaction equations that have to be balanced, or reaction equations that are unbalanced but have upper and lower flux bounds (e.g. metabolite uptake or secretion rates of exchange reactions) [130].

The first GEMM reconstruction constituted the GEMM for *Haemophilus influenzae* [43]. Since then, a collection of GEMMs has been built, including a number of model organisms such as GEMMs for *Escherichia coli*, *Saccharomyces cerevisiae*, *Drosophila melanogaster*, *Mus musculus* and many more [132][54][134][48][175]. The reconstruction of organismal models at the genome-scale level is a laborious and time-consuming task including the assembly of thousands of reactions and the integration of varying degrees of metadata [102], which is why several attempts have been made to automate this process [39][144][2][70][7][86]. However, all these methods follow bottom-up approaches and most are only semi-automated, which often lead to the reconstruction of models not yet ready for simulation, implying additional manual curation [110]. Recently a novel method has been published, suggesting a top-down approach included in a fully automated process, which results in more robust models and thus greatly reduces the amount of manual curation work [110]. However, this new reconstruction method as well as others with full automation level are limited to simpler, prokaryotic organisms [110] [70]. Thus, the generation of models for more complex multi-cellular eukaryotic organisms still shows only a limited level of automation and needs a lot of manual revision.

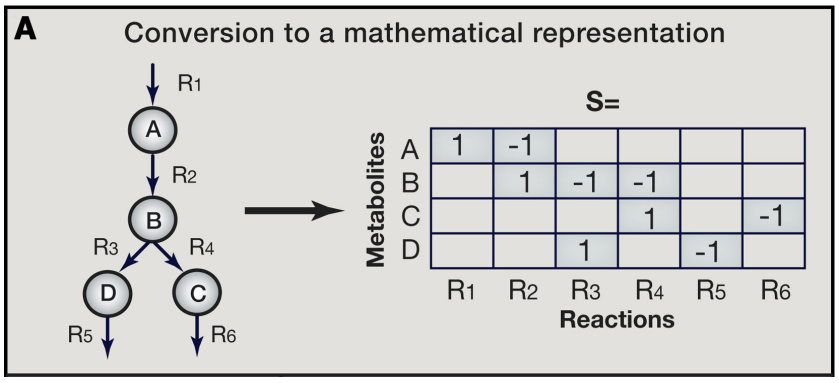

FIGURE 3.1. After the metabolic network has been assembled, it must be converted into a mathematical representation. This conversion is performed using a stoichiometric (S) matrix in which the stoichiometry of each metabolite involved in a reaction is enumerated. Reactions form the columns of this matrix and metabolites the rows. Each metabolite's entry corresponds to its stoichiometric coefficient in the corresponding reaction. Negative coefficient substrates are consumed (reactants) and positive coefficients are produced (products). Figure and figure legend have been reproduced from O'Brian (2015) with permission [130].

3.1.2 Application areas of GEMMs

GEMMs in combination with COBRA methods have now been successfully used for more than 15 years to model phenotypic states and predict a range of metabolic and associated cellular functions based on environmental and genetic parameters [20][130]. The most basic use case consists in predicting cellular growth capabilities under different media compositions. Many other types of applications have been developed, which have been summarized by Oberhardt et al. in five broad categories, namely "(1) contextualization of high-throughput data, (2) guidance of metabolic engineering, (3) directing hypothesis-driven discovery, (4) interrogation of multi-species relationships, and (5) network property discovery" [129]. Each category exhibits studies in diverse areas. The connected areas of application include successes like modeling transcription, translation and metabolism to gain an integrated picture of cell functions [173][150][47][57][108] (1), modeling metabolic effects of genetic perturbations for rational strain design or extitin silico design of media for industrial biochemical production [111][22][184][137] (2), the study of diseases with associated metabolic traits, the discovery of new human metabolic capabilities and the development of cancer drug targets or antibiotic design [188][69][20][102][52][57][91] (3), modeling of metabolic interactions, cross-feeding and nutrient competition between different species within a microbial community [208][202][147][55][162][93](4) and the uncovering of genetic interaction networks, transcriptional regulatory networks and underlying principles for optimal flux states and cellular metabolism, studying enzyme and organismal pathway evolution and assessing the theoretical metabolic capabilities [79][71][174][193][185][13][12][53][136][200][149][166] (5). Depending on the intended modeling approach, the GEMM might need tailoring or extensions

towards specific aspects. However, most of the above-mentioned modeling applications require reliable flux predictions. Thus, GEMMs whose reaction networks accurately reflect the complexity of real organisms' metabolism and whose constraints are well set, e.g. do not violate thermodynamic laws or closely mirror physiological uptake/secretion rates, are a valuable resource for metabolic modeling approaches. Furthermore, a comprehensive set of metadata like reaction-associated gene and protein products (formulated in GPRs) are instrumental for most of these applications.

3.1.3 Current human genome-scale metabolic models and their limitations

Currently available and important human GEMMs are listed in Table III-1.

TABLE 3.1. List of the major releases of human models. The table was compiled from the downloaded models. As a comparison the human genome has 20376 genes annotated in the current genome release (GRCh38.p12, updated Jan 2018) and 11896 reactions are recorded for the human metabolism. *Only literature values available. The number of indicated genes for Recon 2 probably includes transcripts. The number of listed reactions for Recon 2 includes exchange reactions.

Version	# Genes	# Metabolites	# Reactions	# Compartments	Reference	Journal	Date
Recon 1	1496	2766	3337	8	Duarte et al.	PNAS	31.01.2007
Recon 2	1789*	5063*	7440**	8*	Thiele et al.	Nat. Biotechnology	03.03.2013
Recon 2Q	1763	4962	6686	8	Quek et al.	J of Biotechnology	05.06.2014
Recon 2.2	1675	5324	7092	9	Swainston et al.	Metabolomics	07.06.2016
Recon 2M.1	1682	3368	5273	9	Ryu et al.	PNAS	24.10.2017
Recon 2M.2	1663	3368	5290	9	Ryu et al.	PNAS	24.10.2017
Recon 3D	1884	5834	9040	9	Brunk et al.	Nat. Biotechnology	19.02.2018
HMR	3668	5599	7685	8	Mardinoglu et al.	Mol. Systems Biology	19.03.2013
HMR2	3765	5546	7721	8	Mardinoglu et al.	Nat. Communication	14.01.2014

Generally, there are two families of reconstructed human GEMMs, the Recon and the HMR family, of which the Recon family was developed earlier. The first human GEMM released was Recon 1 from Duarte 2007, which represented a mile stone for human metabolic modeling and built the foundation for the following GEMMs. The model encompassed 7.3% of the currently known open reading frames (Ensembl GRCh38.p12, updated Jan 2018) [1] and 28.1% of reactions recorded for the human metabolism (11896 reactions according to Reactome statistics, 2018/09/18) [2] [41] (Table III-1). Since Recon 1, several revised and updated Recon versions have been published. The first revision constituted Recon 2, which not only doubled the number of included reactions and metabolites (including vitamin E metabolism and glycoshpingolipid metabolism), but also experimentally validated model predictions for biomarkers and extracellular metabolites for the first time [187]. It furthermore incorporated additional metadata on drug-enzyme mappings. The next bigger update of Recon 2, in the following called Recon 2Q, was published by Quek et al. and included minor revisions for inconsistencies and duplications in metabolite and reaction names, formulas, balances, charges and annotations [151]. Also reactions where free metabolites were produced were removed, the input and output reactions reduced to a minimum and the biomass

[1] https://www.ensembl.org/Homo_sapiens/Info/Annotation
[2] https://reactome.org/about/statistics

equation was adjusted. More importantly, this model aimed at revising flux predictions, however on the cost of greatly reducing the model to only 357 core reactions mostly from the central carbon metabolism. The following major release encompasses Recon 2.2 [179] which incorporates several smaller and partially independent updates of Recon 2, such as a finer description of lipids and partial removal of unbalanced reactions involving generic metabolites (Recon 2.1), improved transport reactions [159], added drug metabolic reconstruction [160] and the correction of Recon 2Q [151]. Furthermore, extensive manual curation focusing on balancing reactions, a better representation of energy generation on different carbon sources and a revision of reaction consistency was applied. These revisions increased the number of included reactions to 60.0% of the known metabolic reactions taking place in human cells and added the mitochondrial intra-membrane space as a novel compartment to the model. Since then the Recon M.1 and M.2 successions incorporated, based on Recon 2Q, minor revisions and included transcript annotations in the GPRs, which are compatible with transcript level data [158]. Finally, Recon 3D, which appeared early this year and is based on Recon 2, additionally includes three-dimensional metabolite and protein structure data. It also further expands the model by increasing the number of included reactions to 9040 (76.0% of the currently available reactions in the reactome database). Furthermore, it slightly increases the number of included genes, which are now covering 9.2% of the known open reading frames [23]. Until now the HMR series has released only two models, the original HMR model published in 2013 simultaneously with Recon2 and a revised version HMR2 published one year later. HMR was reconstructed based on Recon 1, several databases, e.g. HMDB, and experimental data measuring protein availability [115]. HMR holds, in comparison to the Recon 2 version at that time, more reactions and associated genes, and since it was mainly based on experimental data from adipocytes, a more comprehensive lipid metabolism [115]. HMR2 is an extension of HMR and even further extends the lipid metabolism as well as hepatocyte specific reactions by incorporating clinical, biochemical and genetic studies, large-scale proteomics data and previously published hepatocyte models [116]. HMR2 includes, with 3765 genes, 18.5% of known open reading frames and with 7721 reactions 64.9% of the reactions in the reactome database. Thus, it is comparable in its extent with the newest Recon 3D model.

3.1.4 Aim and approach

At the beginning of this project, no comprehensive human model was available, which reproduced experimentally observed basic phenotypes with FBA. However, as outlined above such a model is indispensable for most modeling applications and the analysis of phenotypes outside of central carbon metabolism. In order to get a human model suitable for analyses like gene-pathway enrichments, omics integration and metabolic flux predictions, reactions, constraints and gene-reaction associations of the human metabolic model HMR2 were revised. We decided to base our model on HMR2 because this model is more comprehensive than the comparable version of Recon 2 (released at the same time) as it holds the bigger collection of reactions, metabolites and genes

(e.g. more vitamin related reactions and metabolites) [187][116]. Furthermore, it exhibits an extended and revised, fatty acid metabolism [116]. The model will be utilized in a later part of this thesis for the integration of experimental omics data, which focuses on the study of an aggressive form of breast cancer with altered lipid metabolism. Thus, a more detailed lipid metabolism could be valuable for the accuracy of the predictions.

For the model revision, the exchange rates of the model were first adapted to experimentally measured values, and transport reactions added where necessary. Second, improvements of other released models were implemented in case they added to the overall accuracy of the model or the flux predictions. Third, flux relevant reactions were identified and revised and flux irrelevant reactions were excluded (e.g. blocked reactions, reactions for protein modification). An important emphasize was put on excluding atomically unbalanced reactions, since they could greatly bias the phenotypic flux predictions by violating the principle of mass conservation and possibly providing "free" metabolites. Furthermore, we introduced directionality constraints for thermodynamically unfavorable reaction fluxes where possible from the software tool "eQuilibrator" [3] and revised the fatty acid beta-oxidation pathway and auxiliary enzyme reactions [51]. Lastly, the gene-reaction associations were revised. After the revisions the model was improved and benchmarked with regard to its capability to predict essential metabolic reactions and experimental data concerning observed metabolic behaviors.

3.2 Materials and Methods

3.2.1 Original human model

The human genome-scale metabolic model HMR2 including its gene-reaction associations was used as a base model for revision [116]. This is a generic human cell model with a revised lipid metabolism. The downloaded HMR2 model (November 2015) contains 7721 reactions (excluding exchange reactions), 5546 compartmentalized metabolites, 8 compartments and 3765 genes associated with the reactions. The revised model and its metadata are available in BioOpt as well as SBML format.

3.2.2 Revisions

3.2.2.1 Exchange and transport reactions

The original HMR2 model does not possess any constraints on exchange or transport reaction fluxes other than those imposed by directionality. Uptake constraints for exchange reaction fluxes were derived from an experimental study of metabolite consumption rates of human cell lines in rich medium conducted by Jain et al. [80]. For exchange reactions whose metabolites were measured, the uptake constraints were set according to the changes in the metabolite

[3] http://equilibrator.weizmann.ac.il

consumption rates after cultivating the cells for up to five days. Therefore, the highest measured consumption rate (biggest depletion in the spent medium) across all 60 cell lines was determined for each metabolite (Table A.15). The highest metabolite consumption rate (fmol / cell / h) was then converted into metabolic uptake fluxes (mmol / (gDW h)) estimating that 10^{10} cells constitute 1 gDW (Table A.15). The determined flux was set as the maximum uptake constraint (upper bounds) of the respective metabolite's exchange reaction flux. Transport and exchange reactions were created in case they didn't yet exist for this metabolite. If none of the cell lines consumed the metabolite, the maximum uptake constraints were set to zero even if the metabolite was enriched in the media. All secretion constraints were generally left open. The implementation of uptake constraints according to cells' experimentally measured consumption rates was followed by a growth feasibility testing with minimal media analysis. This was necessary since the experimental data did not include measurements for all metabolites needed for the cell (due to analytical limitations). In short, starting with a set of experimentally observed uptake/secretion constraints, MILP simulations were run to calculate minimal set of additional metabolites required for cell growth. This procedure was run iteratively to also fine tune the uptake rates for vitamins and other components to minimal amounts needed since these components cannot be used as a carbon/nitrogen source. Additional constraints for uptake reaction fluxes were thus added accordingly to enable feasible growth (Table A.16). Finally, core metabolites were manually checked for their flux values and shadow prices under FBA with growth optimality and changed if necessary to ensure sensible flux routes for these metabolites as well as no artificial limitations on growth (Table A.16). All remaining uptake reactions were constrained to zero.

3.2.2.2 Improvements based on previously published models

The revisions and improvements of the two previously published human GEMM from the Recon family, Recon 2.2 and Recon 2M.1, were systematically checked and implemented in case they were applicable to HMR2 and added to the overall accuracy of the model or the flux predictions. Only these two models were reviewed since Recon 2.2 integrates all changes from previous models (see Introduction chapter) and Recon 2M.1, which was published later, has independent changes implemented. Recon 3D was only published after the revisions were already completed. All integrated changes are listed in Table A.17.

3.2.2.3 Thermodynamically infeasible reaction directionalities

We introduced constraints for reaction directionalities that are thermodynamically unfavorable and thus made them irreversible (Table A.18). For this revision we mainly focused on central carbon metabolism as it carries the highest fluxes and is the pathway from which the fluxes to other pathways are distributed. The software tool "eQuilibrator" [4] was used to calculate the ΔG of reactions [51]. Since the metabolite concentrations are unknown, constraints were

[4] http://equilibrator.weizmann.ac.il

only implemented for reactions with an absolute ΔG bigger than 10 to exclude reactions that reverse upon physiological changes of concentrations. Additionally, reaction directionalities were compared with current knowledge in the literature.

3.2.2.4 Exclusion of reactions with non-metabolic function

We went manually through all groups of pathways in the model and systematically identified reactions, which carried non-(core-)metabolic functions. Since they were neither necessary for growth nor conceptually relevant for flux predictions, we decided to remove these reactions instead of including their products in the biomass equation (Table A.19). The rationale being that their inclusion would skew, e.g., the gene essentiality predictions. Reaction groups that were identified were reactions that contained protein modifications (AA -> [protein]-AA + H20) or were associated with the production of protein or membrane modifications (N-glycan, heparan sulfate, O-Glycan, chondroitin sulfate or keratan sulfate) as well as reactions that were associated with protein biosynthesis, degradation or transport. To account for the energy requirements associated with processes like protein synthesis or modification we introduced maintenance costs in the form of ATP. Therefore the minimal flux of the ATP depletion reaction ATP[c] + H2O[c] => ADP[c] + Pi[c] was varied between 0 and 1 mmol / (gDW h) for simulating different growth independent ATP maintenance requirements.

3.2.2.5 Revision of the beta-oxidation pathway

We manually curated the beta-oxidation pathway and the reactions of auxiliary enzymes as there were inconstancies between the model's reaction topology and the current biochemical knowledge (Table A.20) [72] [146] [73].

3.2.2.6 Atomically unbalanced reactions

Atomically unbalanced reactions were identified with the 'check_elemental_balance' function from the *carve me* package (version 1.2) [110]. All reactions, which were identified as unbalanced and are not exchange reactions or biomass formation reactions, were further manually examined to exclude the violation of the principle of mass conversation (Table A.21).

3.2.2.7 Blocked and isolated reactions

Blocked reactions were identified with the framed python package (version 0.5) for metabolic modeling [110]. First, a complete medium was created for the model by allowing all exchange reactions to carry flux. Blocked reactions were subsequently determined with the 'blocked_reactions' function uTtilizing FVA [113]. Isolated reactions and reaction loops were identified through missing network connectivity with Cytoscape (version 3.5.1) [171]. All blocked and isolated reactions if not already excluded earlier (2.2.4), were removed from the model (Table A.22).

3.2.2.8 GPR associations

The GPR associations of all reactions of the fatty acid beta-oxidation and its auxiliary enzymes as well as of the major growth influencing reactions of the central carbon metabolism and amino acid and vitamin synthesis were manually revised according to databases [5] and literature review (Table A.23) [153] (The UniProt Consortium 2017) [72] [146] [73].

3.2.2.9 Gene essentiality comparison with experimental data

Gene essentiality predictions were compared to experimentally validated data on gene essentiality of human cell lines [192]. For this comparison, a gene was considered experimentally essential if at least three out of the four tested cell lines exhibited an essentiality for this gene in the CRISPR-based screen. The definition of essentiality was taken from the experimental work, namely a growth reduction of more than 10% with an FDR cutoff for the adjusted p-value of less than 0.1 (0.05 in the study). For the simulation of gene essentiality extitin silico the impact of single gene deletions on growth was iteratively evaluated by performing FBA on mutants, in which the respective reactions are blocked according to the GPR associations. The simulations were performed with FBA and maximizing for growth was set as an objective function. A modeled phenotype was defined as non-viable if the predicted growth rate was less than 50% of the maximum growth rate. The media composition of the experimental study was similar to the media composition in Jain et al., which was used to constrain the uptakes of our model. Additional uptakes were implemented in the model in case a metabolite, which affected the predicted viability, was present in the media of the experimental screen and hasn't been measured by Jain et al. (Table A.24). The maximum uptake was set above the metabolite's growth limitation in case its synthesis was impaired. Before its inclusion it was ensured that the metabolite's uptake by human cells has been shown in literature. One major challenge constitutes the chemically undefined component fetal calf serum. Metabolites for which it was unclear, whether they are present in the experimental media or not, were included if classified as a blood component in the human metabolome database (HMDB) [197]. The performance metrics used to evaluate the gene essentiality predictions of the model were defined as follows:

Sensititvity = TP_c/(TP_c + FN_c)
Specificity = TN_c/(TN_c + FP_c)
Precision = TP_c/(TP_c + FP_c)
Accuracy = (TP_c + TN_c)/(TP_c + FP_c + TN_c + FN_c)
F1_score = 2*TP_c/(2*TP_c + FN_c + FP_c)

For the comparison, a subset of genes present in the model and in the experimental data was built.

[5] www.genecards.org and https://www.uniprot.org

3.2.3 Phenotypic flux predictions

After implementing the above-mentioned model curations, phenotypic flux predictions were obtained with flux variability analysis (FVA) of glucose and glutamine uptakes as well as lactate secretions optimizing for growth under a range of different oxygen uptake bounds [113]. Since the effect of oxygen uptake on metabolic fluxes and growth is the greatest in low oxygen conditions, these were sampled more closely. All the simulations were performed with Matlab R2015a v. 8.5.0 using IBM ILOG CPLEX (v. 12.6.1) functions 'cplexlp'.

3.2.4 Technical details

The import/export of SBML files was obtained through the libSBML API using the load_cbmodel of the *framed* python package (version 0.5) for metabolic modeling [18] [110]. BioOpt files were imported through the 'read_cbmodel_from_file' function of *framed*. SBML format was converted into BioOpt format by our internal parser. The IBM ILOG CPLEX Optimizer (version 12.8.0) was used for solving the MILP problems unless noted differently. All simulations were conducted with Python 2.7.13. The biostatistical analysis was conducted using R V.3.3.1 (R Core Team 2018).

3.3 Results and Discussion

3.3.1 Model features

In summary, we added 292 reaction constraints and 70 reactions, changed 198 reactions and 420 GPRs and removed 1569 reactions. Thus the new model was reduced to 6222 active reactions (excluding exchange reactions), 3487 unique genes and 4770 compartmentalized metabolites (without boundary metabolites) distributed amongst 9 compartments. Although smaller than the original HMR2 model it still retains the rich complexity of a genome-scale model.

3.3.2 Newly revised model is condensed focusing on flux relevant changes

In order to build a model consistently usable for flux predictions, HMR2 was first reduced to contain strictly metabolic reactions. A total of 744 reactions were removed from the model since they carried biological functions instead of metabolic functions and were neither necessary for growth nor conceptually relevant for flux predictions (Table A.19). The majority of these reactions were involved in the synthesis of protein or membrane modifications, namely the synthesis of glycans and heparan, chondroitin or keratan sulfates. Alternatively, the produced metabolites could be included in the biomass formulation to account for the impact of the cell's requirements of signaling molecules on metabolism. In this case it would be necessary to ensure that the flux specification implemented for these reactions reflect a metabolic requirement common to all cells. Possibly general maintenance costs for protein and membrane modification, carefully estimated from experimental data, could be included. Attempts have been made to include

regulatory interactions into GEMMs [29] and model the influence of the signaling alterations on metabolism. However, this approach has so far been applied only to organisms with small genomes, such as bacteria. The remaining 117 reactions, which were excluded are reactions associated with the biosynthesis, degradation or transport of specific proteins, such as proteins involved in various biological functions, such as lipid transport (e.g. VLDL), blood coagulation (e.g. fibrinogen), protease inhibitors (e.g. antitrypsin) or globular proteins (e.g. albumin). To account for the energy requirements associated with the general synthesis of proteins or protein modifications we introduced ATP maintenance costs. The amino acid requirements for protein synthesis are already adequately considered in the model and implemented in the biomass equation [116]. The atom balance of all remaining reactions was evaluated next in order to exclude a possible bias on phenotypic flux prediction introduced by free mass generation. The majority of the reactions identified as atomically unbalanced are exchange reactions between the extracellular compartment and the boundary or are involved in biomass formation. Only one of the inspected unbalanced reactions concerning lipid metabolism generated free mass and was therefore corrected (Table A.21). Furthermore, all reactions should be able to carry fluxes when all possible exchange reactions are active. 798 blocked and 9 isolated reactions were excluded from the model (Table A.22). Many of the blocked reactions are involved in the transport between different compartments of the model. Instead of removing these reactions, the availability of these metabolites in the respective compartments as well as their biological function could be carefully evaluated in databases. Additionally, blocked reactions are associated with the synthesis or degradation of membrane lipids, vitamins, hormones and neurotransmitters or involved in biological processes like translation or the biosynthesis of amino acids from rare intermediates. Manual curation and careful consideration would be needed in order to connect these reactions to the rest of the metabolic network and include them in a flux-revised model. Interestingly, a few of the reactions, which were changed according to revisions of reactions in Recon 2.2 are blocked as well [179]. Additional major improvements were the implementation of 80 reaction (i.e. flux) constraints and the restriction of 158 reactions for thermodynamically feasible directions in a biological context (Table A.18). Furthermore, the stoichiometry of 56 reactions was updated, 55 reactions were added and 17 reactions were removed during the revision of the beta-oxidation pathway (Table A.20). We ensured that flux could run through the beta-oxidation pathway after its curation. One of the most flux relevant improvements included in this model, which is taken from previous models, is the implementation of a mitochondrial intra-membrane space [179] (Table A.17). The creation of an additional mitochondrial compartment improves the prediction on respiratory ATP synthesis (see chapter III-3.7). Other improvements incorporated from previous models cover the addition of cofactor reactions and the revision of reactions from the lipid metabolism (Table A.17). TPR reaction-associations of Recon 2M.1 are not adopted in this model since the transcript specific reaction and localization associations are based on predictions from EFICAz2.5 and Wolf PSort only [158]. The manually curated

improvements for reactions identified by this approach are implemented in the revised model (Table A.17). I additionally analyzed the potential of transcript specific reaction and localization associations based on their predictions. I identified 14 cases from the 453 reported transcripts for which different transcripts, which are associated with the same gene are predicted to be found in different compartments (12) or to carry out different reactions (2). Thus, as long as not more comprehensive information is available, the impact of integrating these specific cases on the whole model's prediction is negligible.

3.3.3 Constraining nutrient uptake rates in complex media

Experimentally determined uptake constraints for 101 metabolites were added to the model [80] (Table A.15). Aside from constraints for uptake reactions of glucose and amino acids a wide range of additional metabolites is covered, including nucleotides, amino acid derivatives, glycolysis intermediates, TCA and urea cycle intermediates and vitamins. To ensure the model's growth feasibility, uptakes for a computationally identified minimal set of 23 additional media components were added to the model (Table A.16). The majority of these components encompassed non-measured inorganic chemicals such as water, calcium, potassium or iron or vitamins. Additionally, the uptake bounds of three amino acids and the vitamin derivative pantothenate were edited after manual inspection of flux distributions. Already Recon2Q implemented experimentally measured values for 26 metabolites (mostly amino acids) into their reduced steady-state flux model [151]. However, this media composition presents the first attempt to define uptake flux constraints from a complex media composition in a generic human GEMM.

3.3.4 Tailoring the GPR associations to improve the predictability of flux distributions of GEMMs personalized with omics data

In total the GPR associations of 420 reactions were changed (Table A.23). The revisions encompass different metabolic pathways, the most important being glycolysis, TCA cycle, amino acid synthesis, oxidative phosphorylation, Acyl-CoA hydrolysis, beta-oxidation and vitamin metabolism. For the revision, we implemented the improved gene-reaction associations from the human Recon2.2 model [179], which were in addition manually curated by us. These revisions are crucial for various applications, such as the modeling of drug target efficacy with gene knockouts or the prediction of gene essentiality (see 3.6). The improvement of these GPR associations is specifically valuable for flux predictions in the context of omics data integration. A successful use case will be presented in chapter IV.

3.3.5 Essentiality predictions of the model match experimentally validated human essential genes

To evaluate the predictive capability of the revised HMR2 model including its GPR associations, the predictions of the model on gene essentiality were compared with a set of experimentally determined essential metabolic genes [192] (Figure 3-2a). Since the experimental essentials were determined in a complex media the results of the first comparison were used to review the uptake constraints of our curated model. After manually revising the literature, uptakes for twelve additional metabolites were added and the uptakes of two metabolites were changed (Table A.24).

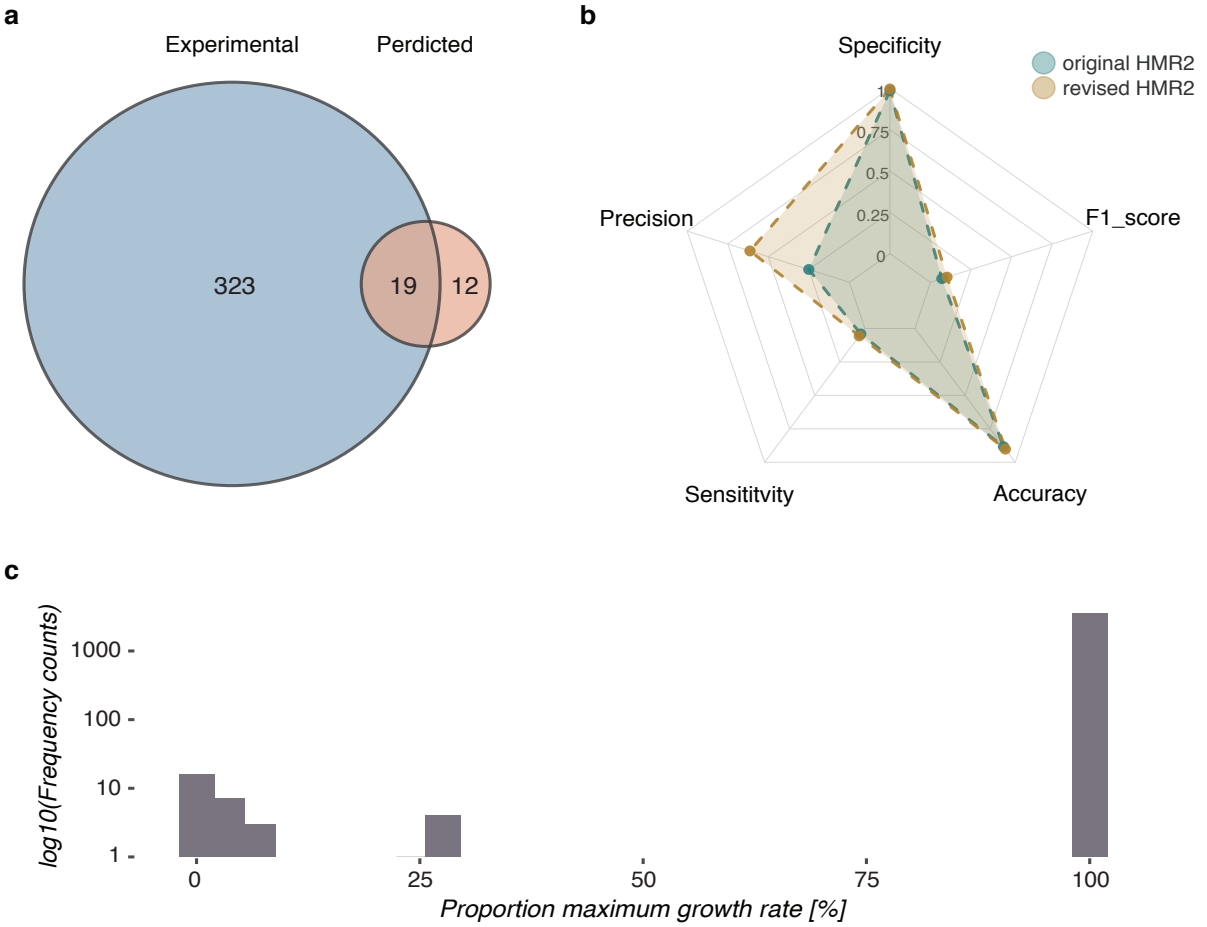

FIGURE 3.2. Comparative assessment of gene essentiality. (a) Intersection of the sets of experimentally determined and model wise predicted essential genes. (b) Quantitative comparison of gene essentiality predictions between the original and revised HMR2 model. (c) Predicted proportion of the model wild type's maximum growth rate after single gene knockouts.

The set of experimentally essential genes is one order of magnitude bigger than the set of the model wise predicted essential genes (342 genes vs. 31 genes, sensitivity = 5.6%, Figure 3-2b). The low sensitivity might be partially owned to the way essentiality is defined in the experimental assay. All genes, which induce a growth reduction of more than 10% compared to the wild type, are considered essential. Increasing this threshold to 25% or 50% does not improve the intersection of the predictions with the experimental gene set. Possibly, the establishment of the assay does not allow the assessment of essentiality beyond the growth reduction threshold of 10%. However, the experimental gene set might still include genes, which are not strictly essential in the definition of non-viable, but might impede growth. The predictions of growth rates as a consequence of gene loss obtained by simulations with a current metabolic model on the contrary are of rather binary behavior and cannot capture continuous changes of viability (Figure 3-2c). Having those two contrary assessment approaches might partially explain the low sensitivity. One additional reason might be the inherently problematic annotation of isoenzymes in a generic human model. Most of the reactions in the model have at least two isoenzymes annotated according to the GPRs (78.7% in the revised model), however in reality only one of these isoenzymes might be actively transcribed in the respective cell type or culturing conditions. For these reasons, the more precise assessment of the predictive capability of gene essentiality of a metabolic model is precision, where only the correctly and incorrectly called essential genes from the model are compared. The precision increased after the model revision from 25.0% to 61.3% in comparison to the original HMR2 model (Figure 3-2b). The wrongly predicted essential genes are mostly connected to nucleotide metabolism and cofactor metabolism and could be further improved. The specificity and accuracy of the revised model's predictions are 99.6% and 90.1%. However, these two measurements are typically inflated in metabolic models due to a large number of true negatives [158].

3.3.6 Model predicts general phenotypes compatible with experimental growth data

To benchmark the performance of the curated HMR2 model we conducted FVA [113] under a range of upper oxygen uptake bounds and compared the results to the simulation predictions obtained from the original HMR2. The flux predictions for reactions consuming or producing major carbon and nitrogen sources in dependence to oxygen availability are depicted in Figure 3-3.

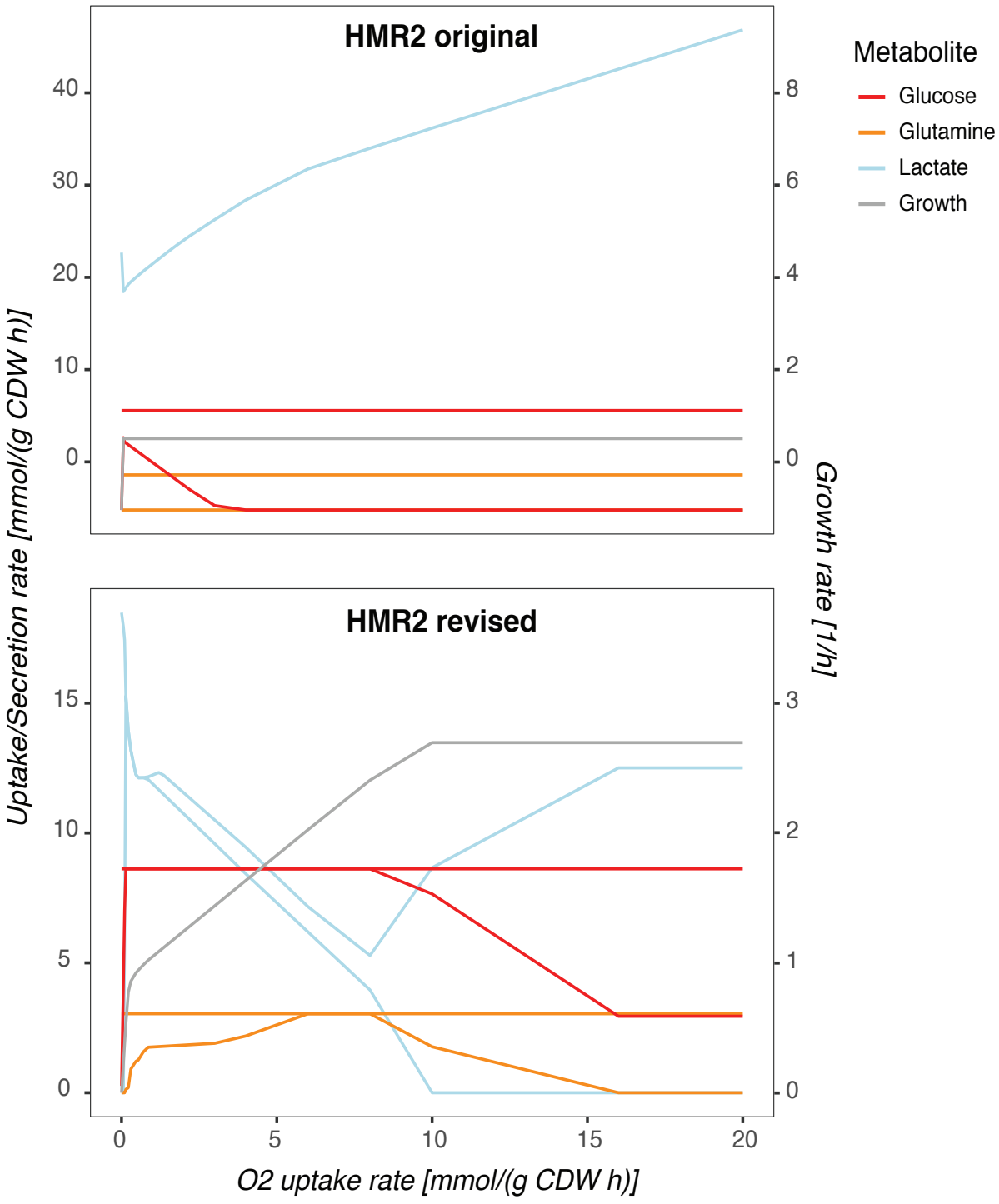

FIGURE 3.3. Phenotypic benchmark of the revised model. Flux variability analysis of the original and curated HMR2 model for growth optimality under a range of upper oxygen uptake bounds. The upper and lower bound of fluxes through reactions consuming the metabolites glucose (D-Glc) and glutamine (L-Gln) and producing the metabolite lactate (L-Lac) are depicted.

The growth limitation under low oxygen availability is more accurately predicted by the revised HMR2 model than by the original model. Furthermore, the revised model also predicts, in contrast to the original model, the simultaneously required lactate secretion. Interestingly, lactate secretion is also possible under high oxygen concentrations, which has been observed in cancer cells [84]. The improved prediction of anaerobic glycolysis is coupled with the more flexible predictions for the uptake reactions of the major carbon and nitrogen sources glucose and glutamine. Under low oxygen conditions, all available glucose has to be uptaken to fulfill the energy demands of the cell. Additionally glutamine is required to be up taken for maximum growth and used to fuel the TCA cycle and the remaining capacity of oxidative phosphorylation [141]. Under high oxygen conditions there is more freedom to distribute the two metabolites and alternatively use them for glycolysis, oxidative phosphorylation and amino acid precursors. The improved prediction behavior of lactate, glucose and glutamine will be particularly important in the context of cancer cell related flux predictions.

3.4 Conclusions and perspectives

In this chapter, the development of a revised human GEMM with improved flux prediction behavior was presented. Major changes involve the implementation of experimental uptake constraints from a complex media composition, the revision of reaction directionalities and gene-reaction associations and the correction of the complete beta-oxidation pathway and auxiliary enzyme reactions. These revisions improved the predictability of human gene essentiality and a more realistic flux behavior of major metabolic pathways like glycolysis and oxidative phosphorylation. Comparing the simulation results with experimental data, the implemented improvements have been shown to be particularly relevant for simulations in cancer related contexts. Further areas of improvements for even more precise flux predictions could be more peripheral pathways, like fatty acid biosynthesis, which up to now are still poorly determined in their flux distributions. These pathways as well as the major metabolic pathways could be improved by incorporating additional flux constraints estimated from acquired metabolite concentrations and ^{13}C labeling data. Furthermore, constraints for secretion reaction fluxes could be set. Additionally, the sensitivity of the model could be improved by systematically incorporating information about reaction and localization depended enzyme isoforms or cell type specific uptake and secretion constraints. The complexity of the model could be improved by systematically reviewing the blocked reactions and if flux relevant reincorporating them into the model instead of only removing them. The GPRs for nucleotides could be further improved, possibly also by incorporating the changes made in the new model Recon 3D. Last, the majority of genes being associated to reactions with non-metabolic functions still remain in the GPR associations even after excluding these reactions. This might hint at the fact that some reactions with a biological instead of metabolic focus remain in the model, which should also be excluded.

CHAPTER 4

METABOLIC REWIRING UNDERLYING MINIMAL RESIDUAL DISEASE IN BREAST CANCER

Summary

This chapter studies how mammalian cells adapt their metabolic networks in response to oncogenic signals and focuses on the robustness of the metabolic network regulation. Particularly, this study investigates the metabolic adaptations accompanying the transition of a differentiated cell to a cancer cell in order to fulfill the demands of a proliferative phenotype as well the metabolic features of the cancer cell after full regression. The reversibility of regulation between different layers of the cell's physiology is studied to explain how metabolic networks are stably rewired even after oncogenic signaling is stopped. For this, we take advantage of a 3D in vitro system of mammary gland organoids to map transcriptome and metabolome of tumorigenic as well as regressed breast cancer cells and integrate these using statistical as well as a metabolic model based approach. The results reveal, for the first time, an oncogenic memory on transcriptional and metabolic level in residual cancer cells. The residual cells showed a stably active glycolysis and urea cycle closer to the tumor state than the healthy tissue as its core features. We validate these findings with in vivo measurements and confirm the increased glycolysis in the regressed cells by in vivo stable isotope carbon tracer measurements. Finally, we investigate the relevance of our findings in patient data by integrating publicly available transcriptome data and comparing them to our results.

*The mouse work, in vivo and in vitro experiments, sample preparation as well as the molecular and histological characterization were carried out by Ksenija Radic from the Jechlinger Group at EMBL Heidelberg. Eleni Kafkia from the Patil group at EMBL Heidelberg collected and analyzed the targeted metabolomics data. Christian Lüchtenborg from the group of Britta Brügger (University of Heidelberg) conducted and analyzed the lipidomics experiments. The untargeted metabolomics data were collected and analyzed by the group of Daniel Sevin at Cellzome, GSK Heidelberg. The sequencing was conducted at the Genecore Facility, EMBL Heidelberg. I performed the bioinformatics analysis including the transcriptome data analysis and integration of the sequencing as well as the omics data. Furthermore, I performed the reporter metabolite analysis, the genome scale flux modeling (with the help of Daniel Machado from the EMBL Heidelberg, who also developed the utilized algorithm for transcriptome data integration) and the comparative analysis of the publically available patient data. I am co-first author of the manuscript (currently in preparation), which I am co-writing (Ksenija Radic, Eleni Kafkia, **Katharina Zirngibl**,Ashna Alladin, Federico Villa, Daniel Machado, Christian Luchtenborg, Daniel Sevin, Britta Brugger, Kiran Raosaheb Patil and Martin Jechlinger, In depth multi-omics analysis reveals an oncogenic memory in a surviving cell population following breast cancer treatment, Manuscript in preparation).*

4.1 Introduction

4.1.1 Breast cancer prevalence

Breast cancer is the most common cancer among females with an estimated incidence of approximately 2 million newly diagnosed cases worldwide in 2018 [83]. It is a heterogeneous disease with the histological and molecular make-up of the tumor providing a predictive measure for patient prognosis. Four groups of sporadic breast cancers can be defined by a immunohistochemical (IHC) determination of hormone receptor status (estrogen and progesteron receptor), human epidermal growth factor receptor 2 (HER2) status as well as the proliferation marker Ki-67: Luminal A (hormone receptor positive, HER2 negative, low levels of Ki-67); Luminal B (hormone receptor positive, HER2 negative or positive, high levels of Ki-67); Triple-negative/basal-like (hormone (estrogen and progesterone) receptor negative, HER2 negative); HER2 overexpression (hormone-receptor negative, HER2 positive). In addition, a fifth group is defined, normal-like breast cancers, having a similar IHC pattern as Luminal A cancers but showing a worse prognosis [34].

While Luminal A breast cancers are the group with best prognosis the triple-negative and HER2-overexpressing groups present the groups with the poorest prognosis, which is associated with a high rate of recurrence. Clinical outcome for the group of HER2-overexpressing tumors has improved with the implementation of targeted therapies using anti-HER2 monoclonal antibodies (trastuzumab). However, 40-60% of HER2-overexpressing tumors develop therapy resistance resulting again in poor patient prognosis [34] [46]. Other molecular features may contribute to the poor outcome of HER2-overexpressing breast cancers including, for example concomitant overexpression of the transcription factor c-MYC, which is potentially associated with trastuzumab resistance [199] [63]. The exact molecular mechanisms that determine clinical outcome and associated recurrence rates, however, still need to be determined.

4.1.2 Minimal residual disease

Patient prognosis for breast cancer may, as described above, be related to the molecular type of the tumor as well as associated recurrence rates. According to the statistics obtained in the US Surveillance program Epidemiology and End Results Program (SEER) in 2012 36.8% of women successfully treated for breast cancer experienced a recurrence within 10 years after first diagnosis. The majority of these recurrences (81.9%) were reported within the first 5 years after diagnosis. After controlling for tumor stage at diagnosis it was reported that the risk of recurrence was significantly increased in hormone receptor negative tumors (other molecular tumor characteristics were not investigated) [31]. One hypothesis for recurrence after seemingly successful therapy refers to minimal residual disease (MRD), a set of resistant cells surviving cancer therapy. These cells may have disseminated from the cancer tissue before therapy and then self-seeded back into the respective tissue after they survived chemotherapy. Another

possibility is that therapy-resistant cells residing in the primary cancer-affected tissue re-initiate carcinogenesis up to several years after treatment. Both cell types are thought to have more potential to form metastasis leading to a poorer prognosis with the recurrent cancer [182]. The therapy-resistant cells remain dormant and clinically unapparent until cancer re-initiation and exact mechanisms for tumor recurrence from these cells are currently unknown. An altered energy metabolism in these cells as compared to healthy tissue has been proposed to play a role in recurrence out of MRD [69].

4.1.3 Metabolic alterations in cancer

Cancer cells have higher metabolic demands compared to their healthy counterparts in order to provide the basis for increased proliferation. More specifically, increased nutrient influx needs to be sustained and nutrient use in metabolic pathways needs to be adjusted for in order to meet the requirements for energy and cellular building-blocks supply for the growing and proliferating cancer cell [141]. A well-known example of this key feature of cancer cells is the increased uptake of glucose that was recognized already in the 1920's by Otto Warburg (Warburg-effect). Paradoxically, cancer cells switch their energy metabolism preferentially to glycolysis with concomitant secretion of lactate, even under aerobic conditions, although this process provides less ATP than compared to oxidative phosphorylation and thus less energy for the cell. It was shown that the increased amount of glucose taken up by the cell as well as the higher rate of glycolysis performed may provide in sum sufficient ATP for the energy needs of the cancer cell. Additionally, through the increased glycolysis the cell sustains the production of molecules ultimately required for cell growth and proliferation, e.g. amino acids and purines and pyrimidines [167][105]. Glutamine is another substrate in addition to glucose that is taken up by cancer cells in increased amounts. In contrast to glucose as a source for carbons, glutamine also delivers nnitrogen required for nucleotide and amino acid biosynthesis. Products of the altered metabolic pathways may also have signaling functions, which exhibit consequences for the carcinogenic potential of the cell. For example, increased production and secretion of lactate as a product of enhanced glycolysis stimulates angiogenesis [141].

4.1.4 Combining multi-omics with metabolic modeling to elucidate molecular alterations in residual breast cancer cells

To investigate the molecular alterations of MRD in an aggressive form of human breast cancer, a transgenic mouse model was used in this study. This model system is based on a chemically inducible breast cancer mouse model harboring two common oncogenes (*c-MYC* and *HER2*) [69]. This model was previously shown to mimic human breast cancer pathology and to be suitable to study breast cancer MRD [69]. The previous study revealed that MRD, although oncogene inactivated, has a stably altered lipid metabolism combined with elevated ROS markers [69].

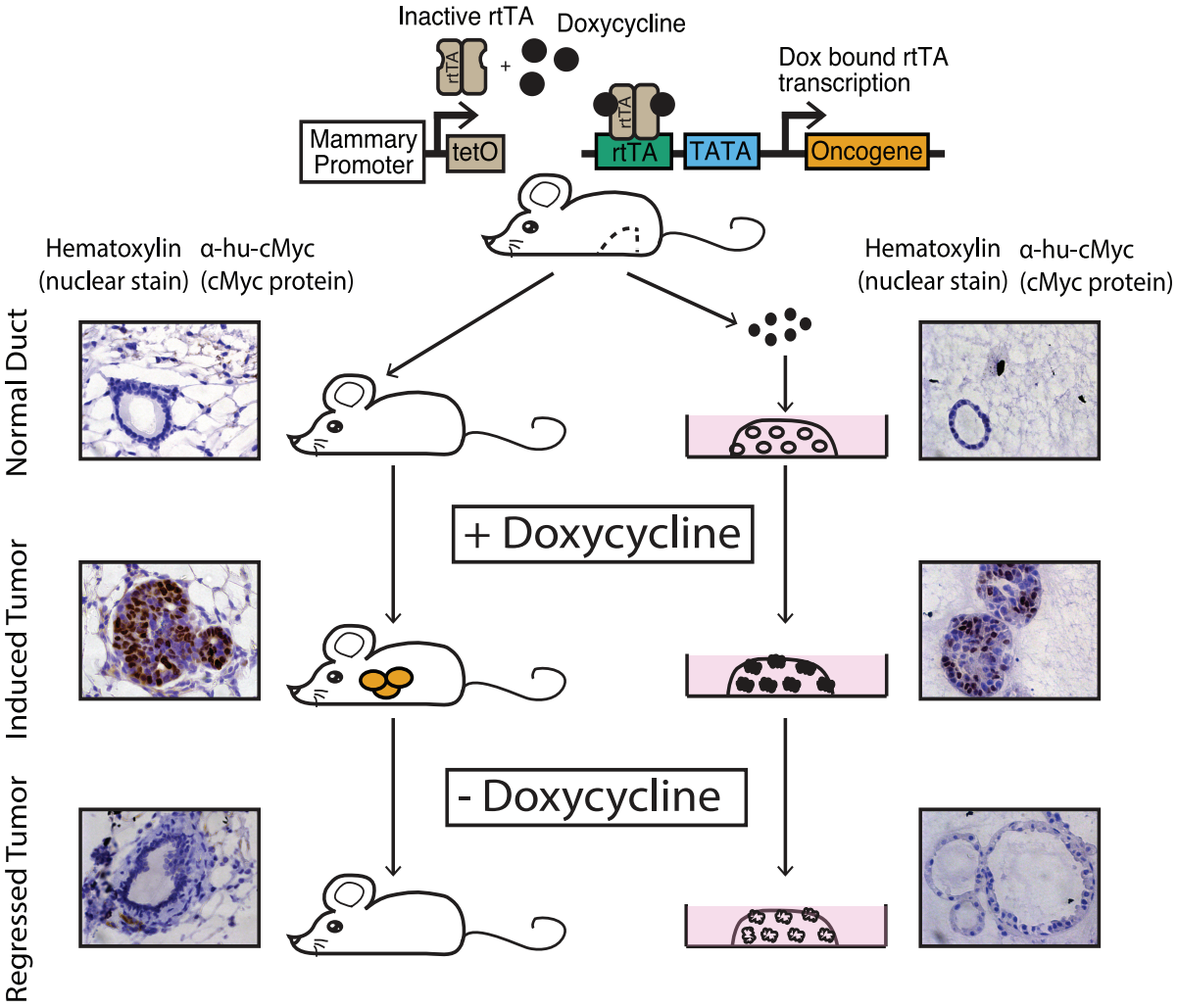

FIGURE 4.1. Heterologous mouse model and culture system to study MRD in human breast cancer. Mouse models of recurrent mammary tumorigenesis were used for *in vivo* studies. These studies were complemented by organoid cultures derived from primary mammary epithelial cells isolated from adult (>8 weeks of age), virgin mice. Orange circles, mammary tumors; white circles, regressed tissue; black-filled dots, *in vitro* tumor correlates; hollow dots, *in vitro* regressed tissue correlates. The corresponding *in vivo* (left panels) and *in vitro* (right panesl) transgene-specific histological c-MYC stainings of acini/mammary glands are depicted next to the schema. Scale bar: 50 μm. This figure and the text in this legend have been adapted from Havas et al. (2017) [69].

Primary mammary epithelial cells isolated from the mouse model were grown in a 3D cell culture system, where they spontaneously form organoids that recapitulate acini[1]. Tumor induction was initiated upon the transcription of the two oncogenes *c-MYC* and *HER2* by adding doxycycline

[1]basic unit of the mammary gland

to the media. The addition of doxycycline to the culture media leads to the transcription of the two trans-oncogenes *c-MYC* and *HER2* and results in tumor formation. After five days in the culture media with doxycycline the lumen of the acini are completely filled with rapidly proliferating luminal endothelial cells. The histology of the organoids resembles an early human breast cancer state. At this time point, doxycycline is excluded from the media, which stops the transcription of the oncogenes and initiates apoptosis. In the following two days the lumen of the acini are cleared and the morphological structure of the acini is fully intact after seven days. The reformed acinus is phenotypically indistinguishable from the healthy control. This regression process mimics an ideal setting of targeted therapy in the patient situation since the expression of the driving oncogenes is regulated by the addition or exclusion of doxycycline in the media. Staining the *in vitro* acini for mammary gland specific morphological markers as well as with transgene-specific antibodies could recapitulate the known physiology of the published *in vitro* culture system with [69]. Caspase3 stains of the *in vitro* culture show that massive apoptosis accompanies the clearance of the lumen and starts after 8 hours of regression. However, not all cells are undergoing apoptosis and about five to ten percent of the cell population survives and reforms acini. Transcriptomics as well as intracellular and extracellular metabolites of the sample groups (healthy control, tumor and regressed cells) were analyzed using three different metabolomics technologies, namely gas-chromatography mass spectrometry (GCMS), untargeted metabolomics on a high-throughput platform and shotgun lipidomics (Table 1). This was complemented with in vivo measurement of the targeted metabolomics as well as fluxomics data for central carbon metabolism. Altogether, this is a one of the most comprehensive metabolomics data sets on a HER2 positive breast cancer in model systems.

TABLE 4.1. Summary of collected experimental omics-data.

System	Compartment	Transcriptomics	GCMS	Lipidomics	Untargeted Metabolomics	Flux Measurements
In vitro	Intracellular	22287 genes	56 metabolites	1472 lipids	2832 ions	-
In vitro	Extracellular	-	30 metabolites	-	3208 ions	-
In vivo	Intracellular	-	52 metabolites	-	-	
In vivo	Extracellular	-	37 metabolites	-	-	

To integrate and interpret the acquired data genome scale metabolic modeling was utilized. Finally, to assess the human relevance of our findings, our results were compared to a combined set of patient microarray data containing healthy tissue samples and biopsies from tumor and regressed tissue.

4.2 Material and Methods

4.2.1 Animals

Breeding and maintenance of mouse colony was done in the LAR (Laboratory Animal Resources) facility of EMBL Heidelberg, under veterinarian supervision and in accordance to the guidelines

of the European Commission, revised Directive 2010/63/EU and AVMA Guidelines 2007. All experiments were performed with the mouse strain TetO-cMyc/TetO-Neu/MMTV-rtTA [1]. For the comparison of metabolic profiles in intracellular GCMS data, an additional strain was used – TetO-cMyc/TetOKrasG12D/MMTV-rtTA [2].

For the *in vitro* experiments, primary mammary epithelial cells were collected from 8 weeks old virgin females through mammary gland tissue digestion and cultured in 3D. For the *in vivo* experiments, the animals have been fed with doxycycline and developed tumors in the period of 4-6 weeks. When the tumor burden was too large, the animals were put on normal food without doxycycline and the tumor regressed to a non-palpable state. Mammary glands of these mice were harvested when tumors fully regressed, 9 weeks after. Wild type animals (age-matched controls) were fed in the same fashion and their mammary glands were collected at the same time and in the same manner.

If not noted otherwise, we had two types of healthy controls for both types of experiments. One control with the transgenes but without doxycycline in the media (never induced, NI) and one control from wild type animals (WT, age-matched) which were supplied with doxycycline in the media or food in the same fashion as the transgenic mice. Their mammary glands were also collected at the same time and in the same manner.

4.2.2 3D Cell culture

Three-dimensional cell cultures were established according to the published protocol [3] with some modifications. Primary mammary epithelial cells were obtained from 8 weeks old virgin females of the described mouse strains through the digestion of mammary glands in 5 mL of digestion media (Lonza/Amaxa DMEM/F12 1:1 Mixture with HEPES, L-Gln, BE12-719F) supplemented with HEPES to the final concentration of 25 mM, 150 U/mL Collagenase type 3 (Worthington, LS004183), 20 μg/mL Liberase Blendzyme 2 (Roche, 05401020001) and 5 ml of Penicillin/Streptomycin (Gibco Life Technologies, 15140-122). After digesting for 15-16 hours at 37 oC in 5 % (vol/vol) CO_2 atmopshere in loosely capped 50 mL polypropylene conical tubes a washing step with 45 mL of phosphate-buffered saline (PBS) was performed. Upon centrifugation at room temperature, 1000 rpm for 5 min, the interphase between the upper fat layer and the cell pellet was removed and 5 mL of 0.25 % trypsin-EDTA (Invitrogen, 25200-056) was added. The suspension was incubated for 40 min at 37 oC, 5 % CO_2 in loosely capped tubes. This was followed by the wash with 25 mL of STOP media (Lonza/Amaxa DMEM/F12 1:1 Mixture with HEPES, L-Gln, BE12-719F supplemented with HEPES to the final concentration of 25 mM and 10 % Tet System Approved Fetal Bovine Serum, Biowest, S181T) and the treatment with 5-15 mg/mL DNase I (ThermoFisher, 18068015). After a second centrifugation step at room temperature, 1000 rpm for 5 min, the dissociated cells were resuspended in MEBM media (Lonza, Mammary Epithelial Cell Basal Medium CC-3151 with supplements from Mammary Epithelial Cell Medium BulletKit CC-3150) and plated onto collagen-coated plates (BD Bioscences, 356400)

for the selection of epithelial cells. On the next day, the cells were washed with PBS and treated with 500 μl of 0,25 % trypsin-EDTA until detachment. Trypsin was inactivated with 9 mL of STOP media (described above), followed by a centrifugation step at room temperature, 1000 rpm for 5 min. Cell pellets were resuspended in PBS, counted, and mixed rapidly on ice with the prepared Matrigel-collagen mixture – Cultrex 3D Culture Matrix Basement Membrane Extract (Biozol, TRE-3445-005-01) and 1,5 mg/mL Cultrex 3D Collagen I rat tail (TEMA Ricerca, 3447-020-01). Mixed droplets in a concentration of 12 500 primary mouse mammary epithelial cells per 100 μl were dispensed into flat bottom wells (Corning CellBIND 12 Well Clear Multiple Well Plates, 3336) or chambered cover glass slides (ThermoFisher Scientific, Nunc LabTek II Chambered Cover glass, 155379). After gel solidifying for 35-40 min at 37°C, 1.5 ml of MEBM serum-free media (supplemented with 2 mL of bovine pituitary extract, 0.5 mL of hEGF, 0.5 mL of hydrocortisone, 0.5 mL of GA-1000, 0.5 mL Insulin from Mammary Epithelial Cell Medium BulletKit CC-3150) was added to each well. Doxycycline (Sigma, Doxycycline hyclate, D9891) was titrated to lower concentration of 200 ng/ml. For the metabolic analyses the same media was used from the start of an experiment until the collection, media was used in volume of 1 mL and changed every day at the same times.

4.2.3 Immunofluorescence

3D culture gels were fixed with 4 % paraformaldehyde (PFA) for 7-10 min for immunofluorescence staining and washed for three times with PBS and once in IF buffer (containing NaCl, Na2HPO4, NaN_3, BSA, TritonX-100, Tween-20; pH 7,4). Blocking was done with 10 % goat serum (Jackson Immuno Research, 005-000-121) for 1.5 h. A standard protocol was applied for the staining with the following antibodies: alpha-6-integrin (BD Biosciences 25-0495-82, diluted 1:80), ZO-1 (Invitrogen 61-7300, diluted 1:500), GM-130 (BD Biosciences, 610823, diluted 1:100), E-cadherin (Invitrogen, 13-1900, diluted 1:200). The nuclei were stained with DAPI (ThermoScientific, 62248, diluted 1:1000). The gels were mounted with Vectashield Anti-fade mounting medium (Vinci Biochem, VC-H-1500-L010) and imaged on a Leica SP5 confocal microscope using 63x water lens and LAS AF imaging software. Anti-rabbit, anti-mouse, and anti-rat antibodies coupled with Alexa Fluor dyes were purchased from Invitrogen (A21247, A11034, A11036). FFPE tissue sections were stained using the standard protocols for the following antibodies: Arg1, Ass1, iNOS, Hk2, PDK1, Lin28A, Ak4 (all from Abcam, diluted 1:250). The tissue sections were mounted using ProLong Gold Antifade (P36930 from ThermoFisher) and scanned using the TissueFAXS Slides system (TissueGnostics). The quantification was done using StrataQuest Analysis Software (TissueGnostics).

4.2.4 RNA sequencing sample preparation and sequencing

Ribonucleic acid (RNA) was harvested from a pool of two 3D gels per condition, using 900 μl of mirVana lysis buffer, and subsequently extracted using mirVana miRNA Isolation Kit with phenol

(Ambion, AM1560). After assessing the RNA quality and concentration with the Bioanalyzer (Agilent 2100, G2939BA), the RNA was sequenced on the Illumina NextSeq 500 platform with a read length of 75 bp. The RNA sequencing (RNAseq) experiment was repeated twice with each time two biological replicates from 2 different animals, except for the healthy control where 4 biological replicates from 4 different animals were used.

4.2.5 Differential expression analysis

The quality of the raw RNA sequencing reads was assessed using FastQC [6] (version 0.11.3). Prior to the alignment, adapter trimming was performed using cutadapt (version 1.9.1) with default options providing the standard lllumina TrueSeq Index adapters. Subsequent quality trimming and filtering was performed with FaQCs (version 1.34) using the following parameters: –q 20 –min_L 30 –n 5 –discard 1. The total reads per sample after trimming and filtering ranged from 34.1 to 52.0 million. The sequencing reads were aligned to the reference genome of M. musculs (GRCm38.p6) which included the sequence for human c-MYC and rat HER2 (FOOTNOTE: https://www.ensembl.org) using tophat2 (D. Kim et al., 2013) (version 2.0.10) with the following parameter: -G -T -x 20 -M –microexon-search –no-coverage-search –no-novel-juncs –mate-std-dev 100 -r 50 –min-segment-intron 20 -i 30 -a 6. Only reads with unique mappings were considered for differential expression analysis. Gene level count tables were obtained using the count script of the HTSeq [4] python library (version 0.6.1p1.) with default options. All reads mapped in total to 19.500 to 20.800 genes. This was followed by statistical analysis using the Bioconductor package DESeq2 [109] (version 1.12.4). Size-factor based normalization to control for batch effects and inter-sample variability and dispersion estimation were conducted using package defaults. The animal was included in the model design. Additionally, genes with a less than 10 counts in total across all data sets were filterd to increase the sensitivity of the detection differential gene expression. The differential expression analysis was also performed with the package defaults, which include multiple testing correction, independent filtering and cooks cutoff [3] for outlier detection. Bonferoni adaption was applied for multiple testing correction. Genes with padj < 0.01 were considered as significantly differentially expressed (DE). Biostatistical analyses were conducted using R V.3.3.1 (R Development Core Team). For performing dimensionality reduction with Principal Component analysis (PCA) and hierarchical clustering rlog DESeq2 [109] transformed transcript counts were utilized. For the calculation of the ellipses on the PCA plots the “stat_ellipse” function from the R package ggplot2 was used [66].

4.2.6 Enrichment analysis

The enrichment analysis was performed using Fisher’s exact test with a foreground of all respective differentially expressed genes and a background, which was composed of a unique set of 5 randomly picked genes per foreground gene exhibiting a similar expression mean over all samples. The chosen p-value cutoff was 0.01.

4.2.7 Collection and extraction of intracellular and extracellular metabolites

In vitro experiments – Before proceeding with the intracellular metabolites collection, 150 μl of the extracellular media was taken from the wells of each condition, snap-frozen and stored at −80°C until the analysis. Organoid structures were then freed from Matrigel upon digestion for 1,5 h at 37°C with 3 μl of liberase and 3 μl of collagenase added to the media. 3 wells were pooled per condition replicate, subsequently washed for three times with PBS, shortly centrifuged (1000 rpm, 2 min, room temperature) and quenched with 200 μl cold (−80°C) HPLC-grade methanol (Biosolve Chimie, 136841). The contamination of the cells with rest media was excluded by comparing the obtained metabolic profiles with 50 μl of each well's used MEBM growth medium and the last washing solution of each well wise the solution (quenched with 100 μl of cold −80°C HPLC-grade methanol). The extraction of the metabolites was done with a 1:1 methanol-water protocol [4–6] with ribitol (Alfa Aesar, 488-81-3) as internal standard. For the *Flow Injection Q-Exactive MS* the extracellular metabolites were measured in extracellular media with a 1:10 dilution. The experiment was repeated twice with each time two biological and two technical replicates from two different animals, except for the wild type control where 3 biological replicates from one animal were used. In vivo experiments – For the glucose labeling experiment mice mammary glands were dissected, minced and digested for 2 hours at 37°C using collagenase and liberase enzymes. The digested cells were then cultured for 8 hours at 37°C and 5 % (vol/vol) CO_2 atmopshere in DMEM glucose- and pyruvate-free media (11966025, ThermoFisher) supplemented with 4,5 g/L labelled D-glucose (U-13C, 99 % from Cambridge Isotope Laboratories, Inc.).) and 2 mL of bovine pituitary extract, 0.5 mL of hEGF, 0.5 mL of hydrocortisone, 0.5 mL of GA-1000 and 0.5 mL insulin from the Mammary Epithelial Cell Medium BulletKit CC-3150. For the non-labeled GCMS metabolomics experiment the mammary glands were dissected and cultured for 8 hours at 37°C and 5 % (vol/vol) CO_2 atmosphere in DMEM 4,5 g/L glucose media (D6429 Sigma), supplemented with 2 mL of bovine pituitary extract, 0.5 mL of hEGF, 0.5 mL of hydrocortisone, 0.5 mL of GA-1000 and 0.5 mL insulin from the Mammary Epithelial Cell Medium BulletKit CC-3150. Extracellular metabolites were collected and snap-frozen in liquid nitrogen. For the harvest of the intracellular metabolites the cells were quickly washed for two times in PBS and quenched with cold methanol. Metabolites were extracted using a 1:1 methanol-water protocol [4–6] with ribitol (Alfa Aesar, 488-81-3) as internal standard. The experiment was repeated once with each time three biological and two technical replicates from three different animals, except for the fluxomics experiment, in which three biological with only one technical replicates from three different animals was used.

Flow Injection Q-Exactive MS. High-throughput discovery metabolomics was modified from the method by Fuhrer et al. [7].

4.2.8 Untargeted metabolomics analysis

As mentioned above, the untargeted metabolomics data collection and analysis was performed by Cellzome, GSK Heidelberg. The pipeline, which is described in the following is an implemented standard pipeline already used in previous publications.

Samples were analyzed on a LC/MS platform consisting of a Thermo Scientific Ultimate 3000 liquid chromatography system with autosampler temperature set to 10°C coupled to a Thermo Scientific Q-Exactive Plus Fourier transform mass spectrometer equipped with a heated electrospray ion source and operated in negative ionization mode. The isocratic flow rate was 150 μL/min of mobile phase consisting of 60:40% (v/v) isopropanol:water buffered with 1 mM ammonium fluoride at pH 9 and containing 10 nM taurocholic acid and 20 nM homotaurine as lock masses. Mass spectra were recorded in profile mode from 50 to 1,000 m/z with the following instrument settings: sheath gas, 35 a.u.; aux gas, 10 a.u.; aux gas heater, 200°C; sweep gas, 1 a.u.; spray voltage, -3 kV; capillary temperature, 250°C; S-lens RF level, 50 a.u; resolution, 70k @ 200 m/z; AGC target, 3x106 ions, max. inject time, 120 ms; acquisition duration, 60 s. Spectral data processing was performed using an automated pipeline in R. Detected ions were tentatively annotated as metabolites using the HMDB database as reference assuming [M-H] and [M-2H] as ionization options and the exchange of one or two ^{13}C with the equivalent number of ^{13}C atoms with the method-inherent disability to distinguish between isomers. The experiment was repeated once with each time four biological and two technical replicates from four different animals, except for wild type control which had two biological and two technical replicates from one different animal.

4.2.9 GCMS analysis

Upon drying, metabolite extracts were derivatized to their (MeOx) TMS-derivatives: 1) with a 50 μL of 20 mg/mL methoxyamine hydrochloride (Alfa Aesar, 593-56-6) solution in pyridine (SigmaAldrich, 437611) for 90 min at 40°C, 2) with 100 μl N-methyl-trimethylsilyl-trifluoroacetamide (MSTFA) (Alfa Aesar, 24589-78-4), for 12 hours at room temperature (6,8). The metabolic profiles of all samples was measured 12 hours after derivatization using a Shimadzu TQ8050 GCMS (triple quadrupole) system (Shimadzu Corp.) and a gas chromatograph with a 30 m x 0.25 mm x 0.25 um DB-50 MS capillary column (Phenomenex, USA). The detector operated both in scan mode (recording in the range of 50-600 m/z) and MRM mode. The samples were normalized to ribitol and total measured metabolite levels.

For the experiment with labeled glucose the metabolites were dried and derivatized to their (MeOx) TMS-derivatives: 1) with 50 μL of 20 mg/mL methoxyamine hydrochloride (Alfa Aesar, 593-56-6) solution in pyridine (SigmaAldrich, 437611) for 90 min at 40°C, 2) with 100 μl N-tert-Butyldimethylsilyl-N-methyltrifluoroacetamide with 1% tert-Butyldimethylchlorosilane (Sigma-Aldrich) for 1h at 60oC and for 12 hours at room temperature (6,8). The samples were further

processed as previously described. P-values were calculated with limma and the adjustment method is Benjamini-Hochberg.

4.2.10 Lipidomics analysis

A modified version of the Bligh & Dyer protocol (9) was used for lipid extraction. Samples were analysed by direct infusion nano-ESI MS using an Qtrap 6500 + coupled with a NanoMate (Sciex). The samples were normalized to 100 % (mol %) of total lipids.

4.2.11 NOS enzymatic assay

Mammary glands were dissected and homogenized in NOS assay buffer and further processed following the Nitric Oxide Synthase Activity Assay kit protocol (Abcam, ab211083) for measuring the enzymatic activity of nitric oxide synthase (NOS).

4.2.12 Reporter metabolite analysis

Metbaolic reactions that are likely to be re-regulated during regression were identified using the reporter metabolite algorithm, a gene set enrichment statistic with genes as keys and metabolites as values from the "piano" R package [188]. The adjusted p-value and log2 fold change (FC) of the respective differentially expressed genes were used to calculate p-values from a theoretical null distribution (10,000 permutations). The gene set was produced from the revised HMR2 model (see chapter 3) whose gene identifiers were translated to mouse orthologs. Multiple testing adjustment was applied using the Benjamini-Hochberg procedure. The threshold for significance was padj < 0.1, but maximally 5% of the total list of tested metabolites. A pathway enrichment was calculated for gene sets of 1 gene per group or bigger.

4.2.13 Genome scale metabolic modeling

A new simulation method was developed to predict differences in the metabolic flux distributions between two conditions based on relative gene expression levels. The method is based in the concept of *enzyme usage constraints* introduced in [112]. This is an extension of classic flux balance analysis, where the total flux carried by each enzyme is explicitly accounted for taking into consideration the complexity of gene-protein-reaction associations (enzyme promiscuity, isozymes, and complex formation). The method is formulated as follows:

$$\min \left\| u^p - \frac{e^p}{e^r} u^r \right\|_1 \tag{4.1}$$

$$s.t. \tag{4.2}$$

$$S_{\text{ext}} \cdot \left| \begin{matrix} v^r \\ u^r \end{matrix} \right| = 0 \tag{4.3}$$

$$S_{\text{ext}} \cdot \left| \begin{matrix} v^p \\ u^p \end{matrix} \right| = 0 \tag{4.4}$$

$$u^r \geq 0 \tag{4.5}$$

$$u^p \geq 0 \tag{4.6}$$

$$lb^r < v^r < ub^r \tag{4.7}$$

$$lb^p < v^p < ub^p \tag{4.8}$$

where u^r and u^p are the enzyme usage vectors in the *reference* and *perturbed* conditions, respectively, $\frac{e^p}{e^r}$ represents the relative gene expression levels between the two conditions, v^r and v^p are the metabolic flux vectors, and S_{ext} is the extended stoichiometric matrix as defined in [112].

The import/export of SBML files was obtained through the libSBML API using the load_cbmodel of the *framed* python package (version 0.5) for metabolic modeling [18] [110]. The IBM ILOG CPLEX Optimizer (version 12.8.0) was used for solving the MILP problems unless noted differently. All simulations were conducted with Python 2.7.13.

4.2.14 Comparison to human breast cancer MRD datasets

Microarray data sets with expression intensities from pre- and post treatment breast cancers biopsies [64] and healthy breast control tissue [114] were downloaded from Gene Expression Omnibus (GEO)[15]. For the analysis first, each data set was prepared on its own including filtering samples for outliers, sample normalization and background correction with the “rma” function of the R package “oligo” filtering genes for minimal intensity filtering and gene annotation of probeset IDs with the removal of multiple mappings of transcript cluster identifiers. Next, the two data sets were combined and subdivided to the set of commonly used probe sets (both Microarray data sets are from Affymetrix but from different gene chip versions, thus they largely overlap in their probe sets). Then the two data sets were combined, normalized, checked for outliers and again, genes with low intensities were filtered. To address the batch affect of the joined data set stemming from the two experimental settings and largely influencing the gene expression, the first principal component of PCA analysis was removed. The “normal” tumor subtype of the data set from Gonzalez-Angulo et al. were removed because it is poorly defined diagnostic category and therefore exhibiting high biological variability.

4.3 Results and Discussion

4.3.1 Tumors as well as phenotypically healthy regressed breast cancer cells possess an altered transcriptome

In order to investigate possible (long-term) changes in the molecular signature through oncogenic signaling, transcriptomics profiles of the tumorigenic and the regressed structures were analyzed in comparison to healthy control structures (age matched NI and WT, see Material and Methods). First, analyzing the tumor reveals that the transcriptome of the tumor cells is heavily altered with 5356 genes being differentially expressed in comparison to the control (Figure A.12). Previous studies analyzing gene expression in cancer[2] in comparison to healthy tissue from patient samples have observed about 2000 to 2500 genes differentially expressed [103] [135]. However, these studies focus on samples from multiple patients and therefore have an increased genetic and environmental heterogeneity, which are confounding the profiles. Also the control tissue, which is often taken from tumor adjacent tissue, is heterogeneous in itself due to inevitable inclusion of other cell types, such as fibroblasts, infiltrating immune cells or adipocytes. Lastly, samples obtained from clinical settings typically possess a lower quality then cell culture data and microarray technologies, which are still the most common method for the transcriptional analysis of clinical samples, are less sensitive and specific in identifying differentially expressed genes than RNASeq [191] [104].

The changes in the tumor transcriptome over the healthy control appear to have a highly proliferative character with genes involved in cell cycle, cell division, DNA repair and gene expression and translation being strongly up regulated (Figure 4-3a). In addition, processes being well established to accompany cancer progression are reflected such as a down regulation of genes involved in cell adhesion and cell recognition and genes synthesizing cell surface markers (Table A.25). Furthermore, the proliferative state of the cells is also reflected by changes in metabolic genes, which are adapted to provide the cell with building blocks for growth as the transcription of genes for glycolytic enzymes, enzymes of the pentose phosphate pathway (PPP), Tricarboxylic acid (TCA) cycle enzymes and enzymes involved in oxidative phosphorylation (OXPHOS) and nucleic acids as well as amino acids biosynthesis are upregulated (Figure A.13). However, the metabolic genes are not enriched amongst the differentially expressed genes, as 21.1% of the enzymes coding genes are differentially expressed genes, which corresponds to the average proportion of metabolic genes in the genome (17.1%)[3].

[2] including breast cancer

[3] The estimate for human metabolic genes is taken from the genes annotated to the revised human GMM, Chapter III

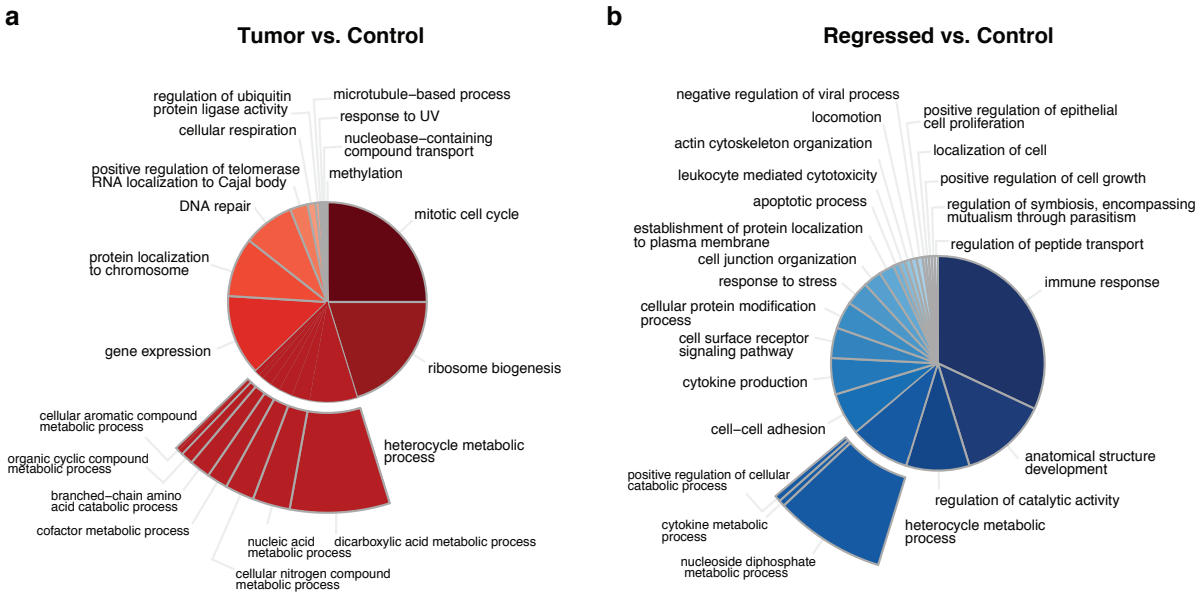

FIGURE 4.2. Transcriptional characterization of breast cancer regression. GO Term enrichment analysis of the upregulated differentially expressed genes of (a) tumorigenic organoids. (b) of regressed organoids in comparison to healthy control organoids.

Surprisingly, the regressed structures have 1525 genes differentially expressed compared to the healthy samples (Figure A.14). 60.9% of the differentially expressed genes overlap and nearly all of them in the same direction (Figure 4-5b). However, their transcriptome profile is less clearly deregulated compared to the healthy controls and the differentially expressed genes spread into diverse categories. Amongst the strongest enriched GO categories of upregulated genes are processes involved in extracellular signaling and reorganization, such as immune response, cell-cell adhesion, cell junction organization, cell surface receptor signaling pathway (also amongst the downregulated genes), but also stress and apoptosis related processes (Figure 4-3b). The upregulation of stress responding genes could be caused by apoptosis being activated as a response to the turning-off of the oncogenic signaling. Even though the sequenced cells are surviving by evading apoptosis, parts of the apoptotic signaling cascade might nevertheless be active. The stress signaling could also be connected to the previously discovered high ROS production in regressed breast cancer cells due to an altered lipid metabolism [69]. With regard to the quiescent status of the regressed cells, expected downregulated processes in the regressed cells over the healthy cells include mitotic cell cycle processes and the associated decrease of nucleotide metabolism as well as processes involved in cell migration and vascularization (Table A.26).

Interestingly, categories positively regulating cell proliferation and cell growth are also found upregulated although phenotypically the cells are growth arrested. Even more intriguingly, genes coding for glycolytic enzymes and enzymes involved in the biosynthesis of amino acids are strongly upregulated (Figure A.15). Furthermore, the genes coding for glycolytic enzymes appear to be concordantly upregulated with genes from the HIF-1 signaling pathway (Figure A.15). HIF-1α is a transcription factor that gets activated by elevated ROS levels and is known to promote cell survival during prolonged hypoxia [145]. It induces the transcription of the two downstream genes *BNIP3* and B*NIP3L*, which in turn induce mitophagy and allow cells to survive in hypoxic condictions by preventing increased levels of ROS [17]. Although the transcript levels of HIF-1α itself do not change[4], the transcript levels of VHL, which binds HIF-1α and thereby targets it for degradation, decreases, suggesting a possible stabilization and thereby activation of the HIF-1α protein [87] [170]. Accordingly, the transcription levels of the transcriptional targets of HIF-1α, *BNIP3* and *BNIP3L*, are strongly differentially expressed in the regressed cells in comparison to the healthy cells with a positive log2 fold change of 2.4 and 0.9, respectively. This could hint at the induction of pro-survival autophagy, counteracting increased ROS levels. Furthermore, active HIF-1α triggers the reprogramming of metabolism towards a glycolytic phenotype by increasing the expression of genes encoding glucose transporters (viz. *GLUT1*, *GLUT3*, *HK1* and *HK2*), enzymes of the glycolytic pathway (viz. *ALDOA*, *ALDOC*, *PGK1*, *ENO1* and *PKM2*) and enzymes directing the flux towards lactate production (viz. *LDHA*, *MCT4*, *PDH1*[5] [170]. A feed-forward

[4] which is expected since the activation of HIF-1α works through the stabilization of the protein

[5] a regulatory gene, which inhibits PDH and thereby prevents pyruvate from entering the TCA cycle and oxidative phosphorylation

mechanism in which increased levels of lactate and pyruvate increase HIF-1α stability has been reported ([118]). Additionally, oncogenic c-MYC has been shown to cooperate with HIF-1α to activate the transcription of *PDK1* and thereby amplify the signal [88] [35]. This regulatory dependence between HIF-1α and glycolysis could explain the close clustering of the glycolytic pathway with the HIF-1 signaling pathway (Figure A.15). Lastly, the increased HIF-1α signaling could also be connected to cell's surviving apoptosis. Depending on the tumor context, HIF-1α has shown diverging results, both inhibiting and promoting apoptosis. Non the less, HIF-1α is generally viewed to promote cell survival and its overexpression has been reported in a variety of human cancers and is typically correlated with resistance to therapy [205] [203] [165] [142] [50]. *VEGFA* one of the most important targets of HIF-1α was shown to counteract apoptosis in hypoxia and exhibits a log2 fold increase of 2.1 in the regressed cells over the healthy control cells [14] [143]. Furthermore, HIF-1α also protects cells from ROS induced apoptosis. This protective effect was accompanied by the increase of HIF-1α target genes *CDKN1A*, enolases and *EPO*, which are also positively differentially expressed in the regressed cells, although mildly (0.50 *CDKN1A*, *ENO1* 0.68, *ENO3* 0.47) [201]. Even more interestingly, the simultaneous upregulation of glycolsis in HIF-1α dependent inhibition of hypoxia and glucose deprivation-induced apoptosis is suspected to play a role in the modulation of apoptosis resistance [58] [76] [87] [19]. The sustained activity of HIF-1α and a simultaneously increased flux through glycolysis could be one of the possible routes by which the surviving regressed breast cancer cells evade apoptosis.

4.3.2 Transcriptome differences between the tumor and the regressed cells converge at the metabolic level

Untargeted metabolomics show that the metabolic status of the tumor cells indeed strongly changes as they cluster apart from the regressed and control cells (Figure 4-4). As suggested by altered transcript levels of enzymes the concentrations of metabolites involved in major growth related pathways like glycolysis, PPP, TCA cycle, Oxphos, nucleotide metabolism and amino acid synthesis/degradation are significantly changed (p-value < 0.05). Like on the transcriptional level, the metabolic status of regressed cells retains features of the tumor cells, as many ions annotated to the above-mentioned pathways remain altered. Hierarchical clustering shows that the regressed samples are overall metabolically even closer to the tumor than the healthy control samples. This suggests that some global transcriptomic and metabolomics alterations are present in the regressed cells, possibly with the progression of the changes in transcript levels up to the metabolite level.

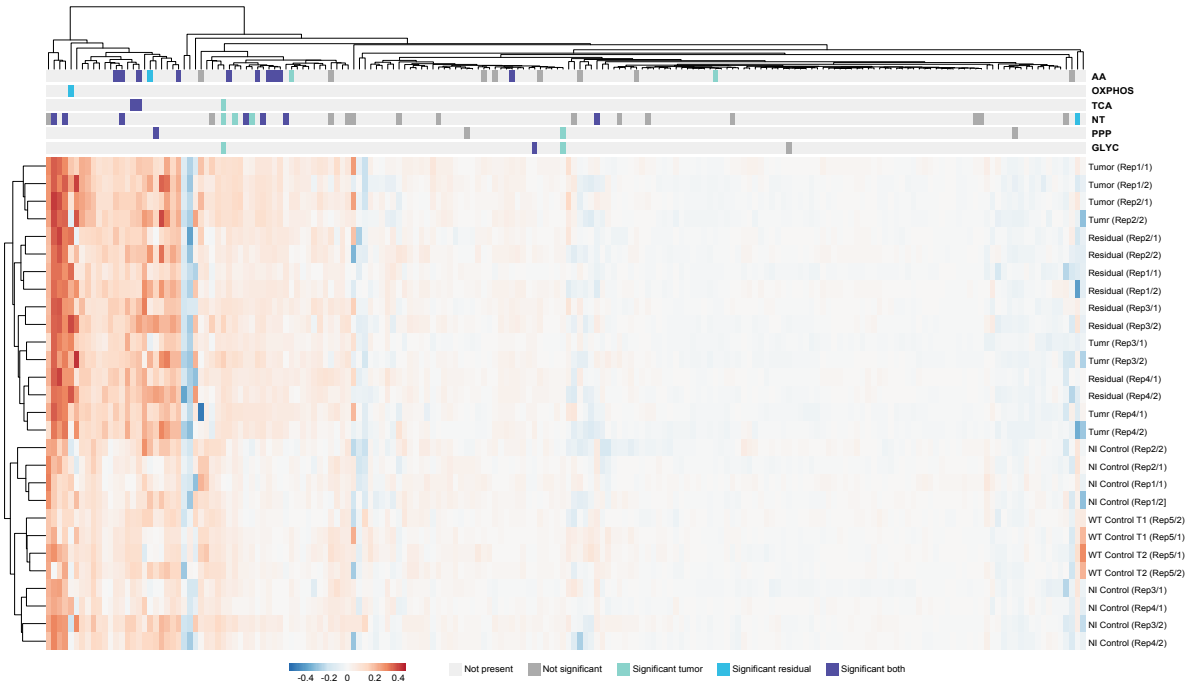

FIGURE 4.3. Intracellular untargeted metabolomics results from regressed organoid structures. Samples are clustered according to high confidence ions. The annotated KEGG pathway is indicated if applicable. AA = amino acid biosynthesis pathway, OXPHOS = Oxidative phosphorylation, TCA = Citrate cycle, NT = Purine and pyrimidine metabolism, PPP = Pentose phosphate pathway, GLYC = Glycolysis/Gluconeogenesis.

In order to gain deeper insights into the metabolic alterations present in regressed breast cancer cells lipidomics as well as targeted metabolomics were measured. Comparing the regressed samples to the healthy controls the different metabolomics data sets repeat the previous observation that the regressed cells do not, in terms of their metabolite levels, return to a healthy status but in contrast cluster closely with the tumor cells (Figure 4-5).

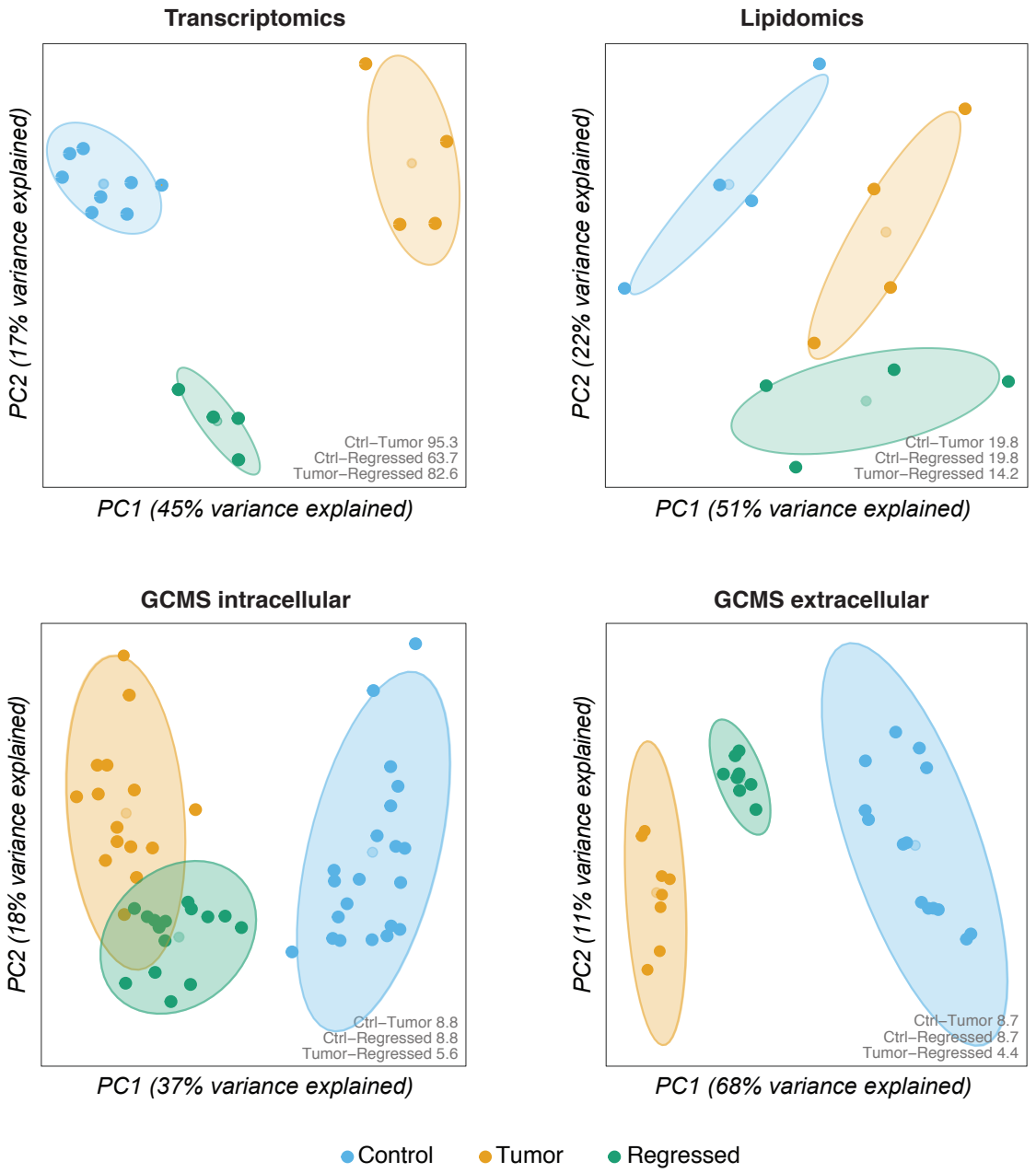

FIGURE 4.4. Dimensionality reduction of transcriptome and metabolome data sets. PCA plots of (a) transcriptomics data (b) intracellular lipidomics data (c) intracellular GCMS data (d) extracellular GCMS data. Blue represents healthy control samples, yellow tumorigenic samples and green regressed samples. All replicates Centroids and ellipses are drawn to represent the center of each sample group considering the first two principal components (PCs). The calculated distance measure is the Euclidean distance between the centroids of the samples based on all principal components. The ellipses represent the 0.95 confidence interval of a multivariate normal distribution. Ctrl – Control samples, Tumor – Tumor samples, Regressed – Regressed samples.

However, comparing the global transcriptomics level amongst the three sample groups, the regressed cells do retain alterations and do not cluster with the healthy controls. But in contrast to the metabolomics levels their status is clearly different from the tumor cells. In fact, they are even transcriptionally closer to the healthy cells. Subdividing the transcriptional data to only metabolic genes does not change the global clustering of the groups (Figure A.16). Thus enzyme levels globally differ between the three groups. One possible explanation could be that in the tumor situation the transcription is highly altered because of the oncogene expression[6], but the extent to which the metabolism can change accordingly is limited/gets saturated,[7]. Hence, even though the transcription in the regressed cells is altered the regressed cells would appear closer to the healthy controls than the tumor cells. 90.5% of all genes possess a log2 fold change of less than 2 between the tumor and the regressed cells and only 2.4% percent exceed a log2 fold change of 3 (Figure A.18). Thus, there is no large isolated group of exceedingly altered genes. However, there are 4655 genes, which are only differentially expressed in the tumor. These genes exhibit on average an absolute log2 fold change of 1.2 over the regressed cells (Figure 4-6a) (Figure A.19a). Clustering the samples with the genes only differentially expressed in the tumor recapitulates the sample clustering with all genes (Figure 4-6a) (Figure A.20a). This confirms that strong drivers of the transcriptomic clustering are the genes that get exclusively altered because of the oncogene expression and tumor formation.

When selecting only the intersection of genes significantly altered in the tumor and the regressed samples (928 genes), the regressed samples still cluster independently but closer to the tumor samples than to the healthy samples (Figure 4-6b) (Figure A.20b). Even though the genes are less strongly changed (average absolute log2 fold change of 0.85), their deregulation pattern is similar to those of the tumor sample for the majority of genes (Figure 4-6b) (Figure A.19b). Thus, only a subset of transcriptional changes from the tumor is present in the regressed cells, but those, which overlap tend to exhibit a similar pattern. Conceivably, part of the metabolic phenotype in the regressed cells could stem from enzyme levels, whose transcription levels are still altered similarly to the tumor cells, just not as strongly. Since many enzymes in the central carbon pathways are known to not reach their metabolic capacity in normal cells it is possible that the enzyme levels in the regressed cells do not need to change to exert a tumorigenic metabolism profile [138] [42]. It is also possible that already a few stronger “driver” pathways or genes are enough to establish a metabolic phenotype similar to the tumor samples. Similarly, metabolites themselves might exert a regulatory feedback function, which maintains a metabolic state.

[6] Oncogenic c-MYC transcript levels are 10.6 times higher than in mouse healthy controls (Figure A.17)

[7] for instance the uptake and secretion of metabolites exhibits an additional regulation of metabolite homeostasis

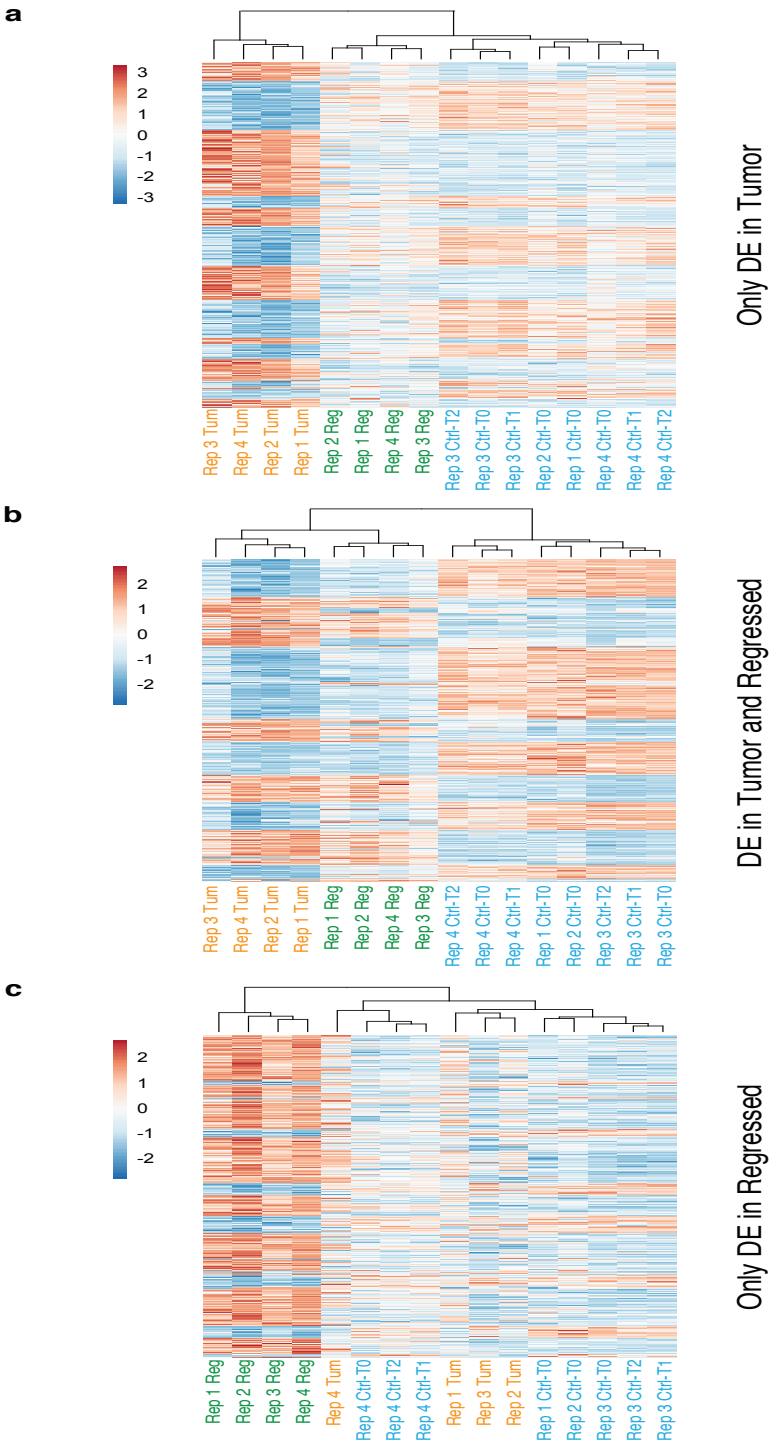

FIGURE 4.5. Detailed analysis of sets of differentially expressed genes Heatmap of rlog transformed transcript counts of differentially expressed genes, which in comparison to the healthy control are differentially expressed (a) only in the tumor samples (b) in the tumor and the regressed samples (c) only in the regressed samples. Ctrl – Control, Tum – Tumor, Reg – Regressed. DE – differentially expressed.

Surprisingly a large proportion of the remaining differentially expressed genes is exclusively changed in the regressed state (597 genes, 39.1% of all DE genes in the regressed state) and separates the regressed cells from the remaining samples. This could possibly be attributed to metabolic network redundancies diverse alterations in transcript levels of enzymes or regulatory genes lead to a similar metabolic phenotype between tumor and regressed samples. Finally, enzyme modifications can also greatly alter the flux of a reaction, but are not detectable on transcript level. In conclusion, significantly different transcriptional changes between the tumor and the regressed state converge on the metabolic level.

4.3.3 Although quiescent, the regressed breast cancer cells maintain high glycolytic flux

Next, we analyzed the concentrations of individual metabolites from the targeted GCMS analysis to identify stably altered metabolic features in regressed cells as compared to healthy cells. As previously observed most of the metabolites, whose concentration levels are significantly changed in the tumor state over the control ($p_{adj} < 0.01$, log2 fold change > 0.5) retain the observed alterations in the regressed state (Figure 4-7, Figure A.21, Table A.27, Table A.28).

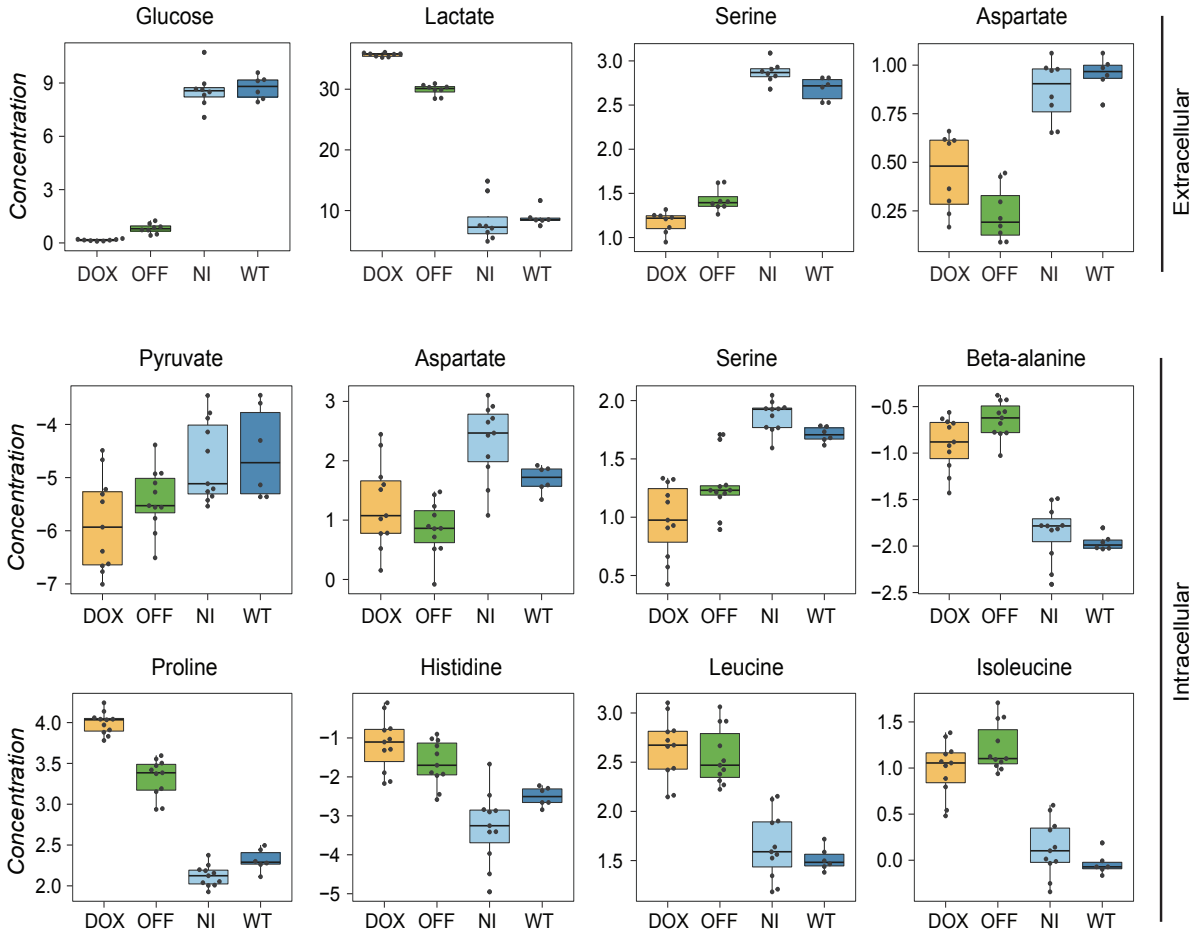

FIGURE 4.6. In vitro targeted GCMS metabolomics analysis of intra- and extracellular metabolite. A selection of significantly altered metabolites ($p_{adj} < 0.01$, log2 fold change > 0.5) in the regressed cells in comparison to the control samples is depicted. The concentration is measured as log2(AUC). AUC = area under the curve, DOX = Tumor

The most prominent metabolic feature in both, the tumor and the regressed cells, is the decrease of glucose in the intracellular samples as well as the media with a concomitant increase of lactate in the media. Taken together with the upregulation of glycolytic enzymes in both samples, this suggests a higher glycolytic flux in regressed than in healthy cells, which is comparable to the flux in tumor cells. *in vivo* measurements of labeled glucose metabolized to lactate confirm that the glycolytic flux in regressed cells indeed significantly increases (one tailed t-test, p-value < 0.05) in comparison to the healthy control cells (Figure 4-8). Notably, the vast majority of glycolytic core enzymes are similarly expressed in the tumor and the regressed samples (Figure A.22). 16 glycolytic enzymes are differentially expressed in the tumor sample in comparison to 15 enzymes in the regressed sample, out of which 12 overlap. The exceptions are a few cases where two different isoenzymes are expressed for the same reaction or additional isoenzymes are upregulated in the tumor. This supports the above-mentioned hypothesis stating that the consistent alteration of a few important core pathways (possibly in combination with metabolites exhibiting regulatory functions) might be enough to drive the metabolic phenotype. Also, the alternating usage of isoenzymes shows that network redundancy is partly responsible in the convergence of the transcriptome to the metabolome.

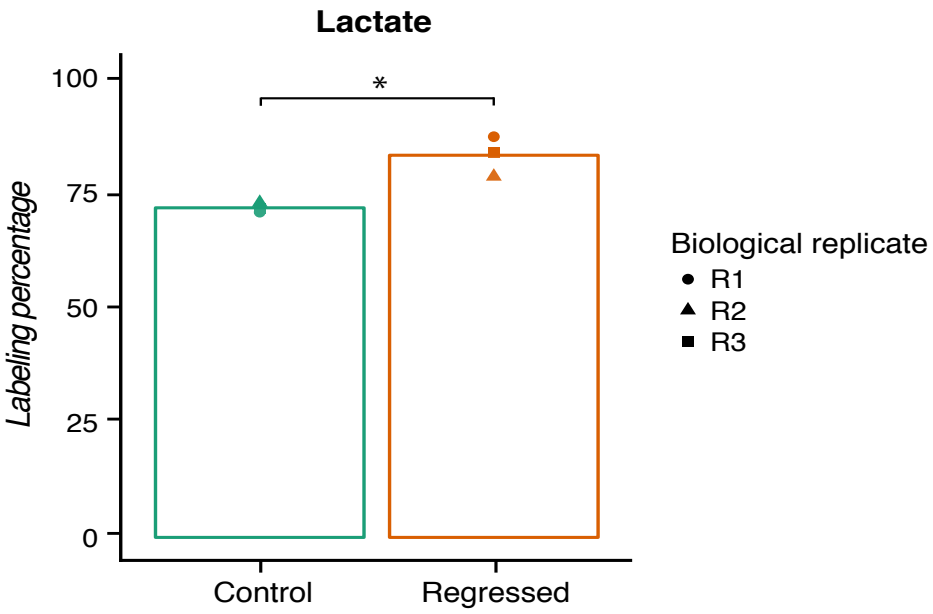

FIGURE 4.7. Glycolytic flux measurements of control and regressed samples. Percentage of intracellular labeled lactate in regressed and healthy control cells.

Additionally the intracellular levels of several amino acids changed in the tumor and the regressed samples in comparison to the healthy control samples (Figure 4-7, Table A.27, Table A.28). These results could also agree with the transcriptional upregulation of genes in the amino acid biosynthesis pathways. Aspartate, which is needed for the synthesis of several other amino acids is decreased intra- and extracellularly, whereas the amino acids beta-alanine, Tyrosine, Phenylalanine, Histidine and Tryptophan, which are synthesized from Aspartate increase intracellularly. Methionine and glutamine, whose increased uptake is one of the most common alterations in cancer metabolism, are only decreasing in the media of the tumor samples [141] [167]. Noteworthy, the urea cycle connected metabolites ornithine, putrescine and urea are increased in both samples intra- and extracellularly over the healthy control as well as the intracellular TCA cycle intermediates succinate, fumarate (not in tumor) and malate. Noteworthy, malate exhibits an intracellular log fold change of 5.39 and 5.84 in the tumor and regressed samples, respectively. Succinate and fumarate are additionally increased in the tumor in comparison to the control. The changes in metabolite levels were confirmed by *in vivo* measurements (ongoing work; personal communication, Ksenija Radic, EMBL Heidelberg). However, it is not possible to derive the direction of the flux change from concentrations measurements of metabolomics data. The same concentration can be reached by a higher or a lower flux in the respective pathway. Additionally, most metabolites typically participate in more reactions than enzymes, thus to redirect the cause for a change in direction is often difficult. In order to gain deeper insights into the nature of the measured metabolite concentration changes such as the metabolites from the urea cycle and the TCA cycle as well as their connection to the transcriptome/the interplay

between the transcriptome and metabolome genome scale metabolic modeling was utilized.

4.3.4 Genome scale metabolic modeling predicts an increased flux through the urea cycle as a second stable metabolic feature of regressed cancer cells

First a reporter metabolite analysis[8] was conducted using the piano tool box [188]. Reporter metabolites can pinpoint to changes in the transcriptome that likely impact the metabolic phenotype. Identifying the consistent reporter metabolites between tumor and regressed cells and overlaying them with the metabolic changes on a network structure can help to pinpoint possible driver pathways. This approach has the advantage that it can identify also distant or isolated pathways of a metabolic network and pick up more subtle trends than other category based enrichment approaches. Further, in cases where the net metabolite concentration does not posses any changes or the metabolite cannot be measured, reporter metabolites supply an additional layer of information. Importantly, reporter metabolites can also help identifying network regions, in which potentially other mechanisms than the transcriptome regulate the metabolome variation, such as e.g. protein modifications, unsaturated enzyme capacities or metabolite concentrations. In this case, metabolites whose concentrations change greatly but without being predicted as reporter metabolites are good candidates. The reporter metabolites predicted for the tumor samples largely overlap with measured metabolites that change (Table A.29). As expected from the GO-Term analysis amongst the predicted reporter metabolites are metabolites participating in glycolysis and oxidative phosphorylation, intermediates from the TCA cycle, glutamine and additional amino acids as well as nucleotides. The reporter metabolites predict changes for nearly all metabolites in the central carbon metabolism, including metabolites, which could not be measured, indicating the glycolysis as a very likely pathway to change. The biggest groups of reporter metabolites consist of metabolites being used in cell surface marker synthesis and cell communication, such as chondroitin, keratan and heparan sulfate derivatives or ceramides (Table A.29). This prediction fits very well with the previous enrichment analysis of GO-categories and metabolites of these families are known to play an important role in cancer progression [186] [1] [168]. Genes of the keratin family and the cadherin superfamily are for instance highly upregulated and collagen family connected genes are highly downregulated (absolute log2 fold changes > 3) in comparison to healthy cells. Additionally, the reporter metabolites predict many metabolites of the glutathione metabolism, including the SAM cycle, as well as a variety of inositol phosphates being altered. In both pathways only a limited number of metabolites can be experimentally measured, thus the reporter metabolites lay stress on these two possibly altered pathways. Overlapping the metabolites with the increase in transcript changes of the respective genes and the decrease in concentration of the few measured metabolites, it is likely that the flux through both pathways increases. An increased glutathione metabolism is a well-established

[8] gene set analysis of genes as keys and metabolites as values

feature of proliferating cells to detoxify the increased amount of reactive oxygen species [9] [37]. Phosphatidylinositols are a diverse group of membrane lipids, whose signaling function, which regulates cellular key processes like differentiation, proliferation and apoptosis in normal and cancer cells, has been recognized over the past decade [204] [45] [33]. An interesting reporter metabolite is the metabolite nitric oxide. The nitric oxide synthesizing genes, especially NOS2, which is participating in the urea cycle, are highly upregulated (log2 fold change of 3.4) in comparison to healthy control cells. Although none of the other urea cycle intermediates (except for mitochondrial aspartate) is predicted, a higher flux in the urea cycle might be an explanation for the increase of the urea cycle metabolites in the media. The reporter metabolite analysis fails to predict most of the observed extracellular metabolite changes. Limited knowledge about transporters and their specificity might be a possible explanation.

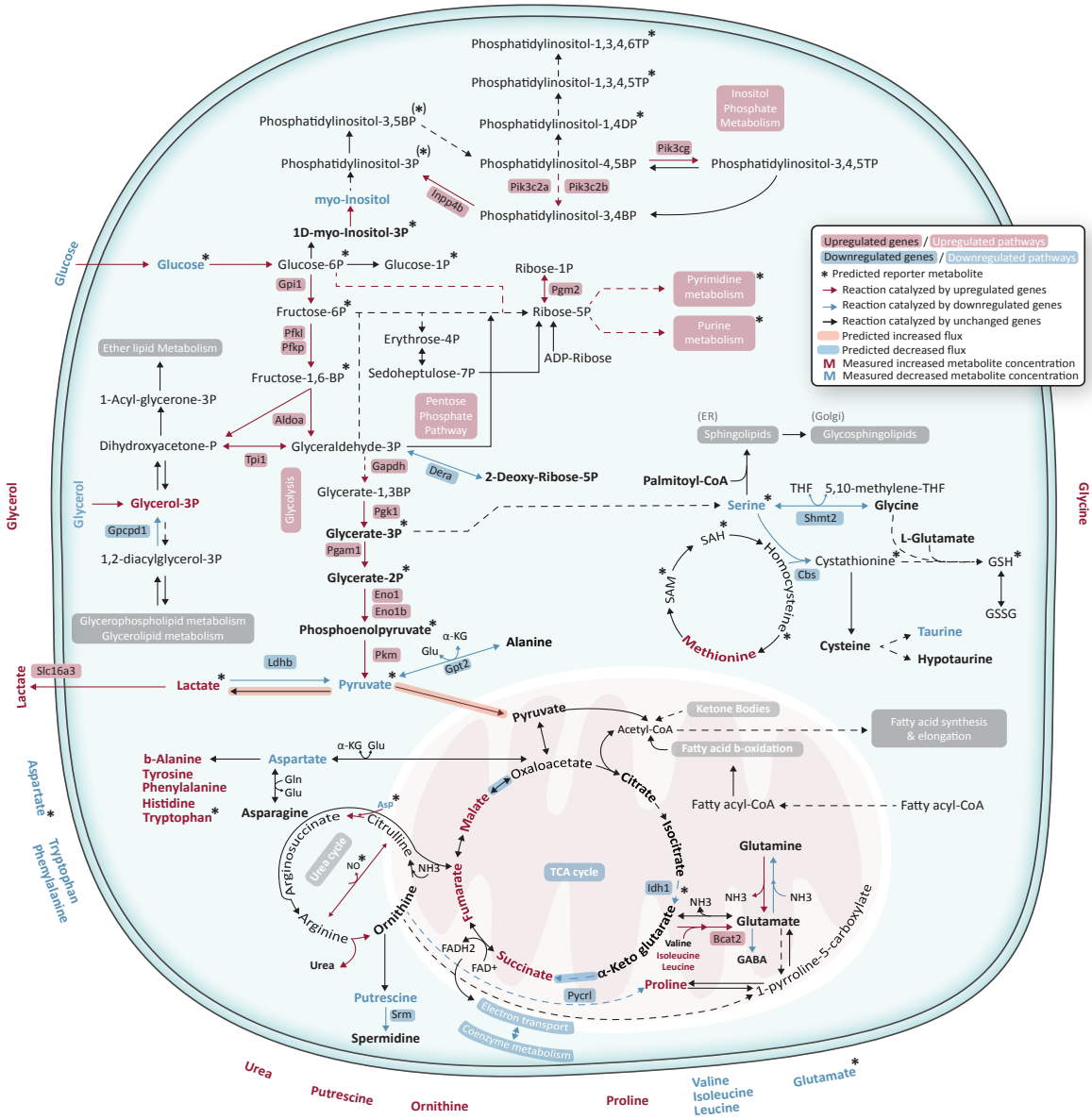

FIGURE 4.8. Overview of molecular changes in the regressed breast cancer cells in comparison to the healthy control cells. A selection of significantly altered genes ($p_{adj} < 0.01$), targeted metabolites ($p_{adj} < 0.01$, log2 fold change > 0.5) and reporter metabolites ($p_{adj} < 0.1$) of core metabolic processes are doverlaid. The two reporter metabolites in brackets are predicted to be changed in the endoplasmic reticulum. The figure design was reproduced from Oatley et al. (2018) and has been originally designed by Gisela Luz Machado. The contents of the original and the presented figure have been developed by myself. Adapted from Oatley et al. (2018). (Oatley 2018).

Overlapping the reporter metabolite predictions from the tumor with the metabolite measurements for the regressed structures shows, as expected, a high level of agreement for metabolites of the glycolysis (Figure 4-9, Table A.30). Probably connected to the higher glycolytic flux also purine and pyrimidine intermediates are still predicted to be changed. Likewise, many reporter metabolites fall into the pathways of phosphatidylinositols and cell surface marker synthesis and are accompanied by the same transcriptional changes. Interestingly, the urea cycle intermediate nitric oxide is consistently predicted. Together with the high upregulation of most genes from the urea cycle in comparison to healthy cells (NOS2 e.g. exhibits a log2 fold change of 6.7) and the persistent increase in the media concentration of its metabolites, this could hint at the possibility that the urea cycle is, aside from the glycolysis, a second pathway whose change/levels influences the metabolic phenotype of the regressed cells. Interestingly, nitric oxide has been shown to be regulated by HIF-1α and itself also to activate HIF-1α. However, for the TCA cycle intermediates as well as the amino acids, the metabolite changes predicted by the transcriptome only partially overlap with measured metabolite levels (Figure 4-9). The first half of the TCA cycle is transcriptionally downregulated in comparison to the healthy control but none of the metabolite concentration changes whereas the concentration of TCA cycle intermediates of the second half increase but without any transcriptional changes associated. The decreased transcription of enzymes in the first half of the TCA cycle could also be connected to the activity of HIF-1α as active HIF-1α leads to an inhibitory post transcriptional modification of PDH. Furthermore, the glutathione pathway is an interesting case, since the same reporter metabolites and metabolite concentrations as in the tumor are predicted and measured, but the connected genes, which are upregulated over the control in the tumor, are unchanged or downregulated in the regressed cells. This could be an example in which the measured metabolite concentrations remain the same, although the flux through the underlying pathway decreases. Lastly, one observation from the reporter metabolites is that in the case of cytosolic aspartate and proline the D-enantiomers are predicted to change. Both metabolites also possess a change in the concentration of the intracellular and extracellular fractions of the regressed samples. Since the measurement cannot distinguish between the L- and the D- variant it is a possibility that the ratio of the enantiomers is altered in the regressed state. Finally, in order to interpret the measured metabolite changes and suggest whether related pathways are likely to be increased or decreased fluxes were predicted from genome scale mouse model, which was tailored by the transcriptome data. Flux predictions have the advantage to take into account the balance of the whole metabolic network when mapping the transcriptional changes. Since the metabolic network has many degrees of freedom, this results at the same time in overall viewer changes then simple enrichment methods. Furthermore, depending on the extent to which the transcriptomic changes are translated into flux changes distant parts of the network might be less likely to exhibit any change in flux distribution. Fluxes can be particularly suited to highlight redundancies in the metabolic network by alternate pathway solutions. The flux predictions correctly show an increased flux through

the glycolytic branching point (Figure 4-9, Table A.31). The uptake pathway is not predicted to change under simulating growth optimality since glucose is the growth limiting metabolite in both models. Notably, the model predicts a decreased flux through the TCA cycle at the entry and exit points of succinate and malate. Furthermore, the flux of malate leaving the mitochondria is predicted to stop completely. Combining this prediction with the potential increase of the flux through the urea cycle, as suggested by the reporter metabolite analysis, could offer a possible explanation for the measured increase of the intracellular concentrations of the TCA cycle intermediates fumarate, malate and succinate. The urea cycle potentially feeds the TCA cycle by producing fumarate, which accumulates because of the decreased enzyme levels and/or fluxes in the TCA cycle. This hypothesis is supported by *in vivo* experiments, which could validate increased protein levels for ARG1 as well as an increase in NOS activity for regressed cells (ongoing work; personal communication, Ksenija Radic, EMBL Heidelberg). Intriguingly, high levels of fumarate and succinate stabilize HIF-1α levels, which in turn inhibits the succinate dehydrogenase oxidizing succinate to fumarate [56] [123]. It is imaginable, that through HIF-1α a metabolite driven (NO, succinate, fumarate) feedback loop is active, which supports HIF-1α activity in regressed cells and reinforces a glycolytic phenotype. An active glycolysis, which on the first sight contradicts the quiescent phenotype, could be one possible mechanism by which the regressed cells circumvent apoptosis [58] [76] [87] [19].

4.3.5 Comparing regressed cells from patient samples high glycolysis and urea cycle can be found in regressed samples of basal like HER2 positive cancer

Next I investigated if the observed transcriptional changes in the regressed breast cancer cells of our model system, which manifest on the metabolome level, translate to the patient situation. Therefore, two different publicly available microarray data sets of pre-treatment breast cancer tumors, post-treatment biopsies and healthy breast tissue were downloaded and analyzed [64] [114]. This comparison takes a novel perspective in the field of breast cancer patient data analysis as there is no study available yet, which collected and comprehensively analyzed all three types of samples. Comparable to our *in vitro* data, the post treatment samples cluster apart from the healthy control tissue as well as the pre-treatment tumor samples (Figure 4-10a). All of the three sample types gather exclusively amongst them, although the tumor samples as well as the regressed samples spread more than the healthy tissue samples. But since the pre- and the post-treatment group are from the same data set, the bigger spread could also be due to batch effects. When displaying the same data according to the diagnosed tumor type, the different groups group surprisingly well amongst each other, albeit their different treatment status. Furthermore, the first PC seems to distinguish between estrogen receptor (ER) positive and negative sample types. The ER status is one of the major markers for classifying breast cancer types and following therapy approaches. Thus, it can be concluded that the biological variation in the integrated

data set is bigger than the technical variation and that despite the treatment the post treatment group carries a substantial tumor memory.

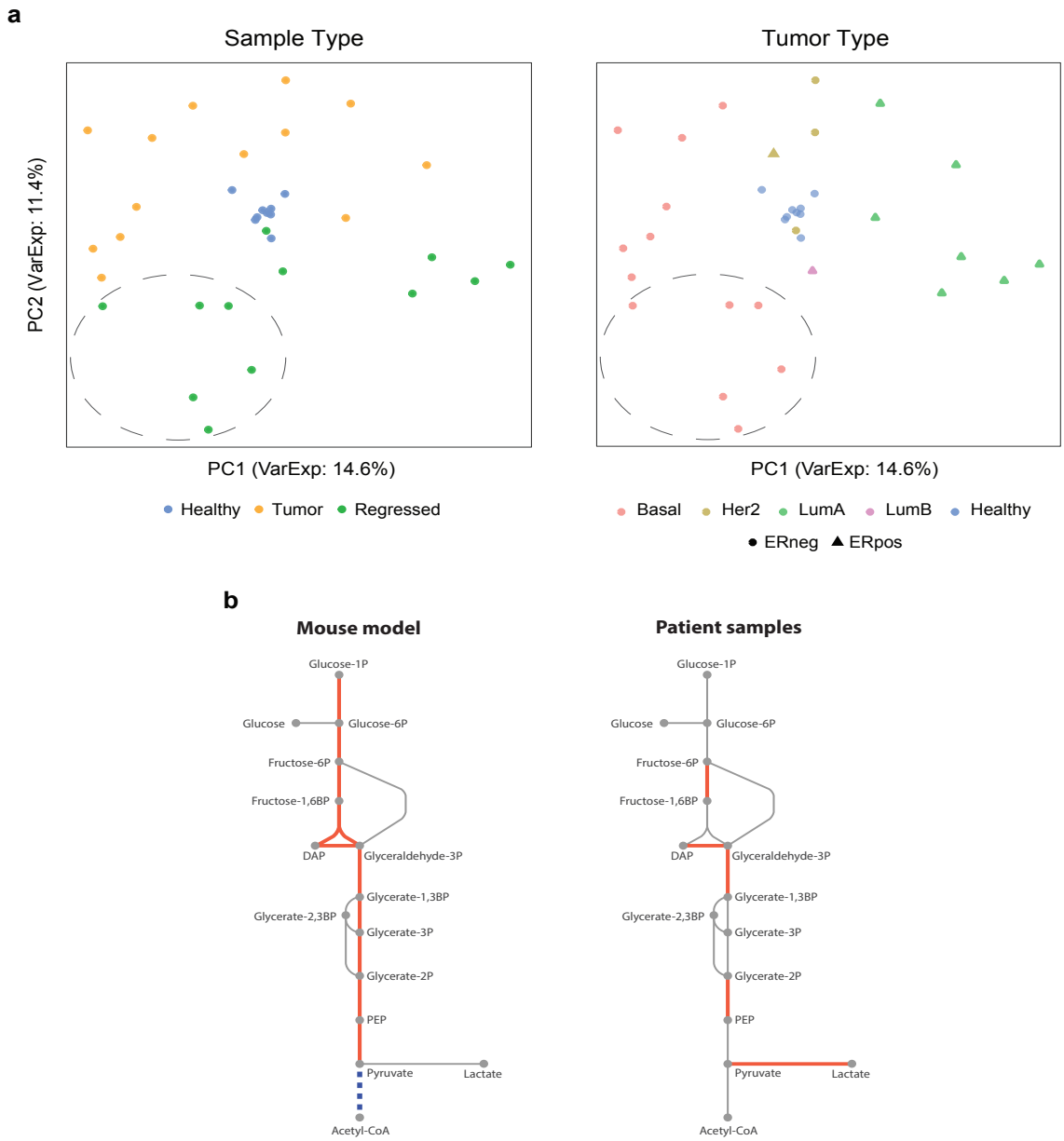

FIGURE 4.9. Joint analysis of publicly available microarray data of patient samples. Pre- and post-treatment breast cancer biopsies were contrasted with samples from healthy breast tissue. (a) Dimensionality reduction plots from the common subset of quantified genes colored by sample group or diagnosed tumor type. Encircled is the regressed basal HER2 negative subgroup, which was taken for the comparison with the *in vitro* data in b. (b) Differentially expressed glycolytic genes from the patient data over the healthy biopsies (p_{adj} <0.1). Differentially expressed glycolytic genes (p_{adj} < 0.01) from the *in vitro* mouse data of the regressed cells are depicted in comparison.

Next, I investigated if similar transcriptional signatures with regard to metabolic changes are present in the combined data as in our *in vitro* samples. Therefore, I decided to compare the data with the subset of basal HER2 negative samples since amongst the present tumor subtypes this sample group is the closest to the cancer type developed in our system. The basal HER2 positive subtype would be even better suited, but unfortunately there is only one sample available of this subtype. Reassuringly, the same glycolytic alterations on the transcript level were found in the basal HER2 negative subgroup, even though a little less pronounced (Figure 4-10b). Increased glycolysis does not seem like a common transcriptional alteration of all regressed cancer samples, as for instance the samples of the (less aggressive) Luminal A+B subtypes exhibited no glycolytic alterations. Increased glycolytic flux could be one feature of cancer cells generally more resistant to therapy. Furthermore, one of the enzymes of the urea cycle exhibited an increased expression in the basal HER2 negative post treatment samples (Figure A.23 a,c). Although not conclusive because of missing replicates, but still noteworthy, the one basal HER2 positive sample also showed a concomitant upregulation of the urea cycle in comparison to the healthy tissue samples having exactly the same enzymes altered as in our model system (Figure A.23 b). Finally, the nucleotide metabolism is also concordantly upregulated in the basal HER2 negative samples in comparison to the healthy samples, which could be connected to the observed upregulation of the glycolytic enzymes as the nucleotide metabolism is fed from glycolytic intermediates (Figure A.24a-c).

4.3.6 Irreversible imprinting of the tumor state on methylome level?

The observation, that the transcriptome of regressed breast cancer cells, *in vitro*, *in vivo* and in patient samples is stably deregulated with an upregulation of genes from the glycolysis and the TCA cycle as a repetitive feature poses the question, how these transcriptional alterations become stably imprinted. This question is even of bigger relevance since we could show that the transcriptomic alterations manifest in a globally altered metabolic state mirroring the metabolic state of tumor cells. A possible explanation could be a permanent change of the epigenetic landscape towards more active transcription. This hypothesis gets supported by the fact that the intracellular metabolic concentrations of the TCA cycle intermediates fumarate and succinate (which are increased in the tumor and the regressed state) have recently been shown to regulate methylation in cancer cells [198] [100] [101]. One additional hint might be the observation that c-MYC unrelated genes with increased expression in the regressed cells in comparison to the healthy cells cluster locally on the genome, as it is for example the case on chromosome 15 (Figure 4-11).

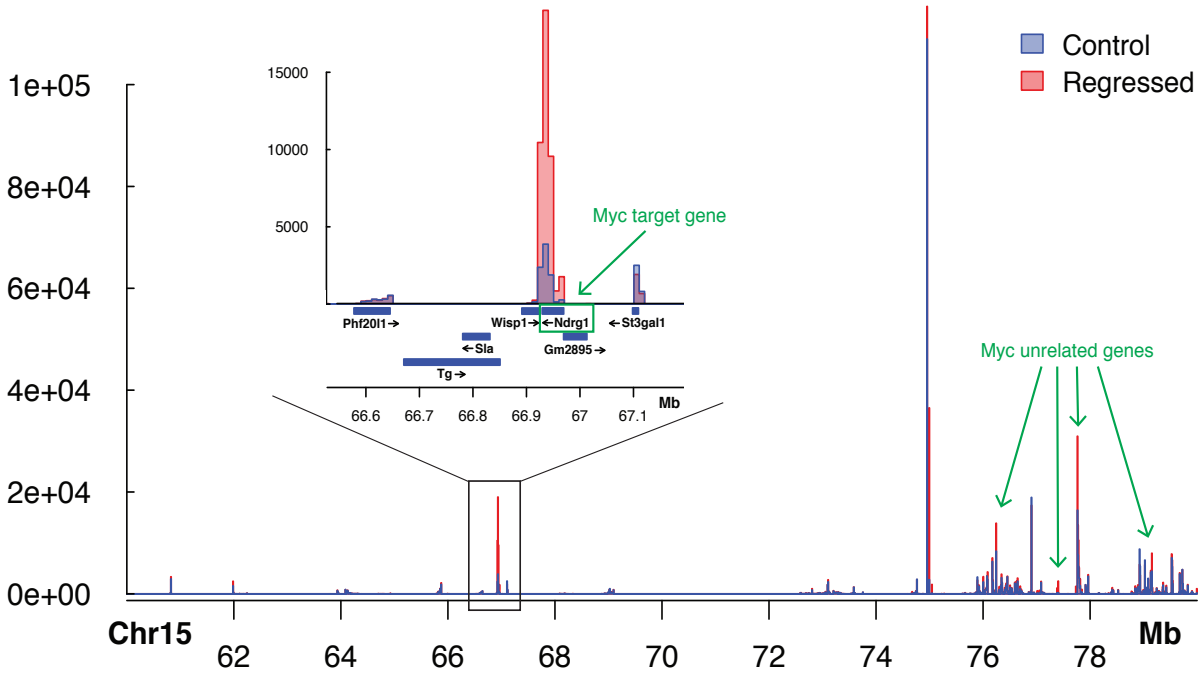

FIGURE 4.10. Read counts aligned at a detail from chromosome 15 as an example of physically clustered c-MYC unrelated genes. Physical read clusters of differentially expressed genes ($p_{adj} < 0.01$) in the regressed cells in comparison to the control of c-MYC target genes and c-MYC unrelated genes.

4.4 Conclusions and future directions

The preceding chapter assessed the molecular adaptations of breast cancer cells during tumor formation and after tumor regression. Surprisingly, although phenotypically undistinguishable from healthy cells, it could be demonstrated that regressed breast cancer established an oncogenic memory after the complete withdrawal of oncogenes. The memory appeared to be more dominant on the metabolome level, with the majority of the measured metabolites coinciding between the tumor and the regressed samples. Intriguingly, however, on the transcriptome level the expression of genes largely varied between tumor and regressed cells with the majority of genes being uniquely altered in the tumor cells. The rather few number of genes, which overlapped between the tumor and the regressed cells on the transcriptome level, in turn, possessed the same trend in their expression levels. The latter observation poses three questions: 1) are the few observed transcriptional changes sufficient to drive or maintain the metabolic tumor phenotype in regressed cells 2) are alternate metabolic paths tunneling into the same metabolic phenotype; 3) do the same metabolite concentrations actually correspond to the same fluxes and therefore metabolic phenotypes. Analysing the transcriptome and metabolome data in greater depth and integrating them with flux data and genome scale modeling techniques, confirmed a high glycolytic flux amongst both, the tumor and the regressed, phenotypically quiescent cancer cells. This increased glycolytic activity is strongly deregulated on the transcriptional and the metabolic level in both cell types analyzed and exhibits a few alternate isoenzymes being differentially expressed. A second potentially important deregulated pathway for maintaining the metabolic cancer phenotype in regressed cells is a concomitant upregulation of enzymes from the urea cycle with a coupled increase of urea cycle intermediates suggesting an increased metabolic flux through the urea cycle. The tight connection between transcriptional and metabolomic changes in these central pathways support the idea that few but important alterations might be sufficient to influence the global metabolite level towards the metabolic cancer phenotype. The TCA cycle metabolism, in contrast, could be an example of how the same metabolite levels could result from different fluxes: In the tumor, an upregulated expression of enzymes from the TCA cycle in comparison to the healthy control is coupled with a highly increased intracellular and extracellular concentration of the TCA cycle intermediates, succinate, fumarate and malate. This suggests an increased flux through the TCA cycle. However in the regressed cells, the same high level of increased metabolite concentrations is coupled with a clear decrease in transcript abundance and the predicted decrease of TCA cycle flux in comparison to the healthy controls. The ROS or hypoxia induced stabilization of HIF-1α as well as the TCA cycle intermediates succinate and fumarate could have a central role in connecting the increased flux through the glycolysis with the increase an decrease of fluxes of the urea cycle and TCA cycle, respectively. Except for isoenzymes in the glycolysis, I found no evidence of alternative pathway routes being active, however it might be difficult to identify them in less central pathways. It might be interesting to investigate probable signaling routes of the oncogenes cMYC and HER2 or the

transcription factor HIF-1α. The presented transcriptomic analysis focused mostly on enzyme levels rather than genes with regulatory functions. By following these signaling routes novel causal crosslinks to other signaling proteins or to metabolic changes may appear. This might however be impeded by posttranslational modifications, playing a major role in regulatory signaling cascades. The interplay between the transcriptional and metabolome level in MRD should be further investigated by integrating the lipidomics and untargeted metabolomics data in the genome scale modeling approach. The genome scale modeling approach could additionally be extended by integrating the measured changes of extracellular metabolite concentrations in the model as uptake and secretion constraints. Therefore, metabolomics measurements of absolute concentrations with calibrated standards need to be performed. Predicting metabolic fluxes with these additional constraints could increase the extent and specificity of the predicted metabolic fluxes that are likely to change. Alternatively, also known posttranscriptional modifications such as the inhibition of PDH under HIF-1α activity could be implemented to increase the precision of the predicted fluxes by minimizing the degrees of freedom. Finally, the mouse GEMM can also be improved by tailoring it to mouse specific reactions. A comprehensive integration of the three metabolomics datasets focusing on the common features amongst them might be gained by integration with MOFA [8]. This might identify additional major "driver" pathways, which could be specifically interesting for detangling potential regulatory roles of phosphatidylinositols. On the experimental side it could be interesting to test whether Hif1α is indeed active and causal for the glycolytic phenotype. In this case it could be further investigated if its activity influences metabolites in the urea and TCA cycle and vice versa. Furthermore, studying whether the glycolytic flux has a flux regulatory role or inhibitory role on apoptosis independent from HIF-1α is another intriguing question. It would furthermore be interesting to analyze whether the epigenetic landscape in regressed cells in comparison to healthy cells and if these changes are influenced by TCA cycle metabolite concentrations and finally if they could be possibly linked to the observed and predicted stable changes in flux patterns.

CHAPTER 5

General Conclusion

In this dissertation, metabolic adaption was analyzed in two different contexts. First towards a new nutritional environment and then in the context of oncogenic signaling. The second chapter showed how metabolic networks quickly adapt to the new stimuli, leveraging two key features of metabolic networks, redundancy and plasticity. The redundancy of metabolic network regulation instantly becomes obvious in the context of glycerol adaptation, where independently two different pathway solutions of adaptation evolved, one via abolishing the HOG pathway and one abolishing the two genes *KGD1* and *UBC13*. However, this study also showed the limitation of the metabolic network redundancy for the alternate carbon source glycerol, as both alternative pathways were tied to metabolic trade-offs in other environments. The results of this thesis show that the two novel mutations *KGD1* and *UBC13* are causative and sufficient for the glycerol growth phenotype. Furthermore, this new metabolic route for glycerol utilization was explained by a shift in the organism's redox-balance under glycerol consumption. This is the first time a mutation in the context of glycerol utilization other than *GUT1* could be mechanistically linked to metabolism. Third, a novel regulatory cross-link between the K63-specific ubiquitinylation machinery and carbon-source driven metabolic fluxes was discovered. In human cells, the extent of plasticity in metabolic network regulation facilitating adaptation was recently demonstrated in the context of hematopoietic stem cell development. The metabolic state of a developing proliferative stem cell population was completely altered to a metabolically quiescent state [128]. These findings illustrate that metabolic adaptations of cells to a new cellular state are an important process occurring during stem cell development. Studying metabolic network adaptation in breast cancer reveals metabolic adaptations accompanying the transition of a differentiated cell to a cancer cell in order to fulfill the demands of a proliferative phenotype. However, after stopping oncogenic signaling, the cells failed to metabolically readapt to their original non-proliferative metabolic state. The metabolic network regulation shows an increase in robustness becoming independent from cellular signaling. The exhibited metabolic network plasticity and redundancy now reversely allow the stable rewiring of the regressed cancer cells prohibiting adaptation. The present findings show for the first time an oncogenic memory on metabolic level in residual cancer cells. Cancer cells are known to lose their metabolic plasticity through the hard wiring of artificial oncogenic signaling. What was unknown though is that this is a stable feature pervading in the regressed states even after the oncogenic signaling is stopped completely. An interesting hypothesis to study in this context will be the question if the robustness is supported by changes in the epigenetic landscape, possibly even induced by the altered metabolism or metabolite levels itself. I showed in this thesis that metabolic adaption is a very important process in eukaryotic cell physiology, ensuring the adequate response to environmental or intrinsic impulses. Plasticity and redundancy of metabolic networks have been shown to be key features of eukaryotic metabolic networks. While high levels of eukaryotic metabolic network plasticity and redundancy in the case of glycerol adaptation and also in cellular development facilitate the adaptive process of metabolism towards novel stimuli, in the context of cancer they enable the establishment of metabolic network

robustness. This on the contrary prohibits adaptation and leads to a stable state insensitive to adaptation mechanisms. During the evolutionary process of glycerol adaptation, natural selection governed adaptation. Similarly, the regulatory systems ensured metabolic adaptation towards the cellular state during the developmental process or at the beginning of oncogenesis. However, prolonged oncogenic signaling deregulates the metabolic regulatory network and lets network plasticity and redundancy enter an irreversible disease state, which is failing adaption. Thus, plasticity and redundancy can be beneficial in the context of adaption as long as the right regulatory mechanisms are in place ensuring an adaptive response to the extrinsic and intrinsic signaling events. To elucidate how plasticity and redundancy can promote metabolic adaptation or contrariwise hinder it, a better understanding of metabolic network regulation is needed. Specifically, the deregulation of metabolic networks in disease contexts such as cancer can be advantageous in deciphering metabolic disease mechanism. I hope this work has brought us closer to understand how adaptive processes alter metabolic networks by taking advantage of their structural properties. From a methodological perspective, genome-scale metabolic modeling has been used successfully to integrate and interpret multi-layer data obtained by various omics technologies such as genomics, transcriptomics, proteomics and metabolomics. Furthermore, I contributed to the field of genome-scale metabolic modeling and omics data integration by providing a revised human model optimized for flux balance analysis. As an extent to this approach the integration of other omics types could enrich the current workflow and explore further mechanisms of metabolic network regulation during adaptation e.g. by studying epigenetic imprints with methylome data. Lastly, as the metabolic network regulation was shown to play a key role in the metabolic adaptation process an integrative approach combining metabolic modeling with the mathematical modeling of kinetic signaling networks could be a valuable approach for future exploration. As the volume and diversity of high-throughput data will likely expand in future, the interpretation and integration of large multi-layered data will remain challenging. This thesis represents one attempt of tackling the question of how we can learn mechanistic insights from large and complex data volumes. Or how a former professor of mine paraphrased it how to “gain knowledge from this mess”.

Abbreviations

ALE - Adaptive laboratory evolution
WT - wild-type
NOX - NADH oxidase
ORF - open reading frame
USER - uracil-specific excision reagent
gDNA - genomic DNA
gRNA - guide RNA
CDW - cell dry weight
MNV - multi-nucleotide variant
SNV - single-nucleotide variant
SNP - single-nucleotide polymorphism
SV - structural variant
MA - mutation accumulation experiments
CNV - copy number variation
HOG - high-osmolarity glycerol
PPP - pentose phosphate pathway
R-GU - Reengineered strain with GUT1 and UBC13 mutation
R-GK - Reengineered strain with GUT1 and KGD1 mutation
R-GKU - Reengineered strain with GUT1, KGD1 and UBC13 mutation
YPD medium - yeast extract peptone dextrose medium
SPO medium - sporulation medium
M medium - mineral medium
MG medium - minimal glycerol medium
MG+ medium - minimal glycerol medium supplemented with amino acids
MD medium - minimal glucose medium
GEMM - genome-scale metabolic model
COBRA - constrained-based reconstruction and analysis
FBA - flux balance analysis
HMDB - human metabolome database
FVA - flux variability analysis
FC - Fold change
NI - Never induced
WT - Wild type
DE - Differentially expression
PPP - pentose phosphate pathway

TCA - Tricarboxylic acid
Oxphos - Oxidative phosphorylation
RNA - Ribonucleic acid
RNASeq - RNA sequencing
PCA - Principal component analysis
MRD - Minimal residual disease

Appendix A

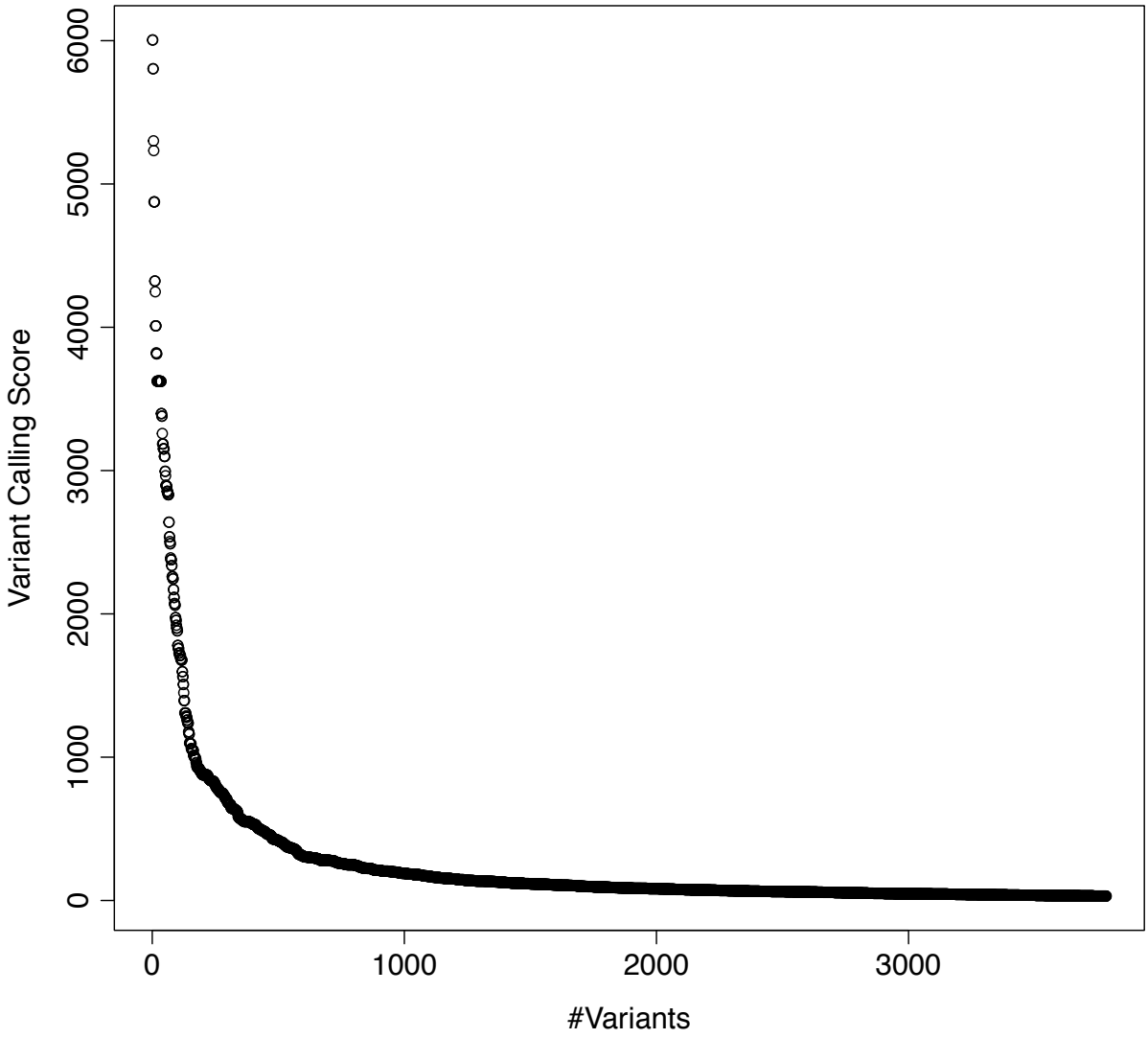

FIGURE A.1. Sorted distribution of variant calling scores from unfiltered variant calls of all WT and NOX endpoint as well as intermediate NOX lineages evolved with mode-I and mode-II.

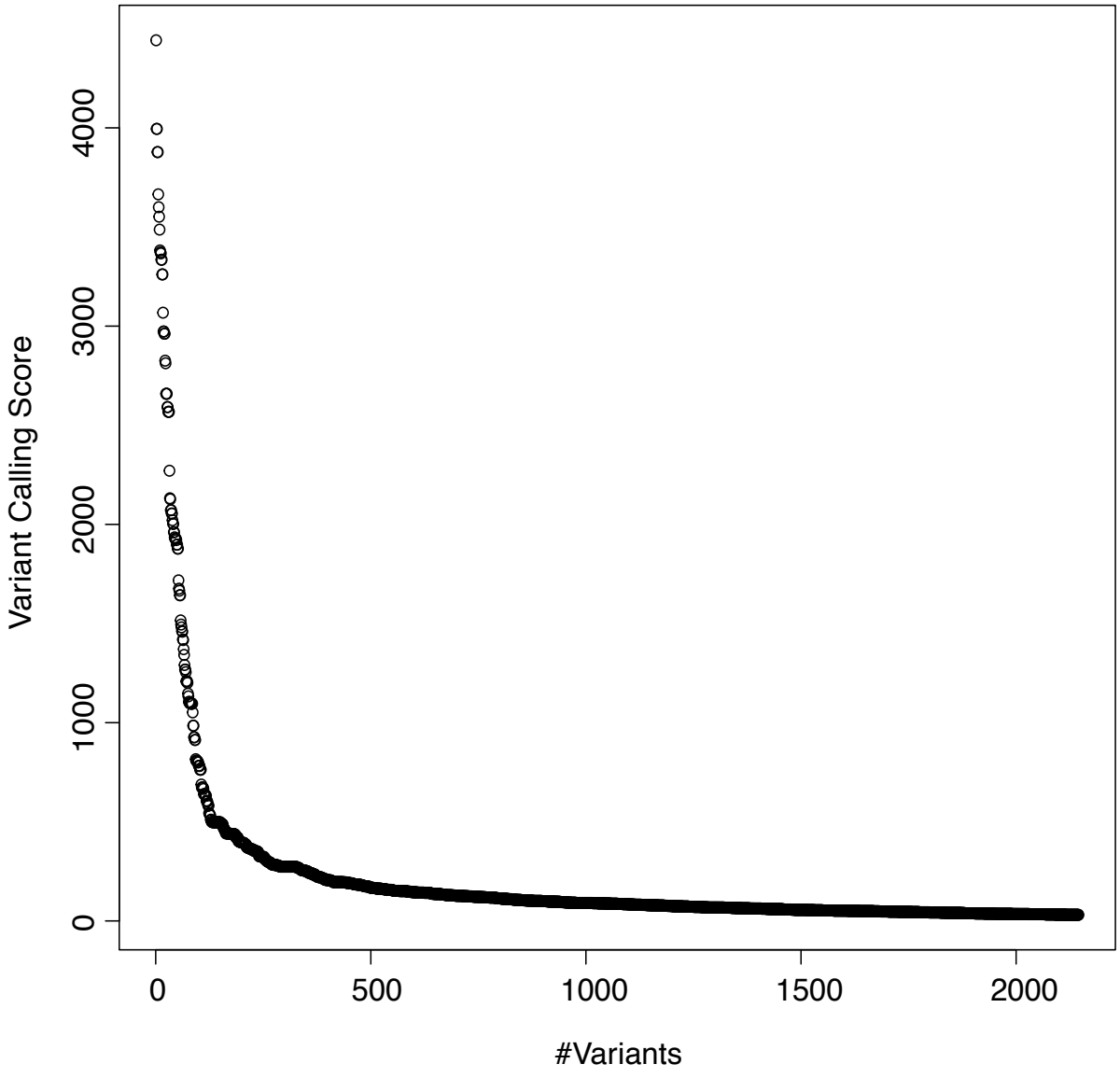

FIGURE A.2. Sorted distribution of variant calling scores from unfiltered variant calls of all sequenced tetrads.

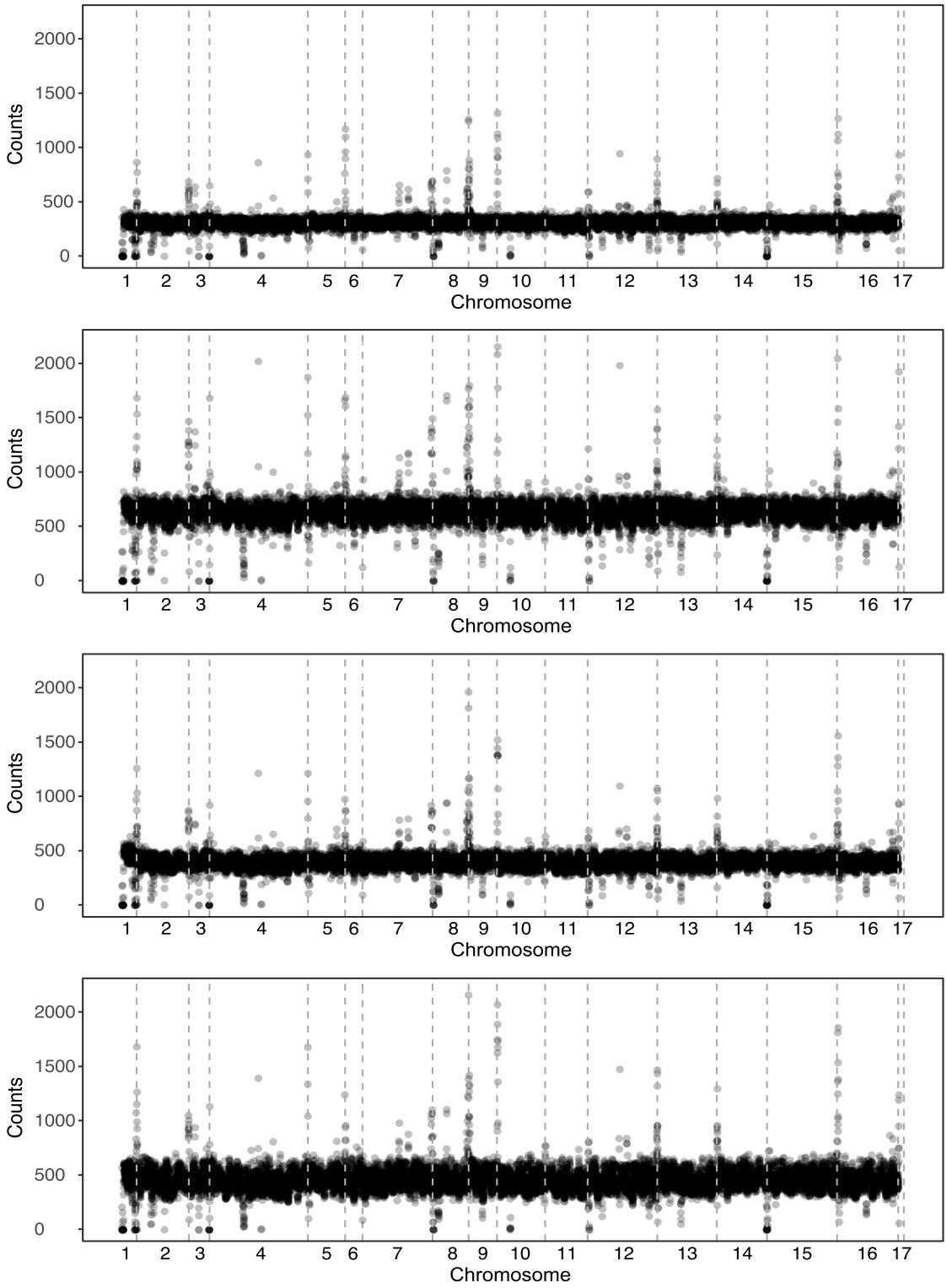

FIGURE A.3. Sequencing reads of the WT parental strain and the mode-II evolved WT lineages ALE1 to ALE3 aligned to the *S. cerevisiae* S288C reference genome and summarized in 1 kb windows.

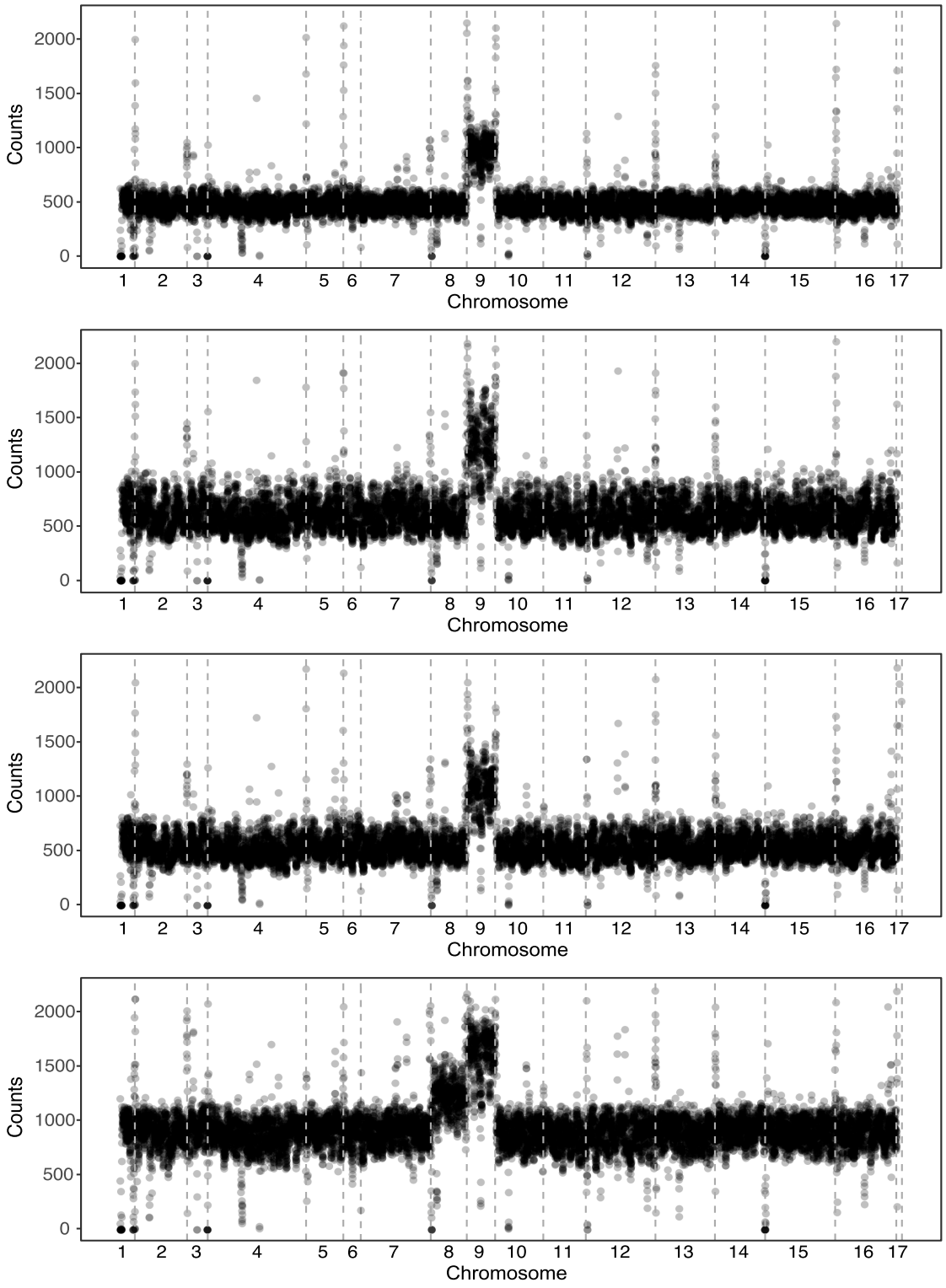
Counts
2000
1500
1000
500
0
1 2 3 4 5 6 7 8 9 10 11 12 13 14 15 16 17
Chromosome

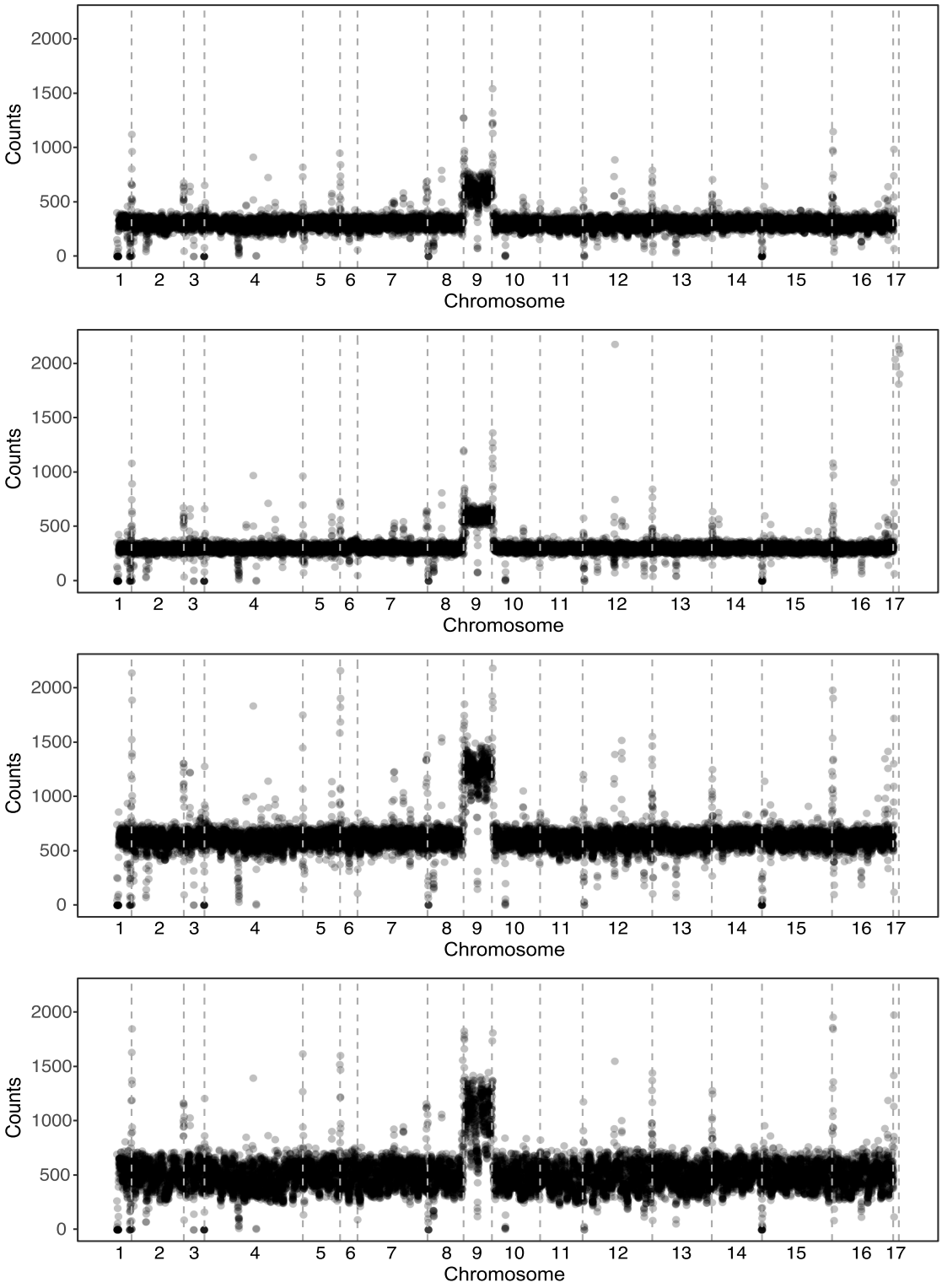

FIGURE A.4. Sequencing reads of the NOX parental strain and the mode-II evolved NOX lineages ALE5 to ALE11 aligned to the *S. cerevisiae* S288C reference genome and summarized in 1 kb windows.

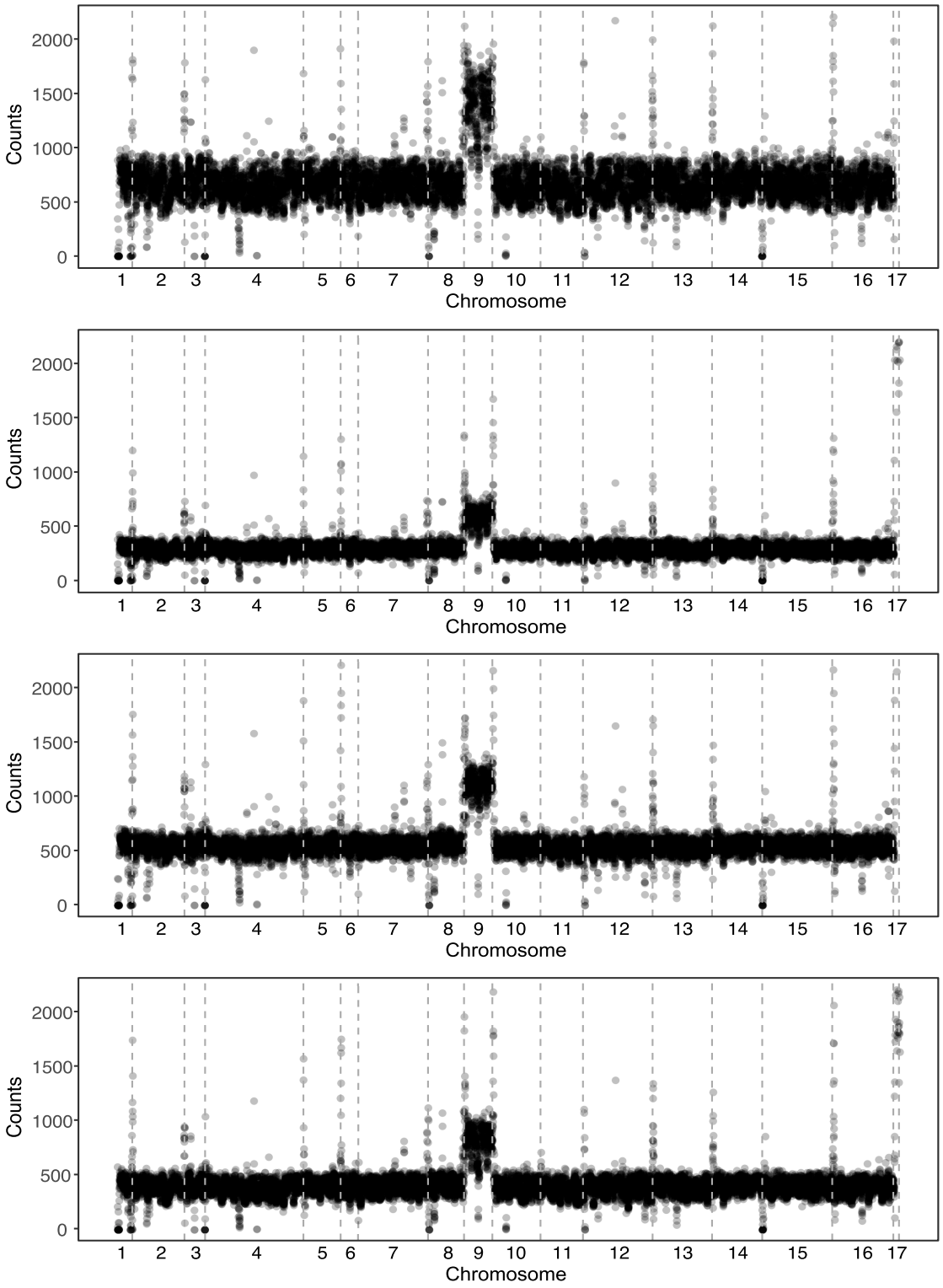
Counts
2000
1500
1000
500
0
1 2 3 4 5 6 7 8 9 10 11 12 13 14 15 16 17
Chromosome

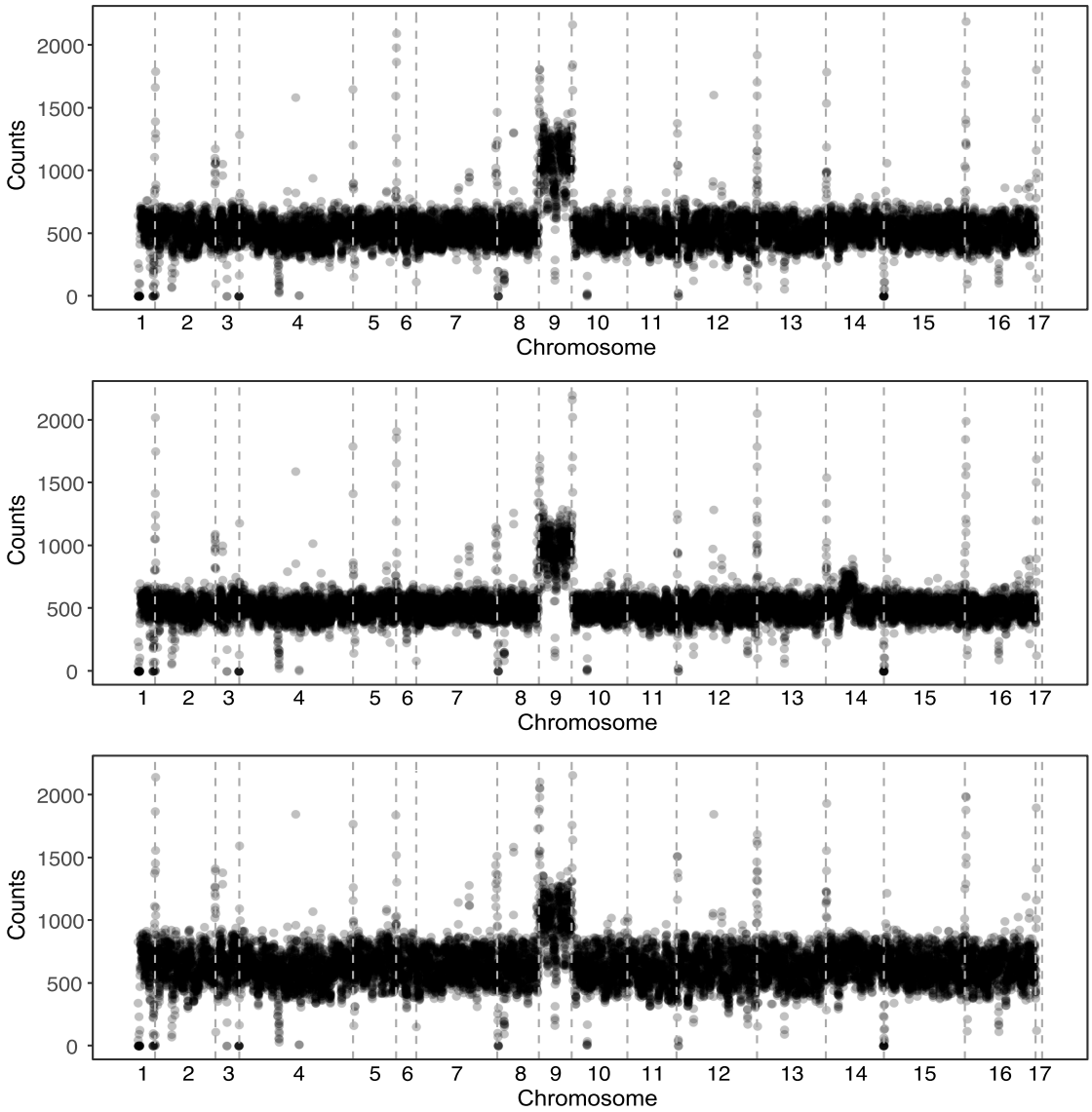

FIGURE A.5. Sequencing reads of the NOX parental strain and the mode-I evolved NOX lineages GEVO5, GEVO9, GEVO17, GEVO25, GEVO29, GEVO26, GEVO30 aligned to the *S. cerevisiae* S288C reference genome and summarized in 1 kb windows.

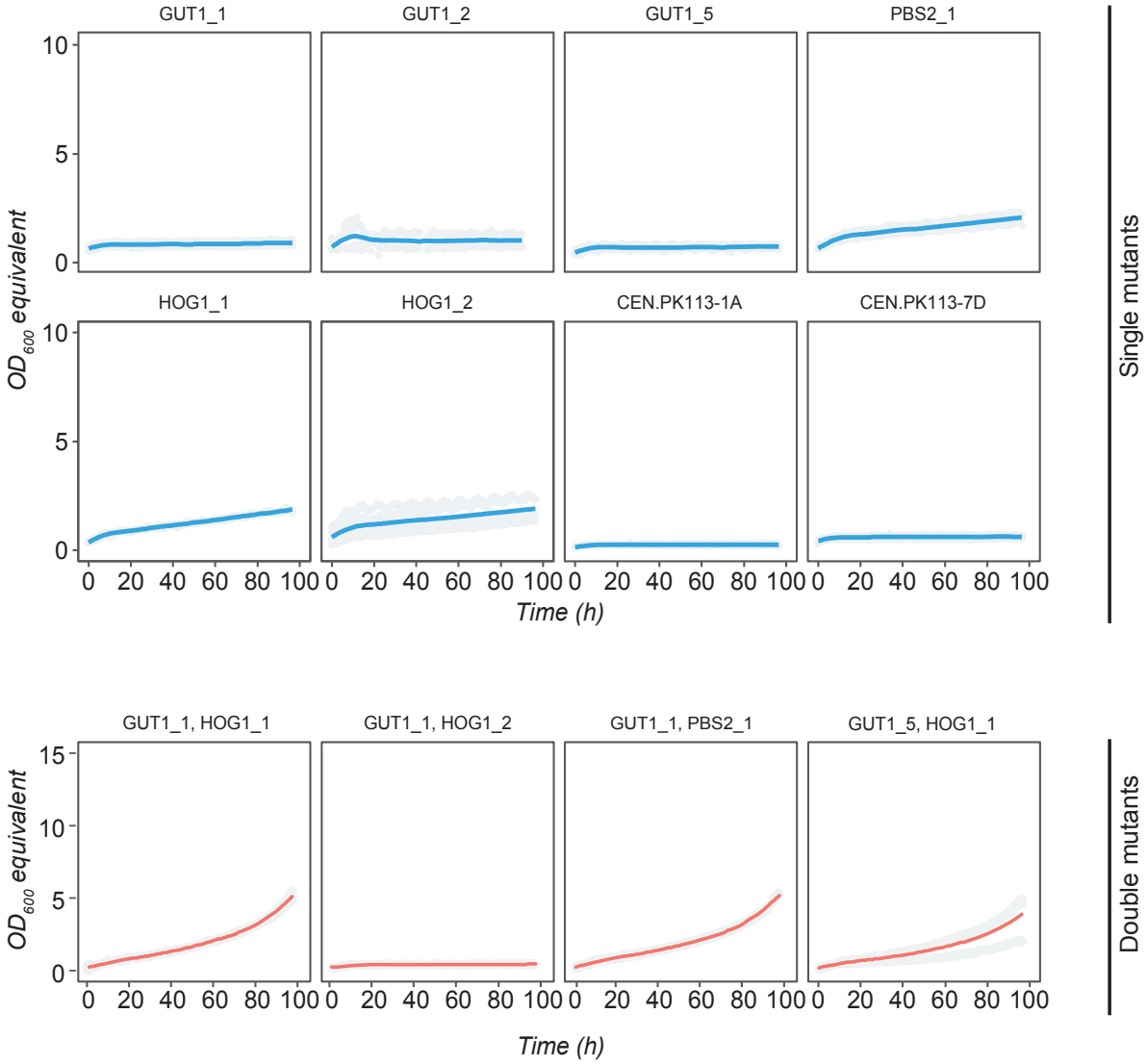

FIGURE A.6. Re-engineered single and double mutations found in evolved NOX lineages in wild-type background CEN.PK strains. Curves are plotted using R language using 'loess' method based on at least two biological replicates per experiment. *This figure and the corresponding legend text have been adapted from Strucko et al. (2018) [178].*

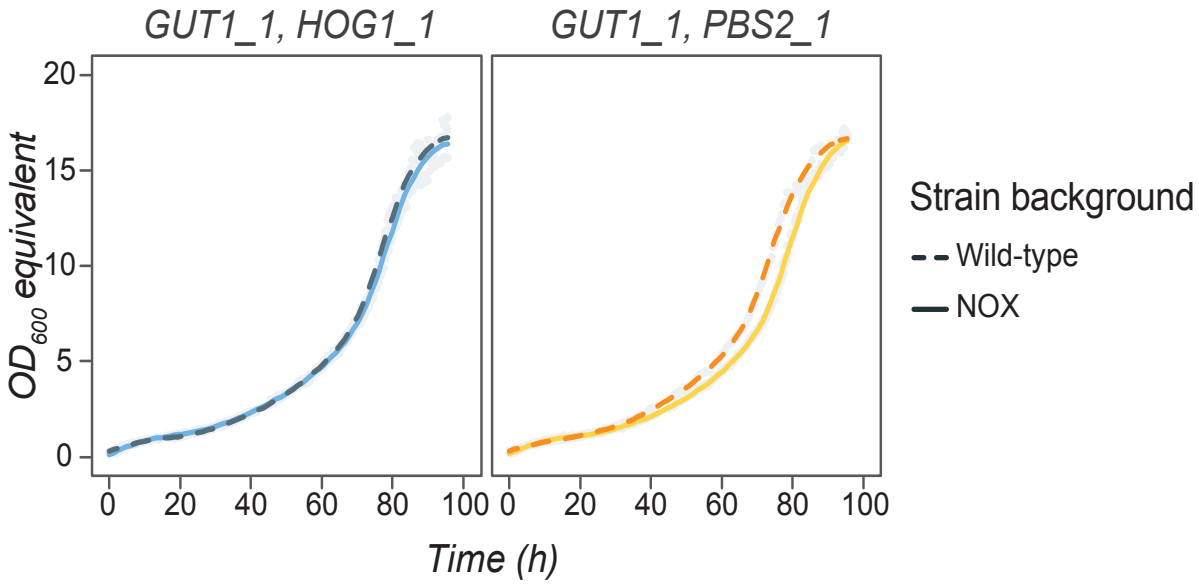

FIGURE A.7. Growth characteristics of double mutations found in evolved NOX lineages re-engineered in WT and NOX backgrounds. Curves are plotted with R language using 'loess' method based on two biological replicates. *This figure and the corresponding legend text have been adapted from Strucko et al. (2018) [178].*

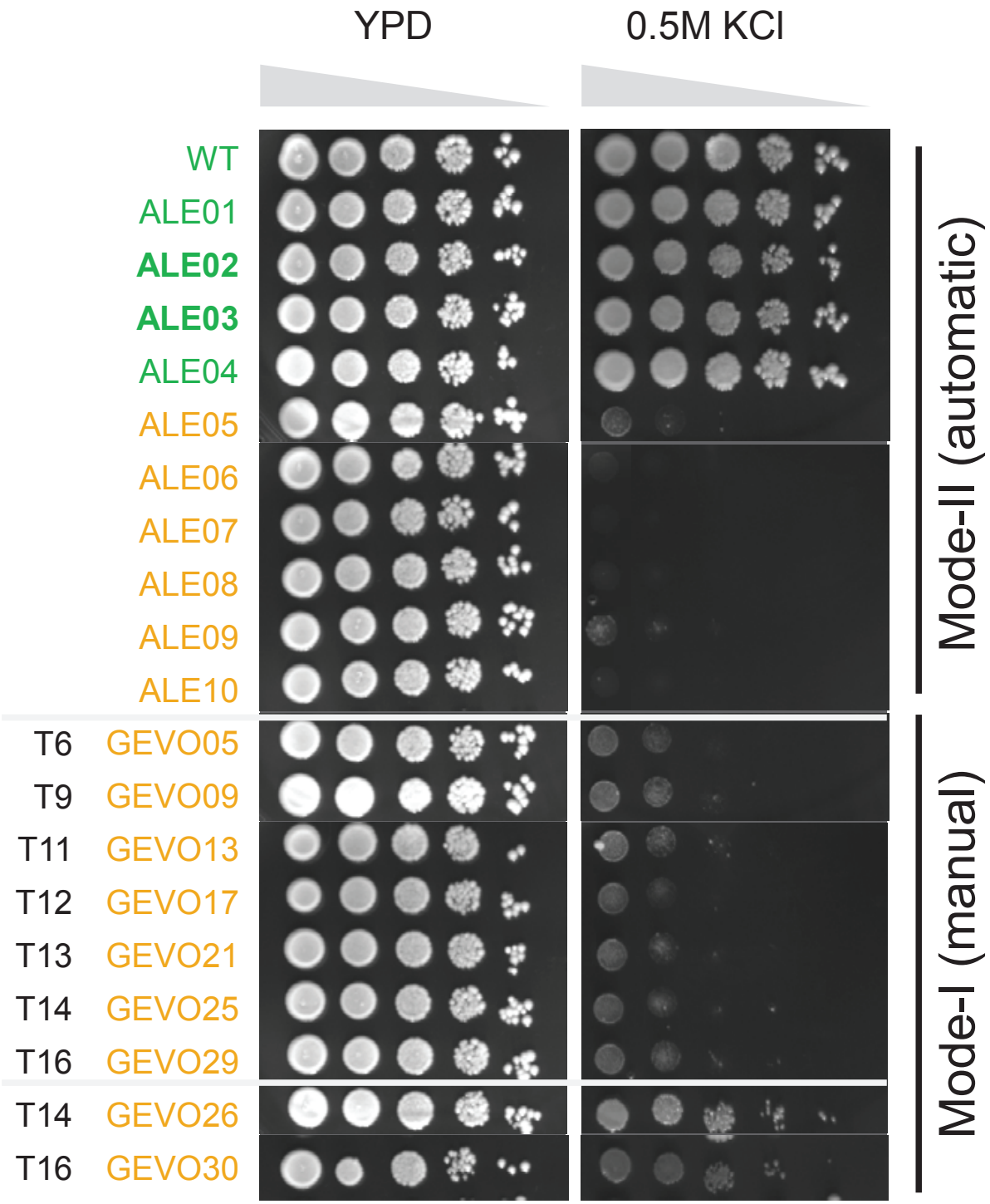

FIGURE A.8. Spot assay on the evolved lineages on the high osmolarity medium. Images were taken after three days incubation at 30 °C. Lineage names depicted in green originated from WT stain background, and in yellow – from NOX strain background. *This figure and the corresponding legend text have been adapted from Strucko et al. (2018) [178].*

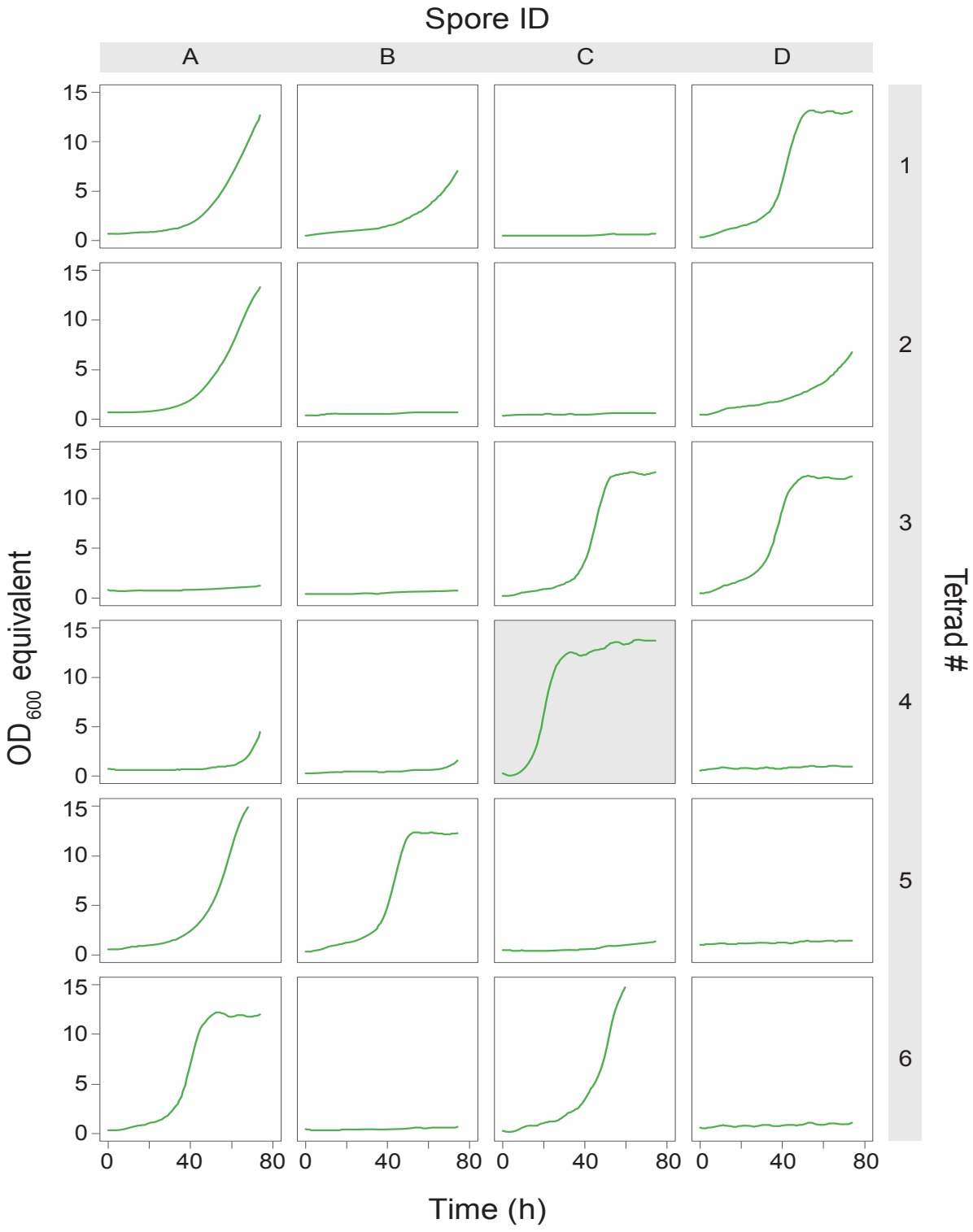

FIGURE A.9. Growth curves of the first generation spores in liquid MG medium. Highlighted squares represent the spore that was used for the following mating/sporulation analysis. Curves are plotted with R language using 'loess' method. *This figure and the corresponding legend text have been adapted from Strucko et al. (2018) [178].*

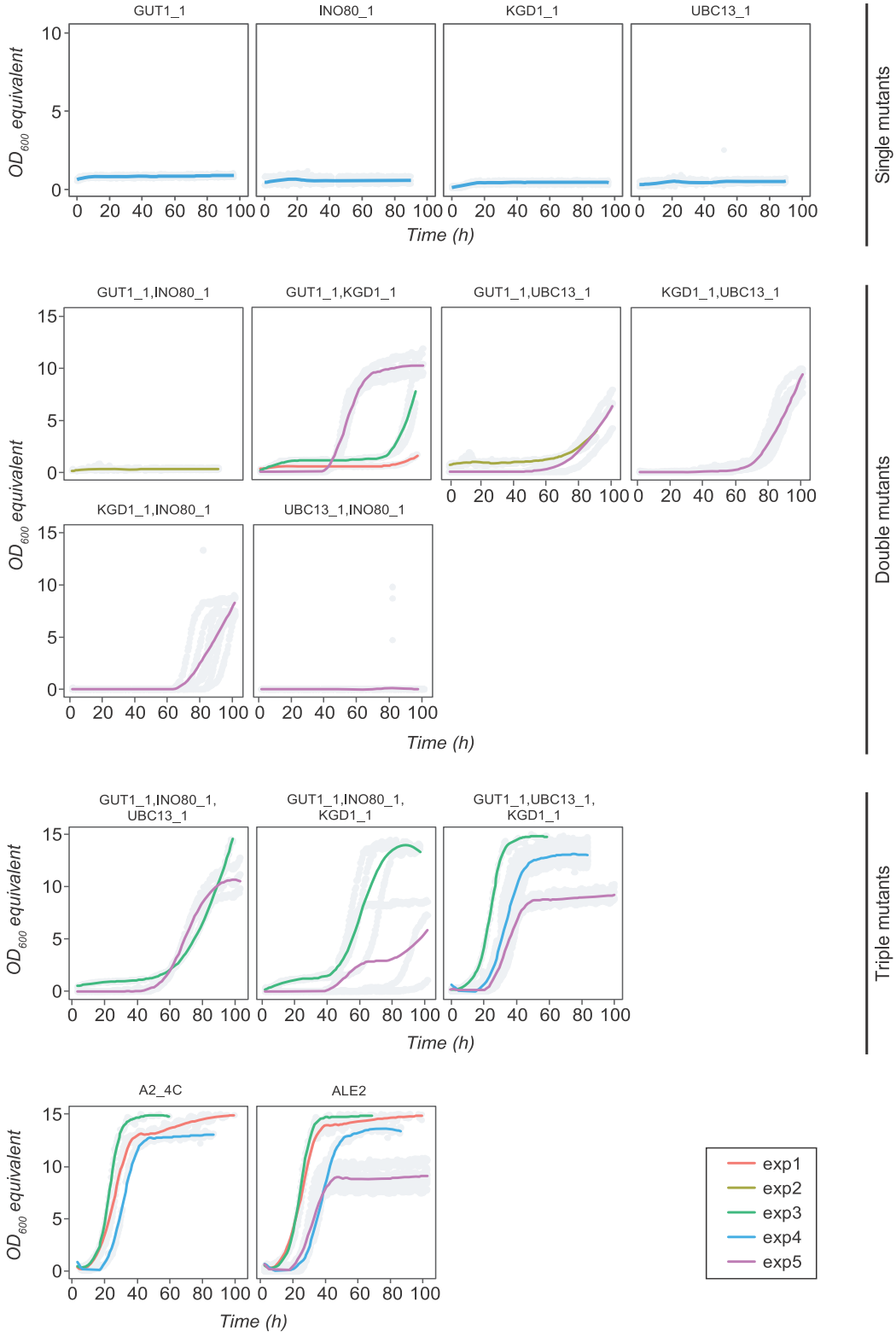

FIGURE A.10. Re-engineered single, double and triple mutations found in the ALE2 lineage in wild-type background CEN.PK strains. Curves are plotted with R language using 'loess' method based on at least two biological replicates per experiment (exp).

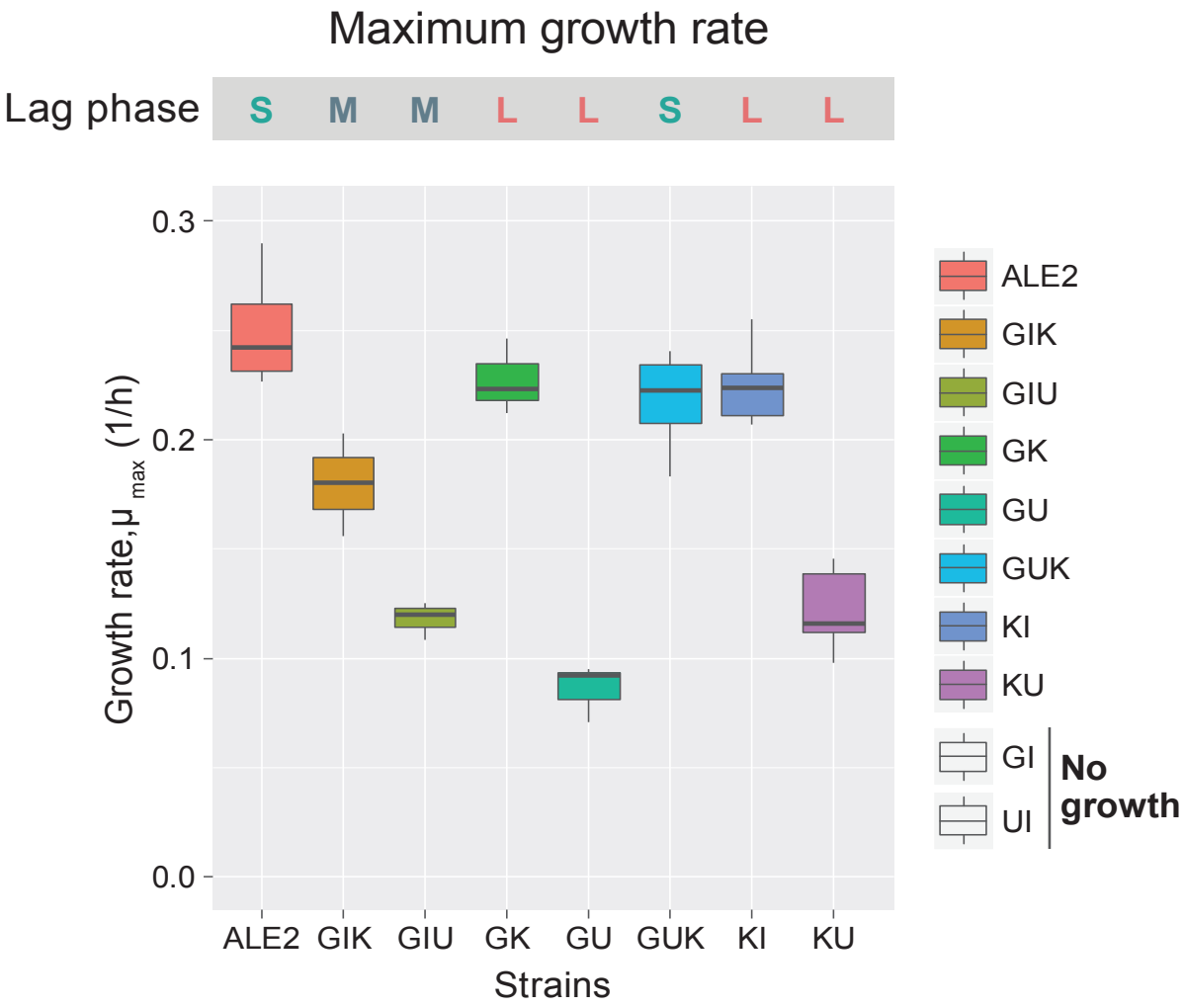

FIGURE A.11. Re-engineered double and triple mutations found in the ALE2 lineage in wild-type background CEN.PK strains. Curves are plotted with R language using 'loess' method based on at least two biological replicates per experiment. Growth rates are estimated using all replicates of five independent experiments. S = short, M = medium, L = long. G = GUT1, I = INO80, K = KGD1, U = UBC13. *This figure and the corresponding legend text have been adapted from Strucko et al. (2018) [178].*

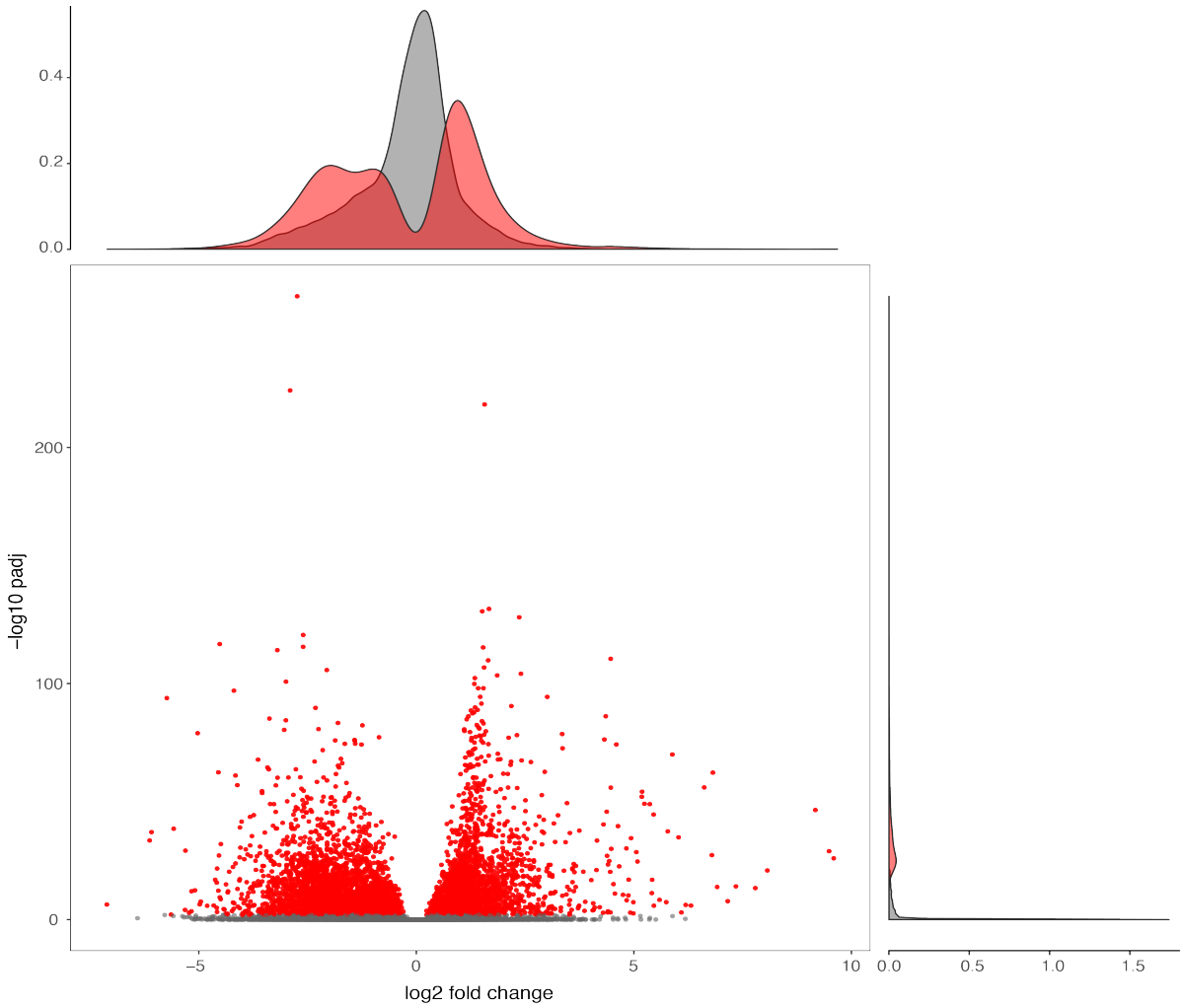

FIGURE A.12. Volcano plot highlighting the 5356 differentially expressed genes (padj < 0.01) comparing the tumor samples with healthy controls.

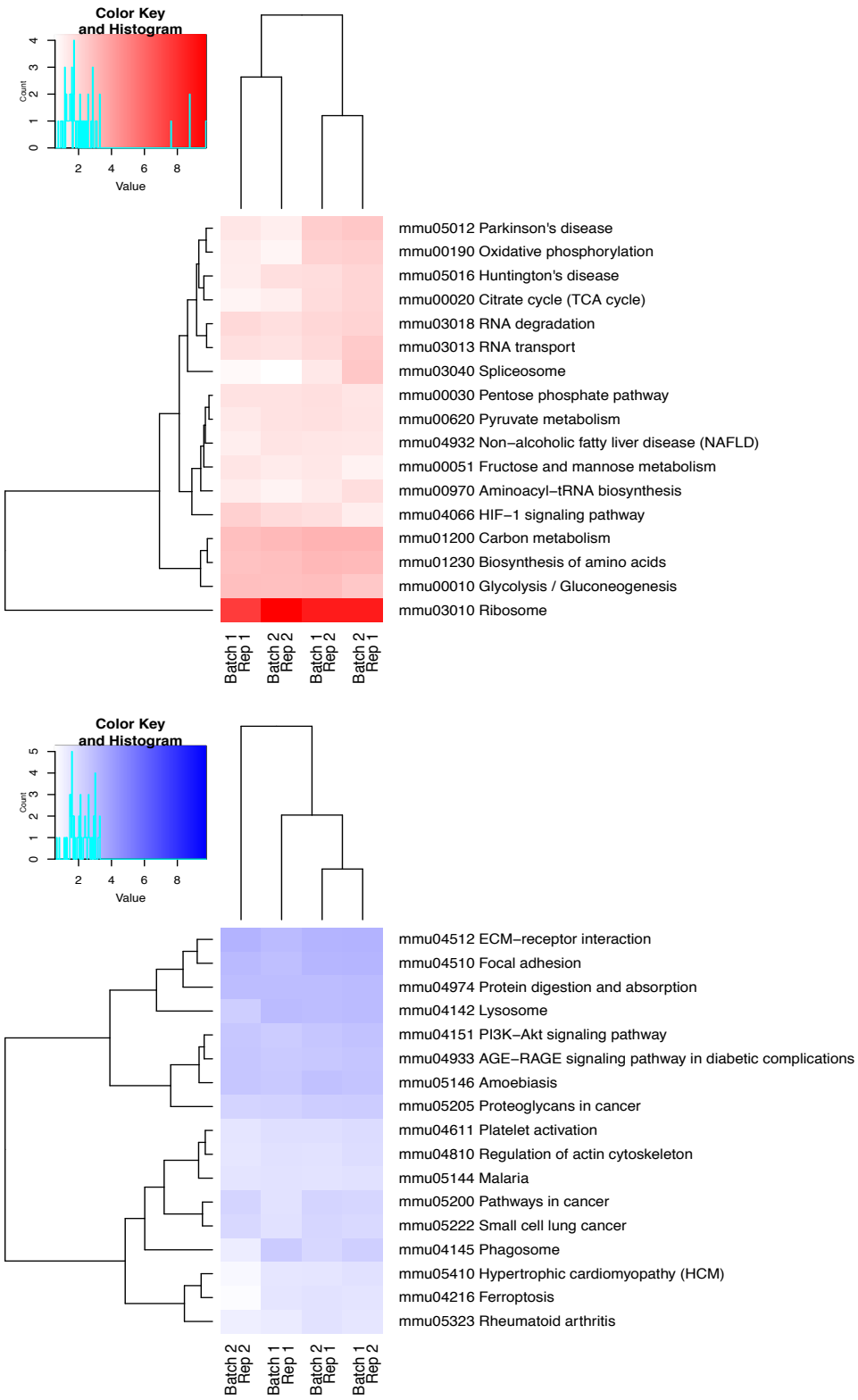

FIGURE A.13. Heatmap of significantly (q-value < 0.1) upregulated (red) and downregulated (blue) KEGG pathways comparing the tumor samples with healthy controls. The batches correspond to different experiments and the replicates to different animals.

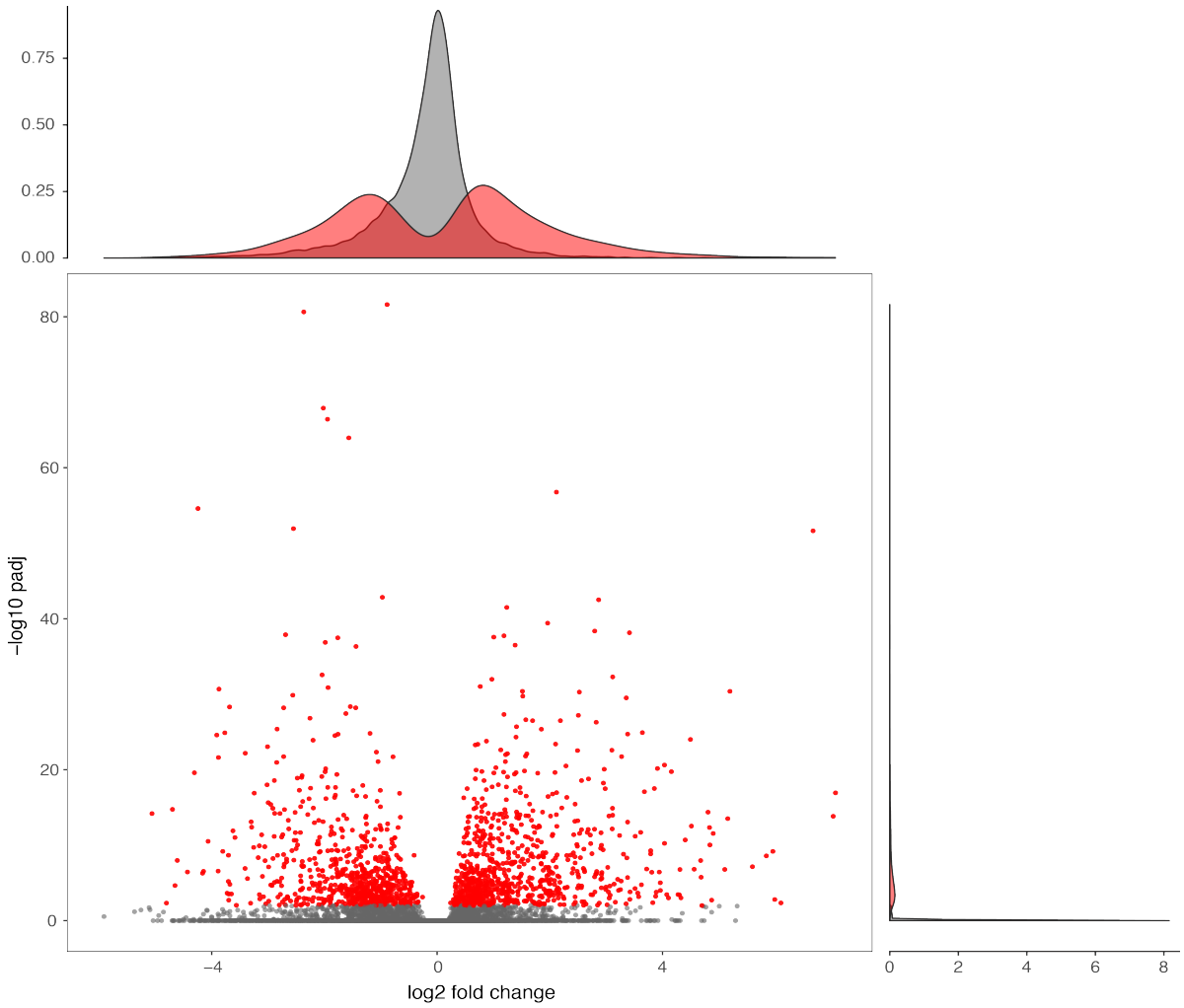

FIGURE A.14. Volcano plot highlighting the 1525 differentially expressed genes (padj < 0.01) comparing the regressed samples with healthy controls.

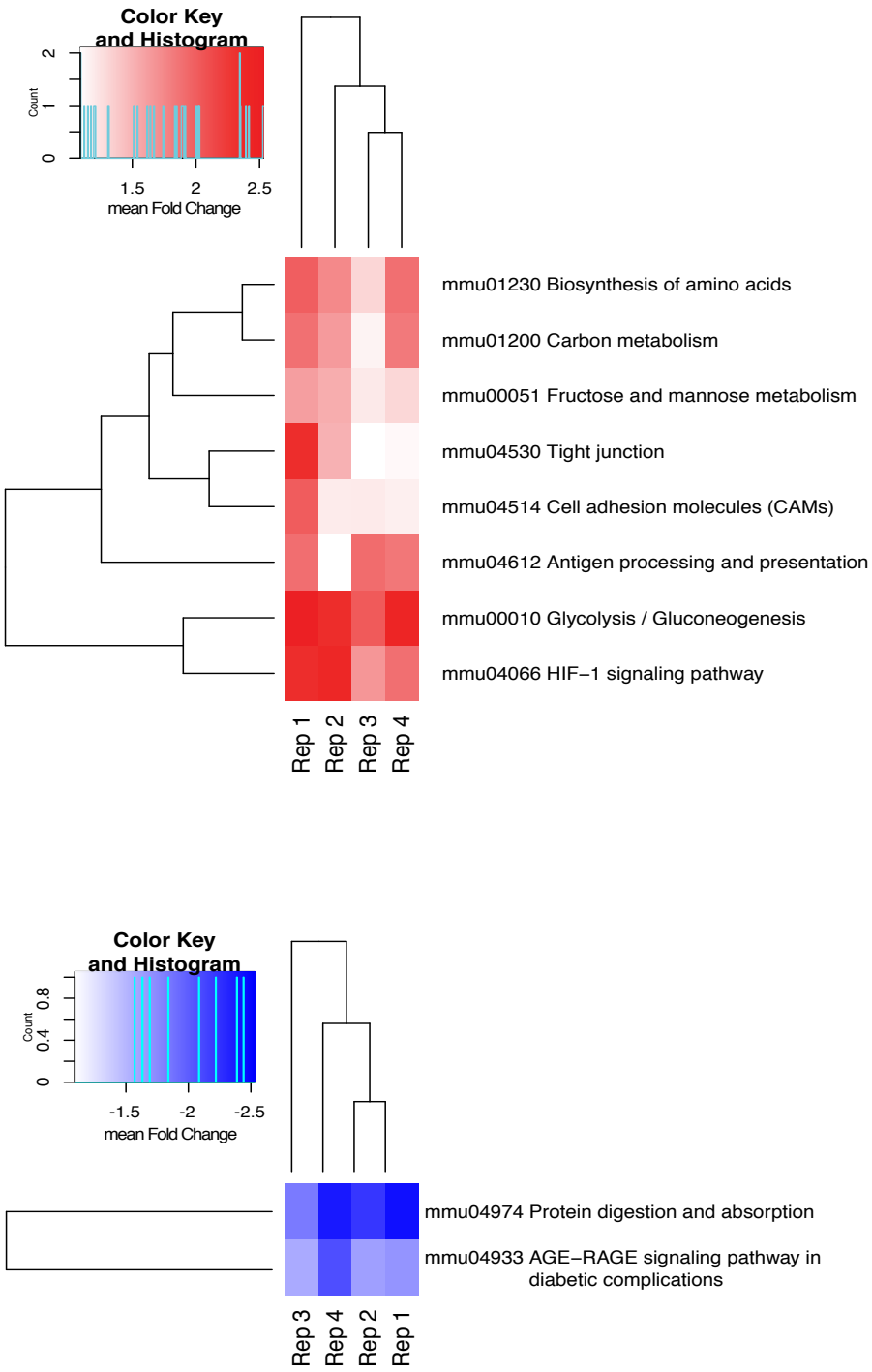

FIGURE A.15. Heatmap of significantly (q-value < 0.1) upregulated (red) and downregulated (blue) KEGG pathways comparing the regressed samples with healthy controls. The batches correspond to different experiments and the replicates to different animals.

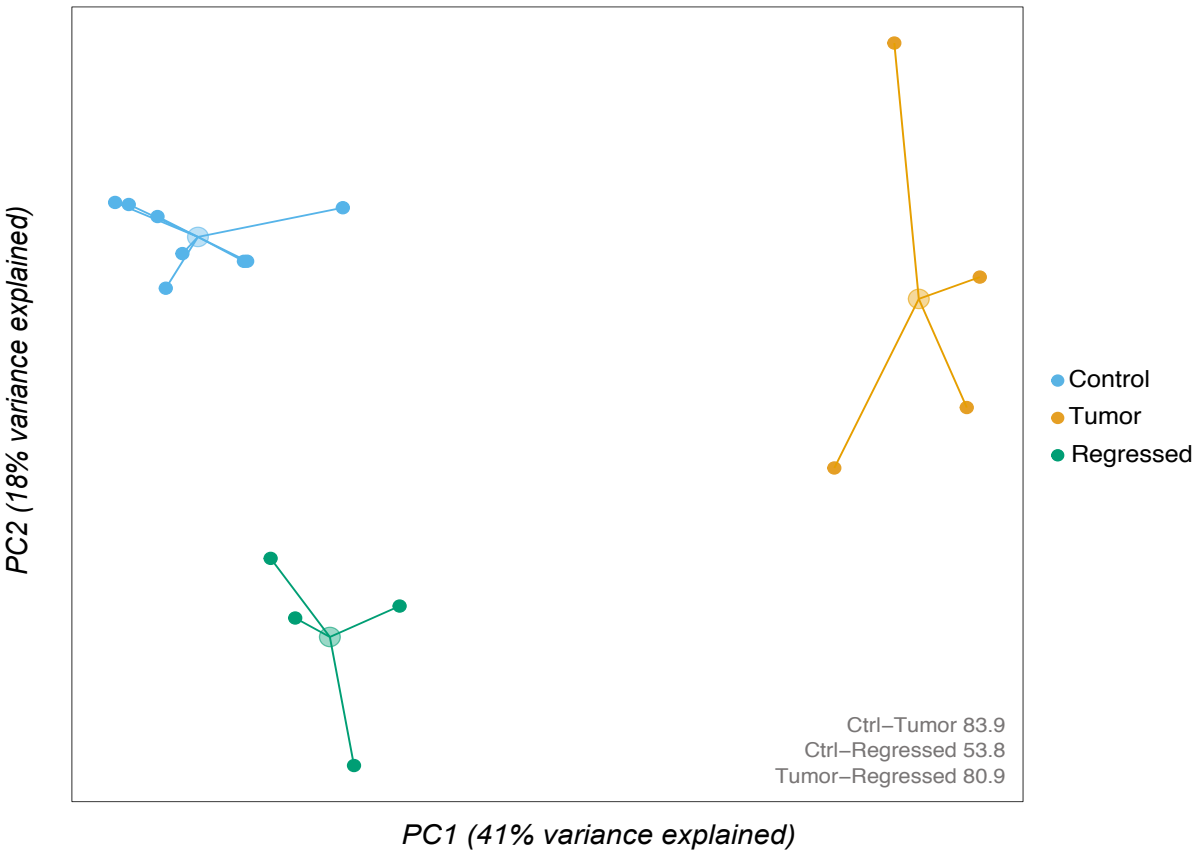

FIGURE A.16. PCA plot of the transcriptome data subsetted to metabolic genes. Blue represents healthy control samples, yellow tumorigenic samples and green regressed samples. Centroids are drawn to represent the center of each sample group considering the first two PCs. The calculated distance measure is the Euclidean distance between the centroids of the samples based on all principal components. Ctrl – Control samples, Tumor – Tumor samples, Regressed – Regressed samples.

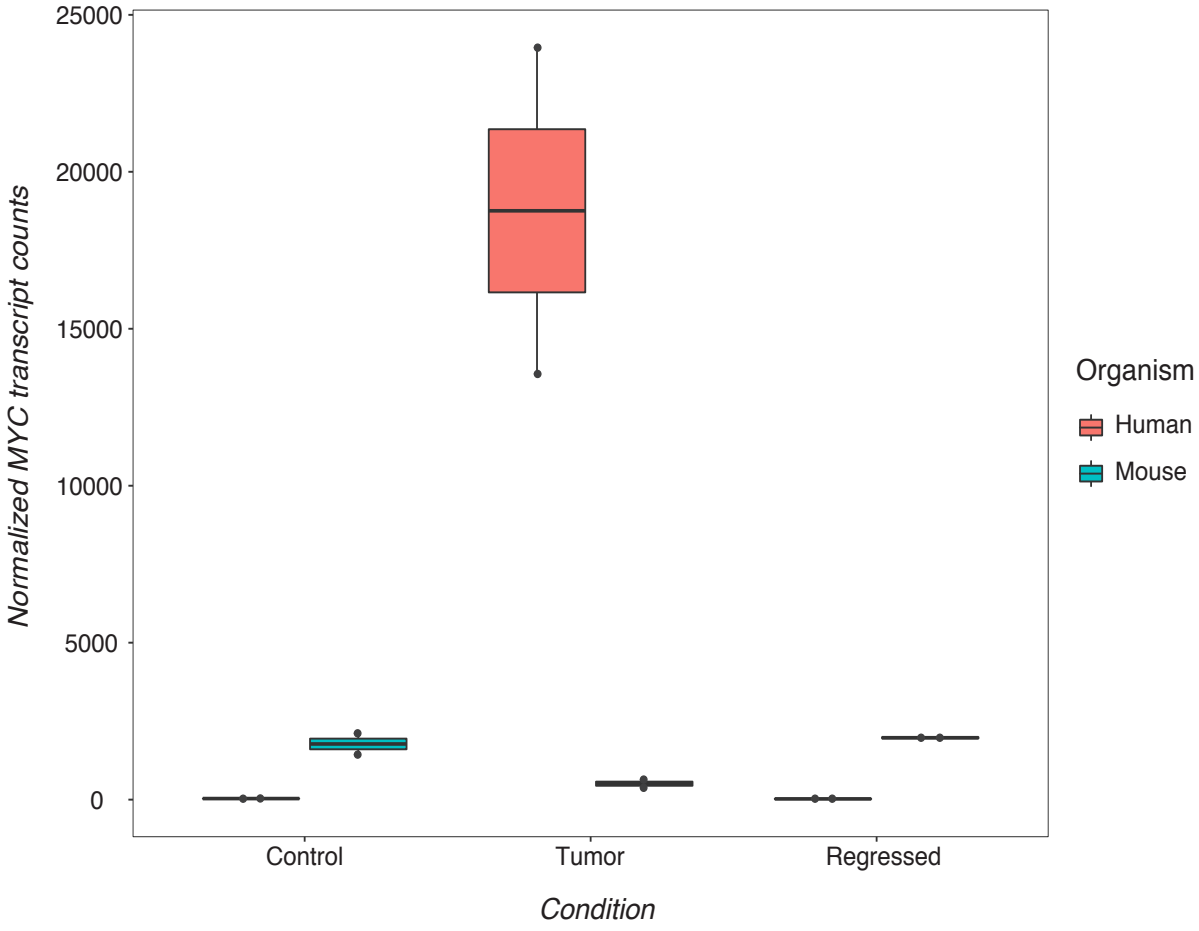

FIGURE A.17. Quantification of normalized transcript counts of heterologous (human) and endogenous (mouse) c-MYC.

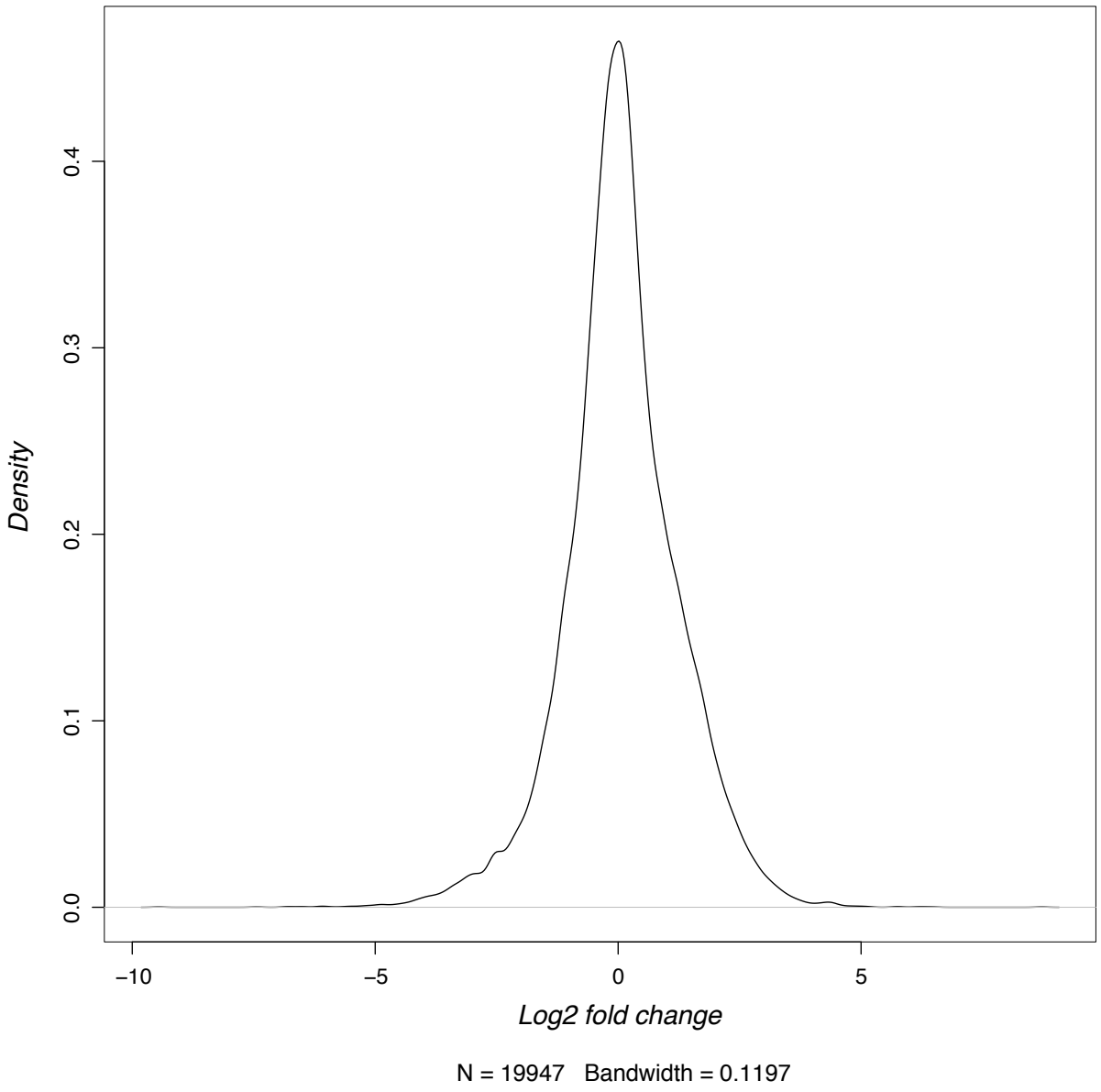

FIGURE A.18. Density distribution of log2 fold changes between the tumor and the regressed organoid samples.

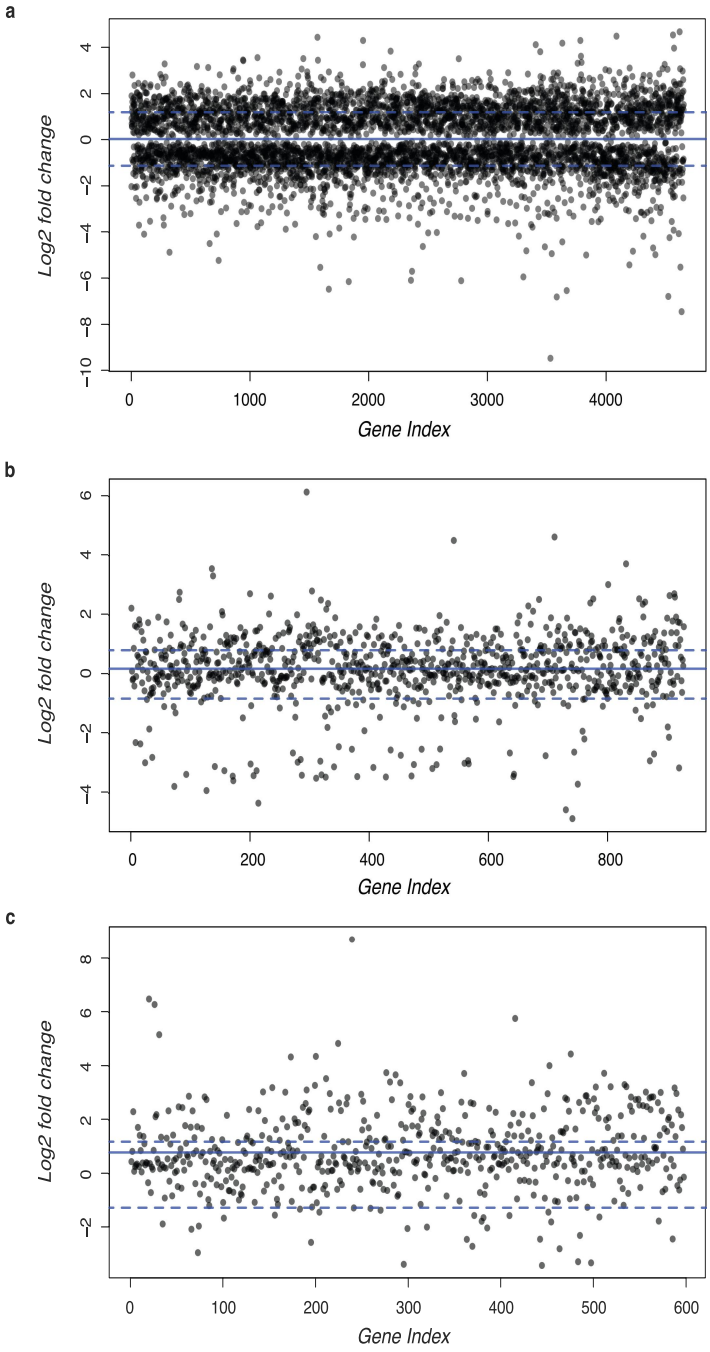

FIGURE A.19. Log2 fold changes of the regressed samples over the tumor samples. Only genes are selected, which in comparison to the healthy control are differentially expressed (a) only in the tumor samples (b) in the tumor and the regressed samples (c) only in the regressed samples. The solid line depicts the mean log2 fold change and the dotted line the absolute mean change in the respective selection of genes.

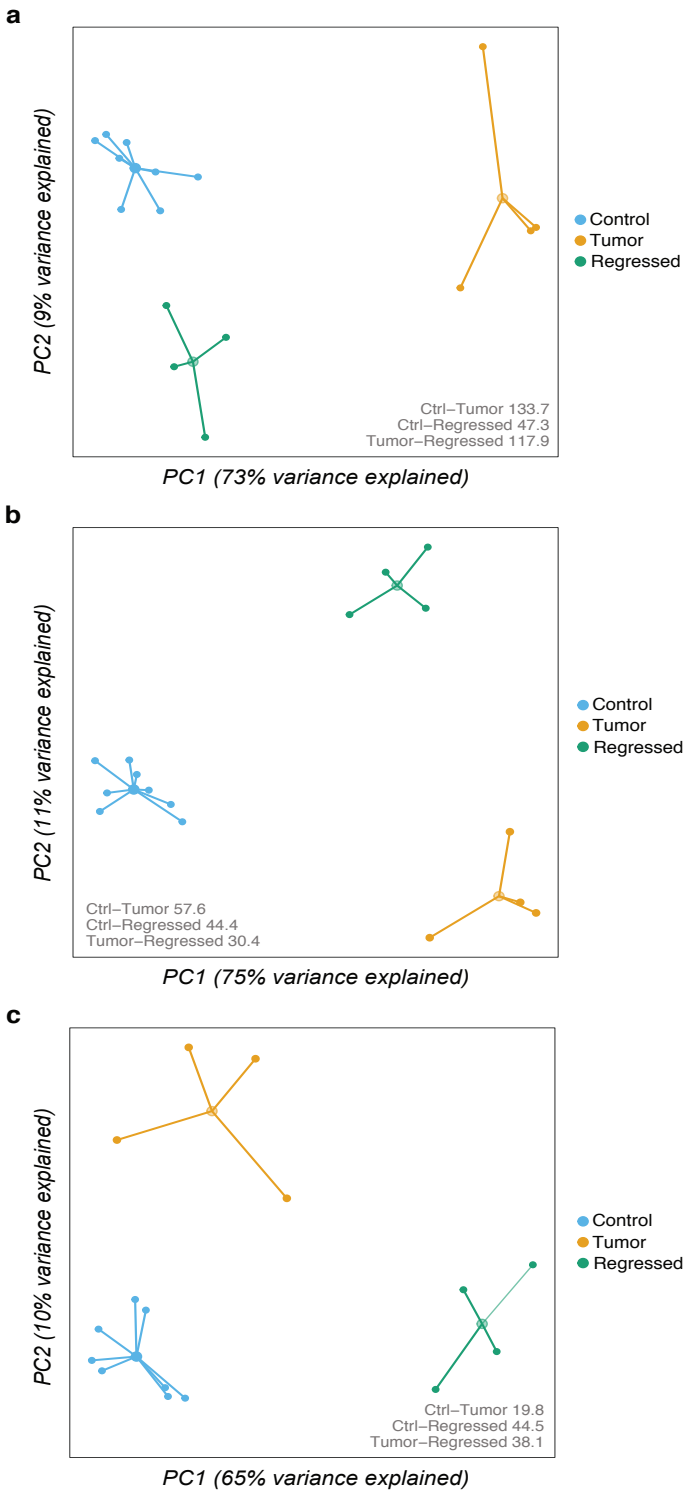

FIGURE A.20. PCA plot of the transcriptome data subsetted to genes uniquely differently expressed (over the healthy control) in (a) the tumor samples (b) the tumor and the regressed samples (c) the regressed samples. Centroids are drawn to represent the center of each sample group considering the first two PCs. The calculated distance measure is the Euclidean distance between the centroids of the samples based on all principal components. Ctrl – Control.

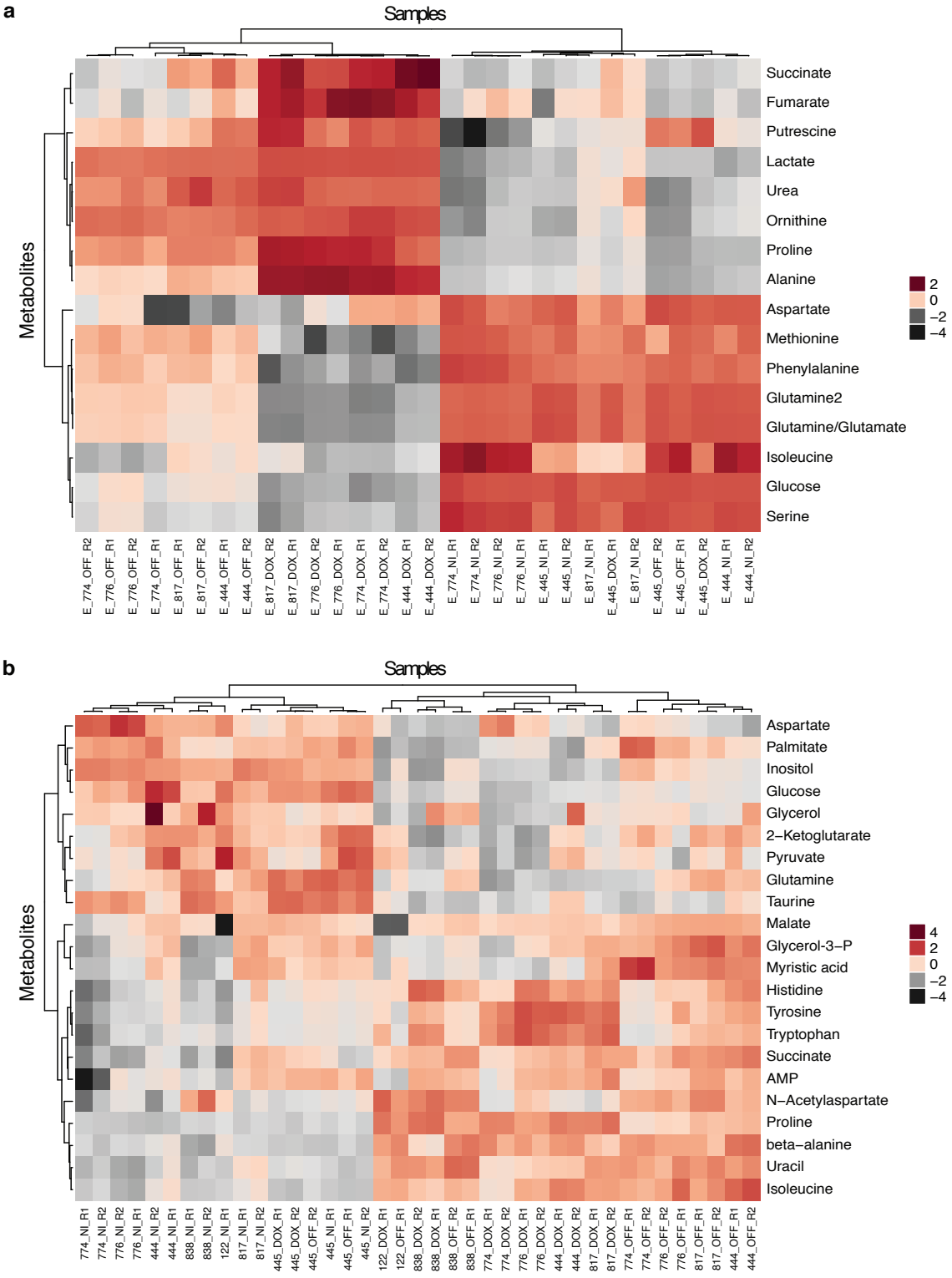

FIGURE A.21. *In vitro* targeted GCMS metabolomics analysis of intra- and extracellular metabolite. Only significantly altered (padj < 0.01) metabolites in either the tumor or the regressed cells in comparison to the control samples are depicted. Sample names.

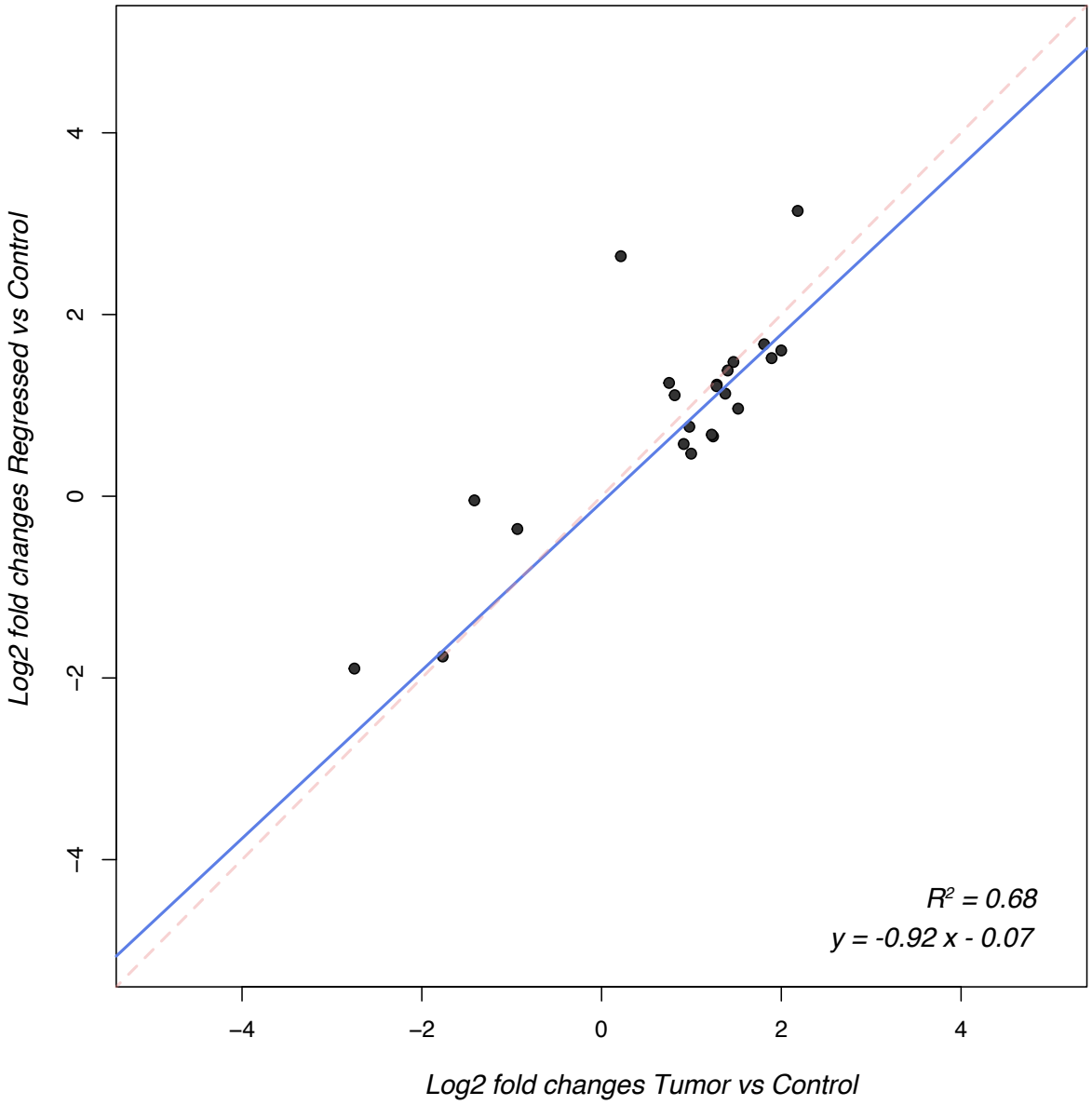

FIGURE A.22. Transcriptomic log2 fold changes of differentially expressed genes in the tumor samples in comparison to the healthy samples plotted against the log2 fold changes of differentially expressed genes in the regressed samples in comparison to the healthy samples for intersecting glycolytic core enzymes. The solid line represents a linear fit through the data. The dotted line depicts the diagonal.

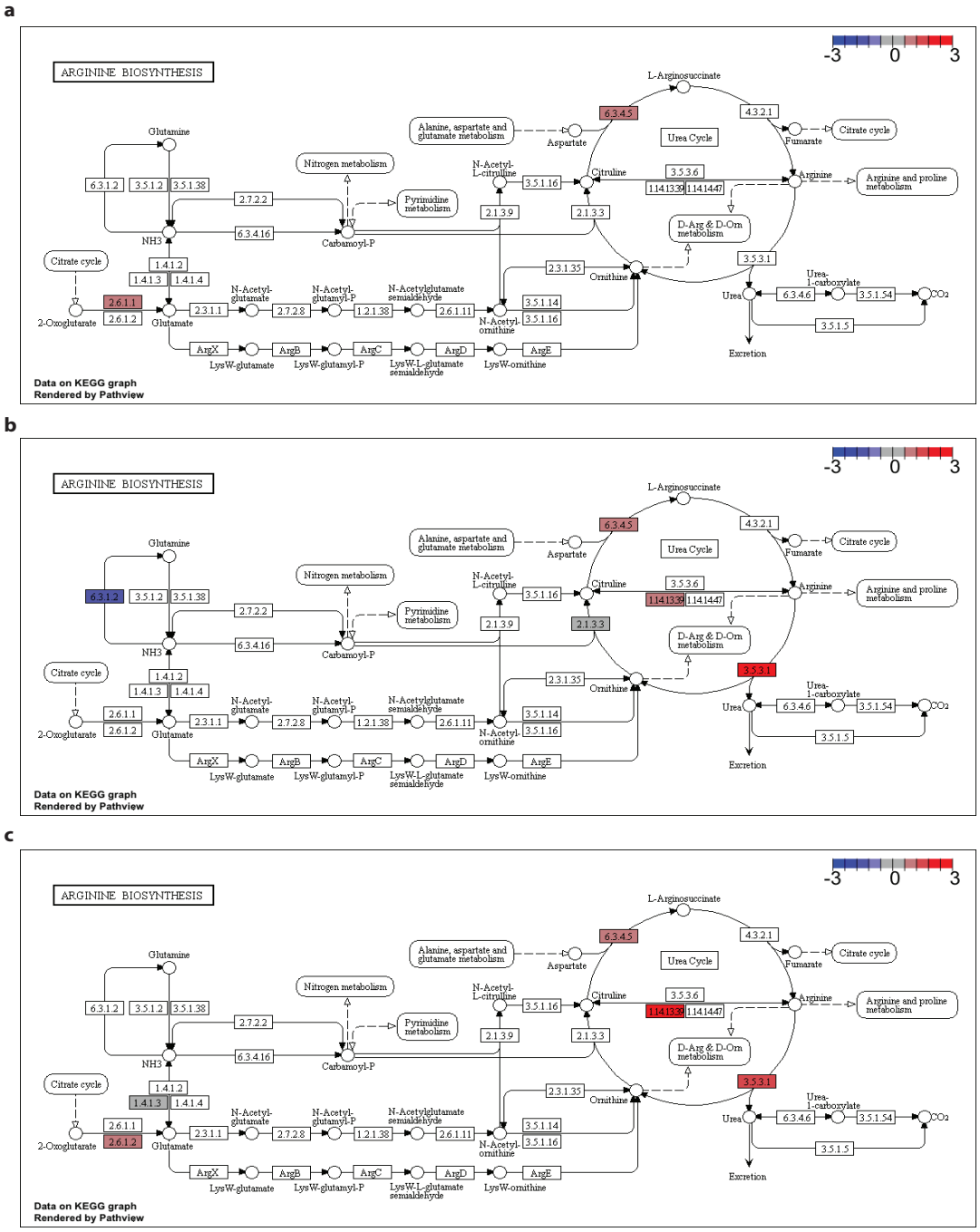

FIGURE A.23. KEGG pathways of arginine biosynthesis with enzymes, whose transcript levels significantly change over the respective healthy control being marked. The coloring represents log2 fold changes. (a) Basal HER2 negative group in comparison to healthy tissue samples. (b) Basal HER2 positive group over healthy tissue samples. (c) *In vitro* tumor cells derived from the mouse model in comparison to healthy control cells. The depicted maps are from the KEGG database

a

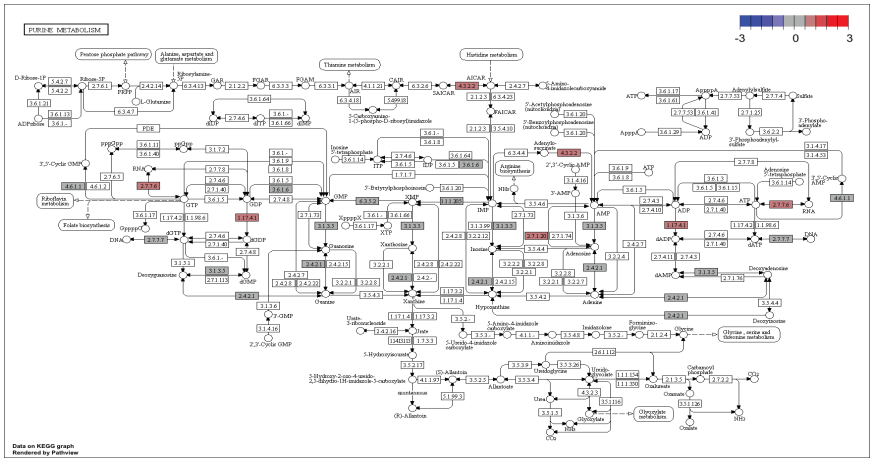

b

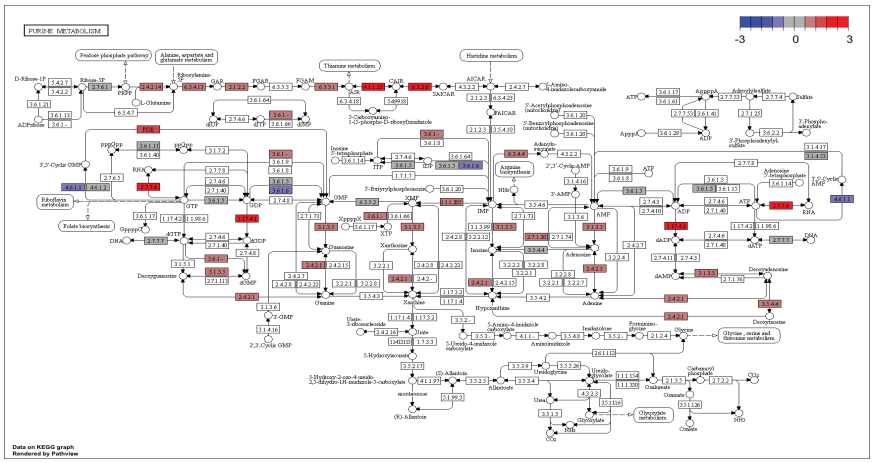

c

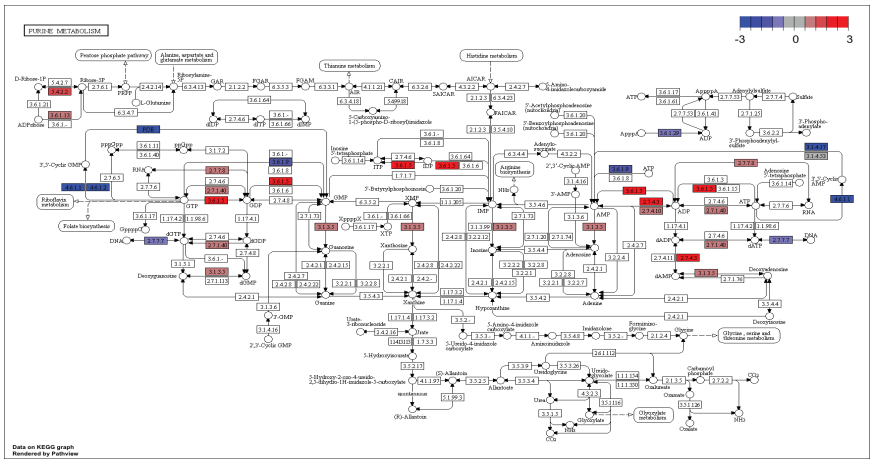

FIGURE A.24. KEGG pathways of purine metabolism with enzymes, whose transcript levels significantly change over the respective healthy control being marked. The coloring represents log2 fold changes. (a) Basal HER2 negative group in comparison to healthy tissue samples. (b) Basal HER2 positive group over healthy tissue samples. (c) *In vitro* tumor cells derived from the mouse model in comparison to healthy control cells The depicted maps are from the KEGG database.

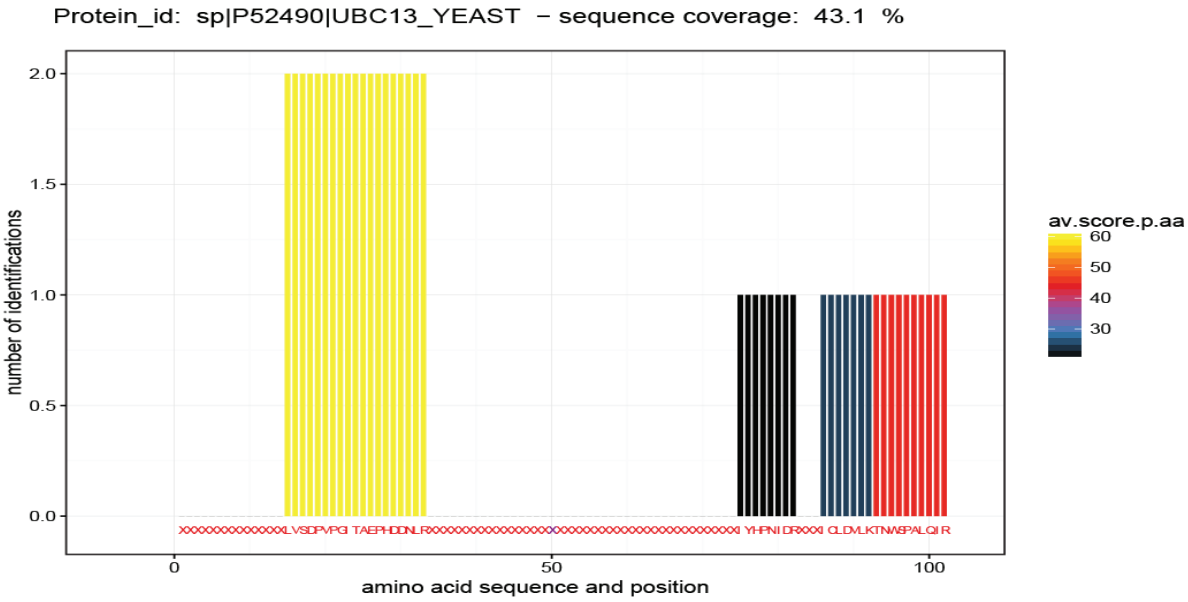

FIGURE A.25. Peptide overlay onto Ubc13 amino acid sequence. Results in the figure show truncated Ubc13 sequence as no confident alignment of MS/MS detected peptides was possible after the 70th amino acid. *This figure and the corresponding legend text have been reproduced from Strucko et al. (2018) with permission and have been originally done and written by myself (Strucko 2018).*

TABLE A.1. List of oligonucleotides. All sequences are displayed in 5' to 3' direction. *This table and the corresponding legend text have been reproduced from Strucko et al. (2018) with permission [178].*

Name	**Target**	**Sequence**
		For USER cloning
PCFB_5	*pTEF1*	acctgcacuttgtaattaaaacttag
PCFB_6	*pTEF1*	cacgcgaugcacacaccatagcttc
PCFB_8	*pPGK1*	atgacagauttgttttatatttgttg
TS_16	*Kp.nox*	ATCTGTCAUATGAGTAAAATCGTTGTAGTCGG
TS_17	*Kp.nox*	CACGCGAUTTATTTTTCAGCCGTAAGGGCAG
		For guide RNA constructs
TS_109	*gRNA_R*	Phos-GATCATTTATCTTTCACTGCG
TS_72	*PPZ2*	CCAATGTTACAAGAGTCTACGTTTTAGAGCTAGAA
TS_73	*GUT1_1*	CATCCACTGCCAGAACCGACGTTTTAGAGCTAGAA
TS_74	*GUT1_3*	GGGCAACTCGCTTACAAACCGTTTTAGAGCTAGAA
TS_76	*KGD1*	CgGCAGCAACAgCACCACTTGTTTTAGAGCTAGAA
TS_77	*PBS2_1*	ATGCAATTCTCCCTATatTGGTTTTAGAGCTAGAA
TS_78	*PBS2_2*	AATTGAGCgCTATTGTTGATGTTTTAGAGCTAGAA
TS_79	*HOG1_1*	CTGAGATGTCAAAGTGTCCGGTTTTAGAGCTAGAA
TS_80	*HOG1_2*	AAACATAGCCTGTCATTTGAGTTTTAGAGCTAGAA
TS_81	*YMR206W*	TGGTGACATTgGTTGAGAGTGTTTTAGAGCTAGAA
TS_110	*GUT1_2*	CATTGCcTTCAAGATAGCCCGTTTTAGAGCTAGAAATAGCAAG
TS_112	*TEA1*	TCATCAACGTACCAGACTTTGTTTTAGAGCTAGAAATAGCAAG
TS_113	*UBC13*	TATATCATCCCAATATTGATGTTTTAGAGCTAGAAATAGCAAG
TS_114	*CYM1*	TATTTGTAAGGTAGGTAAACGTTTTAGAGCTAGAAATAGCAAG
TS_115	*INO80*	GGAATCGATTGGATTGTAGTGTTTTAGAGCTAGAAATAGCAAG
TS_116	*RET1*	TGACTCCGCCTCATGAGTGTGTTTTAGAGCTAGAAATAGCAAG
TJOS-62	(P1F)	CGTGCGAUagggaacaaaagctggagct
TJOS-63	(P2F)	AGTGCAGGUagggaacaaaagctggagct
TJOS-64	(P3F)	ATCTGTCAUagggaacaaaagctggagct
TJOS-65	(P1R)	CACGCGAUtaactaattacatgactcga
TJOS-66	(P2R)	ACCTGCACUtaactaattacatgactcga
TJOS-67	(P3R)	ATGACAGAUtaactaattacatgactcga

Name	Target	Sequence
		Double stranded oligoes (only positive strand shown)
TS_83	*PPZ2*	CAATCATGAATGTGCCAATGTTACAAGAGTgTACGGaTTTTATGATGAATGTAAACtACGTTGTAATATCAAGATTTGGAAAACCTTTGT
TS_84	*GUT1_1*	AGACAGGGACTTTTTAGAGGAAATTTCCGACGTCACATATcAAAAGTCGCCaCTGTCGGTTCTGGCgGTGGATGGCGGGATGTCGAGGTC
TS_85	*GUT1_3*	TGTCTGGGCGACCAAAGCGCATCCATGGTGGGcCAACTCGCTTACAAACCCaGTGCTGCAAAATGTACTTATGGTACCGGTTGCTTTTTA
TS_86	*GUT1_2*	GCTGCCGTGAAGGTGTTTGCTTTCAAGCaAGGGCgATCTTGAAtGCAATGAGTTCTGACGCGTTTTGGTGAAGGTTCCAAAGACAGGGAC
TS_87	*GUT1_5*	AGACAGGGACTTTTTAGAGGAAATTTCCGACGTCACAgATGAAAAGTCGCCaCTGTCGGTTCTGGCgGTGGATGGCGGGATGTCGAGGTC
TS_88	*KGD1*	TAAGGATTTCAAGGTCAGATACTGTGGTAGAAAtCCAAGTGGTGaTGTTGCTGCaGGTAGCAAATCACTACATTTGGCCGAAGAAGATGC
TS_89	*PBS2_1*	CAAATTTTAATGGAACTAGAAGTTTTGCATAAAATGCAATTCTCCCTATTGTcGATTTTTATGGTGCATTCTTTATTGAGGGCGCCGTCTA
TS_90	*PBS2_2*	CCACCAGAAACATACGACAACATTTTCTCTCAATTGAGCcCTATTGTTGATGGaCCGCCACCGAGATTACCTTCAGATAAATTTCAGTTCT
TS_91	*HOG1_1*	CCCGTTGGGATGGGGCATTTGGGTTGGTTTGCTaAGCaACGGAtACTTTGACATCTCAGCCAGTTGCCATTAAGAAAATCATGAAACCT
TS_92	*HOG1_2*	AATGAAAACTGTGATTTGAAGATTTGCaATTTCGGTCTAGCAAGAATTCAAGAtCCTCAAATGACAGGCTATGTTTCCACTAGATACTAC
TS_93	*YMR206W*	CAAAATTACGTACTAAAATTGCAACTCTCGTCACCaAACTCTCAACtAATGTCACCAAGGACTCGGCCGGGCTACCGCCCCTCTTGCTCT
TS_94	*TEA1*	GCTATCAGGGTCGGCTACGACATGGGATTTCAACTGGACgGTAAAGTgTGGTACGTTGATGATAACAATCTGCAGCTGACCCAAAGTGAG
TS_117	*UBC13*	ACGACTATCCAATGGAAGCACCGAAAGTACTTTTTTTAACCAAGATATATCATCCCAATATTGATAGaTTGGGCCGTATATATGTCTTTGATGT
TS_118	*CYM1*	GTATACTGTTTACAGGAGAAACAAAATGAAAAAGAAAGATTTATtCTGTTTTACCTACCTTACAAATAAAAAGACATCCCAAGAGCTGGTGATA
TS_119	*INO80*	CAAGCATCAGAAAGATTAAGAAGAGGAGGTTCACCAATTaTATTGTCACaGACTACAATCCAATCGATTCCAAGTTGAACATCAAAATAAC
TS_120	*RET1*	AGAGTgGGTAAGAAAGTCCTCTTCTTCGACAgAAGATTATTTGACTCCGCCTCATGAGTGTAGaCTTAGAGATATGACATACTCTGCACCA
TJOS-62	(P1F)	CGTGCGGAUagggaacaaaagctggagct
TJOS-63	(P2F)	AGTGCAGGUagggaacaaaagctggagct
TJOS-64	(P3F)	ATCTGTCAUagggaacaaaagctggagct
TJOS-65	(P1R)	CACGCGAUtaactaattacatgactcga
TJOS-66	(P2R)	ACCTGCACUtaactaattacatgactcga
TJOS-67	(P3R)	ATGACAGAUtaactaattacatgactcga

Name	Target	Sequence
		Primers for validation
TS_95	*PPZ2*	GTAAGCAGTCCCTGGAGACC
TS_96	*PPZ2*	TCAGCGATTGGCTAATTTAC
TS_97	*GUT1*	TAGTCAAGAGAAACCTGCCC
TS_98	*GUT1*	ACCTTCTGACTTTGACACAG
TS_99	*KGD1*	ACCCAAGATATTTCCCATCTG
TS_100	*KGD1*	CATCTTTAGGATTGTTGGAAAAC
TS_101	*PBS2*	GGAAGTCCGTTTGGAGCTAG
TS_102	*PBS2*	TAGATAAACCATTCTCACCACG
TS_103	*HOG1*	TAGGACACAGATATTCGGTACAG
TS_104	*HOG1*	CTTACCTTCAATCATTTCGGC
TS_105	*YMR206W*	AAGGACATTCAAAGGATCGC
TS_106	*YMR206W*	TTCTTCTATGGTGATGCCTTG
TS_107	*TEA1*	TGAGCAAAGTACAGCCCGT
TS_108	*TEA1*	ATGGCTTGTTAAAGGTGAGC
TS_121	*UBC13*	AGTAAGTGACCCAGTACCTGGC
TS_122	*UBC13*	TCACTCGGGTTTCTTCTTTGC
TS_123	*CYM1*	TGAGAGCTTGTTGTTTGAGGA
TS_124	*CYM1*	GAGGCTCTGTGGTGTTAGGG
TS_125	*INO80*	AGAACAGGATGACAATGACGA
TS_126	*INO80*	CAACCCGTGTCTAGTGTTG
TS_127	*RET1*	CTGCTCAGGATAAGTGGCAC
TS_128	*RET1*	CATCTGCCTCCACAATAATACG
		Primer for determination of MAT locus
MAT_R	*MAT*	AGTCACATCAAGATCGTTTATGG
MATα_F	*MAT*	ACGGAATATGGGACTACTTCG
MATa_F	*MAT*	ACTCCACTTCAAGTAAGAGTTTG

TABLE A.2. List of the *S. cerevisiae* strains. *This table and the corresponding legend text have been reproduced from Strucko et al. (2018) with permission [178].*

#ID	Name 2	Genotype	Comments (Source)
	CEN.PK113-7D	MATa MAL2-8c SUC2	Peter Koetter
	CEN.PK113-1A	MATα MAL2-8c SUC2	Peter Koetter
	L.1528	MATa/ MATα WT	NZ strains
	CLIB382	MATa/ MATα WT	NZ strains
	7D_Cas9	MATa MAL2-8c SUC2 pCfB2312::KanMX	This study
	1A_Cas9	MATα MAL2-8c SUC2 pCfB2312::KanMX	This study
TS290	TS29 (NOX)	MATα MAL2-8c SUC2 X3::pTEF1::NOX::KanMX	This study
	Mode-I_ALE		
	GEVO05	MATα MAL2-8c SUC2 X3::pTEF1::NOX::KanMX evolved	This study
	GEVO09	MATα MAL2-8c SUC2 X3::pTEF1::NOX::KanMX evolved	This study
	GEVO13	MATα MAL2-8c SUC2 X3::pTEF1::NOX::KanMX evolved	This study
	GEVO17	MATα MAL2-8c SUC2 X3::pTEF1::NOX::KanMX evolved	This study
	GEVO21	MATα MAL2-8c SUC2 X3::pTEF1::NOX::KanMX evolved	This study
	GEVO25	MATα MAL2-8c SUC2 X3::pTEF1::NOX::KanMX evolved	This study
	GEVO26	MATα MAL2-8c SUC2 X3::pTEF1::NOX::KanMX evolved	This study
	GEVO29	MATα MAL2-8c SUC2 X3::pTEF1::NOX::KanMX evolved	This study
	GEVO30	MATα MAL2-8c SUC2 X3::pTEF1::NOX::KanMX evolved	This study

#ID	Name 2	Genotype	Comments (Source)
	Mode-II ALE		
	ALE1	MATa MAL2-8c SUC2 evolved	This study
	ALE2	MATa MAL2-8c SUC2 evolved	This study
	ALE3	MATa MAL2-8c SUC2 evolved	This study
	ALE4	MATa MAL2-8c SUC2 evolved	This study
	ALE5	MATα MAL2-8c SUC2 X3::pTEF1::NOX::KanMX evolved	This study
	ALE6	MATα MAL2-8c SUC2 X3::pTEF1::NOX::KanMX evolved	This study
	ALE7	MATα MAL2-8c SUC2 X3::pTEF1::NOX::KanMX evolved	This study
	ALE8	MATα MAL2-8c SUC2 X3::pTEF1::NOX::KanMX evolved	This study
	ALE9	MATα MAL2-8c SUC2 X3::pTEF1::NOX::KanMX evolved	This study
	ALE10	MATα MAL2-8c SUC2 X3::pTEF1::NOX::KanMX evolved	This study
	CLASSICAL GENETICS		
	ALE2-2A	MAT? MAL2-8c SUC2 spore isolate	1st cross segregant
	ALE2-2B	MAT? MAL2-8c SUC2 spore isolate	1st cross segregant
	ALE2-2C	MAT? MAL2-8c SUC2 spore isolate	1st cross segregant
	ALE2-2D	MAT? MAL2-8c SUC2 spore isolate	1st cross segregant
	ALE2-3A	MAT? MAL2-8c SUC2 spore isolate	1st cross segregant
	ALE2-3B	MAT? MAL2-8c SUC2 spore isolate	1st cross segregant
	ALE2-3C	MAT? MAL2-8c SUC2 spore isolate	1st cross segregant
	ALE2-3D	MAT? MAL2-8c SUC2 spore isolate	1st cross segregant
	ALE2-4A	MAT? MAL2-8c SUC2 spore isolate	1st cross segregant
	ALE2-4B	MAT? MAL2-8c SUC2 spore isolate	1st cross segregant
	ALE2-4C	MAT? MAL2-8c SUC2 spore isolate	1st cross segregant
	ALE2-4D	MAT? MAL2-8c SUC2 spore isolate	1st cross segregant
	4C-2D	MAT? MAL2-8c SUC2 spore isolate	2nd cross segregant
	4C-2D-5C	MAT? MAL2-8c SUC2 spore isolate	3rd cross segredant
	4C-2D-10B	MAT? MAL2-8c SUC2 spore isolate	3rd cross segredant

#ID	Name 2	Genotype	Comments (Source)
	RECONSTRUCTED		
TS105	R-G1	*MATα MAL2-8c SUC2 GUT1(E572Q)*	This study
TS107	R-G5	*MATα MAL2-8c SUC2 GUT1(Y571D)*	This study
TS108	R-P	MATa MAL2-8C SUC2 PBS2(I418fs)	This study
TS110	R-H1	*MATα MAL2-8c SUC2 HOG1(38*stop)*	This study
TS113	R-H2	MATa MAL2-8C SUC2 HOG1(D162N)	This study
TS114	R-T	MATa MAL2-8C SUC2 TAE1(P456A)	This study
TS116	R-PPZ2	MATa MAL2-8C SUC2 PPZ2(R532L)	This study
TS121	R-H2	MATa MAL2-8C SUC2 HOG1(D162N)	This study
TS123	R-K	MATa MAL2-8C SUC2 KGD1(A990D)	This study
TS125	R-K	*MATα MAL2-8C SUC2 KGD1(A990D)*	This study
TS127	R-G1P1	*MATα MAL2-8c SUC2 GUT1(E572Q) PBS2(I418fs)*	This study
TS129	R-G1H1	*MATα MAL2-8c SUC2 GUT1(E572Q) HOG1(38*stop)*	This study
TS131	R-G1H2	*MATα MAL2-8c SUC2 GUT1(E572Q) HOG1(D106Y)*	This study
TS133	R-G5H1	*MATα MAL2-8c SUC2 GUT1(Y571D) HOG1(38*stop)*	This study
TS136	R-TG1	MATa MAL2-8C SUC2 TAE1(P456A) GUT1(E572Q)	This study
TS138	R-PPZ2T	MATa MAL2-8C SUC2 PPZ2(R532L) TAE1(P456A)	This study
TS140	R-PPZ2G1	MATa MAL2-8C SUC2 PPZ2(R532L) GUT1(E572Q)	This study
TS143	R-R	MATa MAL2-8C SUC2 RET1(K109E)	This study
TS144	R-U	MATa MAL2-8C SUC2 UBC13(R70fs)	This study
TS146	R-C	MATa MAL2-8C SUC2 CYM1(S530F)	This study
TS148	R-X	MATa MAL2-8C SUC2 YMR206W(P227L)	This study
TS150	R-I	MATa MAL2-8C SUC2 INO80(C359Y)	This study
TS153	R-GI	*MATα MAL2-8c SUC2 GUT1(E572Q) INO80(C359Y)*	This study
TS154	R-GU	*MATα MAL2-8c SUC2 GUT1(E572Q) UBC13(R70fs)*	This study
TS156	R-RX	MATa MAL2-8C SUC2 RET1(K109E) YMR206W(P227L)	This study
TS164	R-G1P1	*MATα MAL2-8c SUC2 GUT1(E572Q) PBS2(I418fs)*	This study
TS165	R-G1H1	*MATα MAL2-8c SUC2 GUT1(E572Q) HOG1(38*stop)*	This study
TS166	R-G1P1 (5) NOX	*MATα MAL2-8c SUC2 GUT1(E572Q) PBS2(I418fs) X3(pTEF1-S.p.NOX::)*	This study
TS168	R-G1H1 (7) NOX	*MATα MAL2-8c SUC2 GUT1(E572Q) HOG1(38*stop) X3(pTEF1-S.p.NOX::KanMX)*	This study
TS170	R-GK	*MATα MAL2-8c SUC2 GUT1(E572Q) KGD1(A990D)*	This study
TS172	R-GIK	*MATα MAL2-8c SUC2 GUT1(E572Q) INO80(C359Y) KGD1(A990D)*	This study
TS175	R-GIU	*MATα MAL2-8c SUC2 GUT1(E572Q) INO80(C359Y) UBC13(R70fs)*	This study
TS177	R-GUK	*MATα MAL2-8c SUC2 GUT1(E572Q) UBC13(R70fs) KGD1(A990D)*	This study
TS178	R-GUX	*MATα MAL2-8c SUC2 GUT1(E572Q) UBC13(R70fs) YMR206W(P227L)*	This study
TS233	R-KU	*MATα MAL2-8C SUC2 KGD1(A990D) UBC13(R70fs)*	This study
TS235	R-UI	MATa MAL2-8C SUC2 UBC13(R70fs) INO80(C359Y)	This study
TS237	R-KI	*MATα MAL2-8C SUC2 KGD1(A990D) INO80(C359Y)*	This study
TS256	L.1528-GUK	*MATα/a GUT1(E572Q) UBC13(R70fs) KGD1(A990D)*	This study
TS261	CLIB382-GUK	*MATα/a GUT1(E572Q) UBC13(R70fs) KGD1(A990D)*	This study

TABLE A.3. Marker ions used for the quantification of the mentioned metabolites by GC-MS. *This table and the corresponding legend text have been reproduced from Strucko et al. (2018) with permission [178].*

m/z	**Marker Ion (m/z)**
Glucose	319
Pyruvate	174
Lactate	191
Citrate	347
α ketoglutarate	198
Succinate	247
Fumarate	245
Malate	335
γ aminobutyric xacid	174
2-hydroxyglutarate	247
Glycerol 3-phosphate	357
Glycerate 3-phosphate	357

TABLE A.4. Minimum number of re-regulation target fluxes identified with metabolic modeling to achieve optimal glycerol utilization in *S. cerevisiae*. *This table and the corresponding legend text have been reproduced from Strucko et al. (2018) with permission [178].*

UP	**DOWN**
Triosephosphate isomerase	Glucokinase GLK1
Isocitrate dehydrogenase [NADP], cytoplasmic	Phosphofructokinase 2
Isocitrate dehydrogenase [NADP], cytoplasmic	Fructose-biphosphate aldolase
Succinyl-CoA ligase [ADP-forming] subunit beta, mitochondrial	Isocitrate dehydrogenase NAD sbunit 1, mitochondrial
Fructose-1,6-biphosphatase	Alpha-ketoglutarate dehydrogenase
ATP synthase subunit alpha, mitochondrial	Glucose-6-phosphate 1-dehydrogenase
Glutamate decarboxylase	Probable 6-phosphogluconolactonase 1
4-aminobutyrate aminotransferase	6-phosphogluconate dehydrogenase, decarboxylating 2
Succinate-semialdehde dehydrogenase [NADP+]	Ribulose-phosphate 3-epimerase
Glycerol kinase	Ribose-5-phosphate isomerase
Tricarboxylate transport protein	Transketolase 2
Glycerol uptale/efflux facilitator protein	Transketolase 2
Uptake of glycerol	Transaldolase
	Tricarboxylate transport protein
	Low-affinity glucose transporter HXT4
	Uptake of alpha-D-glucose

TABLE A.5. Growth rates of intermediate and final evolved lineages. Growth rates are estimated based on two biological replicates. Results of mode-I (manual ALE) experiment. *This table and the corresponding legend text have been reproduced from Strucko et al. (2018) with permission [178].*

Growth rate, μmax (1/h)		
	Lineage 1	Lineage 2
T6	0,057+0,004	0,074+0,004
T9	0,095+0,004	0,111+0,004
T11	0,087+0,004	0,11+0,004
T12	0,151+0,004	0,120+0,004
T13	0,128+0,004	0,113+0,004
T14	0,182+0,004	0,130+0,004
T16	0,203+0,004	0,122+0,004

TABLE A.6. Growth rates of intermediate and final evolved lineages. Growth rates are estimated based on two biological replicates. Results of mode-II (automatic ALE) experiment. *This table and the corresponding legend text have been reproduced from Strucko et al. (2018) with permission [178].*

Growth rate, μmax (1/h)		
wild-type based	ALE01	ND
	ALE02	0.220 ± 0.004
	ALE03	0.225 ± 0.004
	ALE04	ND
	ALE05	0.215 ± pm0.007
NOX based	ALE06	0.206 ± 0.015
	ALE07	0.229 ± pm0.002
	ALE08	0.216 ± 0.000
	ALE09	0.211 ± 0.004
	ALE10	0.222 ± 0.007

TABLE A.7. All mutations detected in evolved lineages. *This table and the corresponding legend text have been reproduced from Strucko et al. (2018) with permission [178].*

Chromosome	Region (global)	Type	Reference	Allele	Gene	Region (local)	AA Mutation	The closest CDS found upstream of the mutation	The closest CDS found downstream of the mutation	ALE1	ALE2	ALE3	ALE5	ALE6	ALE7	ALE8	ALE9	ALE10	ALE11	GEVO5	GEVO9	GEVO17	GEVO25	GEVO29	GEVO26	GEVO30	
chr01	4568945690	Insertion	-	T	INTER			p_ACS1	p_FLC2					x					x								
chr01	56625	SNV	A	G	SPC72	289T>C	S97P											x									TI
chr02	8179481795	Insertion	-	T	INTER			p_AAR2	t_RPS8B		x								x								
chr02	131443131444	Insertion	-	A	INTER			t_ECM13	t_FUI1		x	x							x								
chr02	444333444334	Insertion	-	T	INTER			t_ATP3	p_FIG1		x				x						x	x					
chr02	310729310730	Insertion	-	A	INTER			p_VID24	p_PHO88				x	x								x	x				
chr03	5665056651	Insertion	-	A	INTER			p_ATG22	t_SRO9	x			x					x									
chr03	2725227253	Insertion	-	A	INTER			p_PEX34-EIW11793.1	p_KAR4		x																
chr03	306167	SNV	T	A	INTER			p_EIW11828.1	t_BIO2		x	x															
chr03	101371101372	Insertion	-	T	INTER			p_EIW11867.1	t_GBP2						x			x	x	x	x	x	x	x	x		
chr03	5682956830	Insertion	-	A	INTER			p_ATG22	t_SRO9							x											
chr03	5666356664	Insertion	-	A	INTER			p_ATG22	t_SRO9											x							
chr04	21268	SNV	C	T	INTER				p_LRG1		x																TI
chr04	1092716	SNV	A	T	OMS1	316A>T	T106S				x																
chr04	954913954914	Insertion	-	A	INTER			p_EIW11867.1	t_GBP2	x		x	x	x	x	x			x			x					
chr04	1346528	SNV	G	A	SSN2	2087C>T	P696L			x																	TI
chr04	629289	Deletion	G	-	UBC13	476delG	R70fs				x	x															
chr04	1079202	SNV	G	C	INTER			p_GIC2	t_SUM1		x	x															
chr04	1250687	SNV	C	A	INTER			p_EIW11598.1	P_SAC7		x	x															
chr04	1325560	SNV	G	A	CYM1	1589C>T	S530F				x	x															TI
chr04	1335093	SNV	G	T	PPZ2	1595G>T	R532L				x	x															
chr04	792793	Insertion	-	T	INTER							x		x											x		
chr04	793794	Insertion	-	T	INTER							x															
chr04	115771	SNV	G	A	INTER			t_ARF1							x												TI
chr04	266930	SNV	C	T	KIN28	379C>T	H128Y								x												TI
chr04	547501547502	Insertion	-	G	INTER			p_RPC1 (RPO31)	t_BAP3							x	x				x						
chr04	195985	SNV	G	T	COP1	838C>A	L280I													x							
chr04	208183	SNV	C	T	RPO21	1031G>A	R344H																			x	TI
chr05	241857241858	Insertion	-	A	INTER			t_SPO73	t_SAP1	x								x									
chr05	333665..333667	MNV	TTT	AAA	INTER			p_DOT6	t_PTC2																x	x	
chr06	100923100924	Insertion	-	A	INTER			p_GNA1		x	x	x		x	x			x		x		x	x		x		
chr06	102603102604	Insertion	-	T	INTER			p_MDJ1		x	x	x	x	x	x						x	x					
chr07	224760	SNV	C	T	INO80	1076G>A	C359Y				x	x															TI
chr07	652925652926	Insertion	-	T	INTER			p_PDC6			x	x	x	x	x	x	x	x	x	x						x	
chr07	737084	SNV	A	C	PPT1	837T>G	F279L								x												
chr07	102534102535	Insertion	-	A	INTER			t_SPT16	t_CHC1								x										
chr07	1011474011475	Insertion	-	T	INTER			p_RAD2	p_TNA1											x							
chr07	4502845029	Insertion	-	A	INTER			p_EIW10317.1	p_KAP114																x		
chr07	935411935412	Insertion	-	TT	INTER			t_CRM1	t_MRPL9		x																
chr08	29959	SNV	C	G	GUT1_1	1711G>C	E572Q				x	x															
chr08	544795544796	Insertion	-	A	INTER				p_PHO1		x							x			x		x				
chr08	30475	SNV	C	T	GUT1_2	1195G>A	G400S						x				x										TI
chr08	30035	SNV	C	A	GUT1_3	1635G>T	K546N							x													
chr08	29976	SNV	A	C	GUT1_4	1694T>G	1566S											x									
chr08	29962	SNV	A	C	GUT1_5	1708T>G	Y571D																	x	x		
chr09	1755317554	Insertion	-	G	INTER					x	x		x	x			x			x		x			x		
chr09	6773167732	Insertion	-	T	INTER			p_ATG32	t_PAN6	x	x		x							x							
chr09	117362	SNV	C	A	KGD1	2969C>A	A990D				x	x															
chr09	130981	SNV	A	C	INTER			p_RPI1	p_RHO3		x	x															
chr10	248360248361	Insertion	-	T	INTER			p_DPB11	p_SIP4				x	x		x			x								
chr10	562623562624	Insertion	-	T	INTER			t_BNA2	t_AIM24						x								x		x		
chr10	161318..161319	Deletion	AT	-	PBS2_1	1252_1253delAT	I418fs											x									
chr10	376267376268	Insertion	-	A	INTER			t_RNR2	p_RRN7										x								
chr10	160839	SNV	C	G	PBS2_2	1732G>C	A578P													x	x	x	x	x			
chr10	9595495955	Insertion	-	T	INTER			p_EIW09701.1	t_JJJ2																	x	
chr10	437771	SNV	G	A	INTER			p_TDH2			x																TI
chr11	462960462961	Insertion	-	C	INTER			p_EIW09251.1	p_PRY2			x								x	x						
chr11	274418	SNV	T	A	MIF2		SILENT						x	x	x	x	x	x	x	x	x	x	x	x			
chr11	617217617218	Insertion	-	T	INTER			t_PTR2											x								
chr11	523716523717	Insertion	-	T	INTER			p_EIW09284.1	t_PET10																x		
chr11	660853660854	Insertion	-	T	INTER																			x			
chr11	222821222822	Insertion	-	A	INTER			p_PRR1	t_APN1																	x	
chr12	284375	SNV	A	G	RAX2		SILENT			x																	TI
chr12	751144751145	Insertion	-	A	INTER			p_TAD3	p_EST2	x																	
chr12	356955	SNV	G	T	HOG1_1	316G>T	D106Y					x					x										
chr12	356755	SNV	C	A	HOG1_2	116C>A	38*							x		x			x								
chr12	527513	SNV	C	A	NMT1	439G>T	A147S							x		x			x								
chr12	10379411037942	Insertion	-	T	INTER			t_FMP27	p_EIW09058.1					x													
chr12	357378	SNV	G	T	HOG1_3	739G>T	247*								x												
chr12	629887629888	Insertion	-	A	INTER			p_NDL1	p_HAP1						x		x										
chr12	3386033861	Insertion	-	A	INTER			p_RPL8B	p_FPS1									x				x					
chr12	411696411697	Insertion	-	G	INTER			t_PUT1	p_EIW08757.1																x		
chr12	357123	SNV	G	A	HOG1_4	484G>A	D162N																			x	TI
chr13	296759	SNV	A	G	ERG5	458T>C	F153S			x																	TI
chr13	670385	SNV	T	A	INTER			p_PFK2	p_EIW08473.1		x	x															
chr13	671263	SNV	C	T	EIW08473.1	680C>T	P227L				x	x															TI
chr13	159120159121	Insertion	-	T	INTER			p_IMD4	p_SPC2				x					x		x				x			
chr14	148742148743	Insertion	-	A	INTER			p_POL2	p_ORC5																	x	
chr14	680966..680967	Deletion	AA	-	INTER			t_PPG1	p_ABZ1		x																
chr15	426599426600	Insertion	-	A	INTER			p_ETT1	t_EIW07486.1	x		x	x		x		x	x		x					x	x	
chr15	732897	SNV	T	C	RET1	325A>G	K109E				x	x															TI
chr15	878076	SNV	G	T	INTER			p_MBF1	p_BUD7		x	x															
chr15	955494	SNV	C	G	TEA1	1366C>G	P456A				x	x															
chr15	204337204338	Insertion	-	T	INTER			p_RIB2	t_INP54				x							x							
chr15	411390	SNV	G	A	WHI2	521G>A	C174Y				x																TI
chr15	553099	SNV	G	T	INTER			p_PFY1	t_LEO1						x				x								
chr15	448654448655	Insertion	-	A	INTER			t_CYT1	p_MSA1								x										
chr15	30573	SNV	G	C	INTER				p_ZPS1																	x	x
chr16	655046655047	Insertion	-	A	INTER			t_RPL43A	t_THP3	x	x															x	
chr16	840664840665	Insertion	-	T	INTER				p_EIW07261.1	x	x			x	x			x	x	x		x	x		x		
chr16	939459	SNV	G	C	ARR2	283C>G	Q95E				x	x															
chr16	900122	SNV	C	T	INTER			p_SEC23	p_SMX3				x				x										TI
chr16	866279	SNV	C	T	SGV1	155G>A	G52E											x									TI

A	8			
T	4			
C	16			
G	15			
		TI	18	43
		TV	25	

TABLE A.8. All mutations detected in tetrad analysis. *This table and the corresponding legend text have been reproduced from Strucko et al. (2018) with permission [178].*

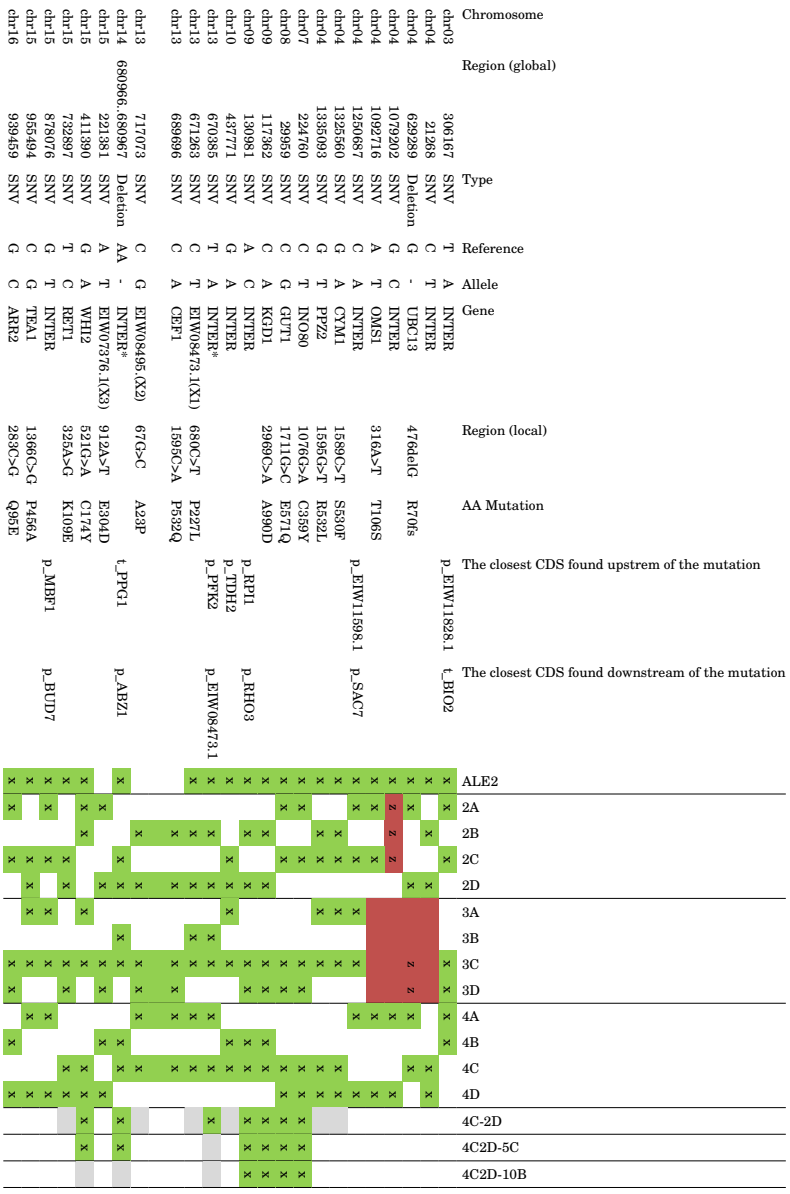

TABLE A.9. Transcriptomics results from the comparison R-GKU vs. ALE2 of genes with multiple testing adjusted q-values of 0.1. The genes are sorted according to their significance. *This table and the corresponding legend text have been reproduced from Strucko et al. (2018) with permission [178].*

CENPK_ID	**GeneID**	**log2FC**	**CENPK_ID**	**GeneID**	**log2FC**
CENPK1137D_2939	Aga2p	2,483	CENPK1137D_2858	hypothetical protein	-0,321
CENPK1137D_2535	Mfa2p	2,231	CENPK1137D_3491	Ser3p	0,480
CENPK1137D_3357	Ste2p	1,668	CENPK1137D_4319	Glt1p	-0,244
CENPK1137D_5045	Bar1p	1,534	CENPK1137D_5435	Msc7p	0,204
CENPK1137D_947	Ste6p	1,385	CENPK1137D_4938	Bdh2p	0,481
CENPK1137D_4287	Mfa1p	1,210	CENPK1137D_648	Pig1p	-0,406
CENPK1137D_1464	Asg7p	1,161	CENPK1137D_3361	Snz3p	0,423
CENPK1137D_4943	Rbg1p	0,538	CENPK1137D_3615	Yef1p	-0,371
CENPK1137D_2886	Mf(alpha)2p	-1,156	CENPK1137D_4116	Dpl1p	-0,232
CENPK1137D_1298	Sag1p	-1,163	CENPK1137D_4099	Pmp3p	-0,210
CENPK1137D_888	hypothetical protein	-3,349	CENPK1137D_3608	hypothetical protein	-0,197
CENPK1137D_1133	Ste3p	-3,634	CENPK1137D_3223	Coq6p	-0,209
CENPK1137D_1940	Mf(alpha)1p	-5,794	CENPK1137D_511	hypothetical protein	-0,267
CENPK1137D_5142	Prm5p	-0,726	CENPK1137D_1293	Pre3p	-0,224
CENPK1137D_1959	Aad15p	1,022	CENPK1137D_4992	Uip3p	0,362
CENPK1137D_4967	Ntg1p	0,539	CENPK1137D_2389	Ald4p	-0,229
CENPK1137D_429	Aqy1p	0,910	CENPK1137D_5119	hypothetical protein	0,399
CENPK1137D_958	Cbt1p	0,508	CENPK1137D_3016	Scm4p	0,377
CENPK1137D_4213	Ato3p	-0,517	CENPK1137D_2139	Gcy1p	0,372
CENPK1137D_649	Mcm5p	-0,424	CENPK1137D_1130	Fre2p	0,353
CENPK1137D_5285	Rim4p	-0,375	CENPK1137D_124	Coq5p	-0,225
CENPK1137D_4936	Erv46p	0,419	CENPK1137D_2402	Fdh1p	-0,405
CENPK1137D_1152	Sry1p	0,535	CENPK1137D_2486	Slz1p	0,394
CENPK1137D_86	Fet3p	0,735	CENPK1137D_1161	Rpt1p	-0,263
CENPK1137D_1481	Ino1p	-0,734	CENPK1137D_4858	Mal32p	0,462
CENPK1137D_4971	Cne1p	0,461	CENPK1137D_3640	Gtt3p	0,255
CENPK1137D_2934	hypothetical protein	0,762	CENPK1137D_3341	Fet5p	-0,165
CENPK1137D_4611	Tip1p	-0,342	CENPK1137D_1769	Spe3p	-0,345
CENPK1137D_1062	Ysr3p	0,591	CENPK1137D_650	Mmp1p	0,285
CENPK1137D_2738	Bio3p	0,377	CENPK1137D_3187	Tos2p	0,258
CENPK1137D_823	Sst2p	-0,590	CENPK1137D_3059	Dbf2p	-0,223
CENPK1137D_582	Hmx1p	0,350	CENPK1137D_501	Avl9p	-0,255
CENPK1137D_2735	Bio5p	0,437	CENPK1137D_4205	Lsm6p	-0,270
CENPK1137D_134	Ypk2p	-0,324	CENPK1137D_287	Faa4p	-0,314
CENPK1137D_3398	Gsy1p	-0,387	CENPK1137D_3344	Ypt1p	-0,132
CENPK1137D_4229	Dit2p	0,519	CENPK1137D_3773	Mch1p	-0,241
CENPK1137D_4977	Efb1p	0,474	CENPK1137D_2633	hypothetical protein	0,309
CENPK1137D_4318	Izh1p	0,495	CENPK1137D_4752	Bem1p	-0,181
CENPK1137D_4961	Ccr4p	0,344	CENPK1137D_2823	Cos12p	0,447
CENPK1137D_1043	Dal80p	-0,700	CENPK1137D_1445	hypothetical protein	0,330
CENPK1137D_166	hypothetical protein	0,381	CENPK1137D_4279	Tsa2p	0,438
CENPK1137D_4949	Bdh1p	0,447	CENPK1137D_738	Cox19p	0,342
CENPK1137D_4980	Nup60p	0,336	CENPK1137D_290	Gim5p	0,241
CENPK1137D_2364	Cin1p	0,433	CENPK1137D_5368	Pho12p	0,390
CENPK1137D_5373	Ecm34p	0,493	CENPK1137D_2070	Bds1p	0,415
CENPK1137D_3142	Atf2p	0,479	CENPK1137D_5439	Sbp1p	-0,195
CENPK1137D_4983	Swd1p	0,358	CENPK1137D_3682	Yat2p	-0,342
CENPK1137D_4974	Spo7p	0,421	CENPK1137D_5106	Cos8p	0,257
CENPK1137D_3823	Nhp10p	0,358	CENPK1137D_4534	Hmlalpha2p	-0,394

CENPK_ID	GeneID	log2FC	CENPK_ID	GeneID	log2FC
CENPK1137D_4637	Nhp6bp	-0,516	CENPK1137D_5105	hypothetical protein	0,292
CENPK1137D_4945	Mtw1p	0,419	CENPK1137D_1851	Gph1p	-0,275
CENPK1137D_5091	Dal1p	0,577	CENPK1137D_538	hypothetical protein	-0,199
CENPK1137D_1480	hypothetical protein	0,491	CENPK1137D_2145	Rga1p	-0,234
CENPK1137D_955	Sfk1p	0,372	CENPK1137D_1820	Ant1p	0,182
CENPK1137D_2248	Mdh2p	-0,513	CENPK1137D_380	Tcb3p	-0,175
CENPK1137D_2416	Izh4p	0,611	CENPK1137D_1541	Tgs1p	0,244
CENPK1137D_4990	hypothetical protein	0,643	CENPK1137D_3623	Mcm3p	-0,215
CENPK1137D_4972	Swc3p	0,410	CENPK1137D_3307	Lys5p	0,345
CENPK1137D_3276	Tpn1p	0,266	CENPK1137D_537	Pcd1p	-0,270
CENPK1137D_3371	Hxt10p	-0,647	CENPK1137D_3266	Adh4p	0,264
CENPK1137D_5024	Prm2p	0,499	CENPK1137D_5238	Hxt4p	0,279
CENPK1137D_898	Gfa1p	-0,302	CENPK1137D_2835	Hfm1p	0,354
CENPK1137D_920	Hot13p	0,561	CENPK1137D_5411	Arg4p	-0,224
CENPK1137D_4986	Bud14p	0,262	CENPK1137D_1591	Thi21p	0,332
CENPK1137D_885	Pau23p	0,497	CENPK1137D_4937	Cdc24p	0,227
CENPK1137D_4948	Prp45p	0,323	CENPK1137D_2448	Emi5p	0,221
CENPK1137D_3402	hypothetical protein	0,381	CENPK1137D_1201	Lsb6p	0,182
CENPK1137D_4940	Cyc3p	0,384	CENPK1137D_3370	hypothetical protein	-0,406
CENPK1137D_4984	Rfa1p	0,307	CENPK1137D_5154	Mob1p	-0,266
CENPK1137D_4942	hypothetical protein	0,545	CENPK1137D_2798	Atg2p	-0,285
CENPK1137D_4956	Mak16p	0,461	CENPK1137D_2408	Shr5p	0,387
CENPK1137D_4657	Alg1p	0,295	CENPK1137D_348	Yme2p	-0,159
CENPK1137D_5396	Gpa1p	-0,312	CENPK1137D_4626	Spt7p	-0,204
CENPK1137D_996	Cce1p	0,481	CENPK1137D_4430	Ahc2p	-0,251
CENPK1137D_2090	Nrt1p	0,355	CENPK1137D_2736	Bio4p	0,306
CENPK1137D_1408	hypothetical protein	0,418	CENPK1137D_4959	Fun26p	0,246
CENPK1137D_4985	Sen34p	0,398	CENPK1137D_151	Asi1p	-0,276
CENPK1137D_1641	Grx5p	-0,265	CENPK1137D_3852	Pst2p	-0,221
CENPK1137D_2397	Fit3p	0,596	CENPK1137D_3872	Cdc34p	-0,249
CENPK1137D_986	Ram2p	0,240	CENPK1137D_1669	Svl3p	0,322
CENPK1137D_489	Erg27p	0,320	CENPK1137D_3794	Slm3p	0,241
CENPK1137D_1443	Hms2p	0,425	CENPK1137D_2819	Flp1p	0,359
CENPK1137D_4944	Fun12p	0,311	CENPK1137D_3674	Spc25p	0,254
CENPK1137D_5330	Aim17p	0,265	CENPK1137D_4535	Taf2p	-0,296
CENPK1137D_2818	Raf1p	0,567	CENPK1137D_4989	Cdc15p	0,270
CENPK1137D_4932	Aim1p	0,444	CENPK1137D_5157	Dph1p	0,214
CENPK1137D_4935	Pta1p	0,369	CENPK1137D_4960	Ecm1p	0,340
CENPK1137D_3785	Prp11p	-0,349	CENPK1137D_1814	Clb5p	0,224
CENPK1137D_91	Arg7p	0,288	CENPK1137D_3267	Dsd1p	0,156
CENPK1137D_1316	Tes1p	0,413	CENPK1137D_2154	Sia1p	-0,227
CENPK1137D_4958	Pmt2p	0,385	CENPK1137D_1643	Sur1p	-0,231
CENPK1137D_3618	Utr4p	-0,393	CENPK1137D_863	Meu1p	-0,202
CENPK1137D_515	Zrt2p	0,338	CENPK1137D_233	Vti1p	-0,168
CENPK1137D_4939	Cln3p	0,338	CENPK1137D_4039	Adr1p	-0,307
CENPK1137D_4954	Saw1p	0,394	CENPK1137D_3356	Gyp8p	0,253
CENPK1137D_4969	Dep1p	0,316	CENPK1137D_4594	Reb1p	-0,211
CENPK1137D_1379	Emc2p	-0,276	CENPK1137D_4199	Frq1p	-0,233
CENPK1137D_85	Aac1p	0,372	CENPK1137D_4973	Mdm10p	0,327
CENPK1137D_3558	Ftr1p	0,396	CENPK1137D_488	hypothetical protein	0,275

CENPK_ID	GeneID	log2FC	CENPK_ID	GeneID	log2FC
CENPK1137D_1946	Cti6p	0,243	CENPK1137D_1267	Tad2p	0,285
CENPK1137D_4299	Trs31p	0,295	CENPK1137D_3789	Prm7p	0,392
CENPK1137D_1157	Mcr1p	0,307	CENPK1137D_2230	Sas5p	0,206
CENPK1137D_4950	Gip4p	0,336	CENPK1137D_848	Jlp1p	0,381
CENPK1137D_3350	Snz2p	0,463	CENPK1137D_3985	Sec1p	0,184
CENPK1137D_3339	Sno3p	0,310	CENPK1137D_2710	Hub1p	-0,325
CENPK1137D_4947	Pop5p	0,423	CENPK1137D_4976	Erp2p	0,358
CENPK1137D_3375	Smc1p	-0,224	CENPK1137D_1503	Ura2p	-0,247
CENPK1137D_5137	Qdr2p	0,452	CENPK1137D_837	hypothetical protein	0,225
CENPK1137D_5444	Aap1p	-0,277	CENPK1137D_3477	Arg5,6p	0,191
CENPK1137D_4422	Kar4p	-0,269	CENPK1137D_4757	Cos111p	-0,244
CENPK1137D_4981	Erp1p	0,354	CENPK1137D_5210	Htd2p	0,200
CENPK1137D_5441	Dog1p	0,440	CENPK1137D_3029	Cox18p	0,320
CENPK1137D_3656	Mnn1p	0,382	CENPK1137D_1476	Far1p	-0,341
CENPK1137D_2449	Nba1p	-0,259	CENPK1137D_5199	Cpr2p	-0,202
CENPK1137D_5350	Aim18p	0,234	CENPK1137D_306	hypothetical protein	0,242
CENPK1137D_4963	Fun30p	0,345	CENPK1137D_2663	Spo1p	0,327
CENPK1137D_1676	Rmi1p	0,280	CENPK1137D_3854	Mrh1p	0,224
CENPK1137D_2805	hypothetical protein	0,468	CENPK1137D_931	Stb6p	0,298
CENPK1137D_1226	Smc3p	-0,216	CENPK1137D_1754	Smk1p	0,318
CENPK1137D_4627	Ubc4p	-0,229	CENPK1137D_2545	hypothetical protein	0,385
CENPK1137D_889	hypothetical protein	-0,425	CENPK1137D_2032	Tir2p	0,344
CENPK1137D_4962	Ats1p	0,413	CENPK1137D_4933	hypothetical protein	0,332
CENPK1137D_4987	Ade1p	0,408	CENPK1137D_1703	Pdh1p	-0,349
CENPK1137D_1371	Bna2p	-0,318	CENPK1137D_3841	Gcv1p	-0,296
CENPK1137D_3907	Afr1p	-0,382	CENPK1137D_2349	Vma4p	-0,162
CENPK1137D_3641	Npp2p	0,255	CENPK1137D_2067	Std1p	0,347
CENPK1137D_2468	Rap1p	-0,221	CENPK1137D_4616	hypothetical protein	-0,201
CENPK1137D_4449	hypothetical protein	0,254	CENPK1137D_4979	Tfc3p	0,283
CENPK1137D_4568	Chs3p	-0,280	CENPK1137D_1022	Pry2p	0,254
CENPK1137D_4584	Fig1p	-0,482	CENPK1137D_5134	Ayr1p	-0,347
CENPK1137D_1673	Erg10p	-0,172	CENPK1137D_5049	Tir3p	0,365
CENPK1137D_5130	Nit1p	0,332	CENPK1137D_3204	Kel2p	0,204
CENPK1137D_4712	Cdc28p	0,215	CENPK1137D_1351	Cdc6p	-0,258
CENPK1137D_4614	Tat1p	0,357	CENPK1137D_683	Cdc25p	-0,262
CENPK1137D_1350	Aps2p	0,344	CENPK1137D_4868	hypothetical protein	0,203
CENPK1137D_4994	hypothetical protein	0,449			

TABLE A.10. Transcriptomics results from the comparison R-GK vs. R-GKU of genes with multiple testing adjusted q-values < 0.1. The genes are sorted according to their significance. *This table and the corresponding legend text have been reproduced from Strucko et al. (2018) with permission [178].*

CENPK_ID	GeneID	log2FC
CENPK1137D_2748	Cos10p	-0,650
CENPK1137D_3608	hypothetical protein	-0,246
CENPK1137D_2735	Bio5p	0,281
CENPK1137D_2439	Zps1p	-0,347
CENPK1137D_3620	Anp1p	-0,157

TABLE A.11. Transcriptomics results from the comparison R-GU vs. R-GKU of genes with multiple testing adjusted q-values of 0.1. The genes are sorted according to their significance. *This table and the corresponding legend text have been reproduced from Strucko et al. (2018) with permission [178].*

CENPK_ID	**GeneID**	**log2FC**	**CENPK_ID**	**GeneID**	**log2FC**
CENPK1137D_1498	hypothetical protein	1,959	CENPK1137D_4111	Nse3	0,343
CENPK1137D_1480	hypothetical protein	1,337	CENPK1137D_2614	Aqr1	0,470
CENPK1137D_3610	Dld3	1,244	CENPK1137D_1676	Rmi1	0,289
CENPK1137D_1444	Bat2	0,856	CENPK1137D_425	Yox1	-0,246
CENPK1137D_3315	Ddi3	0,695	CENPK1137D_4944	Fun12	-0,282
CENPK1137D_476	Alt1	0,705	CENPK1137D_4696	Ysw1	0,409
CENPK1137D_5330	Aim17	0,509	CENPK1137D_3481	Ald5	-0,274
CENPK1137D_2238	Mct1	0,488	CENPK1137D_2895	Fmp37	0,303
CENPK1137D_1702	Cit3	0,905	CENPK1137D_4611	Tip1	0,219
CENPK1137D_2748	Cos10	-0,953	CENPK1137D_2402	Fdh1	-0,417
CENPK1137D_718	Dic1	0,668	CENPK1137D_5024	Prm2	0,380
CENPK1137D_5370	Dur3	0,498	CENPK1137D_5069	Ist3	0,426
CENPK1137D_1739	hypothetical protein	0,616	CENPK1137D_1591	Thi21	0,378
CENPK1137D_4319	Glt1	0,460	CENPK1137D_609	Bna5	0,259
CENPK1137D_1525	Dip5	0,818	CENPK1137D_679	Cda1	0,441
CENPK1137D_2537	Mep2	0,792	CENPK1137D_1899	hypothetical protein	0,256
CENPK1137D_1962	Arg1	0,566	CENPK1137D_4620	Ecm8	0,447
CENPK1137D_4500	Cit2	0,713	CENPK1137D_2677	Ato2	0,446
CENPK1137D_1524	Sam3	-0,525	CENPK1137D_1667	Srl4	0,394
CENPK1137D_2886	Mf(alpha)2	0,605	CENPK1137D_2740	Fre4	0,374
CENPK1137D_3267	Dsd1	0,303	CENPK1137D_4088	Din7	0,305
CENPK1137D_5142	Prm5	0,499	CENPK1137D_4368	hypothetical protein	-0,311
CENPK1137D_1707	Icl2	0,541	CENPK1137D_4708	Ics2	0,398
CENPK1137D_2735	Bio5	0,422	CENPK1137D_3601	Pug1	0,409
CENPK1137D_5373	Ecm34	0,511	CENPK1137D_2397	Fit3	0,439
CENPK1137D_3854	Mrh1	-0,419	CENPK1137D_4609	Nrg2	0,360
CENPK1137D_1049	Gap1	0,439	CENPK1137D_5106	Cos8	0,277
CENPK1137D_3682	Yat2	0,537	CENPK1137D_920	Hot13	0,403
CENPK1137D_712	Gas2	0,648	CENPK1137D_5433	Put2	0,141
CENPK1137D_1163	Jen1	0,456	CENPK1137D_1640	Mfm1	0,318
CENPK1137D_4614	Tat1	0,486	CENPK1137D_2253	Hes1	0,324
CENPK1137D_1600	Aim43	0,388	CENPK1137D_3615	Yef1	-0,343
CENPK1137D_963	Phd1	0,329	CENPK1137D_1062	Ysr3	0,334
CENPK1137D_1703	Pdh1	0,563	CENPK1137D_1438	hypothetical protein	0,344
CENPK1137D_5382	hypothetical protein	-0,376	CENPK1137D_479	Sul2	-0,291
CENPK1137D_1820	Ant1	0,270	CENPK1137D_1737	Gln1	0,328
CENPK1137D_2316	Mum3	0,558	CENPK1137D_4422	Kar4	0,227
CENPK1137D_4336	Gnp1	0,495	CENPK1137D_5133	Kgd1	-0,280
CENPK1137D_28	Ypt7	0,348	CENPK1137D_4478	hypothetical protein	0,407
CENPK1137D_2531	Pga2	0,327	CENPK1137D_3256	Sip2	-0,198
CENPK1137D_183	Imp1	0,314	CENPK1137D_2943	Scw11	-0,325
CENPK1137D_4229	Dit2	0,410	CENPK1137D_2148	Pfk27	0,354
CENPK1137D_612	Thi7	0,356	CENPK1137D_5208	Gos1	-0,191
CENPK1137D_5138	Qdr1	0,420	CENPK1137D_4472	Fus1	0,360
CENPK1137D_1790	Rds3	0,406	CENPK1137D_1434	Met5	-0,301
CENPK1137D_4650	Vid24	0,511	CENPK1137D_412	Cat2	0,326
CENPK1137D_3209	Fmp43	0,339	CENPK1137D_771	Dus3	-0,289
CENPK1137D_5177	Cab2	0,250	CENPK1137D_889	hypothetical protein	0,341

TABLE A.12. Proteomics results of ALE2, R-GKU, R-GU and R-GK of proteins with multiple testing adjusted P-values < 0.1. The genes are sorted according to their significance. *This table and the corresponding legend text have been reproduced from Strucko et al. (2018) with permission [178].*

comparison	protein_id	description	gene_name	mw	logFC	AveExpr	t	P.Value	adj.P.Val	B	qval	lfdr
R-GKU - ALE2	N1P965	Bar1p	CENPK1137D_5045	69932,1	-2,946	20,68	-16,52	6,59E-07	0,0023	4,066	3,75E-13	3,75E-13
R-GKU - ALE2	N1P0N0	Ste3p	CENPK1137D_1133	60889,4	2,606	22,76	14,63	1,52E-06	0,0027	3,766	3,75E-13	3,75E-13
R-GKU - ALE2	N1NYP0	Fet3p	CENPK1137D_86	77485,5	-1,475	23,14	-9,46	2,89E-05	0,0337	2,299	7,67E-10	0,0001
R-GK - R-GKU	N1P6A4	Ubc13p	CENPK1137D_3916	20493,3	3,643	20,54	14,28	1,79E-06	0,0063	-1,510	7,70E-13	7,70E-13
R-GU - R-GKU	N1P8D9	Pho3p	CENPK1137D_4639	58450,1	2,438	21,07	13,94	2,12E-06	0,0074	2,692	2,46E-13	2,46E-13
R-GU - R-GKU	N1P1X2	Cit3p	CENPK1137D_1702	60592,5	1,233	23,68	8,79	4,69E-05	0,0570	1,440	2,46E-13	2,46E-13
R-GU - R-GKU	N1P7B4	Dld3p	CENPK1137D_3610	64714,8	1,291	22,89	8,73	4,90E-05	0,0570	1,418	2,46E-13	2,46E-13

Table A.13: GO term analysis of significant genes (q-value < 0.1) of the comparison ALE2 vs R-GKU. *This table and the corresponding legend text have been reproduced from Strucko et al. (2018) with permission [178].*

ontology	GO.ID	Term	Annotated	Significant	Expected	Fisher.classic
MF	GO:0000772	mating pheromone activity	3	3	0,34	0,0014
MF	GO:0005102	receptor binding	3	3	0,34	0,0014
MF	GO:0005186	pheromone activity	3	3	0,34	0,0014
MF	GO:0030234	enzyme regulator activity	49	11	5,5	0,0153
MF	GO:0008047	enzyme activator activity	25	7	2,81	0,0159
MF	GO:0016705	oxidoreductase activity, acting on paired donors, with incorporation or reduction of molecular oxygen	6	3	0,67	0,0213
MF	GO:0016788	hydrolase activity, acting on ester bonds	54	11	6,06	0,031
MF	GO:0004872	receptor activity	7	3	0,79	0,0343
MF	GO:0060089	molecular transducer activity	7	3	0,79	0,0343
MF	GO:0047429	nucleoside-triphosphate diphosphatase activity	3	2	0,34	0,0347
MF	GO:0005057	receptor signaling protein activity	3	2	0,34	0,0347
MF	GO:0005199	structural constituent of cell wall	3	2	0,34	0,0347
MF	GO:0005096	GTPase activator activity	12	4	1,35	0,0364
MF	GO:0030695	GTPase regulator activity	12	4	1,35	0,0364
MF	GO:0016810	hydrolase activity, acting on carbon-nitrogen (but not peptide) bonds	18	5	2,02	0,042
BP	GO:0044764	multi-organism cellular process	32	15	3,59	2,40E-07
BP	GO:0000746	conjugation	32	15	3,59	2,40E-07
BP	GO:0000747	conjugation with cellular fusion	32	15	3,59	2,40E-07
BP	GO:0019236	response to pheromone	25	13	2,81	3,60E-07
BP	GO:0000749	response to pheromone involved in conjugation with cellular fusion	19	11	2,13	7,50E-07
BP	GO:0071444	cellular response to pheromone	23	12	2,58	1,00E-06
BP	GO:0000750	pheromone-dependent signal transduction involved in conjugation with cellular fusion	9	7	1,01	5,50E-06
BP	GO:0032005	signal transduction involved in conjugation with cellular fusion	9	7	1,01	5,50E-06

ontology	GO.ID	Term	Annotated	Significant	Expected	Fisher.classic
MF	GO:0000772	mating pheromone activity	3	3	0,34	0,0014
MF	GO:0005102	receptor binding	3	3	0,34	0,0014
MF	GO:0005186	pheromone activity	3	3	0,34	0,0014
MF	GO:0030234	enzyme regulator activity	49	11	5,5	0,0153
MF	GO:0008047	enzyme activator activity	25	7	2,81	0,0159
MF	GO:0016705	oxidoreductase activity, acting on paired donors, with incorporation or reduction of molecular oxygen	6	3	0,67	0,0213
MF	GO:0016788	hydrolase activity, acting on ester bonds	54	11	6,06	0,031
MF	GO:0004872	receptor activity	7	3	0,79	0,0343
MF	GO:0060089	molecular transducer activity	7	3	0,79	0,0343
MF	GO:0047429	nucleoside-triphosphate diphosphatase activity	3	2	0,34	0,0347
MF	GO:0005057	receptor signaling protein activity	3	2	0,34	0,0347
MF	GO:0005199	structural constituent of cell wall	3	2	0,34	0,0347
MF	GO:0005096	GTPase activator activity	12	4	1,35	0,0364
MF	GO:0030695	GTPase regulator activity	12	4	1,35	0,0364
MF	GO:0016810	hydrolase activity, acting on carbon-nitrogen (but not peptide) bonds	18	5	2,02	0,042
BP	GO:0044764	multi-organism cellular process	32	15	3,59	2,40E-07
BP	GO:0000746	conjugation	32	15	3,59	2,40E-07
BP	GO:0000747	conjugation with cellular fusion	32	15	3,59	2,40E-07
BP	GO:0019236	response to pheromone	25	13	2,81	3,60E-07
BP	GO:0000749	response to pheromone involved in conjugation with cellular fusion	19	11	2,13	7,50E-07
BP	GO:0071444	cellular response to pheromone	23	12	2,58	1,00E-06
BP	GO:0000750	pheromone-dependent signal transduction involved in conjugation with cellular fusion	9	7	1,01	5,50E-06
BP	GO:0032005	signal transduction involved in conjugation with cellular fusion	9	7	1,01	5,50E-06

ontology	GO.ID	Term	Annotated	Significant	Expected	Fisher.classic
BP	GO:0071310	cellular response to organic substance	35	14	3,93	6,70E-06
BP	GO:0007186	G-protein coupled receptor signaling pathway	10	7	1,12	1,70E-05
BP	GO:0019953	sexual reproduction	64	19	7,18	2,30E-05
BP	GO:0051704	multi-organism process	64	19	7,18	2,30E-05
BP	GO:0044703	multi-organism reproductive process	64	19	7,18	2,30E-05
BP	GO:0022414	reproductive process	120	28	13,46	3,30E-05
BP	GO:0010033	response to organic substance	45	15	5,05	4,10E-05
BP	GO:0000003	reproduction	124	28	13,91	6,40E-05
BP	GO:0070887	cellular response to chemical stimulus	60	17	6,73	0,00013
BP	GO:0042221	response to chemical	80	20	8,98	0,00021
BP	GO:0050896	response to stimulus	204	33	22,89	0,00947
BP	GO:0044700	single organism signaling	59	13	6,62	0,00997
BP	GO:0007165	signal transduction	59	13	6,62	0,00997
BP	GO:0044093	positive regulation of molecular function	30	8	3,37	0,01362
BP	GO:0023052	signaling	62	13	6,96	0,01525
BP	GO:0065009	regulation of molecular function	54	11	6,06	0,03096
BP	GO:0007117	budding cell bud growth	7	3	0,79	0,03431
BP	GO:0006882	cellular zinc ion homeostasis	3	2	0,34	0,03469
BP	GO:0051180	vitamin transport	3	2	0,34	0,03469
BP	GO:0055069	zinc ion homeostasis	3	2	0,34	0,03469
BP	GO:0010243	response to organonitrogen compound	3	2	0,34	0,03469
BP	GO:0000767	cell morphogenesis involved in conjugation	3	2	0,34	0,03469
BP	GO:0000753	cell morphogenesis involved in conjugation with cellular fusion	3	2	0,34	0,03469
BP	GO:0022610	biological adhesion	3	2	0,34	0,03469
BP	GO:0072503	cellular divalent inorganic cation homeostasis	3	2	0,34	0,03469
BP	GO:0072507	divalent inorganic cation homeostasis	3	2	0,34	0,03469

ontology	GO.ID	Term	Annotated	Significant	Expected	Fisher.classic
BP	GO:0045740	positive regulation of DNA replication	3	2	0,34	0,03469
BP	GO:0007155	cell adhesion	3	2	0,34	0,03469
BP	GO:0007154	cell communication	76	14	8,53	0,0354
CC	GO:0005576	extracellular region	15	10	1,68	3,90E-07
CC	GO:0071944	cell periphery	125	32	14,03	7,10E-07
CC	GO:0005886	plasma membrane	92	23	10,32	6,30E-05
CC	GO:0005618	cell wall	23	8	2,58	0,0022
CC	GO:0030312	external encapsulating structure	23	8	2,58	0,0022
CC	GO:0009277	fungal-type cell wall	23	8	2,58	0,0022
CC	GO:0016020	membrane	331	50	37,14	0,004
CC	GO:0031224	intrinsic component of membrane	233	38	26,14	0,004
CC	GO:0044459	plasma membrane part	39	10	4,38	0,0079
CC	GO:0044425	membrane part	270	41	30,29	0,0108
CC	GO:0016021	integral component of membrane	217	33	24,35	0,0248
CC	GO:0031225	anchored component of membrane	16	5	1,8	0,0257
CC	GO:0005887	integral component of plasma membrane	28	7	3,14	0,0294
CC	GO:0098797	plasma membrane protein complex	3	2	0,34	0,0347
CC	GO:0031226	intrinsic component of plasma membrane	30	7	3,37	0,0419

TABLE A.14. Intracellular metabolites. *This table and the corresponding legend text have been reproduced from Strucko et al. (2018) with permission [178].*

substrate/product	ALE2_R1	ALE2_R2	ALE2_R3	TS177(R-GKU)_R1	TS177(R-GKU)_R2	TS177(R-GKU)_R3	TS154(R-GU)_R1	TS154(R-GU)_R2	ALE2		TS177(R-GKU)		TS154(R-GU)		Flux Change
									Average	CoV	Average	CoV	Average	CoV	WT/kgd1
glucose/lactate	7,246391916	2,272082268	7,318373055	3,639363908	6,757009716	3,648512323	1,529628403	1,534414538	5,612282	52%	4,681629	38%	1,532021	0%	0,33
pyruvate/lactate	0,065353444	0,454089682	0,524232275	0,12557921	0,156022676	0,124421356	0,055805204	0,034313264	0,347892	71%	0,135008	13%	0,045059	34%	0,33
citrate/aKG	15,48725054	3,398657416	7,13106586	5,349127789	5,380956819	5,664638881	19,66550337	32,49049429	8,672325	71%	5,464908	3%	26,078	35%	4,77
aKG/succinate	0,283013129	0,479550171	0,518492044	0,667192225	0,363989498	0,528257245	0,046494087	0,048662071	0,427018	30%	0,519813	29%	0,047578	3%	0,09
succinate/fumarate	1,872510141	0,642696869	0,771757407	1,082183331	1,169701458	0,977112778	2,926116413	2,459384683	1,095655	62%	1,076333	9%	2,692751	12%	2,50
GABA/succinate	4,711062558	2,395083012	6,480751452	5,052183647	5,784996861	8,703333333	1,174013652	1,652762468	4,528819	45%	6,513505	30%	1,413388	24%	0,22
2HG/aKG	5,665937323	4,168513552	4,252604173	3,702192467	4,753253364	4,231731145	7,195794575	7,829741855	4,695685	18%	4,229059	12%	7,512768	6%	1,78
glycerol-3p/glycerate-3p	1,076061701	0,908839728	0,754278558	1,136799034	1,175566888	1,114056157	2,956095311	1,613492301	0,913393	18%	1,142141	3%	2,284794	42%	2,00

TABLE A.15. Implemented uptake constraints calculated from experimentally measured consumption rates of human cell lines (Jain 2012). The MetaboliteID indicates the metabolite in the model for which the uptake reaction flux was constrained. An uptake and transport reaction were added to the model in case they did not already exist. Note that the convention for exchange reaction in SBML formatted metabolic models is that uptake constraints have positive values and output constraints have negative values. If no uptake was experimentally observed for a metabolite (no change in medium concentration or an increase in medium concentration) the corresponding uptake flux was constrained to zero in case a transport reaction for that metabolite already existed in the model. *Metabolites that cannot be uniquely identified in the model (none or more than one metabolite matches in the model) **Metabolites for which no literature evidence exists that they can be uptaken by human cells

		Measured consumption rate [f mol/cell/hour]		Fluxes [mmol/gDW/h]	Upper constraint
Metabolite	**MetaboliteID**	**Lowest (all cell lines)**	**Highest (all cell lines)**		
glucose	m01965	-38,901	-861,928	8,619280	8,619280
glutamine	m01975	-13,872	-304,272	3,042720	3,042720
arginine	m01365	2,893	-35,143	0,351430	0,351430
serine	m02896	-2,048	-33,941	0,339410	0,339410
leucine	m02360	-1,977	-26,115	0,261150	0,261150
isoleucine	m02184	-1,063	-21,599	0,215990	0,215990
lysine	m02426	-2,543	-19,234	0,192340	0,192340
asparagine	m01369	2,839	-18,501	0,185010	0,185010
valine	m03135	-1,779	-15,760	0,157600	0,157600
guanidinoacetate	m02036	-1,419	-12,259	0,122590	0,122590
threonine	m02993	-1,379	-12,238	0,122380	0,122380
tyrosine	m03101	-1,052	-10,701	0,107010	0,107010
aspartate	m01370	8,221	-8,645	0,086450	0,086450
phenylalanine	m02724	-0,834	-7,305	0,073050	0,073050
methionine	m02471	-0,700	-7,015	0,070150	0,070150
glyceraldehyde	m01981	0,361	-6,523	0,065230	0,065230
homoserine	m02136	-0,408	-5,770	0,057700	0,057700
glycine	m01986	11,704	-5,650	0,056500	0,056500
cis-hydroxyproline/trans-hydroxyproline	m03037	0,945	-4,368	0,043680	0,043680
glutamate	m01974	96,547	-3,823	0,038230	0,038230
alpha-glycerophosphocholine*	-	83,958	-3,534	0,035340	-
tryptophan	m03089	-0,027	-3,491	0,034910	0,034910
ornithine	m02658	9,966	-3,290	0,032900	0,032900
alanine	m01307	65,407	-2,750	0,027500	0,027500
choline	m01513	0,261	-2,298	0,022980	0,022980
creatine	m01619	0,312	-1,594	0,015940	0,015940
proline	m02770	5,782	-1,194	0,011940	0,011940
niacinamide	m02583	0,028	-0,919	0,009190	0,009190
taurine	m02961	0,029	-0,612	0,006120	0,006120
bilirubin	m01396	0,639	-0,455	0,004550	0,004550
citrulline	m01588	0,062	-0,373	0,003730	0,003730
glycerol_1	m01983	4,174	-0,356	0,003560	0,003560
thiamine	m02982	0,249	-0,331	0,003310	0,003310
hypoxanthine	m02159	0,040	-0,227	0,002270	0,002270
oxalate	m02661	0,108	-0,175	0,001750	0,001750
urate	m03120	0,106	-0,153	0,001530	0,001530
succinate	m02943	0,639	-0,141	0,001410	0,001410
citrate	m01587	6,372	-0,133	0,001330	0,001330
betaine	m01393	0,204	-0,133	0,001330	0,001330
uracil	m03118	0,482	-0,123	0,001230	0,001230
uridine	m03123	0,296	-0,079	0,000790	0,000790
carnitine	m02348	0,012	-0,078	0,000780	0,000780
serotonin	m02897	0,140	-0,075	0,000750	0,000750
acetoacetate	m01253	4,026	-0,073	0,000730	0,000730
carnosine	m01423	0,038	-0,066	0,000660	0,000660
cytidine	m01630	0,047	-0,042	0,000420	0,000420
dimethylglycine	m01708	0,029	-0,041	0,000410	0,000410
pantothenate	m02680	0,003	-0,038	0,000380	0,000380
aminoisobutyrate*	-	0,005	-0,034	0,000340	-
kynurenine	m02319	1,143	-0,030	0,000300	0,000300
2'-deoxycytidine	m01668	1,563	-0,029	0,000290	0,000290
2'-deoxyuridine	m01673	0,044	-0,024	0,000240	0,000240
folate	m01830	0,099	-0,023	0,000230	0,000230
thymidine	m02996	0,072	-0,020	0,000200	0,000200
spermidine	m02923	0,035	-0,018	0,000180	0,000180
isocitrate	m02183	0,070	-0,017	0,000170	0,000170
2-aminoadipate	m02322	0,077	-0,017	0,000170	0,000170
kynurenate	m00990	0,028	-0,016	0,000160	0,000160
propionate	m02772	0,033	-0,016	0,000160	0,000160

Metabolite	MetaboliteID	Measured consumption rate [f mol/cell/hour] Lowest (all cell lines)	Highest (all cell lines)	Fluxes [mmol/gDW/h]	Upper constraint
anthranilate	m01342	0,198	-0,014	0,000140	0,000140
lactose	m02332	0,122	-0,013	0,000130	0,000130
spermine	m02926	0,028	-0,013	0,000130	0,000130
homocysteine	m02133	0,219	-0,012	0,000120	0,000120
5-HIAA	m01103	0,053	-0,007	0,000070	0,000070
glycodeoxycholate/glycochenodeoxycholate*	m01989/m01987	0,001	-0,007	0,000070	-
3-phosphoglycerate	m00913	0,050	-0,006	0,000060	0,000060
xanthosine	m03149	0,012	-0,006	0,000060	0,000060
thymine	m02997	0,036	-0,004	0,000040	0,000040
creatinine**	m01621	1,073	-0,003	0,000030	0,000000
phosphoethanolamine	m01798	0,218	-0,003	0,000030	0,000030
glucuronate	m01973	0,038	-0,003	0,000030	0,000030
sucrose	m02945	0,025	-0,003	0,000030	0,000030
taurodeoxycholate/taurochenodeoxycholate*	-	0,003	-0,003	0,000030	-
XMP	m03150	0,042	-0,003	0,000030	0,000030
2-phosphoglycerate	m00674	0,057	-0,002	0,000020	0,000020
4-hydroxybenzoate	m00995	0,012	-0,002	0,000020	0,000020
alpha-ketoglutarate**	m01306	0,026	-0,002	0,000020	0,000000
glycocholate**	m01988	0,000	-0,002	0,000020	0,000000
IMP	m02167	0,004	-0,002	0,000020	0,000020
GABA	m00970	0,344	-0,001	0,000010	0,000010
4-pyridoxate	m01033	0,003	-0,001	0,000010	0,000010
adenine	m01279	0,018	-0,001	0,000010	0,000010
AMP	m01334	0,054	-0,001	0,000010	0,000010
cystathionine	m02349	0,259	-0,001	0,000010	0,000010
glutathione oxidized	m02027	0,911	-0,001	0,000010	0,000010
inosine	m02170	0,026	-0,001	0,000010	0,000010
niacin	m02586	0,001	-0,001	0,000010	0,000010
PEP	m02696	0,017	-0,001	0,000010	0,000010
quinolinate**	m02822	0,003	-0,001	0,000010	0,000000
taurocholate**	m02963	0,000	-0,001	0,000010	0,000000
thyroxine	m02998	0,000	-0,001	0,000010	0,000010
methylmalonate	m02479	0,000	0,000	0,000000	-
allantoin	m01313	0,000	0,000	0,000000	-
ADMA	m02577	0,000	0,000	0,000000	-
maleate*	-	0,000	0,000	0,000000	-
malonate	m02440	0,000	0,000	0,000000	0,000000
lithocholate	m02402	0,000	0,000	0,000000	-
citrate/isocitrate*	-	0,000	0,000	0,000000	-
cotinine*	-	0,000	0,000	0,000000	-
trimethylamine-N-oxide	m03054	0,000	0,000	0,000000	-
phenylacetylglycine	m02723	0,000	0,000	0,000000	0,000000
biotin	m01401	0,000	0,000	0,000000	0,000000
hippurate	m02123	0,000	0,000	0,000000	-
hyodeoxycholate/ursodeoxycholate*	m02155/m03129	0,000	0,000	0,000000	-
salicylurate*	-	0,000	0,000	0,000000	-
ascorbate	m01368	0,000	0,000	0,000000	0,000000
fru-1,6-DP/fru-2,6-DP/glc-1,6-DP*	-	0,000	0,000	0,000000	-
chenodeoxycholate/deoxycholate*	-	0,000	0,000	0,000000	-
taurolithocholate	m02965	0,000	0,000	0,000000	-
glycerol_2*	-	0,000	0,000	0,000000	-
UDP-galactose/UDP-glucose*	m03107/m03108	0,000	0,000	0,000000	-
homocystine*	-	0,000	0,000	0,000000	-
OH-phenylpyruvate	m02725	0,081	0,000	0,000000	-
3-hydroxyanthranilate	m00775	0,284	0,000	0,000000	-
adenosine	m01280	0,068	0,000	0,000000	0,000000
5'-adenosylhomocysteine	m02871	0,023	0,000	0,000000	-
N-carbamoyl-beta-alanine	m00923	0,199	0,000	0,000000	-
CMP	m01590	0,037	0,000	0,000000	0,000000
2'-deoxyadenosine	m01666	0,000	0,000	0,000000	0,000000
dCMP	m01644	0,001	0,000	0,000000	-
DHAP	m01690	0,086	0,000	0,000000	-
GMP	m02016	0,038	0,000	0,000000	0,000000
3-OH-kynurenate	m00788	0,010	0,000	0,000000	-
nicotinic acid mononucleotide*	-	0,001	0,000	0,000000	-
orotate	m02659	0,027	0,000	0,000000	0,000000
OMP	m02660	0,001	0,000	0,000000	-
triiodothyronine	m03052	0,000	0,000	0,000000	0,000000
UDP-glucuronate	m03109	0,001	0,000	0,000000	-
UMP	m03114	0,082	0,000	0,000000	0,000000
xanthine	m03148	0,233	0,000	0,000000	-
aconitate	m01580	0,000	0,000	0,000000	-
adipate*	-	0,000	0,000	0,000000	-
pyruvate	m02819	0,000	0,000	0,000000	0,000000
NMMA*	-	0,000	0,000	0,000000	-
alpha-glycerophosphate	m02914	0,167	0,001	-0,000010	-
sorbitol	m01682	0,339	0,005	-0,000050	0,000000
fumarate	m01862	0,361	0,008	-0,000080	-
phosphocholine	m02738	2,631	0,013	-0,000130	-
malate	m02439	1,663	0,042	-0,000420	-
lactate	m02403	1345,141	32,349	-0,323490	0,000000

TABLE A.16. Model constraints for uptake reactions fluxes, which were implemented in addition to the constraints added from (Jain et al. 2012). The MetaboliteID indicates the metabolite in the model for which the uptake reaction flux was constrained. The column "Constraints" shows the lower and the upper bounds in brackets. The reactions were either added because of the minimal media analysis or because of manual curation.

Metabolite	**MetaboliteID**	**Constraints**	**Added by**
alpha-tocopherol	m01327	[0, 0.01]	Minimal media analysis
[B12] aquacob(III)alamin	m01361	[0, 0.01]	Minimal media analysis
biotin	m01401	[0, 0.01]	Minimal media analysis
Ca2+	m01413	[0, 1000]	Minimal media analysis
chloride	m01442	[0, 1000]	Minimal media analysis
CO2	m01596	[0, 0.01]	Minimal media analysis
Fe2+	m01821	[0, 1000]	Minimal media analysis
Fe3+	m01822	[0, 1000]	Minimal media analysis
folate	m01830	[0, 0.01]	Minimal media analysis
gamma-tocopherol	m01935	[0, 0.01]	Minimal media analysis
H+	m02039	[0, 1000]	Minimal media analysis
H2O	m02040	[0, 1000]	Minimal media analysis
HCO3-	m02046	[0, 1000]	Minimal media analysis
histidine	m02125	[0, 1.7]	Minimal media analysis
K+	m02200	[0, 1000]	Minimal media analysis
lipoic acid	m02394	[0, 0.01]	Minimal media analysis
lithocholate	m02402	[0, 0.0001]	Minimal media analysis
malonate	m02440	[0, 0.001]	Minimal media analysis
O2	m02630	[0, 2]	Minimal media analysis
Pi	m02751	[0, 2]	Minimal media analysis
retinol	m02834	[0, 0.01]	Minimal media analysis
riboflavin	m02842	[0, 0.01]	Minimal media analysis
sulfate	m02946	[0, 1000]	Minimal media analysis
arginine	m01365	[0, 0.01]	Manual curation
lysine	m02426	[0, 0.0565]	Manual curation
pantothenate	m02680	[0, 0.01]	Manual curation
phenylalanine	m02724	[0, 0.01]	Manual curation

TABLE A.17. Implemeted improvements from the previous models Recon 2.2 and Recon 2M.1. “Stoich” includes changes in the reaction directionality as well.

ReactionID	Reaction	From	Change
HMR_3818	L-glutamate 5-semialdehyde[c] <=> L-glutamate 5-semialdehyde[m]	Recon 2M.1	Remove
R_SW1	H+[i] => H+[m]	Recon 2.2	Added
R_SW2	ubiquinone[m] + sn-glycerol-3-phosphate[m] => DHAP[m] + ubiquinol[m]	Recon 2.2	Added
R_SYL1	ATP[n] + GMP[n] <=> ADP[n] + GDP[n]	Recon 2M.1	Added
R_SYL2	GTP[c] + H2O[c] => GDP[c] + Pi[c]	Recon 2M.1	Added
R_SYL3	GTP[n] + H2O[n] => GDP[n] + Pi[n]	Recon 2M.1	Added
R_SYL4	OAA[m] => pyruvate[m] + CO2[m]	Recon 2M.1	Added
R_SYL5	2-aminoadipate 6-semialdehyde[c] + H2O[c] + NADP+[c] <=> H+[c] + L-2-aminoadipate[c] + NADPH[c]	Recon 2M.1	Added
R_SYL6	2-aminoadipate 6-semialdehyde[m] + H2O[m] + NADP+[m] <=> H+[m] + L-2-aminoadipate[m] + NADPH[m]	Recon 2M.1	Added
R_SYL7	glutamine[c] + phenylpyruvate[c] <=> 2-oxoglutaramate[c] + phenylalanine[c]	Recon 2M.1	Added
R_SYL8	dCTP[c] + H2O[c] => dCMP[c] + PPi[c]	Recon 2M.1	Added
R_SYL9	dCTP[m] + H2O[m] => dCMP[m] + PPi[m]	Recon 2M.1	Added
R_SYL10	dCTP[n] + H2O[n] => dCMP[n] + PPi[n]	Recon 2M.1	Added
R_SYL11	H+[c] + NADPH[c] + estrone[c] => NADP+[c] + estradiol-17beta[c]	Recon 2M.1	Added
R_SYL12	Thiosulfate[m] + Cyanide ion[m] <=> Sulfite[m] + Thiocyanate[m]	Recon 2M.1	Added
R_SYL13	ATP[n] + Uridine[n] <=> ADP[n] + UMP[n]	Recon 2M.1	Added
HMR_6914	8 H+[m] + O2[m] + 4 ferrocytochrome C[m] => 4 H+[i] + 2 H2O[m] + 4 ferricytochrome C[m]	Recon 2.2	Stoich
HMR_6916	ADP[m] + 4 H+[i] + Pi[m] => ATP[m] + 4 H+[m] + H2O[m]	Recon 2.2	Stoich
HMR_6918	2 H+[m] + 2 ferricytochrome C[m] + ubiquinol[m] => 4 H+[i] + 2 ferrocytochrome C[m] + ubiquinone[m]	Recon 2.2	Stoich
HMR_6921	5 H+[m] + NADH[m] + ubiquinone[m] => 4 H+[i] + NAD+[m] + ubiquinol[m]	Recon 2.2	Stoich
HMR_3825	H+[i] + aspartate[m] + glutamate[c] => H+[m] + aspartate[c] + glutamate[m]	Recon 2.2	Stoich
HMR_2590	L-carnitine[m] => L-carnitine[c]	Recon 2.2	Stoich
HMR_2600	L-carnitine[c] + malonyl-carnitin[m] => L-carnitine[m] + malonyl-carnitin[c]	Recon 2.2	Stoich
HMR_2592	L-carnitine[c] + O-acetylcarnitine[m] => L-carnitine[m] + O-acetylcarnitine[c]	Recon 2.2	Stoich
HMR_4704	H2O[c] + O2[c] + gentisate aldehyde[c] => 2,5-dihydroxybenzoate[c] + H2O2[c] + H+[c]	Recon 2.2	Stoich
HMR_0156	ATP[m] + CoA[m] + butyrate[m] => AMP[m] + PPi[m] + butyryl-CoA[m]	Recon 2.2	Stoich
HMR_0165	ATP[m] + CoA[m] + valeric acid[m] => AMP[m] + PPi[m] + pentanoyl-CoA[m]	Recon 2.2	Stoich
HMR_0168	ATP[m] + CoA[m] + hexanoic acid[m] => AMP[m] + PPi[m] + hexanoyl-CoA[m]	Recon 2.2	Stoich
HMR_0171	ATP[m] + CoA[m] + heptylic acid[m] => AMP[m] + PPi[m] + heptanoyl-CoA[m]	Recon 2.2	Stoich
HMR_0174	ATP[m] + CoA[m] + octanoic acid[m] => AMP[m] + PPi[m] + octanoyl-CoA[m]	Recon 2.2	Stoich
HMR_0177	ATP[m] + CoA[m] + nonanoic acid[m] => AMP[m] + PPi[m] + nonanoyl-CoA[m]	Recon 2.2	Stoich
HMR_0180	ATP[m] + CoA[m] + decanoic acid[m] => AMP[m] + PPi[m] + decanoyl-CoA[m]	Recon 2.2	Stoich
HMR_0184	ATP[m] + CoA[m] + undecylic acid[m] => AMP[m] + PPi[m] + undecanoyl-CoA[m]	Recon 2.2	Stoich
HMR_0188	ATP[c] + CoA[c] + lauric acid[c] => AMP[c] + PPi[c] + lauroyl-CoA[c]	Recon 2.2	Stoich
HMR_0192	ATP[c] + CoA[c] + tridecylic acid[c] => AMP[c] + PPi[c] + tridecanoyl-CoA[c]	Recon 2.2	Stoich
HMR_0196	ATP[c] + CoA[c] + myristic acid[c] => AMP[c] + PPi[c] + myristoyl-CoA[c]	Recon 2.2	Stoich
HMR_0200	(9E)-tetradecenoic acid[c] + ATP[c] + CoA[c] => (9E)-tetradecenoyl-CoA[c] + AMP[c] + PPi[c]	Recon 2.2	Stoich
HMR_0204	(7Z)-tetradecenoic acid[c] + ATP[c] + CoA[c] => (7Z)-tetradecenoyl-CoA[c] + AMP[c] + PPi[c]	Recon 2.2	Stoich
HMR_0209	ATP[c] + CoA[c] + physeteric acid[c] => 5-tetradecenoyl-CoA[c] + AMP[c] + PPi[c]	Recon 2.2	Stoich
HMR_0213	ATP[c] + CoA[c] + pentadecylic acid[c] => AMP[c] + PPi[c] + pentadecanoyl-CoA[c]	Recon 2.2	Stoich

ReactionID	Reaction	From	Change
HMR_0217	ATP[c] + CoA[c] + palmitate[c] => AMP[c] + PPi[c] + palmitoyl-CoA[c]	Recon 2.2	Stoich
HMR_0226	ATP[c] + CoA[c] + palmitolate[c] => AMP[c] + PPi[c] + palmitoleoyl-CoA[c]	Recon 2.2	Stoich
HMR_0233	7-palmitoleic acid[c] + ATP[c] + CoA[c] => 7-hexadecenoyl-CoA[c] + AMP[c] + PPi[c]	Recon 2.2	Stoich
HMR_0237	ATP[c] + CoA[c] + margaric acid[c] => AMP[c] + PPi[c] + heptadecanoyl-CoA[c]	Recon 2.2	Stoich
HMR_0241	(10Z)-heptadecenoic acid[c] + ATP[c] + CoA[c] => (10Z)-heptadecenoyl-CoA[c] + AMP[c] + PPi[c]	Recon 2.2	Stoich
HMR_0245	9-heptadecylenic acid[c] + ATP[c] + CoA[c] => 9-heptadecenoyl-CoA[c] + AMP[c] + PPi[c]	Recon 2.2	Stoich
HMR_0249	ATP[c] + CoA[c] + stearate[c] => AMP[c] + PPi[c] + stearoyl-CoA[c]	Recon 2.2	Stoich
HMR_0255	(13Z)-octadecenoic acid[c] + ATP[c] + CoA[c] => (13Z)-octadecenoyl-CoA[c] + AMP[c] + PPi[c]	Recon 2.2	Stoich
HMR_0259	ATP[c] + CoA[c] + cis-vaccenic acid[c] => AMP[c] + PPi[c] + cis-vaccenoyl-CoA[c]	Recon 2.2	Stoich
HMR_0263	ATP[c] + CoA[c] + oleate[c] => AMP[c] + PPi[c] + oleoyl-CoA[c]	Recon 2.2	Stoich
HMR_0267	ATP[c] + CoA[c] + elaidate[c] => (9E)-octadecenoyl-CoA[c] + AMP[c] + PPi[c]	Recon 2.2	Stoich
HMR_0271	(7Z)-octadecenoic acid[c] + ATP[c] + CoA[c] => (13Z)-octadecenoyl-CoA[c] + AMP[c] + PPi[c]	Recon 2.2	Stoich
HMR_0275	(6Z,9Z)-octadecadienoic acid[c] + ATP[c] + CoA[c] => (6Z,9Z)-octadecadienoyl-CoA[c] + AMP[c] + PPi[c]	Recon 2.2	Stoich
HMR_0279	ATP[c] + CoA[c] + nonadecylic acid[c] => AMP[c] + PPi[c] + nonadecanoyl-CoA[c]	Recon 2.2	Stoich
HMR_0283	ATP[c] + CoA[c] + eicosanoate[c] => AMP[c] + PPi[c] + eicosanoyl-CoA[c]	Recon 2.2	Stoich
HMR_0289	(13Z)-eicosenoic acid[c] + ATP[c] + CoA[c] => (13Z)-eicosenoyl-CoA[c] + AMP[c] + PPi[c]	Recon 2.2	Stoich
HMR_0293	ATP[c] + CoA[c] + cis-gondoic acid[c] => (11Z)-eicosenoyl-CoA[c] + AMP[c] + PPi[c]	Recon 2.2	Stoich
HMR_0297	9-eicosenoic acid[c] + ATP[c] + CoA[c] => 9-eicosenoyl-CoA[c] + AMP[c] + PPi[c]	Recon 2.2	Stoich
HMR_0301	8,11-eicosadienoic acid[c] + ATP[c] + CoA[c] => (8Z,11Z)-eicosadienoyl-CoA[c] + AMP[c] + PPi[c]	Recon 2.2	Stoich
HMR_0305	ATP[c] + CoA[c] + mead acid[c] => (5Z,8Z,11Z)-eicosatrienoyl-CoA[c] + AMP[c] + PPi[c]	Recon 2.2	Stoich
HMR_0309	ATP[c] + CoA[c] + henicosanoic acid[c] => AMP[c] + PPi[c] + heneicosanoyl-CoA[c]	Recon 2.2	Stoich
HMR_0313	ATP[c] + CoA[c] + behenic acid[c] => AMP[c] + PPi[c] + docosanoyl-CoA[c]	Recon 2.2	Stoich
HMR_0319	ATP[c] + CoA[c] + cis-erucic acid[c] => (13Z)-docosenoyl-CoA[c] + AMP[c] + PPi[c]	Recon 2.2	Stoich
HMR_0323	ATP[c] + CoA[c] + cis-cetoleic acid[c] => (11Z)-docosenoyl-CoA[c] + AMP[c] + PPi[c]	Recon 2.2	Stoich
HMR_0327	ATP[c] + CoA[c] + tricosanoic acid[c] => AMP[c] + PPi[c] + tricosanoyl-CoA[c]	Recon 2.2	Stoich
HMR_0331	ATP[c] + CoA[c] + lignocerate[c] => AMP[c] + PPi[c] + tetracosanoyl-CoA[c]	Recon 2.2	Stoich
HMR_0337	ATP[c] + CoA[c] + nervonic acid[c] => (15Z)-tetracosenoyl-CoA[c] + AMP[c] + PPi[c]	Recon 2.2	Stoich
HMR_0341	ATP[c] + CoA[c] + cerotic acid[c] => AMP[c] + PPi[c] + hexacosanoyl-CoA[c]	Recon 2.2	Stoich
HMR_0345	ATP[c] + CoA[c] + ximenic acid[c] => AMP[c] + PPi[c] + hexacosenoyl-CoA[c]	Recon 2.2	Stoich
HMR_0349	ATP[c] + CoA[c] + linolenate[c] => AMP[c] + PPi[c] + linolenoyl-CoA[c]	Recon 2.2	Stoich
HMR_0353	ATP[c] + CoA[c] + stearidonic acid[c] => (6Z,9Z,12Z,15Z)-octadecatetraenoyl-CoA[c] + AMP[c] + PPi[c]	Recon 2.2	Stoich
HMR_0357	ATP[c] + CoA[c] + omega-3-arachidonic acid[c] => (8Z,11Z,14Z,17Z)-eicosatetraenoyl-CoA[c] + AMP[c] + PPi[c]	Recon 2.2	Stoich
HMR_0361	ATP[c] + CoA[c] + EPA[c] => (5Z,8Z,11Z,14Z,17Z)-eicosapentaenoyl-CoA[c] + AMP[c] + PPi[c]	Recon 2.2	Stoich
HMR_0365	ATP[c] + CoA[c] + DPA[c] => (7Z,10Z,13Z,16Z,19Z)-docosapentaenoyl-CoA[c] + AMP[c] + PPi[c]	Recon 2.2	Stoich
HMR_0369	(9Z,12Z,15Z,18Z,21Z)-TPA[c] + ATP[c] + CoA[c] => (9Z,12Z,15Z,18Z,21Z)-tetracosapentaenoyl-CoA[c] + AMP[c] + PPi[c]	Recon 2.2	Stoich
HMR_0373	(6Z,9Z,12Z,15Z,18Z,21Z)-THA[c] + ATP[c] + CoA[c] => (6Z,9Z,12Z,15Z,18Z,21Z)-tetracosahexaenoyl-CoA[c] + AMP[c] + PPi[c]	Recon 2.2	Stoich
HMR_0377	ATP[c] + CoA[c] + DHA[c] => (4Z,7Z,10Z,13Z,16Z,19Z)-docosahexaenoyl-CoA[c] + AMP[c] + PPi[c]	Recon 2.2	Stoich
HMR_0381	(11Z,14Z,17Z)-eicosatrienoic acid[c] + ATP[c] + CoA[c] => (11Z,14Z,17Z)-eicosatrienoyl-CoA[c] + AMP[c] + PPi[c]	Recon 2.2	Stoich
HMR_0385	13,16,19-docosatrienoic acid[c] + ATP[c] + CoA[c] => 13,16,19-docosatrienoyl-CoA[c] + AMP[c] + PPi[c]	Recon 2.2	Stoich
HMR_0389	10,13,16,19-docosatetraenoic acid[c] + ATP[c] + CoA[c] => 10,13,16,19-docosatetraenoyl-CoA[c] + AMP[c] + PPi[c]	Recon 2.2	Stoich
HMR_0393	12,15,18,21-tetracosatetraenoic acid[c] + ATP[c] + CoA[c] => 12,15,18,21-tetracosatetraenoyl-CoA[c] + AMP[c] + PPi[c]	Recon 2.2	Stoich
HMR_0397	ATP[c] + CoA[c] + linoleate[c] => AMP[c] + PPi[c] + linoleoyl-CoA[c]	Recon 2.2	Stoich
HMR_0401	ATP[c] + CoA[c] + gamma-linolenate[c] => AMP[c] + PPi[c] + gamma-linolenoyl-CoA[c]	Recon 2.2	Stoich
HMR_0405	ATP[c] + CoA[c] + dihomo-gamma-linolenate[c] => AMP[c] + PPi[c] + dihomo-gamma-linolenoyl-CoA[c]	Recon 2.2	Stoich
HMR_0409	ATP[c] + CoA[c] + arachidonate[c] => AMP[c] + PPi[c] + arachidonyl-CoA[c]	Recon 2.2	Stoich
HMR_0413	ATP[c] + CoA[c] + adrenic acid[c] => (7Z,10Z,13Z,16Z)-docosatetraenoyl-CoA[c] + AMP[c] + PPi[c]	Recon 2.2	Stoich
HMR_0417	(9Z,12Z,15Z,18Z)-TTA[c] + ATP[c] + CoA[c] => (9Z,12Z,15Z,18Z)-tetracosatetraenoyl-CoA[c] + AMP[c] + PPi[c]	Recon 2.2	Stoich
HMR_0421	(6Z,9Z,12Z,15Z,18Z)-TPA[c] + ATP[c] + CoA[c] => (6Z,9Z,12Z,15Z,18Z)-tetracosapentaenoyl-CoA[c] + AMP[c] + PPi[c]	Recon 2.2	Stoich
HMR_0425	(4Z,7Z,10Z,13Z,16Z)-DPA[c] + ATP[c] + CoA[c] => (4Z,7Z,10Z,13Z,16Z)-docosapentaenoyl-CoA[c] + AMP[c] + PPi[c]	Recon 2.2	Stoich
HMR_0429	(11Z,14Z)-eicosadienoic acid[c] + ATP[c] + CoA[c] => (11Z,14Z)-eicosadienoyl-CoA[c] + AMP[c] + PPi[c]	Recon 2.2	Stoich
HMR_0433	(13Z,16Z)-docosadienoic acid[c] + ATP[c] + CoA[c] => (13Z,16Z)-docosadienoyl-CoA[c] + AMP[c] + PPi[c]	Recon 2.2	Stoich
HMR_0437	10,13,16-docosatriynoic acid[c] + ATP[c] + CoA[c] => 10,13,16-docosatrienoyl-CoA[c] + AMP[c] + PPi[c]	Recon 2.2	Stoich
HMR_2942	ATP[r] + CoA[r] + lauric acid[r] => AMP[r] + PPi[r] + lauroyl-CoA[r]	Recon 2.2	Stoich
HMR_2943	ATP[r] + CoA[r] + tridecylic acid[r] => AMP[r] + PPi[r] + tridecanoyl-CoA[r]	Recon 2.2	Stoich
HMR_2944	ATP[r] + CoA[r] + myristic acid[r] => AMP[r] + PPi[r] + myristoyl-CoA[r]	Recon 2.2	Stoich
HMR_2945	ATP[r] + CoA[r] + physeteric acid[r] => 5-tetradecenoyl-CoA[r] + AMP[r] + PPi[r]	Recon 2.2	Stoich
HMR_2946	(9E)-tetradecenoic acid[r] + ATP[r] + CoA[r] => (9E)-tetradecenoyl-CoA[r] + AMP[r] + PPi[r]	Recon 2.2	Stoich
HMR_2947	(7Z)-tetradecenoic acid[r] + ATP[r] + CoA[r] => (7Z)-tetradecenoyl-CoA[r] + AMP[r] + PPi[r]	Recon 2.2	Stoich
HMR_2948	ATP[r] + CoA[r] + pentadecylic acid[r] => AMP[r] + PPi[r] + pentadecanoyl-CoA[r]	Recon 2.2	Stoich
HMR_2949	ATP[r] + CoA[r] + palmitate[r] => AMP[r] + PPi[r] + palmitoyl-CoA[r]	Recon 2.2	Stoich
HMR_2951	7-palmitoleic acid[r] + ATP[r] + CoA[r] => 7-hexadecenoyl-CoA[r] + AMP[r] + PPi[r]	Recon 2.2	Stoich
HMR_2952	ATP[r] + CoA[r] + palmitolate[r] => AMP[r] + PPi[r] + palmitoleoyl-CoA[r]	Recon 2.2	Stoich
HMR_2954	ATP[r] + CoA[r] + margaric acid[r] => AMP[r] + PPi[r] + heptadecanoyl-CoA[r]	Recon 2.2	Stoich

ReactionID	Reaction	From	Change
HMR_2955	(10Z)-heptadecenoic acid[r] + ATP[r] + CoA[r] => (10Z)-heptadecenoyl-CoA[r] + AMP[r] + PPi[r]	Recon 2.2	Stoich
HMR_2956	9-heptadecylenic acid[r] + ATP[r] + CoA[r] => 9-heptadecenoyl-CoA[r] + AMP[r] + PPi[r]	Recon 2.2	Stoich
HMR_2957	ATP[r] + CoA[r] + stearate[r] => AMP[r] + PPi[r] + stearoyl-CoA[r]	Recon 2.2	Stoich
HMR_2959	ATP[r] + CoA[r] + oleate[r] => AMP[r] + PPi[r] + oleoyl-CoA[r]	Recon 2.2	Stoich
HMR_2961	ATP[r] + CoA[r] + elaidate[r] => (9E)-octadecenoyl-CoA[r] + AMP[r] + PPi[r]	Recon 2.2	Stoich
HMR_2962	(13Z)-octadecenoic acid[r] + ATP[r] + CoA[r] => (13Z)-octadecenoyl-CoA[r] + AMP[r] + PPi[r]	Recon 2.2	Stoich
HMR_2963	ATP[r] + CoA[r] + cis-vaccenic acid[r] => AMP[r] + PPi[r] + cis-vaccenoyl-CoA[r]	Recon 2.2	Stoich
HMR_2964	(6Z,9Z)-octadecadienoic acid[r] + ATP[r] + CoA[r] => (6Z,9Z)-octadecadienoyl-CoA[r] + AMP[r] + PPi[r]	Recon 2.2	Stoich
HMR_2965	ATP[r] + CoA[r] + nonadecylic acid[r] => AMP[r] + PPi[r] + nonadecanoyl-CoA[r]	Recon 2.2	Stoich
HMR_2966	ATP[r] + CoA[r] + eicosanoate[r] => AMP[r] + PPi[r] + eicosanoyl-CoA[r]	Recon 2.2	Stoich
HMR_2967	ATP[r] + CoA[r] + cis-gondoic acid[r] => (11Z)-eicosenoyl-CoA[r] + AMP[r] + PPi[r]	Recon 2.2	Stoich
HMR_2968	(13Z)-eicosenoic acid[r] + ATP[r] + CoA[r] => (13Z)-eicosenoyl-CoA[r] + AMP[r] + PPi[r]	Recon 2.2	Stoich
HMR_2969	9-eicosenoic acid[r] + ATP[r] + CoA[r] => 9-eicosenoyl-CoA[r] + AMP[r] + PPi[r]	Recon 2.2	Stoich
HMR_2970	8,11-eicosadienoic acid[r] + ATP[r] + CoA[r] => (8Z,11Z)-eicosadienoyl-CoA[r] + AMP[r] + PPi[r]	Recon 2.2	Stoich
HMR_2971	ATP[r] + CoA[r] + mead acid[r] => (5Z,8Z,11Z)-eicosatrienoyl-CoA[r] + AMP[r] + PPi[r]	Recon 2.2	Stoich
HMR_2972	ATP[r] + CoA[r] + henicosanoic acid[r] => AMP[r] + PPi[r] + heneicosanoyl-CoA[r]	Recon 2.2	Stoich
HMR_2973	ATP[r] + CoA[r] + behenic acid[r] => AMP[r] + PPi[r] + docosanoyl-CoA[r]	Recon 2.2	Stoich
HMR_2974	ATP[r] + CoA[r] + cis-erucic acid[r] => (13Z)-docosenoyl-CoA[r] + AMP[r] + PPi[r]	Recon 2.2	Stoich
HMR_2975	ATP[r] + CoA[r] + cis-cetoleic acid[r] => (11Z)-docosenoyl-CoA[r] + AMP[r] + PPi[r]	Recon 2.2	Stoich
HMR_2976	ATP[r] + CoA[r] + tricosanoic acid[r] => AMP[r] + PPi[r] + tricosanoyl-CoA[r]	Recon 2.2	Stoich
HMR_2977	ATP[r] + CoA[r] + lignocerate[r] => AMP[r] + PPi[r] + tetracosanoyl-CoA[r]	Recon 2.2	Stoich
HMR_2978	ATP[r] + CoA[r] + nervonic acid[r] => (15Z)-tetracosenoyl-CoA[r] + AMP[r] + PPi[r]	Recon 2.2	Stoich
HMR_2979	ATP[r] + CoA[r] + cerotic acid[r] => AMP[r] + PPi[r] + hexacosanoyl-CoA[r]	Recon 2.2	Stoich
HMR_2980	ATP[r] + CoA[r] + ximenic acid[r] => AMP[r] + PPi[r] + hexacosenoyl-CoA[r]	Recon 2.2	Stoich
HMR_2981	ATP[r] + CoA[r] + linolenate[r] => AMP[r] + PPi[r] + linolenoyl-CoA[r]	Recon 2.2	Stoich
HMR_2982	ATP[r] + CoA[r] + stearidonic acid[r] => (6Z,9Z,12Z,15Z)-octadecatetraenoyl-CoA[r] + AMP[r] + PPi[r]	Recon 2.2	Stoich
HMR_2983	ATP[r] + CoA[r] + omega-3-arachidonic acid[r] => (8Z,11Z,14Z,17Z)-eicosatetraenoyl-CoA[r] + AMP[r] + PPi[r]	Recon 2.2	Stoich
HMR_2984	ATP[r] + CoA[r] + EPA[r] => (5Z,8Z,11Z,14Z,17Z)-eicosapentaenoyl-CoA[r] + AMP[r] + PPi[r]	Recon 2.2	Stoich
HMR_2985	ATP[r] + CoA[r] + DPA[r] => (7Z,10Z,13Z,16Z,19Z)-docosapentaenoyl-CoA[r] + AMP[r] + PPi[r]	Recon 2.2	Stoich
HMR_2986	(9Z,12Z,15Z,18Z,21Z)-TPA[r] + ATP[r] + CoA[r] => (9Z,12Z,15Z,18Z,21Z)-tetracosapentaenoyl-CoA[r] + AMP[r] + PPi[r]	Recon 2.2	Stoich
HMR_2987	(6Z,9Z,12Z,15Z,18Z,21Z)-THA[r] + ATP[r] + CoA[r] => (6Z,9Z,12Z,15Z,18Z,21Z)-tetracosahexaenoyl-CoA[r] + AMP[r] + PPi[r]	Recon 2.2	Stoich
HMR_2988	ATP[r] + CoA[r] + DHA[r] => (4Z,7Z,10Z,13Z,16Z,19Z)-docosahexaenoyl-CoA[r] + AMP[r] + PPi[r]	Recon 2.2	Stoich
HMR_2989	(11Z,14Z,17Z)-eicosatrienoic acid[r] + ATP[r] + CoA[r] => (11Z,14Z,17Z)-eicosatrienoyl-CoA[r] + AMP[r] + PPi[r]	Recon 2.2	Stoich
HMR_2990	13,16,19-docosatrienoic acid[r] + ATP[r] + CoA[r] => 13,16,19-docosatrienoyl-CoA[r] + AMP[r] + PPi[r]	Recon 2.2	Stoich
HMR_2991	ATP[r] + CoA[r] + linoleate[r] => AMP[r] + PPi[r] + linoleoyl-CoA[r]	Recon 2.2	Stoich
HMR_2992	ATP[r] + CoA[r] + gamma-linolenate[r] => AMP[r] + PPi[r] + gamma-linolenoyl-CoA[r]	Recon 2.2	Stoich
HMR_2994	ATP[r] + CoA[r] + dihomo-gamma-linolenate[r] => AMP[r] + PPi[r] + dihomo-gamma-linolenoyl-CoA[r]	Recon 2.2	Stoich
HMR_2996	ATP[r] + CoA[r] + arachidonate[r] => AMP[r] + PPi[r] + arachidonyl-CoA[r]	Recon 2.2	Stoich

ReactionID	Reaction	From	Change
HMR_2998	ATP[r] + CoA[r] + adrenic acid[r] => (7Z,10Z,13Z,16Z)-docosatetraenoyl-CoA[r] + AMP[r] + PPi[r]	Recon 2.2	Stoich
HMR_2999	(9Z,12Z,15Z,18Z)-TTA[r] + ATP[r] + CoA[r] => (9Z,12Z,15Z,18Z)-tetracosatetraenoyl-CoA[r] + AMP[r] + PPi[r]	Recon 2.2	Stoich
HMR_3000	(6Z,9Z,12Z,15Z,18Z)-TPA[r] + ATP[r] + CoA[r] => (6Z,9Z,12Z,15Z,18Z)-tetracosapentaenoyl-CoA[r] + AMP[r] + PPi[r]	Recon 2.2	Stoich
HMR_3001	(4Z,7Z,10Z,13Z,16Z)-DPA[r] + ATP[r] + CoA[r] => (4Z,7Z,10Z,13Z,16Z)-docosapentaenoyl-CoA[r] + AMP[r] + PPi[r]	Recon 2.2	Stoich
HMR_3002	(11Z,14Z)-eicosadienoic acid[r] + ATP[r] + CoA[r] => (11Z,14Z)-eicosadienoyl-CoA[r] + AMP[r] + PPi[r]	Recon 2.2	Stoich
HMR_3003	(13Z,16Z)-docosadienoic acid[r] + ATP[r] + CoA[r] => (13Z,16Z)-docosadienoyl-CoA[r] + AMP[r] + PPi[r]	Recon 2.2	Stoich
HMR_4548	H+[c] + melatonin[c] + NADPH[c] + O2[c] => 6-hydroxymelatonin[c] + NADP+[c] + H2O[c]	Recon 2.2	Stoich
HMR_6818	adrenaline[c] + O2[c] => 5 H+[c] + adrenochrome[c]	Recon 2.2	Stoich
HMR_6822	noradrenaline[c] + O2[c] => 5 H+[c] + noradrenochrome[c]	Recon 2.2	Stoich
HMR_2451	1-hydroperoxy-8-carboxyoctyl-3,4-epoxynon-(2E)-enyl-ether[c] + NAD+[c] <=> 4-oxo-2-nonenal[c] + 3 H+[c] + azelaic acid[c]	Recon 2.2	Stoich
HMR_6602	alloxan[c] + urea[c] => H2O2[c] + urate[c]	Recon 2.2	Stoich
HMR_6603	alloxan[s] + urea[s] => H2O2[s] + urate[s]	Recon 2.2	Stoich
HMR_1430	17-hydroperoxy-H4-neuroprostane[c] + ascorbate[c] <=> 17-hydroxy-E4-neuroprostane[c] + H2O[c] + dehydroascorbic acid[c]	Recon 2.2	Stoich
HMR_1431	17-hydroperoxy-H4-neuroprostane[c] + ascorbate[c] <=> 17-hydroxy-D4-neuroprostane[c] + H2O[c] + dehydroascorbic acid[c]	Recon 2.2	Stoich
HMR_1427	13-hydroperoxy-H4-neuroprostane[c] + ascorbate[c] <=> 13-hydroxy-D4-neuroprostane[c] + H2O[c] + dehydroascorbic acid[c]	Recon 2.2	Stoich
HMR_1418	4-hydroperoxy-H4-neuroprostane[c] + ascorbate[c] <=> 4-hydroxy-D4-neuroprostane[c] + H2O[c] + dehydroascorbic acid[c]	Recon 2.2	Stoich
HMR_1419	4-hydroperoxy-H4-neuroprostane[c] + ascorbate[c] <=> 4-hydroxy-E4-neuroprostane[c] + H2O[c] + dehydroascorbic acid[c]	Recon 2.2	Stoich
R_SW1	ENSG00000115159	Recon2.2	GPR
HMR_6518	ENSG00000128309	Recon 2M.1	GPR
R_SYL1	ENSG00000143774	Recon 2M.1	GPR
R_SYL2	ENSG00000125877	Recon 2M.1	GPR
R_SYL3	ENSG00000125877	Recon 2M.1	GPR
R_SYL4	ENSG00000082212	Recon 2M.1	GPR
R_SYL5	ENSG00000164904	Recon 2M.1	GPR
R_SYL6	ENSG00000137124;ENSG00000164904	Recon 2M.1	GPR
R_SYL7	ENSG00000171097	Recon 2M.1	GPR
R_SYL8	ENSG00000179958	Recon 2M.1	GPR
R_SYL9	ENSG00000179958	Recon 2M.1	GPR
R_SYL10	ENSG00000179958	Recon 2M.1	GPR
R_SYL11	ENSG00000025423;ENSG00000086696;ENSG00000108786;ENSG00000132196;ENSG00000149084;ENSG00000198189	Recon 2M.1	GPR
R_SYL13	ENSG00000130717;ENSG00000198276;ENSG00000143179	Recon 2M.1	GPR

Table A.18: Implemented constraints for reaction fluxes with infeasible reaction directionalities.

Reaction	**Introduced Constraint**	**Reaction**	**Introduced Constraint**
HMR_0156	[0, 1000]	HMR_2956	[0, 1000]
HMR_0165	[0, 1000]	HMR_2957	[0, 1000]
HMR_0168	[0, 1000]	HMR_2959	[0, 1000]
HMR_0171	[0, 1000]	HMR_2961	[0, 1000]
HMR_0174	[0, 1000]	HMR_2962	[0, 1000]
HMR_0177	[0, 1000]	HMR_2963	[0, 1000]
HMR_0180	[0, 1000]	HMR_2964	[0, 1000]
HMR_0184	[0, 1000]	HMR_2965	[0, 1000]
HMR_0188	[0, 1000]	HMR_2966	[0, 1000]
HMR_0192	[0, 1000]	HMR_2967	[0, 1000]
HMR_0196	[0, 1000]	HMR_2968	[0, 1000]
HMR_0200	[0, 1000]	HMR_2969	[0, 1000]
HMR_0204	[0, 1000]	HMR_2970	[0, 1000]
HMR_0209	[0, 1000]	HMR_2971	[0, 1000]
HMR_0213	[0, 1000]	HMR_2972	[0, 1000]
HMR_0217	[0, 1000]	HMR_2973	[0, 1000]
HMR_0226	[0, 1000]	HMR_2974	[0, 1000]
HMR_0233	[0, 1000]	HMR_2975	[0, 1000]
HMR_0237	[0, 1000]	HMR_2976	[0, 1000]
HMR_0241	[0, 1000]	HMR_2977	[0, 1000]
HMR_0245	[0, 1000]	HMR_2978	[0, 1000]
HMR_0249	[0, 1000]	HMR_2979	[0, 1000]
HMR_0255	[0, 1000]	HMR_2980	[0, 1000]
HMR_0259	[0, 1000]	HMR_2981	[0, 1000]
HMR_0263	[0, 1000]	HMR_2982	[0, 1000]
HMR_0267	[0, 1000]	HMR_2983	[0, 1000]
HMR_0271	[0, 1000]	HMR_2984	[0, 1000]
HMR_0275	[0, 1000]	HMR_2985	[0, 1000]
HMR_0279	[0, 1000]	HMR_2986	[0, 1000]
HMR_0283	[0, 1000]	HMR_2987	[0, 1000]
HMR_0289	[0, 1000]	HMR_2988	[0, 1000]
HMR_0293	[0, 1000]	HMR_2989	[0, 1000]
HMR_0297	[0, 1000]	HMR_2990	[0, 1000]
HMR_0301	[0, 1000]	HMR_2991	[0, 1000]
HMR_0305	[0, 1000]	HMR_2992	[0, 1000]
HMR_0309	[0, 1000]	HMR_2994	[0, 1000]
HMR_0313	[0, 1000]	HMR_2996	[0, 1000]
HMR_0319	[0, 1000]	HMR_2998	[0, 1000]
HMR_0323	[0, 1000]	HMR_2999	[0, 1000]

Reaction	Introduced Constraint	Reaction	Introduced Constraint
HMR_0327	[0, 1000]	HMR_3000	[0, 1000]
HMR_0331	[0, 1000]	HMR_3001	[0, 1000]
HMR_0337	[0, 1000]	HMR_3002	[0, 1000]
HMR_0341	[0, 1000]	HMR_3003	[0, 1000]
HMR_0345	[0, 1000]	HMR_4459	[0, 1000]
HMR_0349	[0, 1000]	HMR_4460	[0, 1000]
HMR_0353	[0, 1000]	HMR_4727	[0, 1000]
HMR_0357	[0, 1000]	HMR_4071	[-1000, 0]
HMR_0361	[0, 1000]	HMR_3769	[-1000, 0]
HMR_0365	[0, 1000]	HMR_4686	[-1000, 0]
HMR_0369	[0, 1000]	HMR_4687	[-1000, 0]
HMR_0373	[0, 1000]	HMR_4442	[0, 1000]
HMR_0377	[0, 1000]	HMR_4444	[0, 1000]
HMR_0381	[0, 1000]	HMR_4654	[0, 1000]
HMR_0385	[0, 1000]	HMR_4655	[0, 1000]
HMR_0389	[0, 1000]	HMR_4332	[0, 1000]
HMR_0393	[0, 1000]	HMR_4333	[0, 1000]
HMR_0397	[0, 1000]	HMR_4335	[0, 1000]
HMR_0401	[0, 1000]	HMR_4145	[0, 1000]
HMR_0405	[0, 1000]	HMR_4315	[0, 1000]
HMR_0409	[0, 1000]	HMR_4316	[0, 1000]
HMR_0413	[0, 1000]	HMR_3995	[-1000, 0]
HMR_0417	[0, 1000]	HMR_3996	[-1000, 0]
HMR_0421	[0, 1000]	HMR_8682	[-1000, 0]
HMR_0425	[0, 1000]	HMR_8530	[0, 1000]
HMR_0429	[0, 1000]	HMR_4085	[-1000, 0]
HMR_0433	[0, 1000]	HMR_4086	[-1000, 0]
HMR_0437	[0, 1000]	HMR_5351	[0, 1000]
HMR_2942	[0, 1000]	HMR_4586	[0, 1000]
HMR_2943	[0, 1000]	HMR_0453	[0, 1000]
HMR_2944	[0, 1000]	HMR_4700	[0, 1000]
HMR_2945	[0, 1000]	HMR_8097	[-1000, 0]
HMR_2946	[0, 1000]	HMR_7702	[0, 1000]
HMR_2947	[0, 1000]	HMR_3802	[-1000, 0]
HMR_2948	[0, 1000]	HMR_3804	[-1000, 0]
HMR_2949	[0, 1000]	HMR_8507	[-1000, 0]
HMR_2951	[0, 1000]	HMR_8508	[-1000, 0]
HMR_2952	[0, 1000]	HMR_3838	[-1000, 0]
HMR_2954	[0, 1000]	HMR_3819	[-1000, 0]
HMR_2955	[0, 1000]	HMR_3820	[-1000, 0]

TABLE A.19. Flux irrelevant reactions, which carry biological instead of metabolic function and were therefore removed from the model. PM = protein modification, P = protein assembly, degradation or transport, BGB = blood group biosynthesis.

Reaction ID	Reaction Group	Reaction ID	Reaction Group	Reaction ID	Reaction Group	Reaction ID	Reaction Group
HMR_5415	PMM	HMR_7490	PMM	HMR_7411	PMM	HMR_8284	PMM
HMR_5416	PMM	HMR_7491	PMM	HMR_7412	PMM	HMR_8285	PMM
HMR_5417	PMM	HMR_7492	PMM	HMR_7413	PMM	HMR_8286	PMM
HMR_6983	PMM	HMR_7493	PMM	HMR_7414	PMM	HMR_8287	PMM
HMR_6984	PMM	HMR_7494	PMM	HMR_7415	PMM	HMR_8288	PMM
HMR_6985	PMM	HMR_7495	PMM	HMR_7416	PMM	HMR_8291	PMM
HMR_8025	PMM	HMR_7496	PMM	HMR_7417	PMM	HMR_8292	PMM
HMR_8026	PMM	HMR_7497	PMM	HMR_7418	PMM	HMR_8293	PMM
HMR_8027	PMM	HMR_7498	PMM	HMR_7419	PMM	HMR_8294	PMM
HMR_8029	PMM	HMR_7509	PMM	HMR_7420	PMM	HMR_8295	PMM
HMR_7171	PMM	HMR_7510	PMM	HMR_7421	PMM	HMR_8298	PMM
HMR_7172	PMM	HMR_7519	PMM	HMR_7422	PMM	HMR_8301	PMM
HMR_7174	PMM	HMR_7520	PMM	HMR_7423	PMM	HMR_8302	PMM
HMR_7175	PMM	HMR_7521	PMM	HMR_7424	PMM	HMR_8305	PMM
HMR_7180	PMM	HMR_7522	PMM	HMR_7425	PMM	HMR_8306	PMM
HMR_7181	PMM	HMR_7534	PMM	HMR_7426	PMM	HMR_8307	PMM
HMR_7183	PMM	HMR_7535	PMM	HMR_7427	PMM	HMR_8308	PMM
HMR_7197	PMM	HMR_7536	PMM	HMR_7455	PMM	HMR_8309	PMM
HMR_7436	PMM	HMR_7537	PMM	HMR_7456	PMM	HMR_8316	PMM
HMR_7438	PMM	HMR_7538	PMM	HMR_7457	PMM	HMR_8317	PMM
HMR_7440	PMM	HMR_7551	PMM	HMR_7458	PMM	HMR_8318	PMM
HMR_8254	PMM	HMR_7552	PMM	HMR_7459	PMM	HMR_8319	PMM
HMR_8255	PMM	HMR_7553	PMM	HMR_7460	PMM	HMR_8322	PMM
HMR_8256	PMM	HMR_7554	PMM	HMR_7461	PMM	HMR_8325	PMM
HMR_8257	PMM	HMR_7501	PMM	HMR_7462	PMM	HMR_8326	PMM
HMR_8258	PMM	HMR_7502	PMM	HMR_7463	PMM	HMR_8327	PMM
HMR_8260	PMM	HMR_7503	PMM	HMR_7464	PMM	HMR_8330	PMM
HMR_8261	PMM	HMR_7504	PMM	HMR_7465	PMM	HMR_8331	PMM
HMR_1532	PMM	HMR_7505	PMM	HMR_7466	PMM	HMR_8332	PMM
HMR_7254	PMM	HMR_7506	PMM	HMR_7467	PMM	HMR_8333	PMM
HMR_7255	PMM	HMR_7507	PMM	HMR_7468	PMM	HMR_8334	PMM
HMR_7256	PMM	HMR_7508	PMM	HMR_7469	PMM	HMR_8337	PMM
HMR_7258	PMM	HMR_7513	PMM	HMR_7484	PMM	HMR_8270	PMM
HMR_7259	PMM	HMR_7525	PMM	HMR_7485	PMM	HMR_8273	PMM
HMR_7260	PMM	HMR_7526	PMM	HMR_7486	PMM	HMR_8283	PMM
HMR_7261	PMM	HMR_7527	PMM	HMR_7487	PMM	HMR_8300	PMM
HMR_7263	PMM	HMR_7528	PMM	HMR_7488	PMM	HMR_8304	PMM
HMR_7264	PMM	HMR_7529	PMM	HMR_7489	PMM	HMR_8311	PMM
HMR_7265	PMM	HMR_7530	PMM	HMR_7623	PMM	HMR_8313	PMM
HMR_7266	PMM	HMR_7531	PMM	HMR_7625	PMM	HMR_8315	PMM
HMR_7267	PMM	HMR_7532	PMM	HMR_9490	PMM	HMR_8321	PMM
HMR_7268	PMM	HMR_7533	PMM	HMR_9491	PMM	HMR_8324	PMM
HMR_7269	PMM	HMR_7541	PMM	HMR_9492	PMM	HMR_8265	PMM
HMR_7270	PMM	HMR_7542	PMM	HMR_9493	PMM	HMR_8269	PMM
HMR_7271	PMM	HMR_7543	PMM	HMR_9494	PMM	HMR_8272	PMM
HMR_7274	PMM	HMR_7544	PMM	HMR_9495	PMM	HMR_8282	PMM
HMR_7275	PMM	HMR_7545	PMM	HMR_9496	PMM	HMR_8289	PMM
HMR_7276	PMM	HMR_7546	PMM	HMR_9498	PMM	HMR_8296	PMM
HMR_7277	PMM	HMR_7547	PMM	HMR_9499	PMM	HMR_8299	PMM
HMR_7278	PMM	HMR_7548	PMM	HMR_9500	PMM	HMR_8303	PMM
HMR_7279	PMM	HMR_7549	PMM	HMR_9501	PMM	HMR_8310	PMM
HMR_7280	PMM	HMR_7550	PMM	HMR_9502	PMM	HMR_8312	PMM
HMR_7281	PMM	HMR_7557	PMM	HMR_9503	PMM	HMR_8314	PMM
HMR_7285	PMM	HMR_7558	PMM	HMR_9505	PMM	HMR_8320	PMM
HMR_7286	PMM	HMR_7559	PMM	HMR_9512	PMM	HMR_8323	PMM
HMR_7287	PMM	HMR_7560	PMM	HMR_9531	PMM	HMR_8328	PMM
HMR_7288	PMM	HMR_7561	PMM	HMR_9532	PMM	HMR_8335	PMM
HMR_7289	PMM	HMR_7562	PMM	HMR_9541	PMM	HMR_8338	PMM
HMR_7290	PMM	HMR_7563	PMM	HMR_9542	PMM	HMR_8874	PMM
HMR_7291	PMM	HMR_7564	PMM	HMR_9543	PMM	HMR_9320	PMM
HMR_7292	PMM	HMR_7565	PMM	HMR_9545	PMM	HMR_9323	PMM
HMR_7293	PMM	HMR_7566	PMM	HMR_9547	PMM	HMR_9324	PMM
HMR_7294	PMM	HMR_7567	PMM	HMR_9548	PMM	HMR_9325	PMM

Reaction ID	Reaction Group	Reaction ID	Reaction Group	Reaction ID	Reaction Group	Reaction ID	Reaction Group
HMR_7295	PMM	HMR_7225	PMM	HMR_9549	PMM	HMR_9326	PMM
HMR_7296	PMM	HMR_7226	PMM	HMR_9551	PMM	HMR_9327	PMM
HMR_7297	PMM	HMR_7227	PMM	HMR_9553	PMM	HMR_9328	PMM
HMR_7298	PMM	HMR_7228	PMM	HMR_9577	PMM	HMR_9332	PMM
HMR_7299	PMM	HMR_7229	PMM	HMR_9578	PMM	HMR_9333	PMM
HMR_7300	PMM	HMR_7230	PMM	HMR_9579	PMM	HMR_9334	PMM
HMR_7301	PMM	HMR_7231	PMM	HMR_7173	PMM	HMR_5165	P
HMR_7302	PMM	HMR_7232	PMM	HMR_7184	PMM	HMR_5166	P
HMR_7303	PMM	HMR_7233	PMM	HMR_7223	PMM	HMR_5167	P
HMR_7304	PMM	HMR_7234	PMM	HMR_7372	PMM	HMR_5168	P
HMR_7305	PMM	HMR_7235	PMM	HMR_7453	PMM	HMR_5169	P
HMR_7306	PMM	HMR_7236	PMM	HMR_7482	PMM	HMR_5170	P
HMR_7308	PMM	HMR_7237	PMM	HMR_7499	PMM	HMR_5171	P
HMR_7309	PMM	HMR_7238	PMM	HMR_7511	PMM	HMR_5172	P
HMR_7310	PMM	HMR_7239	PMM	HMR_7523	PMM	HMR_5173	P
HMR_7311	PMM	HMR_7240	PMM	HMR_7539	PMM	HMR_5174	P
HMR_7312	PMM	HMR_7241	PMM	HMR_7555	PMM	HMR_5258	P
HMR_7313	PMM	HMR_7242	PMM	HMR_7579	PMM	HMR_5259	P
HMR_7314	PMM	HMR_7243	PMM	HMR_7583	PMM	HMR_5260	P
HMR_7315	PMM	HMR_7244	PMM	HMR_8023	PMM	HMR_5261	P
HMR_7316	PMM	HMR_7245	PMM	HMR_9635	PMM	HMR_5262	P
HMR_7317	PMM	HMR_7246	PMM	HMR_9636	PMM	HMR_5263	P
HMR_7318	PMM	HMR_7247	PMM	HMR_9648	PMM	HMR_5264	P
HMR_7319	PMM	HMR_7248	PMM	HMR_9653	PMM	HMR_5265	P
HMR_7320	PMM	HMR_7249	PMM	HMR_9654	PMM	HMR_5266	P
HMR_7321	PMM	HMR_7250	PMM	HMR_9655	PMM	HMR_5267	P
HMR_7322	PMM	HMR_7251	PMM	HMR_9658	PMM	HMR_5268	P
HMR_7323	PMM	HMR_7335	PMM	HMR_9660	PMM	HMR_5269	P
HMR_7324	PMM	HMR_7336	PMM	HMR_9661	PMM	HMR_5270	P
HMR_7325	PMM	HMR_7337	PMM	HMR_9662	PMM	HMR_5271	P
HMR_7326	PMM	HMR_7338	PMM	HMR_9663	PMM	HMR_5272	P
HMR_7327	PMM	HMR_7339	PMM	HMR_9720	PMM	HMR_5273	P
HMR_7328	PMM	HMR_7340	PMM	HMR_9731	PMM	HMR_5274	P
HMR_7329	PMM	HMR_7341	PMM	HMR_8024	PMM	HMR_5275	P
HMR_7332	PMM	HMR_7342	PMM	HMR_8028	PMM	HMR_5276	P
HMR_7333	PMM	HMR_7343	PMM	HMR_7199	PMM	HMR_5277	P
HMR_7334	PMM	HMR_7344	PMM	HMR_7224	PMM	HMR_5278	P
HMR_7428	PMM	HMR_7345	PMM	HMR_7283	PMM	HMR_5279	P
HMR_7429	PMM	HMR_7346	PMM	HMR_7374	PMM	HMR_5280	P
HMR_7574	PMM	HMR_7347	PMM	HMR_7454	PMM	HMR_5281	P
HMR_7575	PMM	HMR_7348	PMM	HMR_7483	PMM	HMR_5282	P
HMR_7576	PMM	HMR_7349	PMM	HMR_7500	PMM	HMR_5283	P
HMR_7577	PMM	HMR_7350	PMM	HMR_7512	PMM	HMR_5284	P
HMR_7578	PMM	HMR_7351	PMM	HMR_7524	PMM	HMR_5285	P
HMR_7580	PMM	HMR_7352	PMM	HMR_7540	PMM	HMR_5286	P
HMR_7582	PMM	HMR_7353	PMM	HMR_7556	PMM	HMR_5287	P
HMR_7585	PMM	HMR_7354	PMM	HMR_7581	PMM	HMR_5288	P
HMR_7586	PMM	HMR_7355	PMM	HMR_7584	PMM	HMR_5289	P
HMR_7587	PMM	HMR_7356	PMM	HMR_7907	PMM	HMR_5290	P
HMR_8691	PMM	HMR_7357	PMM	HMR_8908	PMM	HMR_5291	P
HMR_8692	PMM	HMR_7358	PMM	HMR_7198	PMM	HMR_9817	P
HMR_8693	PMM	HMR_7359	PMM	HMR_7284	PMM	HMR_9818	P
HMR_8694	PMM	HMR_7360	PMM	HMR_4955	PMM	HMR_1924	P
HMR_8695	PMM	HMR_7361	PMM	HMR_7201	PMM	HMR_1926	P
HMR_7282	PMM	HMR_7362	PMM	HMR_7431	PMM	HMR_0024	P
HMR_7616	PMM	HMR_7363	PMM	HMR_7437	PMM	HMR_0025	P
HMR_7617	PMM	HMR_7364	PMM	HMR_8259	PMM	HMR_0026	P
HMR_7618	PMM	HMR_7365	PMM	HMR_9667	PMM	HMR_0027	P
HMR_7619	PMM	HMR_7366	PMM	HMR_9668	PMM	HMR_0028	P
HMR_9735	PMM	HMR_7367	PMM	HMR_9669	PMM	HMR_0029	P
HMR_7621	PMM	HMR_7368	PMM	HMR_9670	PMM	HMR_0030	P
HMR_7622	PMM	HMR_7369	PMM	HMR_9671	PMM	HMR_5198	P
HMR_7624	PMM	HMR_7370	PMM	HMR_7182	PMM	HMR_5200	P
HMR_7626	PMM	HMR_7371	PMM	HMR_7330	PMM	HMR_5202	P
HMR_6404	PMM	HMR_7442	PMM	HMR_7432	PMM	HMR_5206	P

Reaction ID	Reaction Group	Reaction ID	Reaction Group	Reaction ID	Reaction Group	Reaction ID	Reaction Group
HMR_7165	PMM	HMR_7443	PMM	HMR_7307	PMM	HMR_5213	P
HMR_7166	PMM	HMR_7444	PMM	HMR_7257	PMM	HMR_5215	P
HMR_7167	PMM	HMR_7445	PMM	HMR_7262	PMM	HMR_5216	P
HMR_7168	PMM	HMR_7446	PMM	HMR_7272	PMM	HMR_5219	P
HMR_7169	PMM	HMR_7447	PMM	HMR_7273	PMM	HMR_5221	P
HMR_7170	PMM	HMR_7448	PMM	HMR_8030	PMM	HMR_5231	P
HMR_7188	PMM	HMR_7449	PMM	HMR_8382	PMM	HMR_5237	P
HMR_8378	PMM	HMR_7450	PMM	HMR_9629	PMM	HMR_5240	P
HMR_8379	PMM	HMR_7451	PMM	HMR_9630	PMM	HMR_5241	P
HMR_7185	PMM	HMR_7452	PMM	HMR_9631	PMM	HMR_1925	P
HMR_8380	PMM	HMR_7471	PMM	HMR_9632	PMM	HMR_5222	P
HMR_7186	PMM	HMR_7472	PMM	HMR_9633	PMM	HMR_5223	P
HMR_8381	PMM	HMR_7473	PMM	HMR_9732	PMM	HMR_5225	P
HMR_7187	PMM	HMR_7474	PMM	HMR_9111	PMM	HMR_5227	P
HMR_8383	PMM	HMR_7475	PMM	HMR_9113	PMM	HMR_5197	P
HMR_8384	PMM	HMR_7476	PMM	HMR_9114	PMM	HMR_5199	P
HMR_8385	PMM	HMR_7477	PMM	HMR_9115	PMM	HMR_5201	P
HMR_8387	PMM	HMR_7478	PMM	HMR_9116	PMM	HMR_5204	P
HMR_8388	PMM	HMR_7479	PMM	HMR_9117	PMM	HMR_5212	P
HMR_8389	PMM	HMR_7480	PMM	HMR_9118	PMM	HMR_5214	P
HMR_8390	PMM	HMR_7481	PMM	HMR_9119	PMM	HMR_5217	P
HMR_8391	PMM	HMR_7373	PMM	HMR_9120	PMM	HMR_5218	P
HMR_8392	PMM	HMR_7375	PMM	HMR_9121	PMM	HMR_5220	P
HMR_8393	PMM	HMR_7376	PMM	HMR_9124	PMM	HMR_5224	P
HMR_8394	PMM	HMR_7377	PMM	HMR_9125	PMM	HMR_5226	P
HMR_8395	PMM	HMR_7378	PMM	HMR_9126	PMM	HMR_5228	P
HMR_8396	PMM	HMR_7379	PMM	HMR_9127	PMM	HMR_5230	P
HMR_8397	PMM	HMR_7380	PMM	HMR_9128	PMM	HMR_5203	P
HMR_8398	PMM	HMR_7381	PMM	HMR_9204	PMM	HMR_5205	P
HMR_8399	PMM	HMR_7382	PMM	HMR_9389	PMM	HMR_5207	P
HMR_8401	PMM	HMR_7383	PMM	HMR_9681	PMM	HMR_5209	P
HMR_8402	PMM	HMR_7384	PMM	HMR_9686	PMM	HMR_5210	P
HMR_8403	PMM	HMR_7385	PMM	HMR_9687	PMM	HMR_5211	P
HMR_8404	PMM	HMR_7386	PMM	HMR_9700	PMM	HMR_5245	P
HMR_8405	PMM	HMR_7387	PMM	HMR_9703	PMM	HMR_9025	P
HMR_8406	PMM	HMR_7388	PMM	HMR_9704	PMM	HMR_9027	P
HMR_8407	PMM	HMR_7389	PMM	HMR_9705	PMM	HMR_9029	P
HMR_7200	PMM	HMR_7390	PMM	HMR_9706	PMM	HMR_9031	P
HMR_7202	PMM	HMR_7391	PMM	HMR_9709	PMM	HMR_9049	P
HMR_7203	PMM	HMR_7392	PMM	HMR_9710	PMM	HMR_9051	P
HMR_7205	PMM	HMR_7393	PMM	HMR_9711	PMM	HMR_9053	P
HMR_7206	PMM	HMR_7394	PMM	HMR_9712	PMM	HMR_9055	P
HMR_7207	PMM	HMR_7395	PMM	HMR_9714	PMM	HMR_9130	P
HMR_7208	PMM	HMR_7396	PMM	HMR_9721	PMM	HMR_9730	P
HMR_7209	PMM	HMR_7397	PMM	HMR_8262	PMM	HMR_5151	P
HMR_7210	PMM	HMR_7398	PMM	HMR_8263	PMM	HMR_5152	P
HMR_7211	PMM	HMR_7399	PMM	HMR_8264	PMM	HMR_5153	P
HMR_7212	PMM	HMR_7400	PMM	HMR_8267	PMM	HMR_5154	P
HMR_7213	PMM	HMR_7401	PMM	HMR_8268	PMM	HMR_5155	P
HMR_7214	PMM	HMR_7402	PMM	HMR_8271	PMM	HMR_5156	P
HMR_7215	PMM	HMR_7403	PMM	HMR_8274	PMM	HMR_5157	P
HMR_7216	PMM	HMR_7404	PMM	HMR_8275	PMM	HMR_5158	P
HMR_7217	PMM	HMR_7405	PMM	HMR_8276	PMM	HMR_5159	P
HMR_7218	PMM	HMR_7406	PMM	HMR_8277	PMM	HMR_5160	P
HMR_7219	PMM	HMR_7407	PMM	HMR_8278	PMM	HMR_5161	P
HMR_7220	PMM	HMR_7408	PMM	HMR_8279	PMM	HMR_5162	P
HMR_7221	PMM	HMR_7409	PMM	HMR_8280	PMM	HMR_5163	P
HMR_7222	PMM	HMR_7410	PMM	HMR_8281	PMM	HMR_5164	P

TABLE A.20. Implemented revisions in connection with the beta-oxidation pathway. "reaction stoich changed" includes changes in the reaction directionality as well.

Rection ID	Reaction	Implemented Change
HMR_1176	8(R)-hydroxy-hexadeca-(2E,4E,6E,10Z)-tetraenoate[m] + H+[m] + NADPH[m] => 8(R)-hydroxy-hexadeca-(2E,6E,10Z)-trienoate[m] + NADP+[m]	reaction removed
HMR_1180	6(R)-hydroxy-tetradeca-(4E,8Z)-dienoate[m] + O2[m] => 6(R)-hydroxy-tetradeca-(2E,4E,8Z)-trienoate[m] + H2O2[m]	reaction removed
HMR_1181	6(R)-hydroxy-tetradeca-(2E,4E,8Z)-trienoate[m] + H+[m] + NADPH[m] <=> 6(R)-hydroxy-tetradeca-(2E,8Z)-dienoate[m] + NADP+[m]	reaction removed
HMR_1182	6(R)-hydroxy-tetradeca-(2E,8Z)-dienoate[m] + H2O[m] => 3(S),6(R)-dihydroxy-tetradec-(8Z)-enoate[m]	reaction removed
HMR_1183	3(S)-6(R)-dihydroxy-tetradec-(8Z)-enoate[m] + NAD+[m] => 3-oxo-6(R)-hydroxy-tetradec-8-cis-enoate[m] + H+[m] + NADH[m]	reaction removed
HMR_1184	3-oxo-6(R)-hydroxy-tetradec-8-cis-enoate[m] + CoA[m] => 4(R)-hydroxy-dodec-(6Z)-enoate[m] + acetyl-CoA[m]	reaction removed
HMR_1185	4(R)-hydroxy-dodec-(6Z)-enoate[m] + CoA[m] => (2E)-dodecenoyl-CoA[m] + 2 H+[m] + O2[m]	reaction removed
HMR_1227	4(S)-hydroxy-dodec-(6Z)-enoate[m] + CoA[m] => (2E)-dodecenoyl-CoA[m] + 2 H+[m] + O2[m]	reaction removed
HMR_0157	butyryl-CoA[c] => butyryl-CoA[m]	reaction removed
HMR_0158	L-carnitine[c] + butyryl-CoA[m] <=> L-carnitine[m] + butyryl-CoA[c]	reaction removed
HMR_0166	pentanoyl-CoA[c] <=> pentanoyl-CoA[m]	reaction removed
HMR_0169	hexanoyl-CoA[c] <=> hexanoyl-CoA[m]	reaction removed
HMR_0172	heptanoyl-CoA[c] <=> heptanoyl-CoA[m]	reaction removed
HMR_0175	octanoyl-CoA[c] <=> octanoyl-CoA[m]	reaction removed
HMR_0178	nonanoyl-CoA[c] <=> nonanoyl-CoA[m]	reaction removed
HMR_0182	decanoyl-CoA[c] <=> decanoyl-CoA[m]	reaction removed
HMR_0185	undecanoyl-CoA[c] <=> undecanoyl-CoA[m]	reaction removed
HMR_3288	cis,cis-3,6-dodecadienoyl-CoA[m] => trans,cis-lauro-2,6-dienoyl-CoA[m]	reaction stoich changed
HMR_3322	2-trans-4-cis-decadienoyl-CoA[p] + NADP+[p] => trans-3-decenoyl-CoA[p] + H+[p] + NADPH[p]	reaction stoich changed
HMR_3409	(6Z,9Z)-octadecadienoyl-CoA[m] + 8 CoA[m] + 7 FAD[m] + 8 H2O[m] + 8 NAD+[m] + NADPH[m] => 7 FADH2[m] + 7 H+[m] + 8 NADH[m] + NADP+[m] + 9 acetyl-CoA[m]	reaction stoich changed
HMR_3413	(8Z,11Z)-eicosadienoyl-CoA[m] + 9 CoA[m] + 8 FAD[m] + 9 H2O[m] + 9 NAD+[m] + NADPH[m] => 8 FADH2[m] + 8 H+[m] + 9 NADH[m] + NADP+[m] + 10 acetyl-CoA[m]	reaction stoich changed
HMR_3414	(5Z,8Z,11Z)-eicosatrienoyl-CoA[m] + 9 CoA[m] + 6 FAD[m] + 9 H2O[m] + 9 NAD+[m] + NADPH[m] => 6 FADH2[m] + 8 H+[m] + 9 NADH[m] + NADP+[m] + 10 acetyl-CoA[m]	reaction stoich changed
HMR_3421	(7Z,10Z,13Z,16Z)-docosatetraenoyl-CoA[m] + 10 CoA[m] + 8 FAD[m] + 10 H2O[m] + 10 NAD+[m] + 2 NADPH[m] => 8 FADH2[m] + 8 H+[m] + 10 NADH[m] + 2 NADP+[m] + 11 acetyl-CoA[m]	reaction stoich changed
HMR_3422	(4Z,7Z,10Z,13Z,16Z)-docosapentaenoyl-CoA[m] + 10 CoA[m] + 8 FAD[m] + 10 H2O[m] + 10 NAD+[m] + 3 NADPH[m] => 8 FADH2[m] + 7 H+[m] + 10 NADH[m] + 3 NADP+[m] + 11 acetyl-CoA[m]	reaction stoich changed
HMR_3423	(11Z,14Z)-eicosadienoyl-CoA[m] + 9 CoA[m] + 8 FAD[m] + 9 H2O[m] + 9 NAD+[m] + NADPH[m] => 8 FADH2[m] + 8 H+[m] + 9 NADH[m] + NADP+[m] + 10 acetyl-CoA[m]	reaction stoich changed
HMR_3424	(13Z,16Z)-docosadienoyl-CoA[m] + 10 CoA[m] + 9 FAD[m] + 10 H2O[m] + 10 NAD+[m] + NADPH[m] => 9 FADH2[m] + 9 H+[m] + 10 NADH[m] + NADP+[m] + 11 acetyl-CoA[m]	reaction stoich changed
HMR_3425	10,13,16-docosatrienoyl-CoA[m] + 10 CoA[m] + 7 FAD[m] + 10 H2O[m] + 10 NAD+[m] => 7 FADH2[m] + 10 H+[m] + 10 NADH[m] + 11 acetyl-CoA[m]	reaction stoich changed
HMR_3426	linolenoyl-CoA[m] + 8 CoA[m] + 7 FAD[m] + 8 H2O[m] + 8 NAD+[m] + NADPH[m] => 7 FADH2[m] + 7 H+[m] + 8 NADH[m] + NADP+[m] + 9 acetyl-CoA[m]	reaction stoich changed
HMR_3427	(8Z,11Z,14Z,17Z)-eicosatetraenoyl-CoA[m] + 9 CoA[m] + 8 FAD[m] + 9 H2O[m] + 9 NAD+[m] + 2 NADPH[m] => 8 FADH2[m] + 7 H+[m] + 9 NADH[m] + 2 NADP+[m] + 10 acetyl-CoA[m]	reaction stoich changed
HMR_3428	(5Z,8Z,11Z,14Z,17Z)-eicosapentaenoyl-CoA[m] + 9 CoA[m] + 6 FAD[m] + 9 H2O[m] + 9 NAD+[m] + 2 NADPH[m] => 6 FADH2[m] + 7 H+[m] + 9 NADH[m] + 2 NADP+[m] + 10 acetyl-CoA[m]	reaction stoich changed
HMR_3429	(7Z,10Z,13Z,16Z,19Z)-docosapentaenoyl-CoA[m] + 10 CoA[m] + 8 FAD[m] + 10 H2O[m] + 10 NAD+[m] + 2 NADPH[m] => 8 FADH2[m] + 8 H+[m] + 10 NADH[m] + 2 NADP+[m] + 11 acetyl-CoA[m]	reaction stoich changed
HMR_3430	(4Z,7Z,10Z,13Z,16Z,19Z)-docosahexaenoyl-CoA[m] + 10 CoA[m] + 7 FAD[m] + 10 H2O[m] + 10 NAD+[m] + 3 NADPH[m] => 7 FADH2[m] + 7 H+[m] + 10 NADH[m] + 3 NADP+[m] + 11 acetyl-CoA[m]	reaction stoich changed
HMR_3431	(11Z,14Z,17Z)-eicosatrienoyl-CoA[m] + 9 CoA[m] + 7 FAD[m] + 9 H2O[m] + 9 NAD+[m] + NADPH[m] => 7 FADH2[m] + 8 H+[m] + 9 NADH[m] + NADP+[m] + 10 acetyl-CoA[m]	reaction stoich changed
HMR_3432	13,16,19-docosatrienoyl-CoA[m] + 10 CoA[m] + 7 FAD[m] + 10 H2O[m] + 10 NAD+[m] => 7 FADH2[m] + 10 H+[m] + 10 NADH[m] + 11 acetyl-CoA[m]	reaction stoich changed
HMR_3433	10,13,16,19-docosatetraenoyl-CoA[m] + 10 CoA[m] + 7 FAD[m] + 10 H2O[m] + 10 NAD+[m] + NADPH[m] => 7 FADH2[m] + 9 H+[m] + 10 NADH[m] + NADP+[m] + 11 acetyl-CoA[m]	reaction stoich changed
HMR_3053	12,15,18,21-tetracosatetraenoyl-CoA[p] + 11 CoA[p] + 11 H2O[p] + 11 NAD+[p] + 7 O2[p] => 10 H+[p] + 7 H2O2[p] + 11 NADH[p] + 12 acetyl-CoA[p]	reaction stoich changed
HMR_3054	(9Z,12Z,15Z,18Z,21Z)-tetracosapentaenoyl-CoA[p] + 11 CoA[p] + 11 H2O[p] + 11 NAD+[p] + 8 O2[p] + 2 NADPH[p] => 9 H+[p] + 8 H2O2[p] + 11 NADH[p] + 2 NADP+[p] + 12 acetyl-CoA[p]	reaction stoich changed
HMR_3055	(9Z,12Z,15Z,18Z)-tetracosatetraenoyl-CoA[p] + 11 CoA[p] + 11 H2O[p] + 11 NAD+[p] + 10 O2[p] + 2 NADPH[p] => 9 H+[p] + 10 H2O2[p] + 11 NADH[p] + 2 NADP+[p] + 12 acetyl-CoA[p]	reaction stoich changed

Rection ID	Reaction	Implemented Change
HMR_3396	(10Z)-heptadecenoyl-CoA[m] + 7 CoA[m] + 6 FAD[m] + 7 H2O[m] + 7 NAD+[m] + NADPH[m] => 6 FADH2[m] + 6 H+[m] + 7 NADH[m] + NADP+[m] + 7 acetyl-CoA[m] + propanoyl-CoA[m]	reaction stoich changed
HMR_1174	3-oxo-10(R)-hydroxy-octadeca-(6E,8E,12Z)-trienoyl-CoA[m] + CoA[m] => 8(R)-hydroxy-hexadeca-(4E,6E,10Z)-trienoyl-CoA[m] + acetyl-CoA[m]	reaction stoich changed
HMR_1175	8(R)-hydroxy-hexadeca-(4E,6E,10Z)-trienoyl-CoA[m] + FAD[m] => 8(R)-hydroxy-hexadeca-(2E,4E,6E,10Z)-tetraenoyl-CoA[m] + FADH2[m]	reaction stoich changed
HMR_1177	8(R)-hydroxy-hexadeca-(2E,4E,6E,10Z)-tetraenoyl-CoA[m] + H2O[m] => 3(S),8(R)-dihydroxy-hexadeca-(4E,6E,10Z)-trienoyl-CoA[m]	reaction stoich changed
HMR_1178	3(S),8(R)-dihydroxy-hexadeca-(4E,6E,10Z)-trienoyl-CoA[m] + NAD+[m] => 3-oxo-8(R)-hydroxy-hexadeca-(4E,6E,10Z)-trienoyl-CoA[m] + H+[m] + NADH[m]	reaction stoich changed
HMR_1179	3-oxo-8(R)-hydroxy-hexadeca-(4E,6E,10Z)-trienoyl-CoA[m] + CoA[m] => 6(R)-hydroxy-tetradeca-(2E,4E,8Z)-trienoyl-CoA[m] + acetyl-CoA[m]	reaction stoich changed
HMR_1216	3-oxo-10(S)-hydroxy-octadeca-(6E,8E,12Z)-trienoyl-CoA[m] + CoA[m] => 8(S)-hydroxy-hexadeca-(4E,6E,10Z)-trienoyl-CoA[m] + acetyl-CoA[m]	reaction stoich changed
HMR_1217	8(S)-hydroxy-hexadeca-(4E,6E,10Z)-trienoyl-CoA[m] + FAD[m] => 8(S)-hydroxy-hexadeca-(2E,4E,6E,10Z)-tetraenoyl-CoA[m] + FADH2[m]	reaction stoich changed
HMR_1218	8(S)-hydroxy-hexadeca-(2E,4E,6E,10Z)-tetraenoyl-CoA[m] + H+[m] + NADPH[m] => 8(S)-hydroxy-hexadeca-(2E,6E,10Z)-trienoyl-CoA[m] + NADP+[m]	reaction stoich changed
HMR_1219	8(S)-hydroxy-hexadeca-(2E,6E,10Z)-trienoyl-CoA[m] + H2O[m] => 3(S),8(S)-dihydroxy-hexadeca-(6E,10Z)-dienoyl-CoA[m]	reaction stoich changed
HMR_1220	3(S),8(S)-dihydroxy-hexadeca-(6E,10Z)-dienoyl-CoA[m] + NAD+[m] <=> 3-oxo-8(S)-hydroxy-hexadeca-(6E,10Z)-dienoyl-CoA[m] + H+[m] + NADH[m]	reaction stoich changed
HMR_1221	3-oxo-8(S)-hydroxy-hexadeca-(6E,10Z)-dienoyl-CoA[m] + CoA[m] <=> 6(S)-hydroxy-tetradeca-(4E,8Z)-dienoyl-CoA[m] + acetyl-CoA[m]	reaction stoich changed
HMR_1222	6(S)-hydroxy-tetradeca-(2E,4E,8Z)-trienoyl-CoA[m] + H+[m] + NADPH[m] <=> 6(S)-hydroxy-tetradeca-(2E,8Z)-dienoyl-CoA[m] + NADP+[m]	reaction stoich changed
HMR_1223	6(S)-hydroxy-tetradeca-(4E,8Z)-dienoyl-CoA[m] + FAD[m] => 6(S)-hydroxy-tetradeca-(2E,4E,8Z)-trienoyl-CoA[m] + FADH2[m]	reaction stoich changed
HMR_1224	6(S)-hydroxy-tetradeca-(2E,8Z)-dienoyl-CoA[m] + H2O[m] => 3(S),6(S)-dihydroxy-tetradec-(8Z)-enoyl-CoA[m]	reaction stoich changed
HMR_1225	3(S),6(S)-dihydroxy-tetradec-(8Z)-enoyl-CoA[m] + NAD+[m] => 3-oxo-6(S)-hydroxy-tetradec-(8Z)-enoyl-CoA[m] + H+[m] + NADH[m]	reaction stoich changed
HMR_1226	3-oxo-6(S)-hydroxy-tetradec-(8Z)-enoyl-CoA[m] + CoA[m] => 4(S)-hydroxy-dodec-(6Z)-enoyl-CoA[m] + acetyl-CoA[m]	reaction stoich changed
HMR_3244	FAD[m] + cis-vaccenoyl-CoA[m] => FADH2[m] + trans,cis-octadeca-2,11-dienoyl-CoA[m]	reaction stoich changed
HMR_3272	(2E)-dodecenoyl-CoA[m] <=> (3E)-dodecenoyl-CoA[m]	reaction stoich changed
HMR_3375	(2E)-dodecenoyl-CoA[p] <=> (3E)-dodecenoyl-CoA[p]	reaction stoich changed
HMR_3296	2-trans-4-cis-decadienoyl-CoA[m] + NADP+[m] => trans-3-decenoyl-CoA[m] + H+[m] + NADPH[m]	reaction stoich changed
HMR_3316	cis,cis-3,6-dodecadienoyl-CoA[p] => trans,cis-lauro-2,6-dienoyl-CoA[p]	reaction stoich changed
HMR_3321	4-cis-decenoyl-CoA[p] + O2[p] => 2-trans-4-cis-decadienoyl-CoA[p] + H2O2[p] + 2 H+[p]	reaction stoich changed
HMR_3480	ATP[c] + CoA[c] + phytanic acid[c] => AMP[c] + PPi[c] + phytanoyl-CoA[c]	reaction stoich changed
HMR_3482	ATP[p] + CoA[p] + phytanic acid[p] => AMP[p] + PPi[p] + phytanoyl-CoA[p]	reaction stoich changed
HMR_3493	ATP[p] + CoA[p] + pristanic acid[p] => (2R)-pristanoyl-CoA[p] + AMP[p] + PPi[p]	reaction stoich changed
HMR_3797	ATP[m] + CoA[m] + propanoate[m] => AMP[m] + PPi[m] + propanoyl-CoA[m]	reaction stoich changed
HMR_5295	ATP[c] + H2O[c] + 2 K+[s] + 3 Na+[c] => ADP[c] + 2 K+[c] + 3 Na+[s] + Pi[c]	reaction stoich changed
HMR_0449	FAD[m] + sn-glycerol-3-phosphate[c] => DHAP[c] + FADH2[m]	reaction stoich changed
HMR_0216	palmitate[s] <=> palmitate[c]	reaction stoich changed
HMR_0225	palmitolate[s] <=> palmitolate[c]	reaction stoich changed
HMR_4459	ATP[c] + propanoate[c] => PPi[c] + propinol adenylate[c]	reaction stoich changed
HMR_4460	ATP[m] + propanoate[m] => PPi[m] + propinol adenylate[m]	reaction stoich changed
HMR_4727	ATP[c] + phosphopantetheine[c] => PPi[c] + dephospho-CoA[c]	reaction stoich changed
R_a1	3(S),6(R)-dihydroxy-tetradeca-(4E,8Z)-dienoyl-CoA[m] + NAD+[m] => 3-oxo-6(R)-hydroxy-tetradeca-(4E,8Z)-dienoyl-CoA[m] + H+[m] + NADH[m]	reaction added
R_a2	3-oxo-6(R)-hydroxy-tetradeca-(4E,8Z)-dienoyl-CoA[m] + CoA[m] => 4(R)-hydroxy-dodeca-(2E,6Z)-dienoyl-CoA[m] + acetyl-CoA[m]	reaction added
R_a3	4(R)-hydroxy-dodeca-(2E,6Z)-dienoyl-CoA[m] + H2O[m] => 3(S),4(R)-dihydroxy-dodec-(6Z)-enoyl-CoA[m]	reaction added
R_a4	3(S),4(R)-dihydroxy-dodec-(6Z)-enoyl-CoA[m] + NAD+[m] => 3-oxo-4(R)-hydroxy-dodec-(6Z)-enoyl-CoA[m] + H+[m] + NADH[m]	reaction added
R_a5	3-oxo-4(R)-hydroxy-dodec-(6Z)-enoyl-CoA[m] + CoA[m] => 2(R)-hydroxy-dec-(4Z)-enoyl-CoA[m] + acetyl-CoA[m]	reaction added

Rection ID	Reaction	Implemented Change
R_a6	2(R)-hydroxy-dec-(4Z)-enoyl-CoA[m] + H2O[m] => 2(R)-hydroxy-dec-(4Z)-enoate[m] + CoA[m]	reaction added
R_a7	2(R)-hydroxy-dec-(4Z)-enoate[m] <=> 2(R)-hydroxy-dec-(4Z)-enoate[c]	reaction added
R_a8	2(R)-hydroxy-dec-(4Z)-enoate[c] <=> 2(R)-hydroxy-dec-(4Z)-enoate[r]	reaction added
R_a9	ATP[r] + CoA[r] + 2(R)-hydroxy-dec-(4Z)-enoate[r] => AMP[r] + PPi[r] + 2(R)-hydroxy-dec-(4Z)-enoyl-CoA[r]	reaction added
R_a10	2(R)-hydroxy-dec-(4Z)-enoate[c] <=> 2(R)-hydroxy-dec-(4Z)-enoate[p]	reaction added
R_a11	ATP[p] + CoA[p] + 2(R)-hydroxy-dec-(4Z)-enoate[p] => AMP[p] + PPi[p] + 2(R)-hydroxy-dec-(4Z)-enoyl-CoA[p]	reaction added
R_a12	2(R)-hydroxy-dec-(4Z)-enoyl-CoA[p] => (3Z)-nonenoic aldehyde[p] + formyl-CoA[p]	reaction added
R_a13	(3Z)-nonenoic aldehyde[p] + H2O[p] + NAD+[p] => (3Z)-nonenoate[p] + H+[p] + NADH[p]	reaction added
R_a14	(3Z)-nonenoate[p] <=> (3Z)-nonenoate[c]	reaction added
R_a15	(3Z)-nonenoate[c] <=> (3Z)-nonenoate[m]	reaction added
R_a16	ATP[m] + (3Z)-nonenoate[m] + CoA[m] => (3Z)-nonenoyl-CoA[m] + AMP[m] + PPi[m]	reaction added
R_a17	(3Z)-nonenoyl-CoA[m] <=> (2E)-nonenoyl-CoA[m]	reaction added
R_a18	2(R)-hydroxy-dec-(4Z)-enoyl-CoA[r] => (3Z)-nonenoic aldehyde[r] + formyl-CoA[r]	reaction added
R_a19	H2O[r] + formyl-CoA[r] => CoA[r] + formate[r]	reaction added
R_a20	(3Z)-nonenoic aldehyde[r] + H2O[r] + NAD+[r] => (3Z)-nonenoate[r] + H+[r] + NADH[r]	reaction added
R_a21	(3Z)-nonenoate[r] <=> (3Z)-nonenoate[c]	reaction added
R_a22	(3Z)-nonenoate[c] <=> (3Z)-nonenoate[m]	reaction added
R_a23	3-oxo-10(S)-hydroxy-octadeca-(6E,8E,12Z)-trienoate[m] + CoA[m] + ATP[m] => 3-oxo-10(S)-hydroxy-octadeca-(6E,8E,12Z)-trienoyl-CoA[m] + PPi[m] + AMP[m]	reaction added
R_a24	4(S)-hydroxy-dodec-(6Z)-enoyl-CoA[m] + FAD[m] => 4(S)-hydroxy-dodeca-(2E,6Z)-dienoyl-CoA[m] + FADH2[m]	reaction added
R_a25	4(S)-hydroxy-dodeca-(2E,6Z)-dienoyl-CoA[m] + H2O[m] => 3(S),4(S)-dihydroxy-dodec-(6Z)-enoyl-CoA[m]	reaction added
R_a26	3(S),4(S)-dihydroxy-dodec-(6Z)-enoyl-CoA[m] + NAD+[m] => 3-oxo-4(S)-hydroxy-dodec-(6Z)-enoyl-CoA[m] + H+[m] + NADH[m]	reaction added
R_a27	3-oxo-4(S)-hydroxy-dodec-(6Z)-enoyl-CoA[m] + CoA[m] => 2(S)-hydroxy-dec-(4Z)-enoyl-CoA[m] + acetyl-CoA[m]	reaction added
R_a28	2(S)-hydroxy-dec-(4Z)-enoyl-CoA[m] + H2O[m] => 2(S)-hydroxy-dec-(4Z)-enoate[m]	reaction added
R_a29	2(S)-hydroxy-dec-(4Z)-enoate[m] <=> 2(S)-hydroxy-dec-(4Z)-enoate[c]	reaction added
R_a30	2(S)-hydroxy-dec-(4Z)-enoate[c] <=> 2(S)-hydroxy-dec-(4Z)-enoate[r]	reaction added
R_a31	ATP[r] + CoA[r] + 2(S)-hydroxy-dec-(4Z)-enoate[r] => AMP[r] + PPi[r] + 2(S)-hydroxy-dec-(4Z)-enoyl-CoA[r]	reaction added
R_a32	2(S)-hydroxy-dec-(4Z)-enoate[c] <=> 2(S)-hydroxy-dec-(4Z)-enoate[p]	reaction added
R_a33	ATP[p] + CoA[p] + 2(S)-hydroxy-dec-(4Z)-enoate[p] => AMP[p] + PPi[p] + 2(S)-hydroxy-dec-(4Z)-enoyl-CoA[p]	reaction added
R_a34	2(S)-hydroxy-dec-(4Z)-enoyl-CoA[p] => (3Z)-nonenoic aldehyde[p] + formyl-CoA[p]	reaction added
R_a35	2(S)-hydroxy-dec-(4Z)-enoyl-CoA[r] => (3Z)-nonenoic aldehyde[r] + formyl-CoA[r]	reaction added
R_a36	(5Z)-dodecenoyl-CoA[m] + FAD[m] => FADH2[m] + (2E,5Z)-dodecadienoyl-CoA[m]	reaction added
R_a37	(2E,5Z)-dodecadienoyl-CoA[m] <=> (3E,5Z)-dodecadienoyl-CoA[m]	reaction added
R_a38	(3E,5Z)-dodecadienoyl-CoA[m] <=> (2E,4Z)-dodecadienoyl-CoA[m]	reaction added
R_a39	(2E,4Z)-dodecadienoyl-CoA[m] + NADPH[m] <=> (3E)-dodecenoyl-CoA[m] + NADP+[m]	reaction added
R_a40	(5Z)-dodecenoyl-CoA[p] + O2[p] => H2O2[p] + (2E,5Z)-dodecadienoyl-CoA[p]	reaction added
R_a41	(2E,5Z)-dodecadienoyl-CoA[p] <=> (3E,5Z)-dodecadienoyl-CoA[p]	reaction added
R_a42	(3E,5Z)-dodecadienoyl-CoA[p] <=> (2E,4Z)-dodecadienoyl-CoA[p]	reaction added
R_a43	(2E,4Z)-dodecadienoyl-CoA[p] + NADPH[p] <=> (3E)-dodecenoyl-CoA[p] + NADP+[p]	reaction added
R_a52	6(R)-hydroxy-tetradeca-(2E,4E,8Z)-trienoyl-CoA[m] + H2O[m] => 3(S),6(R)-dihydroxy-tetradeca-(4E,8Z)-dienoyl-CoA[m]	reaction added
R_a53	formate[p] <=> formate[c]	reaction added
R_a39	butyrate[c] <=> butyrate[m]	reaction added
R_a40	valeric acid[c] <=> valeric acid[m]	reaction added
R_a41	hexanoic acid[c] <=> hexanoic acid[m]	reaction added
R_a42	heptylic acid[c] <=> heptylic acid[m]	reaction added
R_a43	octanoic acid[c] <=> octanoic acid[m]	reaction added
R_a44	nonanoic acid[c] <=> nonanoic acid[m]	reaction added
R_a45	decanoic acid[c] <=> decanoic acid[m]	reaction added
R_a46	undecylic acid[c] <=> undecylic acid[m]	reaction added
R_m02675	palmitolate[x] <=> palmitolate[s]	reaction added
R_m02674	palmitate[x] <=> palmitate[s]	reaction added

Table A.21: Atomically unbalanced reaction, which was changed in the revised model.

Rection ID	**Original reaction**	**Revised reaction**
HMR_0013	HDL[s] => 160 cholesterol-ester pool[s] + 20 cholesterol[s] + HDL remnant[s]	HDL[s] => HDL remnant[s]

TABLE A.22. Blocked or isolated reactions, which remain after the removal of reactions with biological functions. All listed reactions were excluded from the model.

ReactionID	Type	ReactionID	Type	ReactionID	Type	ReactionID	Type
HMR_8652	Blocked	HMR_3995	Blocked	HMR_1835	Blocked	HMR_9539	Blocked
HMR_4831	Blocked	HMR_3996	Blocked	HMR_1836	Blocked	HMR_9540	Blocked
HMR_4832	Blocked	HMR_4072	Blocked	HMR_1837	Blocked	HMR_9544	Blocked
HMR_8766	Blocked	HMR_5388	Blocked	HMR_1840	Blocked	HMR_9546	Blocked
HMR_4310	Blocked	HMR_5418	Blocked	HMR_1841	Blocked	HMR_9550	Blocked
HMR_4317	Blocked	HMR_5419	Blocked	HMR_1842	Blocked	HMR_9552	Blocked
HMR_4318	Blocked	HMR_6523	Blocked	HMR_1843	Blocked	HMR_9801	Blocked
HMR_4320	Blocked	HMR_8641	Blocked	HMR_1844	Blocked	HMR_9807	Blocked
HMR_4356	Blocked	HMR_8682	Blocked	HMR_1845	Blocked	HMR_9554	Blocked
HMR_4401	Blocked	HMR_8683	Blocked	HMR_1848	Blocked	HMR_9555	Blocked
HMR_4402	Blocked	HMR_4688	Blocked	HMR_1403	Blocked	HMR_9556	Blocked
HMR_4403	Blocked	HMR_7132	Blocked	HMR_1404	Blocked	HMR_9557	Blocked
HMR_4594	Blocked	HMR_7134	Blocked	HMR_1405	Blocked	HMR_9558	Blocked
HMR_3855	Blocked	HMR_7135	Blocked	HMR_1406	Blocked	HMR_9559	Blocked
HMR_8500	Blocked	HMR_7136	Blocked	HMR_1407	Blocked	HMR_9560	Blocked
HMR_8507	Blocked	HMR_7137	Blocked	HMR_1408	Blocked	HMR_9561	Blocked
HMR_8508	Blocked	HMR_7138	Blocked	HMR_1409	Blocked	HMR_9562	Blocked
HMR_8509	Blocked	HMR_7139	Blocked	HMR_1410	Blocked	HMR_9563	Blocked
HMR_3212	Blocked	HMR_7620	Blocked	HMR_1411	Blocked	HMR_9564	Blocked
HMR_0718	Blocked	HMR_8640	Blocked	HMR_1412	Blocked	HMR_9565	Blocked
HMR_0719	Blocked	HMR_8689	Blocked	HMR_1413	Blocked	HMR_9566	Blocked
HMR_7709	Blocked	HMR_8690	Blocked	HMR_1414	Blocked	HMR_9567	Blocked
HMR_4476	Blocked	HMR_4124	Blocked	HMR_1415	Blocked	HMR_9568	Blocked
HMR_9799	Blocked	HMR_7696	Blocked	HMR_1416	Blocked	HMR_9570	Blocked
HMR_9800	Blocked	HMR_7697	Blocked	HMR_1417	Blocked	HMR_9571	Blocked
HMR_4086	Blocked	HMR_7698	Blocked	HMR_1418	Blocked	HMR_9572	Blocked
HMR_4135	Blocked	HMR_8672	Blocked	HMR_1419	Blocked	HMR_9573	Blocked
HMR_4451	Blocked	HMR_8674	Blocked	HMR_1420	Blocked	HMR_9574	Blocked
HMR_6601	Blocked	HMR_8675	Blocked	HMR_1421	Blocked	HMR_9575	Blocked
HMR_6602	Blocked	HMR_5130	Blocked	HMR_1422	Blocked	HMR_9580	Blocked
HMR_6603	Blocked	HMR_5131	Blocked	HMR_1423	Blocked	HMR_9585	Blocked
HMR_6609	Blocked	HMR_5132	Blocked	HMR_1424	Blocked	HMR_9588	Blocked
HMR_6610	Blocked	HMR_5133	Blocked	HMR_1425	Blocked	HMR_9798	Blocked
HMR_6611	Blocked	HMR_5134	Blocked	HMR_1426	Blocked	HMR_9806	Blocked
HMR_4211	Blocked	HMR_5135	Blocked	HMR_1427	Blocked	HMR_5238	Blocked
HMR_6613	Blocked	HMR_5136	Blocked	HMR_1428	Blocked	HMR_5239	Blocked
HMR_7744	Blocked	HMR_5137	Blocked	HMR_1429	Blocked	HMR_5243	Blocked
HMR_7894	Blocked	HMR_5138	Blocked	HMR_1430	Blocked	HMR_5244	Blocked
HMR_7895	Blocked	HMR_5139	Blocked	HMR_1431	Blocked	HMR_5257	Blocked

ReactionID	Type	ReactionID	Type	ReactionID	Type	ReactionID	Type
HMR_8445	Blocked	HMR_5140	Blocked	HMR_1432	Blocked	HMR_0006	Blocked
HMR_8484	Blocked	HMR_5141	Blocked	HMR_1433	Blocked	HMR_0019	Blocked
HMR_8493	Blocked	HMR_5142	Blocked	HMR_3992	Blocked	HMR_4931	Blocked
HMR_8494	Blocked	HMR_5143	Blocked	HMR_4267	Blocked	HMR_6512	Blocked
HMR_8495	Blocked	HMR_5144	Blocked	HMR_4268	Blocked	HMR_6991	Blocked
HMR_6968	Blocked	HMR_5145	Blocked	HMR_4279	Blocked	HMR_7629	Blocked
HMR_6969	Blocked	HMR_5146	Blocked	HMR_7677	Blocked	HMR_7630	Blocked
HMR_6970	Blocked	HMR_5147	Blocked	HMR_7678	Blocked	HMR_7631	Blocked
HMR_6971	Blocked	HMR_5148	Blocked	HMR_4499	Blocked	HMR_7632	Blocked
HMR_6972	Blocked	HMR_5149	Blocked	HMR_6567	Blocked	HMR_7660	Blocked
HMR_3819	Blocked	HMR_5150	Blocked	HMR_6568	Blocked	HMR_7798	Blocked
HMR_4605	Blocked	HMR_4188	Blocked	HMR_6573	Blocked	HMR_7901	Blocked
HMR_6929	Blocked	HMR_4842	Blocked	HMR_6574	Blocked	HMR_7903	Blocked
HMR_6930	Blocked	HMR_7704	Blocked	HMR_6575	Blocked	HMR_8687	Blocked
HMR_6931	Blocked	HMR_2437	Blocked	HMR_6580	Blocked	HMR_8720	Blocked
HMR_6933	Blocked	HMR_2438	Blocked	HMR_6584	Blocked	HMR_8923	Blocked
HMR_6934	Blocked	HMR_2443	Blocked	HMR_6588	Blocked	HMR_8929	Blocked
HMR_6936	Blocked	HMR_2444	Blocked	HMR_6589	Blocked	HMR_9180	Blocked
HMR_6938	Blocked	HMR_2445	Blocked	HMR_8799	Blocked	HMR_9182	Blocked
HMR_6939	Blocked	HMR_2446	Blocked	HMR_8800	Blocked	HMR_9196	Blocked
HMR_6940	Blocked	HMR_2447	Blocked	HMR_8803	Blocked	HMR_9639	Blocked
HMR_6941	Blocked	HMR_2448	Blocked	HMR_8804	Blocked	HMR_9015	Blocked
HMR_6942	Blocked	HMR_2449	Blocked	HMR_8805	Blocked	HMR_9019	Blocked
HMR_6943	Blocked	HMR_2450	Blocked	HMR_8818	Blocked	HMR_9020	Blocked
HMR_6944	Blocked	HMR_2461	Blocked	HMR_8825	Blocked	HMR_1173	Blocked
HMR_6945	Blocked	HMR_2462	Blocked	HMR_8827	Blocked	HMR_2590	Blocked
HMR_6946	Blocked	HMR_6397	Blocked	HMR_7145	Blocked	HMR_3921	Blocked
HMR_6947	Blocked	HMR_2581	Blocked	HMR_7146	Blocked	HMR_4266	Blocked
HMR_6948	Blocked	HMR_2583	Blocked	HMR_7147	Blocked	HMR_4684	Blocked
HMR_6949	Blocked	HMR_3445	Blocked	HMR_6394	Blocked	HMR_5022	Blocked
HMR_6950	Blocked	HMR_3460	Blocked	HMR_6405	Blocked	HMR_5036	Blocked
HMR_6951	Blocked	HMR_0941	Blocked	HMR_8349	Blocked	HMR_5112	Blocked
HMR_6952	Blocked	HMR_0988	Blocked	HMR_8621	Blocked	HMR_5117	Blocked
HMR_6953	Blocked	HMR_0989	Blocked	HMR_8622	Blocked	HMR_6408	Blocked
HMR_6954	Blocked	HMR_0990	Blocked	HMR_8623	Blocked	HMR_6455	Blocked
HMR_6955	Blocked	HMR_1030	Blocked	HMR_8624	Blocked	HMR_6513	Blocked
HMR_6956	Blocked	HMR_1045	Blocked	HMR_8625	Blocked	HMR_7723	Blocked
HMR_6957	Blocked	HMR_1053	Blocked	HMR_4763	Blocked	HMR_7757	Blocked
HMR_6958	Blocked	HMR_1079	Blocked	HMR_4764	Blocked	HMR_7760	Blocked
HMR_6959	Blocked	HMR_1160	Blocked	HMR_4768	Blocked	HMR_7897	Blocked
HMR_6960	Blocked	HMR_1162	Blocked	HMR_4769	Blocked	HMR_7899	Blocked

ReactionID	Type	ReactionID	Type	ReactionID	Type	ReactionID	Type
HMR_6961	Blocked	HMR_1164	Blocked	HMR_8634	Blocked	HMR_8528	Blocked
HMR_6962	Blocked	HMR_1166	Blocked	HMR_9717	Blocked	HMR_8562	Blocked
HMR_6963	Blocked	HMR_1168	Blocked	HMR_6635	Blocked	HMR_8785	Blocked
HMR_6964	Blocked	HMR_1170	Blocked	HMR_6636	Blocked	HMR_8910	Blocked
HMR_6965	Blocked	HMR_1171	Blocked	HMR_6637	Blocked	HMR_9676	Blocked
HMR_6966	Blocked	HMR_1302	Blocked	HMR_6639	Blocked	HMR_0707	Blocked
HMR_6967	Blocked	HMR_3009	Blocked	HMR_6640	Blocked	HMR_1172	Blocked
HMR_6973	Blocked	HMR_0159	Blocked	HMR_6663	Blocked	HMR_3026	Blocked
HMR_8416	Blocked	HMR_3032	Blocked	HMR_6666	Blocked	HMR_3948	Blocked
HMR_8425	Blocked	HMR_8419	Blocked	HMR_6667	Blocked	HMR_6928	Blocked
HMR_8603	Blocked	HMR_0160	Blocked	HMR_6670	Blocked	HMR_6937	Blocked
HMR_8604	Blocked	HMR_0161	Blocked	HMR_6671	Blocked	HMR_8422	Blocked
HMR_8605	Blocked	HMR_2778	Blocked	HMR_6681	Blocked	HMR_9179	Blocked
HMR_8608	Blocked	HMR_2780	Blocked	HMR_6683	Blocked	HMR_9181	Blocked
HMR_3750	Blocked	HMR_2783	Blocked	HMR_6684	Blocked	HMR_9017	Blocked
HMR_3771	Blocked	HMR_2785	Blocked	HMR_6685	Blocked	HMR_4538	Blocked
HMR_3772	Blocked	HMR_0001	Blocked	HMR_6686	Blocked	HMR_7765	Blocked
HMR_3782	Blocked	HMR_3491	Blocked	HMR_6694	Blocked	HMR_7767	Blocked
HMR_3794	Blocked	HMR_3493	Blocked	HMR_6695	Blocked	HMR_7861	Blocked
HMR_4199	Blocked	HMR_9722	Blocked	HMR_6697	Blocked	HMR_7862	Blocked
HMR_4466	Blocked	HMR_1931	Blocked	HMR_6699	Blocked	HMR_8840	Blocked
HMR_4937	Blocked	HMR_1932	Blocked	HMR_6704	Blocked	HMR_8638	Blocked
HMR_4426	Blocked	HMR_1933	Blocked	HMR_6705	Blocked	HMR_8642	Blocked
HMR_5336	Blocked	HMR_1934	Blocked	HMR_8703	Blocked	HMR_4314	Blocked
HMR_5337	Blocked	HMR_1935	Blocked	HMR_8704	Blocked	HMR_9016	Blocked
HMR_5340	Blocked	HMR_1942	Blocked	HMR_8706	Blocked	HMR_9018	Blocked
HMR_8783	Blocked	HMR_1943	Blocked	HMR_8712	Blocked	HMR_0929	Blocked
HMR_8784	Blocked	HMR_1950	Blocked	HMR_4546	Blocked	HMR_2040	Blocked
HMR_8786	Blocked	HMR_1951	Blocked	HMR_4547	Blocked	HMR_4903	Blocked
HMR_4241	Blocked	HMR_6793	Blocked	HMR_4548	Blocked	HMR_4907	Blocked
HMR_8563	Blocked	HMR_6794	Blocked	HMR_4549	Blocked	HMR_5048	Blocked
HMR_8566	Blocked	HMR_1978	Blocked	HMR_4550	Blocked	HMR_5049	Blocked
HMR_4685	Blocked	HMR_2020	Blocked	HMR_4551	Blocked	HMR_5050	Blocked
HMR_4687	Blocked	HMR_2022	Blocked	HMR_4552	Blocked	HMR_5051	Blocked
HMR_4702	Blocked	HMR_2024	Blocked	HMR_4553	Blocked	HMR_5052	Blocked
HMR_4703	Blocked	HMR_2050	Blocked	HMR_4554	Blocked	HMR_5053	Blocked
HMR_4704	Blocked	HMR_2056	Blocked	HMR_4555	Blocked	HMR_5054	Blocked
HMR_8630	Blocked	HMR_2062	Blocked	HMR_4556	Blocked	HMR_5055	Blocked
HMR_6924	Blocked	HMR_2077	Blocked	HMR_4557	Blocked	HMR_5056	Blocked
HMR_6925	Blocked	HMR_3702	Blocked	HMR_4561	Blocked	HMR_5057	Blocked
HMR_6926	Blocked	HMR_3730	Blocked	HMR_4563	Blocked	HMR_5058	Blocked

ReactionID	Type	ReactionID	Type	ReactionID	Type	ReactionID	Type
HMR_6927	Blocked	HMR_3731	Blocked	HMR_4564	Blocked	HMR_5059	Blocked
HMR_3743	Blocked	HMR_3742	Blocked	HMR_8746	Blocked	HMR_5060	Blocked
HMR_4227	Blocked	HMR_0715	Blocked	HMR_8003	Blocked	HMR_5061	Blocked
HMR_4232	Blocked	HMR_0716	Blocked	HMR_8004	Blocked	HMR_5062	Blocked
HMR_4248	Blocked	HMR_0733	Blocked	HMR_8005	Blocked	HMR_5063	Blocked
HMR_6707	Blocked	HMR_8237	Blocked	HMR_8012	Blocked	HMR_5064	Blocked
HMR_6708	Blocked	HMR_0463	Blocked	HMR_8013	Blocked	HMR_5065	Blocked
HMR_6709	Blocked	HMR_0484	Blocked	HMR_6423	Blocked	HMR_5066	Blocked
HMR_6710	Blocked	HMR_0613	Blocked	HMR_6456	Blocked	HMR_7252	Blocked
HMR_6711	Blocked	HMR_8423	Blocked	HMR_6457	Blocked	HMR_7430	Blocked
HMR_6712	Blocked	HMR_0840	Blocked	HMR_6458	Blocked	HMR_7710	Blocked
HMR_6713	Blocked	HMR_0856	Blocked	HMR_6459	Blocked	HMR_8355	Blocked
HMR_6714	Blocked	HMR_0857	Blocked	HMR_6460	Blocked	HMR_8490	Blocked
HMR_6715	Blocked	HMR_0858	Blocked	HMR_6461	Blocked	HMR_8491	Blocked
HMR_6722	Blocked	HMR_0928	Blocked	HMR_6499	Blocked	HMR_8492	Blocked
HMR_6723	Blocked	HMR_0813	Blocked	HMR_6500	Blocked	HMR_8688	Blocked
HMR_6726	Blocked	HMR_0861	Blocked	HMR_6501	Blocked	HMR_8875	Blocked
HMR_6727	Blocked	HMR_0862	Blocked	HMR_7051	Blocked	HMR_8928	Blocked
HMR_6735	Blocked	HMR_0863	Blocked	HMR_7091	Blocked	HMR_0612	Blocked
HMR_6737	Blocked	HMR_0871	Blocked	HMR_7092	Blocked	HMR_0652	Blocked
HMR_6738	Blocked	HMR_0879	Blocked	HMR_7093	Blocked	HMR_0717	Blocked
HMR_6739	Blocked	HMR_0880	Blocked	HMR_7094	Blocked	HMR_0917	Blocked
HMR_6740	Blocked	HMR_0881	Blocked	HMR_7095	Blocked	HMR_4125	Blocked
HMR_6744	Blocked	HMR_0882	Blocked	HMR_7096	Blocked	HMR_4902	Blocked
HMR_6747	Blocked	HMR_0888	Blocked	HMR_7097	Blocked	HMR_6577	Blocked
HMR_6748	Blocked	HMR_0896	Blocked	HMR_7098	Blocked	HMR_6578	Blocked
HMR_6749	Blocked	HMR_0897	Blocked	HMR_6535	Blocked	HMR_7204	Blocked
HMR_6750	Blocked	HMR_0790	Blocked	HMR_6536	Blocked	HMR_7435	Blocked
HMR_6751	Blocked	HMR_0792	Blocked	HMR_5127	Blocked	HMR_7694	Blocked
HMR_6753	Blocked	HMR_0834	Blocked	HMR_5128	Blocked	HMR_7695	Blocked
HMR_6754	Blocked	HMR_0915	Blocked	HMR_7741	Blocked	HMR_7759	Blocked
HMR_6755	Blocked	HMR_0921	Blocked	HMR_9464	Blocked	HMR_7761	Blocked
HMR_6757	Blocked	HMR_1996	Blocked	HMR_9465	Blocked	HMR_8496	Blocked
HMR_6759	Blocked	HMR_1320	Blocked	HMR_9466	Blocked	HMR_8527	Blocked
HMR_6771	Blocked	HMR_1335	Blocked	HMR_9467	Blocked	HMR_8673	Blocked
HMR_6788	Blocked	HMR_1346	Blocked	HMR_9468	Blocked	HMR_8856	Blocked
HMR_6792	Blocked	HMR_1352	Blocked	HMR_9469	Blocked	HMR_8857	Blocked
HMR_6798	Blocked	HMR_1355	Blocked	HMR_9470	Blocked	HMR_8920	Blocked
HMR_6799	Blocked	HMR_1356	Blocked	HMR_9471	Blocked	HMR_9199	Blocked
HMR_6800	Blocked	HMR_1357	Blocked	HMR_9472	Blocked	HMR_4313	Blocked
HMR_6801	Blocked	HMR_1358	Blocked	HMR_9473	Blocked	HMR_1306	Blocked

ReactionID	Type	ReactionID	Type	ReactionID	Type	ReactionID	Type
HMR_6927	Blocked	HMR_3731	Blocked	HMR_4564	Blocked	HMR_5059	Blocked
HMR_6802	Blocked	HMR_1359	Blocked	HMR_9474	Blocked	HMR_2777	Blocked
HMR_6803	Blocked	HMR_1360	Blocked	HMR_9475	Blocked	HMR_4126	Blocked
HMR_6806	Blocked	HMR_1361	Blocked	HMR_9476	Blocked	HMR_4860	Blocked
HMR_6807	Blocked	HMR_1362	Blocked	HMR_9477	Blocked	HMR_7784	Blocked
HMR_6808	Blocked	HMR_1363	Blocked	HMR_9478	Blocked	HMR_8369	Blocked
HMR_6811	Blocked	HMR_1401	Blocked	HMR_9479	Blocked	HMR_8651	Blocked
HMR_6813	Blocked	HMR_1402	Blocked	HMR_9480	Blocked	HMR_8681	Blocked
HMR_6814	Blocked	HMR_0705	Blocked	HMR_9481	Blocked	HMR_8919	Blocked
HMR_6815	Blocked	HMR_0706	Blocked	HMR_9482	Blocked	HMR_8921	Blocked
HMR_6817	Blocked	HMR_0708	Blocked	HMR_9483	Blocked	HMR_9200	Blocked
HMR_6818	Blocked	HMR_7604	Blocked	HMR_9484	Blocked	HMR_9625	Blocked
HMR_6819	Blocked	HMR_7605	Blocked	HMR_9485	Blocked	HMR_9024	Blocked
HMR_6820	Blocked	HMR_7606	Blocked	HMR_9487	Blocked	HMR_9077	Blocked
HMR_6822	Blocked	HMR_7607	Blocked	HMR_9497	Blocked	HMR_9080	Blocked
HMR_6823	Blocked	HMR_7610	Blocked	HMR_9504	Blocked	HMR_9081	Blocked
HMR_6824	Blocked	HMR_7514	Blocked	HMR_9506	Blocked	HMR_9082	Blocked
HMR_6827	Blocked	HMR_7515	Blocked	HMR_9507	Blocked	HMR_9149	Blocked
HMR_6828	Blocked	HMR_7516	Blocked	HMR_9508	Blocked	HMR_9150	Blocked
HMR_6830	Blocked	HMR_7517	Blocked	HMR_9509	Blocked	HMR_9157	Blocked
HMR_6835	Blocked	HMR_7518	Blocked	HMR_9510	Blocked	HMR_9162	Blocked

Table A.23: Revised GPRs implemented in the model.

Reaction ID	Genes	Reaction ID	Genes
HMR_3322	ENSG00000242612	HMR_3093	ENSG00000060971
HMR_1218	ENSG00000104325	HMR_3094	ENSG00000161533
HMR_1220	ENSG00000084754	HMR_3097	ENSG00000060971
HMR_1222	ENSG00000104325	HMR_3098	ENSG00000161533
HMR_1225	ENSG00000084754	HMR_3101	ENSG00000060971
HMR_3375	ENSG00000198721	HMR_3102	ENSG00000161533
HMR_1178	ENSG00000084754	HMR_3171	ENSG00000084754
R_a1	ENSG00000084754	HMR_3175	ENSG00000084754
R_a4	ENSG00000084754	HMR_3486	ENSG00000131373
R_a12	ENSG00000131373	HMR_3505	ENSG00000060971
R_a13	ENSG00000072210	HMR_3510	ENSG00000060971
R_a18	ENSG00000105135	HMR_3515	ENSG00000060971
R_a20	ENSG00000072210	HMR_3242	ENSG00000084754
R_a26	ENSG00000084754	HMR_3246	ENSG00000084754
R_a34	ENSG00000131373	HMR_3254	ENSG00000084754
R_a35	ENSG00000105135	HMR_3262	ENSG00000084754
R_a38	ENSG00000104823	HMR_3359	ENSG00000060971
R_a39	ENSG00000104325	HMR_3363	ENSG00000060971
R_a41	ENSG00000198721	HMR_3220	ENSG00000084754
R_a42	ENSG00000104823	HMR_3224	ENSG00000084754
R_a43	ENSG00000242612	HMR_3228	ENSG00000084754
HMR_3522	ENSG00000117054	HMR_3232	ENSG00000084754
HMR_3523	ENSG00000127884	HMR_3236	ENSG00000084754
HMR_3525	ENSG00000167315	HMR_3329	ENSG00000060971
HMR_3527	ENSG00000117054	HMR_3333	ENSG00000060971
HMR_3528	ENSG00000127884	HMR_3337	ENSG00000060971
HMR_3530	ENSG00000167315	HMR_3341	ENSG00000060971
HMR_3531	ENSG00000117054	HMR_3345	ENSG00000060971
HMR_3532	ENSG00000127884	HMR_3349	ENSG00000060971
HMR_3534	ENSG00000167315	HMR_3353	ENSG00000060971
HMR_3278	ENSG00000084754	HMR_3355	ENSG00000198721
HMR_3282	ENSG00000084754	HMR_3368	ENSG00000060971
HMR_3286	ENSG00000084754	HMR_3373	ENSG00000060971
HMR_3292	ENSG00000084754	HMR_4332	ENSG00000228716
HMR_3294	ENSG00000117054	HMR_4333	ENSG00000228716
HMR_3305	ENSG00000060971	HMR_4654	ENSG00000228716
HMR_3310	ENSG00000060971	HMR_4655	ENSG00000228716
HMR_3315	ENSG00000060971	HMR_4391	ENSG00000111669
HMR_3320	ENSG00000060971	HMR_6912	ENSG00000138777
HMR_3323	ENSG00000198721	HMR_2118	ENSG00000111012
HMR_3108	ENSG00000084754	HMR_2129	ENSG00000019186
HMR_3112	ENSG00000084754	HMR_2130	ENSG00000019186
HMR_3116	ENSG00000084754	HMR_2131	ENSG00000019186
HMR_3143	ENSG00000127884	HMR_2132	ENSG00000019186
HMR_3150	ENSG00000127884	HMR_2133	ENSG00000019186
HMR_3157	ENSG00000127884	HMR_2134	ENSG00000019186
HMR_3057	ENSG00000161533	HMR_2135	ENSG00000019186
HMR_3058	ENSG00000113790	HMR_2138	ENSG00000019186
HMR_3059	ENSG00000113790	HMR_2139	ENSG00000111012
HMR_3060	ENSG00000060971	HMR_2140	ENSG00000111012
HMR_3062	ENSG00000161533	HMR_2144	ENSG00000019186
HMR_3063	ENSG00000113790	HMR_2145	ENSG00000019186
HMR_3064	ENSG00000113790	HMR_8003	ENSG00000111012
HMR_3065	ENSG00000060971	HMR_8005	ENSG00000019186
HMR_3066	ENSG00000161533	HMR_8006	ENSG00000111012
HMR_3067	ENSG00000113790	HMR_8514	ENSG00000166816
HMR_3068	ENSG00000113790	HMR_3288	ENSG00000167969 OR ENSG00000198721
HMR_3069	ENSG00000060971	HMR_1175	ENSG00000072778 OR ENSG00000115361
HMR_3070	ENSG00000161533	HMR_1216	ENSG00000138029 OR ENSG00000167315
HMR_3073	ENSG00000060971	HMR_1217	ENSG00000072778 OR ENSG00000115361
HMR_3074	ENSG00000161533	HMR_1219	ENSG00000084754 OR ENSG00000127884
HMR_3077	ENSG00000060971	HMR_1221	ENSG00000138029 OR ENSG00000167315
HMR_3078	ENSG00000161533	HMR_1223	ENSG00000072778 OR ENSG00000115361
HMR_3081	ENSG00000060971	HMR_1224	ENSG00000084754 OR ENSG00000127884
HMR_3082	ENSG00000161533	HMR_1226	ENSG00000138029 OR ENSG00000167315
HMR_3085	ENSG00000060971	HMR_3244	ENSG00000072778 OR ENSG00000115361
HMR_3086	ENSG00000161533	HMR_3272	ENSG00000167969 OR ENSG00000198721
HMR_3089	ENSG00000060971	HMR_1179	ENSG00000138029 OR ENSG00000167315
HMR_3090	ENSG00000161533	R_a2	ENSG00000138029 OR ENSG00000167315

Reaction ID	Genes
R_a3	ENSG00000084754 OR ENSG00000127884
R_a5	ENSG00000138029 OR ENSG00000167315
R_a24	ENSG00000072778 OR ENSG00000115361
R_a25	ENSG00000084754 OR ENSG00000127884
R_a27	ENSG00000138029 OR ENSG00000167315
R_a37	ENSG00000167969 OR ENSG00000198721
R_a40	ENSG00000161533 OR ENSG00000087008
R_a52	ENSG00000084754 OR ENSG00000127884
HMR_3240	ENSG00000072778 OR ENSG00000115361
HMR_3250	ENSG00000072778 OR ENSG00000115361
HMR_3258	ENSG00000072778 OR ENSG00000115361
HMR_3524	ENSG00000072506 OR ENSG00000138796
HMR_3529	ENSG00000072506 OR ENSG00000138796
HMR_3533	ENSG00000072506 OR ENSG00000138796
HMR_3275	ENSG00000072778 OR ENSG00000115361
HMR_3280	ENSG00000072778 OR ENSG00000115361
HMR_3284	ENSG00000072778 OR ENSG00000115361
HMR_3302	ENSG00000113790 OR ENSG00000133835
HMR_3307	ENSG00000113790 OR ENSG00000133835
HMR_3312	ENSG00000113790 OR ENSG00000133835
HMR_3317	ENSG00000113790 OR ENSG00000133835
HMR_3107	ENSG00000072778 OR ENSG00000115361
HMR_3109	ENSG00000072506 OR ENSG00000084754
HMR_3110	ENSG00000138029 OR ENSG00000167315
HMR_3111	ENSG00000072778 OR ENSG00000115361
HMR_3113	ENSG00000072506 OR ENSG00000084754
HMR_3114	ENSG00000138029 OR ENSG00000167315
HMR_3117	ENSG00000072506 OR ENSG00000084754
HMR_3118	ENSG00000138029 OR ENSG00000167315
HMR_3123	ENSG00000072506 OR ENSG00000084754
HMR_3125	ENSG00000138029 OR ENSG00000167315
HMR_3128	ENSG00000072778 OR ENSG00000115361
HMR_3130	ENSG00000072506 OR ENSG00000084754
HMR_3132	ENSG00000138029 OR ENSG00000167315
HMR_3139	ENSG00000138029 OR ENSG00000167315
HMR_3146	ENSG00000138029 OR ENSG00000167315
HMR_3153	ENSG00000138029 OR ENSG00000167315
HMR_3156	ENSG00000117054 OR ENSG00000196177
HMR_3160	ENSG00000138029 OR ENSG00000167315
HMR_3071	ENSG00000113790 OR ENSG00000133835
HMR_3075	ENSG00000113790 OR ENSG00000133835
HMR_3079	ENSG00000113790 OR ENSG00000133835
HMR_3083	ENSG00000113790 OR ENSG00000133835
HMR_3087	ENSG00000113790 OR ENSG00000133835
HMR_3091	ENSG00000113790 OR ENSG00000133835
HMR_3095	ENSG00000113790 OR ENSG00000133835
HMR_3099	ENSG00000113790 OR ENSG00000133835
HMR_3103	ENSG00000113790 OR ENSG00000133835
HMR_3172	ENSG00000072506 OR ENSG00000084754
HMR_3173	ENSG00000138029 OR ENSG00000167315
HMR_3176	ENSG00000072506 OR ENSG00000084754
HMR_3177	ENSG00000138029 OR ENSG00000167315
HMR_3498	ENSG00000087008 OR ENSG00000168306
HMR_3501	ENSG00000113790 OR ENSG00000133835
HMR_3506	ENSG00000087008 OR ENSG00000168306
HMR_3508	ENSG00000113790 OR ENSG00000133835
HMR_3512	ENSG00000087008 OR ENSG00000168306
HMR_3513	ENSG00000113790 OR ENSG00000133835
HMR_3243	ENSG00000138029 OR ENSG00000167315
HMR_3247	ENSG00000138029 OR ENSG00000167315
HMR_3256	ENSG00000138029 OR ENSG00000167315
HMR_3264	ENSG00000138029 OR ENSG00000167315
HMR_3357	ENSG00000113790 OR ENSG00000133835
HMR_3358	ENSG00000113790 OR ENSG00000133835
HMR_3361	ENSG00000113790 OR ENSG00000133835
HMR_3362	ENSG00000113790 OR ENSG00000133835
HMR_3218	ENSG00000072778 OR ENSG00000115361
HMR_3221	ENSG00000138029 OR ENSG00000167315
HMR_3222	ENSG00000072778 OR ENSG00000115361
HMR_3225	ENSG00000138029 OR ENSG00000167315
HMR_3226	ENSG00000072778 OR ENSG00000115361
HMR_3229	ENSG00000138029 OR ENSG00000167315
HMR_3230	ENSG00000072778 OR ENSG00000115361
HMR_3233	ENSG00000138029 OR ENSG00000167315
HMR_3234	ENSG00000072778 OR ENSG00000115361
HMR_3237	ENSG00000138029 OR ENSG00000167315
HMR_3239	ENSG00000167969 OR ENSG00000198721
HMR_3327	ENSG00000113790 OR ENSG00000133835
HMR_3328	ENSG00000113790 OR ENSG00000133835
HMR_3331	ENSG00000113790 OR ENSG00000133835
HMR_3332	ENSG00000113790 OR ENSG00000133835
HMR_3335	ENSG00000113790 OR ENSG00000133835
HMR_3336	ENSG00000113790 OR ENSG00000133835
HMR_3339	ENSG00000113790 OR ENSG00000133835
HMR_3340	ENSG00000113790 OR ENSG00000133835
HMR_3343	ENSG00000113790 OR ENSG00000133835
HMR_3344	ENSG00000113790 OR ENSG00000133835
HMR_3347	ENSG00000113790 OR ENSG00000133835
HMR_3348	ENSG00000113790 OR ENSG00000133835
HMR_3351	ENSG00000113790 OR ENSG00000133835
HMR_3352	ENSG00000113790 OR ENSG00000133835
HMR_3365	ENSG00000113790 OR ENSG00000133835
HMR_3367	ENSG00000113790 OR ENSG00000133835
HMR_3370	ENSG00000113790 OR ENSG00000133835
HMR_3372	ENSG00000113790 OR ENSG00000133835
HMR_1457	ENSG00000160752 OR ENSG00000152904
HMR_1460	ENSG00000160752 OR ENSG00000152904
R_a36	ENSG00000072778 OR ENSG00000115361 OR ENSG00000117054
HMR_3115	ENSG00000072778 OR ENSG00000115361 OR ENSG00000177646
HMR_3121	ENSG00000072778 OR ENSG00000115361 OR ENSG00000177646
HMR_3122	ENSG00000072506 OR ENSG00000084754 OR ENSG00000127884
HMR_3129	ENSG00000072506 OR ENSG00000084754 OR ENSG00000127884
HMR_3135	ENSG00000072778 OR ENSG00000115361 OR ENSG00000117054
HMR_3170	ENSG00000072778 OR ENSG00000115361 OR ENSG00000177646
HMR_3174	ENSG00000072778 OR ENSG00000115361 OR ENSG00000177646
HMR_3202	ENSG00000196177 OR ENSG00000117054 OR ENSG00000177646
HMR_0459	ENSG00000111275 OR ENSG00000137124 OR ENSG00000164904
HMR_8784	ENSG00000111275 OR ENSG00000137124 OR ENSG00000164904
HMR_9563	ENSG00000111275 OR ENSG00000137124 OR ENSG00000164904
HMR_3975	ENSG00000107902 OR ENSG00000143363 OR ENSG00000180817
HMR_3977	ENSG00000107902 OR ENSG00000143363 OR ENSG00000180817
HMR_3979	ENSG00000107902 OR ENSG00000143363 OR ENSG00000180817
HMR_2115	ENSG00000186104 OR ENSG00000135929 OR ENSG00000118816
HMR_2117	ENSG00000186104 OR ENSG00000135929 OR ENSG00000118816
HMR_7996	ENSG00000186104 OR ENSG00000135929 OR ENSG00000118816
HMR_4281	ENSG00000134333 OR ENSG00000111716 OR ENSG00000171989
HMR_4280	ENSG00000134333 OR ENSG00000111716 OR ENSG00000171989
HMR_4239	ENSG00000091140 AND ENSG00000119689 AND ENSG00000105953
HMR_5297	ENSG00000091140 AND ENSG00000119689 AND ENSG00000105953
R_a11	ENSG00000068366 OR ENSG00000123983 OR ENSG00000151726 OR ENSG00000164398
R_a33	ENSG00000068366 OR ENSG00000123983 OR ENSG00000151726 OR ENSG00000164398
HMR_1692	ENSG00000072210 OR ENSG00000006534 OR ENSG00000108602 OR ENSG00000132746
HMR_1132	ENSG00000072210 OR ENSG00000006534 OR ENSG00000108602 OR ENSG00000132746
HMR_1134	ENSG00000072210 OR ENSG00000006534 OR ENSG00000108602 OR ENSG00000132746
HMR_1289	ENSG00000072210 OR ENSG00000006534 OR ENSG00000108602 OR ENSG00000132746
HMR_3923	ENSG00000091140 AND ENSG00000140905 AND ENSG00000145020 AND ENSG00000178445
HMR_6409	ENSG00000091140 AND ENSG00000140905 AND ENSG00000145020 AND ENSG00000178445
HMR_8433	ENSG00000091140 AND ENSG00000140905 AND ENSG00000145020 AND ENSG00000178445
HMR_8434	ENSG00000091140 AND ENSG00000140905 AND ENSG00000145020 AND ENSG00000178445
HMR_8435	ENSG00000091140 AND ENSG00000140905 AND ENSG00000145020 AND ENSG00000178445
HMR_8436	ENSG00000091140 AND ENSG00000140905 AND ENSG00000145020 AND ENSG00000178445
HMR_8437	ENSG00000091140 AND ENSG00000140905 AND ENSG00000145020 AND ENSG00000178445

Reaction ID	Genes
R_a6	ENSG00000119673 OR ENSG00000112304 OR ENSG00000123130 OR ENSG00000159445 OR ENSG00000196407
R_a28	ENSG00000119673 OR ENSG00000112304 OR ENSG00000123130 OR ENSG00000159445 OR ENSG00000196407
HMR_4388	ENSG00000134333 OR ENSG00000111716 OR ENSG00000166796 OR ENSG00000166800 OR ENSG00000171989
HMR_3056	ENSG00000087008 AND ENSG00000161533 AND ENSG00000133835 AND ENSG00000113790 AND ENSG00000060971
HMR_0738	ENSG00000090054 AND (ENSG00000100596 OR ENSG00000172296) AND (ENSG00000165389 OR ENSG00000196542)
R_a9	ENSG00000103740 OR ENSG00000068366 OR ENSG00000123983 OR ENSG00000151726 OR ENSG00000164398 OR ENSG00000197142
R_a16	ENSG00000005187 OR ENSG00000066813 OR ENSG00000166743 OR ENSG00000183549 OR ENSG00000183747 OR ENSG00000215009
R_a31	ENSG00000103740 OR ENSG00000068366 OR ENSG00000123983 OR ENSG00000151726 OR ENSG00000164398 OR ENSG00000197142
HMR_0154	ENSG00000097021 OR ENSG00000136881 OR ENSG00000177465 OR ENSG00000184227 OR ENSG00000205669 OR ENSG00000205794
HMR_0189	ENSG00000097021 OR ENSG00000136881 OR ENSG00000177465 OR ENSG00000184227 OR ENSG00000205669 OR ENSG00000205794
HMR_0193	ENSG00000097021 OR ENSG00000136881 OR ENSG00000177465 OR ENSG00000184227 OR ENSG00000205669 OR ENSG00000205794
HMR_0197	ENSG00000097021 OR ENSG00000136881 OR ENSG00000177465 OR ENSG00000184227 OR ENSG00000205669 OR ENSG00000205794
HMR_0201	ENSG00000097021 OR ENSG00000136881 OR ENSG00000177465 OR ENSG00000184227 OR ENSG00000205669 OR ENSG00000205794
HMR_0206	ENSG00000097021 OR ENSG00000136881 OR ENSG00000177465 OR ENSG00000184227 OR ENSG00000205669 OR ENSG00000205794
HMR_0210	ENSG00000097021 OR ENSG00000136881 OR ENSG00000177465 OR ENSG00000184227 OR ENSG00000205669 OR ENSG00000205794
HMR_0214	ENSG00000097021 OR ENSG00000136881 OR ENSG00000177465 OR ENSG00000184227 OR ENSG00000205669 OR ENSG00000205794
HMR_0223	ENSG00000097021 OR ENSG00000136881 OR ENSG00000177465 OR ENSG00000184227 OR ENSG00000205669 OR ENSG00000205794
HMR_0230	ENSG00000097021 OR ENSG00000136881 OR ENSG00000177465 OR ENSG00000184227 OR ENSG00000205669 OR ENSG00000205794
HMR_0234	ENSG00000097021 OR ENSG00000136881 OR ENSG00000177465 OR ENSG00000184227 OR ENSG00000205669 OR ENSG00000205794
HMR_0238	ENSG00000097021 OR ENSG00000136881 OR ENSG00000177465 OR ENSG00000184227 OR ENSG00000205669 OR ENSG00000205794
HMR_0242	ENSG00000097021 OR ENSG00000136881 OR ENSG00000177465 OR ENSG00000184227 OR ENSG00000205669 OR ENSG00000205794
HMR_0246	ENSG00000097021 OR ENSG00000136881 OR ENSG00000177465 OR ENSG00000184227 OR ENSG00000205669 OR ENSG00000205794
HMR_0250	ENSG00000097021 OR ENSG00000136881 OR ENSG00000177465 OR ENSG00000184227 OR ENSG00000205669 OR ENSG00000205794
HMR_0256	ENSG00000097021 OR ENSG00000136881 OR ENSG00000177465 OR ENSG00000184227 OR ENSG00000205669 OR ENSG00000205794
HMR_0260	ENSG00000097021 OR ENSG00000136881 OR ENSG00000177465 OR ENSG00000184227 OR ENSG00000205669 OR ENSG00000205794
HMR_0264	ENSG00000097021 OR ENSG00000136881 OR ENSG00000177465 OR ENSG00000184227 OR ENSG00000205669 OR ENSG00000205794
HMR_0268	ENSG00000097021 OR ENSG00000136881 OR ENSG00000177465 OR ENSG00000184227 OR ENSG00000205669 OR ENSG00000205794
HMR_0272	ENSG00000097021 OR ENSG00000136881 OR ENSG00000177465 OR ENSG00000184227 OR ENSG00000205669 OR ENSG00000205794
HMR_0276	ENSG00000097021 OR ENSG00000136881 OR ENSG00000177465 OR ENSG00000184227 OR ENSG00000205669 OR ENSG00000205794
HMR_0280	ENSG00000097021 OR ENSG00000136881 OR ENSG00000177465 OR ENSG00000184227 OR ENSG00000205669 OR ENSG00000205794
HMR_0284	ENSG00000097021 OR ENSG00000136881 OR ENSG00000177465 OR ENSG00000184227 OR ENSG00000205669 OR ENSG00000205794
HMR_0290	ENSG00000097021 OR ENSG00000136881 OR ENSG00000177465 OR ENSG00000184227 OR ENSG00000205669 OR ENSG00000205794
HMR_0294	ENSG00000097021 OR ENSG00000136881 OR ENSG00000177465 OR ENSG00000184227 OR ENSG00000205669 OR ENSG00000205794
HMR_0298	ENSG00000097021 OR ENSG00000136881 OR ENSG00000177465 OR ENSG00000184227 OR ENSG00000205669 OR ENSG00000205794
HMR_0302	ENSG00000097021 OR ENSG00000136881 OR ENSG00000177465 OR ENSG00000184227 OR ENSG00000205669 OR ENSG00000205794
HMR_0306	ENSG00000097021 OR ENSG00000136881 OR ENSG00000177465 OR ENSG00000184227 OR ENSG00000205669 OR ENSG00000205794
HMR_0310	ENSG00000097021 OR ENSG00000136881 OR ENSG00000177465 OR ENSG00000184227 OR ENSG00000205669 OR ENSG00000205794
HMR_0314	ENSG00000097021 OR ENSG00000136881 OR ENSG00000177465 OR ENSG00000184227 OR ENSG00000205669 OR ENSG00000205794
HMR_0320	ENSG00000097021 OR ENSG00000136881 OR ENSG00000177465 OR ENSG00000184227 OR ENSG00000205669 OR ENSG00000205794
HMR_0324	ENSG00000097021 OR ENSG00000136881 OR ENSG00000177465 OR ENSG00000184227 OR ENSG00000205669 OR ENSG00000205794
HMR_0328	ENSG00000097021 OR ENSG00000136881 OR ENSG00000177465 OR ENSG00000184227 OR ENSG00000205669 OR ENSG00000205794

Reaction ID	Genes
HMR_0332	ENSG00000097021 OR ENSG00000136881 OR ENSG00000177465 OR ENSG00000184227 OR ENSG00000205669 OR ENSG00000205794
HMR_0338	ENSG00000097021 OR ENSG00000136881 OR ENSG00000177465 OR ENSG00000184227 OR ENSG00000205669 OR ENSG00000205794
HMR_0342	ENSG00000097021 OR ENSG00000136881 OR ENSG00000177465 OR ENSG00000184227 OR ENSG00000205669 OR ENSG00000205794
HMR_0346	ENSG00000097021 OR ENSG00000136881 OR ENSG00000177465 OR ENSG00000184227 OR ENSG00000205669 OR ENSG00000205794
HMR_0350	ENSG00000097021 OR ENSG00000136881 OR ENSG00000177465 OR ENSG00000184227 OR ENSG00000205669 OR ENSG00000205794
HMR_0354	ENSG00000097021 OR ENSG00000136881 OR ENSG00000177465 OR ENSG00000184227 OR ENSG00000205669 OR ENSG00000205794
HMR_0358	ENSG00000097021 OR ENSG00000136881 OR ENSG00000177465 OR ENSG00000184227 OR ENSG00000205669 OR ENSG00000205794
HMR_0362	ENSG00000097021 OR ENSG00000136881 OR ENSG00000177465 OR ENSG00000184227 OR ENSG00000205669 OR ENSG00000205794
HMR_0366	ENSG00000097021 OR ENSG00000136881 OR ENSG00000177465 OR ENSG00000184227 OR ENSG00000205669 OR ENSG00000205794
HMR_0370	ENSG00000097021 OR ENSG00000136881 OR ENSG00000177465 OR ENSG00000184227 OR ENSG00000205669 OR ENSG00000205794
HMR_0374	ENSG00000097021 OR ENSG00000136881 OR ENSG00000177465 OR ENSG00000184227 OR ENSG00000205669 OR ENSG00000205794
HMR_0378	ENSG00000097021 OR ENSG00000136881 OR ENSG00000177465 OR ENSG00000184227 OR ENSG00000205669 OR ENSG00000205794
HMR_0382	ENSG00000097021 OR ENSG00000136881 OR ENSG00000177465 OR ENSG00000184227 OR ENSG00000205669 OR ENSG00000205794
HMR_0386	ENSG00000097021 OR ENSG00000136881 OR ENSG00000177465 OR ENSG00000184227 OR ENSG00000205669 OR ENSG00000205794
HMR_0390	ENSG00000097021 OR ENSG00000136881 OR ENSG00000177465 OR ENSG00000184227 OR ENSG00000205669 OR ENSG00000205794
HMR_0394	ENSG00000097021 OR ENSG00000136881 OR ENSG00000177465 OR ENSG00000184227 OR ENSG00000205669 OR ENSG00000205794
HMR_0398	ENSG00000097021 OR ENSG00000136881 OR ENSG00000177465 OR ENSG00000184227 OR ENSG00000205669 OR ENSG00000205794
HMR_0402	ENSG00000097021 OR ENSG00000136881 OR ENSG00000177465 OR ENSG00000184227 OR ENSG00000205669 OR ENSG00000205794
HMR_0406	ENSG00000097021 OR ENSG00000136881 OR ENSG00000177465 OR ENSG00000184227 OR ENSG00000205669 OR ENSG00000205794
HMR_0410	ENSG00000097021 OR ENSG00000136881 OR ENSG00000177465 OR ENSG00000184227 OR ENSG00000205669 OR ENSG00000205794
HMR_0414	ENSG00000097021 OR ENSG00000136881 OR ENSG00000177465 OR ENSG00000184227 OR ENSG00000205669 OR ENSG00000205794
HMR_0418	ENSG00000097021 OR ENSG00000136881 OR ENSG00000177465 OR ENSG00000184227 OR ENSG00000205669 OR ENSG00000205794
HMR_0422	ENSG00000097021 OR ENSG00000136881 OR ENSG00000177465 OR ENSG00000184227 OR ENSG00000205669 OR ENSG00000205794
HMR_0426	ENSG00000097021 OR ENSG00000136881 OR ENSG00000177465 OR ENSG00000184227 OR ENSG00000205669 OR ENSG00000205794
HMR_0430	ENSG00000097021 OR ENSG00000136881 OR ENSG00000177465 OR ENSG00000184227 OR ENSG00000205669 OR ENSG00000205794
HMR_0434	ENSG00000097021 OR ENSG00000136881 OR ENSG00000177465 OR ENSG00000184227 OR ENSG00000205669 OR ENSG00000205794
HMR_0438	ENSG00000097021 OR ENSG00000136881 OR ENSG00000177465 OR ENSG00000184227 OR ENSG00000205669 OR ENSG00000205794
HMR_3009	ENSG00000097021 OR ENSG00000136881 OR ENSG00000177465 OR ENSG00000184227 OR ENSG00000205669 OR ENSG00000205794
HMR_8605	ENSG00000143149 OR ENSG00000164904 OR ENSG00000184254 OR ENSG00000165092 OR ENSG00000128918 OR ENSG00000118514
HMR_4079	ENSG00000143149 OR ENSG00000164904 OR ENSG00000184254 OR ENSG00000165092 OR ENSG00000128918 OR ENSG00000118514
HMR_7993	ENSG00000143149 OR ENSG00000164904 OR ENSG00000184254 OR ENSG00000165092 OR ENSG00000128918 OR ENSG00000118514
HMR_0456	ENSG00000143149 OR ENSG00000164904 OR ENSG00000184254 OR ENSG00000165092 OR ENSG00000128918 OR ENSG00000118514
HMR_4737	ENSG00000143149 OR ENSG00000164904 OR ENSG00000184254 OR ENSG00000165092 OR ENSG00000128918 OR ENSG00000118514
HMR_4233	ENSG00000143149 OR ENSG00000164904 OR ENSG00000184254 OR ENSG00000165092 OR ENSG00000128918 OR ENSG00000118514
HMR_6714	ENSG00000143149 OR ENSG00000164904 OR ENSG00000184254 OR ENSG00000165092 OR ENSG00000128918 OR ENSG00000118514
HMR_1568	ENSG00000143149 OR ENSG00000164904 OR ENSG00000184254 OR ENSG00000165092 OR ENSG00000128918 OR ENSG00000118514
HMR_8503	ENSG00000143149 OR ENSG00000164904 OR ENSG00000184254 OR ENSG00000165092 OR ENSG00000128918 OR ENSG00000118514
HMR_8504	ENSG00000143149 OR ENSG00000164904 OR ENSG00000184254 OR ENSG00000165092 OR ENSG00000128918 OR ENSG00000118514
HMR_6646	ENSG00000143149 OR ENSG00000164904 OR ENSG00000184254 OR ENSG00000165092 OR ENSG00000128918 OR ENSG00000118514
HMR_6647	ENSG00000143149 OR ENSG00000164904 OR ENSG00000184254 OR ENSG00000165092 OR ENSG00000128918 OR ENSG00000118514
HMR_6652	ENSG00000143149 OR ENSG00000164904 OR ENSG00000184254 OR ENSG00000165092 OR ENSG00000128918 OR ENSG00000118514

Reaction ID	Genes
HMR_6674	ENSG00000143149 OR ENSG00000164904 OR ENSG00000184254 OR ENSG00000165092 OR ENSG00000128918 OR ENSG00000118514
HMR_6675	ENSG00000143149 OR ENSG00000164904 OR ENSG00000184254 OR ENSG00000165092 OR ENSG00000128918 OR ENSG00000118514
HMR_6676	ENSG00000143149 OR ENSG00000164904 OR ENSG00000184254 OR ENSG00000165092 OR ENSG00000128918 OR ENSG00000118514
HMR_4559	ENSG00000143149 OR ENSG00000164904 OR ENSG00000184254 OR ENSG00000165092 OR ENSG00000128918 OR ENSG00000118514
HMR_8775	ENSG00000143149 OR ENSG00000164904 OR ENSG00000184254 OR ENSG00000165092 OR ENSG00000128918 OR ENSG00000118514
HMR_4683	ENSG00000143149 OR ENSG00000164904 OR ENSG00000184254 OR ENSG00000165092 OR ENSG00000128918 OR ENSG00000118514
HMR_4686	ENSG00000143149 OR ENSG00000164904 OR ENSG00000184254 OR ENSG00000165092 OR ENSG00000128918 OR ENSG00000118514
HMR_4797	ENSG00000143149 OR ENSG00000164904 OR ENSG00000184254 OR ENSG00000165092 OR ENSG00000128918 OR ENSG00000118514
HMR_3053	ENSG00000087008 AND ENSG00000161533 AND ENSG00000133835 AND ENSG00000113790 AND ENSG00000060971 AND ENSG00000167969
HMR_4137	ENSG00000091140 AND ENSG00000110435 AND (ENSG00000131828 OR ENSG00000163114) AND ENSG00000168291 AND ENSG00000150768
HMR_4605	ENSG00000111275 OR ENSG00000137124 OR ENSG00000164904 OR ENSG00000112294 OR ENSG00000164904 OR ENSG00000119711 OR ENSG00000159423
HMR_4688	ENSG00000111275 OR ENSG00000137124 OR ENSG00000164904 OR ENSG00000112294 OR ENSG00000164904 OR ENSG00000119711 OR ENSG00000159423
HMR_8357	ENSG00000111275 OR ENSG00000137124 OR ENSG00000164904 OR ENSG00000112294 OR ENSG00000164904 OR ENSG00000119711 OR ENSG00000159423
HMR_8786	ENSG00000111275 OR ENSG00000137124 OR ENSG00000164904 OR ENSG00000112294 OR ENSG00000164904 OR ENSG00000119711 OR ENSG00000159423
HMR_9564	ENSG00000111275 OR ENSG00000137124 OR ENSG00000164904 OR ENSG00000112294 OR ENSG00000164904 OR ENSG00000119711 OR ENSG00000159423
HMR_1133	ENSG00000111275 OR ENSG00000137124 OR ENSG00000164904 OR ENSG00000112294 OR ENSG00000164904 OR ENSG00000119711 OR ENSG00000159423
HMR_4739	ENSG00000111275 OR ENSG00000137124 OR ENSG00000164904 OR ENSG00000112294 OR ENSG00000164904 OR ENSG00000119711 OR ENSG00000159423
HMR_8506	ENSG00000111275 OR ENSG00000137124 OR ENSG00000164904 OR ENSG00000112294 OR ENSG00000164904 OR ENSG00000119711 OR ENSG00000159423
HMR_8778	ENSG00000111275 OR ENSG00000137124 OR ENSG00000164904 OR ENSG00000112294 OR ENSG00000164904 OR ENSG00000119711 OR ENSG00000159423
HMR_8563	ENSG00000111275 OR ENSG00000137124 OR ENSG00000164904 OR ENSG00000112294 OR ENSG00000164904 OR ENSG00000119711 OR ENSG00000159423
HMR_4685	ENSG00000111275 OR ENSG00000137124 OR ENSG00000164904 OR ENSG00000112294 OR ENSG00000164904 OR ENSG00000119711 OR ENSG00000159423
HMR_4687	ENSG00000111275 OR ENSG00000137124 OR ENSG00000164904 OR ENSG00000112294 OR ENSG00000164904 OR ENSG00000119711 OR ENSG00000159423
HMR_3759	ENSG00000111275 OR ENSG00000137124 OR ENSG00000164904 OR ENSG00000112294 OR ENSG00000164904 OR ENSG00000119711 OR ENSG00000159423
HMR_3054	ENSG00000087008 AND ENSG00000161533 AND ENSG00000133835 AND ENSG00000113790 AND ENSG00000060971 AND ENSG00000167969 AND ENSG00000242612
HMR_3055	ENSG00000087008 AND ENSG00000161533 AND ENSG00000133835 AND ENSG00000113790 AND ENSG00000060971 AND ENSG00000167969 AND ENSG00000242612

Reaction ID	Genes
HMR_3489	ENSG00000068366 OR ENSG00000103740 OR ENSG00000123983 OR ENSG00000130377 OR ENSG00000140284 OR ENSG00000151726 OR ENSG00000164398 OR ENSG00000197142
HMR_0249	ENSG00000068366 OR ENSG00000103740 OR ENSG00000123983 OR ENSG00000130377 OR ENSG00000140284 OR ENSG00000151726 OR ENSG00000164398 OR ENSG00000197142
HMR_2957	ENSG00000068366 OR ENSG00000103740 OR ENSG00000123983 OR ENSG00000130377 OR ENSG00000140284 OR ENSG00000151726 OR ENSG00000164398 OR ENSG00000197142
HMR_3432	ENSG00000167315 AND (ENSG00000072778 OR ENSG00000115361) AND (ENSG00000117054 OR ENSG00000177646) AND ENSG00000084754 AND (ENSG00000138796 OR ENSG00000072506) AND (ENSG00000127884 OR ENSG00000084754) AND (ENSG00000138029 OR ENSG00000167315) AND (ENSG00000198721 OR ENSG00000167969)
HMR_3398	ENSG00000167315 AND (ENSG00000072778 OR ENSG00000115361) AND (ENSG00000117054 OR ENSG00000177646) AND ENSG00000084754 AND (ENSG00000138796 OR ENSG00000072506) AND (ENSG00000127884 OR ENSG00000084754) AND (ENSG00000138029 OR ENSG00000167315) AND (ENSG00000198721 OR ENSG00000167969)
HMR_3406	ENSG00000167315 AND (ENSG00000072778 OR ENSG00000115361) AND (ENSG00000117054 OR ENSG00000177646) AND ENSG00000084754 AND (ENSG00000138796 OR ENSG00000072506) AND (ENSG00000127884 OR ENSG00000084754) AND (ENSG00000138029 OR ENSG00000167315) AND (ENSG00000198721 OR ENSG00000167969)
HMR_3407	ENSG00000167315 AND (ENSG00000072778 OR ENSG00000115361) AND (ENSG00000117054 OR ENSG00000177646) AND ENSG00000084754 AND (ENSG00000138796 OR ENSG00000072506) AND (ENSG00000127884 OR ENSG00000084754) AND (ENSG00000138029 OR ENSG00000167315) AND (ENSG00000198721 OR ENSG00000167969)
HMR_3408	ENSG00000167315 AND (ENSG00000072778 OR ENSG00000115361) AND (ENSG00000117054 OR ENSG00000177646) AND ENSG00000084754 AND (ENSG00000138796 OR ENSG00000072506) AND (ENSG00000127884 OR ENSG00000084754) AND (ENSG00000138029 OR ENSG00000167315) AND (ENSG00000198721 OR ENSG00000167969)
HMR_3411	ENSG00000167315 AND (ENSG00000072778 OR ENSG00000115361) AND (ENSG00000117054 OR ENSG00000177646) AND ENSG00000084754 AND (ENSG00000138796 OR ENSG00000072506) AND (ENSG00000127884 OR ENSG00000084754) AND (ENSG00000138029 OR ENSG00000167315) AND (ENSG00000198721 OR ENSG00000167969)
HMR_3416	ENSG00000167315 AND (ENSG00000072778 OR ENSG00000115361) AND (ENSG00000117054 OR ENSG00000177646) AND ENSG00000084754 AND (ENSG00000138796 OR ENSG00000072506) AND (ENSG00000127884 OR ENSG00000084754) AND (ENSG00000138029 OR ENSG00000167315) AND (ENSG00000198721 OR ENSG00000167969)
HMR_3397	ENSG00000167315 AND (ENSG00000072778 OR ENSG00000115361) AND (ENSG00000117054 OR ENSG00000177646) AND ENSG00000084754 AND (ENSG00000138796 OR ENSG00000072506) AND (ENSG00000127884 OR ENSG00000084754) AND (ENSG00000138029 OR ENSG00000167315) AND (ENSG00000198721 OR ENSG00000167969)
HMR_3414	ENSG00000167315 AND (ENSG00000072778 OR ENSG00000115361) AND (ENSG00000117054 OR ENSG00000177646) AND ENSG00000084754 AND (ENSG00000138796 OR ENSG00000072506) AND (ENSG00000127884 OR ENSG00000084754) AND (ENSG00000138029 OR ENSG00000167315) AND (ENSG00000198721 OR ENSG00000167969) AND ENSG00000104325
HMR_3421	ENSG00000167315 AND (ENSG00000072778 OR ENSG00000115361) AND (ENSG00000117054 OR ENSG00000177646) AND ENSG00000084754 AND (ENSG00000138796 OR ENSG00000072506) AND (ENSG00000127884 OR ENSG00000084754) AND (ENSG00000138029 OR ENSG00000167315) AND (ENSG00000198721 OR ENSG00000167969) AND ENSG00000104325
HMR_3422	ENSG00000167315 AND (ENSG00000072778 OR ENSG00000115361) AND (ENSG00000117054 OR ENSG00000177646) AND ENSG00000084754 AND (ENSG00000138796 OR ENSG00000072506) AND (ENSG00000127884 OR ENSG00000084754) AND (ENSG00000138029 OR ENSG00000167315) AND (ENSG00000198721 OR ENSG00000167969) AND ENSG00000104325
HMR_3423	ENSG00000167315 AND (ENSG00000072778 OR ENSG00000115361) AND (ENSG00000117054 OR ENSG00000177646) AND ENSG00000084754 AND (ENSG00000138796 OR ENSG00000072506) AND (ENSG00000127884 OR ENSG00000084754) AND (ENSG00000138029 OR ENSG00000167315) AND (ENSG00000198721 OR ENSG00000167969) AND ENSG00000104325
HMR_3424	ENSG00000167315 AND (ENSG00000072778 OR ENSG00000115361) AND (ENSG00000117054 OR ENSG00000177646) AND ENSG00000084754 AND (ENSG00000138796 OR ENSG00000072506) AND (ENSG00000127884 OR ENSG00000084754) AND (ENSG00000138029 OR ENSG00000167315) AND (ENSG00000198721 OR ENSG00000167969) AND ENSG00000104325
HMR_3425	ENSG00000167315 AND (ENSG00000072778 OR ENSG00000115361) AND (ENSG00000117054 OR ENSG00000177646) AND ENSG00000084754 AND (ENSG00000138796 OR ENSG00000072506) AND (ENSG00000127884 OR ENSG00000084754) AND (ENSG00000138029 OR ENSG00000167315) AND (ENSG00000198721 OR ENSG00000167969) AND ENSG00000104325
HMR_3426	ENSG00000167315 AND (ENSG00000072778 OR ENSG00000115361) AND (ENSG00000117054 OR ENSG00000177646) AND ENSG00000084754 AND (ENSG00000138796 OR ENSG00000072506) AND (ENSG00000127884 OR ENSG00000084754) AND (ENSG00000138029 OR ENSG00000167315) AND (ENSG00000198721 OR ENSG00000167969) AND ENSG00000104325
HMR_9719	ENSG00000167315 AND (ENSG00000072778 OR ENSG00000115361) AND (ENSG00000117054 OR ENSG00000177646) AND ENSG00000084754 AND (ENSG00000138796 OR ENSG00000072506) AND (ENSG00000127884 OR ENSG00000084754) AND (ENSG00000138029 OR ENSG00000167315) AND (ENSG00000198721 OR ENSG00000167969) AND ENSG00000104325
HMR_3427	ENSG00000167315 AND (ENSG00000072778 OR ENSG00000115361) AND (ENSG00000117054 OR ENSG00000177646) AND ENSG00000084754 AND (ENSG00000138796 OR ENSG00000072506) AND (ENSG00000127884 OR ENSG00000084754) AND (ENSG00000138029 OR ENSG00000167315) AND (ENSG00000198721 OR ENSG00000167969) AND ENSG00000104325

Reaction ID	Genes
HMR_3428	ENSG00000167315 AND (ENSG00000072778 OR ENSG00000115361) AND (ENSG00000117054 OR ENSG00000177646) AND ENSG00000084754 AND (ENSG00000138796 OR ENSG00000072506) AND (ENSG00000127884 OR ENSG00000084754) AND (ENSG00000138029 OR ENSG00000167315) AND (ENSG00000198721 OR ENSG00000167969) AND ENSG00000104325
HMR_3429	ENSG00000167315 AND (ENSG00000072778 OR ENSG00000115361) AND (ENSG00000117054 OR ENSG00000177646) AND ENSG00000084754 AND (ENSG00000138796 OR ENSG00000072506) AND (ENSG00000127884 OR ENSG00000084754) AND (ENSG00000138029 OR ENSG00000167315) AND (ENSG00000198721 OR ENSG00000167969) AND ENSG00000104325
HMR_3430	ENSG00000167315 AND (ENSG00000072778 OR ENSG00000115361) AND (ENSG00000117054 OR ENSG00000177646) AND ENSG00000084754 AND (ENSG00000138796 OR ENSG00000072506) AND (ENSG00000127884 OR ENSG00000084754) AND (ENSG00000138029 OR ENSG00000167315) AND (ENSG00000198721 OR ENSG00000167969) AND ENSG00000104325
HMR_3431	ENSG00000167315 AND (ENSG00000072778 OR ENSG00000115361) AND (ENSG00000117054 OR ENSG00000177646) AND ENSG00000084754 AND (ENSG00000138796 OR ENSG00000072506) AND (ENSG00000127884 OR ENSG00000084754) AND (ENSG00000138029 OR ENSG00000167315) AND (ENSG00000198721 OR ENSG00000167969) AND ENSG00000104325
HMR_3433	ENSG00000167315 AND (ENSG00000072778 OR ENSG00000115361) AND (ENSG00000117054 OR ENSG00000177646) AND ENSG00000084754 AND (ENSG00000138796 OR ENSG00000072506) AND (ENSG00000127884 OR ENSG00000084754) AND (ENSG00000138029 OR ENSG00000167315) AND (ENSG00000198721 OR ENSG00000167969) AND ENSG00000104325
HMR_3396	ENSG00000167315 AND (ENSG00000072778 OR ENSG00000115361) AND (ENSG00000117054 OR ENSG00000177646) AND ENSG00000084754 AND (ENSG00000138796 OR ENSG00000072506) AND (ENSG00000127884 OR ENSG00000084754) AND (ENSG00000138029 OR ENSG00000167315) AND (ENSG00000198721 OR ENSG00000167969) AND ENSG00000104325
HMR_3409	ENSG00000167315 AND (ENSG00000072778 OR ENSG00000115361) AND (ENSG00000117054 OR ENSG00000177646) AND ENSG00000084754 AND (ENSG00000138796 OR ENSG00000072506) AND (ENSG00000127884 OR ENSG00000084754) AND (ENSG00000138029 OR ENSG00000167315) AND (ENSG00000198721 OR ENSG00000167969) AND ENSG00000104325
HMR_3413	ENSG00000167315 AND (ENSG00000072778 OR ENSG00000115361) AND (ENSG00000117054 OR ENSG00000177646) AND ENSG00000084754 AND (ENSG00000138796 OR ENSG00000072506) AND (ENSG00000127884 OR ENSG00000084754) AND (ENSG00000138029 OR ENSG00000167315) AND (ENSG00000198721 OR ENSG00000167969) AND ENSG00000104325
HMR_6916	ENSG00000099624 AND ENSG00000110955 AND ENSG00000116459 AND ENSG00000124172 AND ENSG00000152234 AND (ENSG00000159199 OR ENSG00000135390 OR ENSG00000154518) AND ENSG00000154723 AND ENSG00000165629 AND ENSG00000167283 AND ENSG00000167863 AND ENSG00000169020 AND ENSG00000198899 AND ENSG00000241468 AND ENSG00000241837 AND ENSG00000154518 AND ENSG00000228253

TABLE A.24. Model constraints for uptake reaction fluxes, which were implemented after manual literature revision of metabolites pointed out by the comparative study of gene essentiality. The MetaboliteID indicates the metabolite in the model for which the flux of the uptake reaction was constraint. The constraints are shown with the lower and the upper bounds in brackets. An uptake and transport reaction was added to the model in case it did not already exist. Note that HDL remnant is a composition of diverse lipids including cholesterols, cholesterol esters, phosphatidylcholines, phosphatidylserines, phosphatidylethanolamines and sphingomyelins.

Metabolite	**MetaboliteID**	**Constraints from Jain et al.**	**Constraints**	**Literature evidence**
cysteine	m01628	-	[0, 0.01]	Arriza et al. 1993
L-cystine	m01629	-	[0, 0.08645]	Sato et al. 1999
i-Inositol	m02171	-	[0, 0.1]	Schneider 2015
protoheme	m02049	-	[0, 0.1]	Anwar and Quigley 2011
L-carnitine	m02348	[0, 0.000780]	[0, 0.01]	Longo et al. 2006
proline	m02770	[0, 0.011940]	[0, 0.038]	Takanaga et al. 2005
vitamin A derivatives	m03139	-	[0, 0.01]	Kawaguchi et al. 2015
vitamin D derivatives	m03140	-	[0, 0.01]	Rowling et al. 2006
vitamin E derivatives	m03143	-	[0, 0.01]	Saito et al. 2004
cholesterol	m01450	-	[0, 0.1]	Röhrl and Stangl 2013; Murakami et al. 1990
ubiquinone	m03103	-	[0, 0.1]	Fernández-Ayala et al. 2005
tetrahydrobiopterin	m02978	-	[0,0.1]	Yamamoto et al. 1996
FAD+	m01802	-	[0,0.1]	Jin et al. 2017
HDL remnant	m02047	-	[0,0.1]	Brown and Rader 2009

Table A.25: Enriched GO Terms sorted by category of differentially down regulated genes (padj < 0.01) comparing the tumor samples with NI and WT controls.

Term ID	**Description**	**Occurrences**
GO:0042254	ribosome biogenesis	43
GO:0046483	heterocycle metabolic process	25
GO:0034502	protein localization to chromosome	16
GO:0090304	nucleic acid metabolic process	16
GO:0048856	anatomical structure development	7
GO:0010467	gene expression	7
GO:0001503	ossification	7
GO:0007165	signal transduction	6
GO:1904874	positive regulation of telomerase RNA localization to Cajal body	6
GO:0034641	cellular nitrogen compound metabolic process	6
GO:0016477	cell migration	5
GO:1901135	carbohydrate derivative metabolic process	5
GO:0009081	branched-chain amino acid metabolic process	5
GO:0043062	extracellular structure organization	3
GO:0000278	mitotic cell cycle	2
GO:0007155	cell adhesion	1
GO:1904666	regulation of ubiquitin protein ligase activity	1
GO:0090287	regulation of cellular response to growth factor stimulus	1
GO:0006725	cellular aromatic compound metabolic process	1
GO:1901360	organic cyclic compound metabolic process	1

Table A.26: Enriched GO Terms sorted by category of differentially down regulated genes (padj < 0.01) comparing the regressed samples with NI and WT controls.

Term ID	Description	Occurrences
GO:1903047	mitotic cell cycle process	51
GO:0009190	cyclic nucleotide biosynthetic process	17
GO:0048285	organelle fission	17
GO:0007399	nervous system development	14
GO:0007267	cell-cell signaling	12
GO:0030334	regulation of cell migration	8
GO:0048856	anatomical structure development	7
GO:0072358	cardiovascular system development	5
GO:0030154	cell differentiation	4
GO:0007155	cell adhesion	3
GO:0007165	signal transduction	3
GO:0090304	nucleic acid metabolic process	3
GO:0043062	extracellular structure organization	2
GO:0006939	smooth muscle contraction	2
GO:0071840	cellular component organization or biogenesis	1
GO:0006928	movement of cell or subcellular component	1
GO:0007017	microtubule-based process	1
GO:0071467	cellular response to pH	1
GO:0072006	nephron development	1
GO:0042474	middle ear morphogenesis	1
GO:0001503	ossification	1

Table A.27: Targeted GCMS metabolomics analysis of extracellular metabolites from *In vitro* cultures.

Metabolite	log2FC Tum-Ctrl	Pval Tum-Ctrl	adjPval Tum-Ctrl	log2FC Reg-Ctrl	Pval Reg-Ctrl	adjPval Reg-Ctrl	log2FC Reg-Tum	Pval Reg-Tum	adjPval Reg-Tum
Alanine-2TMS	1,57	1,31E-08	3,56E-08	0,55	1,23E-02	1,47E-02	-1,01	2,98E-05	9,92E-05
Asparagine-3TMS	-0,22	6,49E-02	7,21E-02	-0,35	4,56E-03	5,95E-03	-0,13	2,65E-01	4,42E-01
Aspartic acid-3TMS	-1,10	5,40E-04	7,05E-04	-2,12	1,76E-08	7,55E-08	-1,02	1,18E-03	2,96E-03
Cysteine-3TMS	-0,11	5,77E-01	5,77E-01	-0,21	2,91E-01	3,01E-01	-0,10	6,13E-01	7,51E-01
Fumaric acid-2TMS	1,17	3,31E-05	5,23E-05	-0,05	8,32E-01	8,32E-01	-1,22	1,76E-05	6,62E-05
Glucose-meto-5TMS(2)	-5,80	4,02E-26	1,21E-24	-3,48	3,48E-19	1,05E-17	2,32	4,41E-14	3,31E-13
Glutamic acid-3TMS	0,23	1,18E-01	1,27E-01	-0,67	6,45E-05	1,38E-04	-0,90	5,72E-07	2,45E-06
Glutamine_pool_2	-1,08	4,00E-25	6,00E-24	-0,42	9,11E-13	6,84E-12	0,67	1,39E-18	4,16E-17
Glutamine\Glutamate pool	-1,01	3,84E-24	3,84E-23	-0,42	6,91E-13	6,84E-12	0,59	5,80E-17	8,71E-16
Glycerol-3TMS	0,76	5,89E-04	7,29E-04	0,72	1,02E-03	1,39E-03	-0,04	8,44E-01	8,73E-01
Glycine-3TMS	0,80	1,88E-09	5,65E-09	0,52	5,74E-06	1,44E-05	-0,27	8,71E-03	1,87E-02
Histidine-3TMS	-0,21	4,83E-01	5,00E-01	-0,34	2,52E-01	2,70E-01	-0,13	6,51E-01	7,51E-01
Inositol-6TMS(1)	-0,33	1,23E-05	2,05E-05	-0,46	3,70E-08	1,23E-07	-0,13	5,56E-02	9,81E-02
Isoleucine-2TMS	-1,07	3,32E-08	8,30E-08	-0,98	2,03E-07	6,08E-07	0,09	5,35E-01	7,51E-01
Lactic acid-2TMS	2,20	2,44E-04	3,33E-04	1,94	9,44E-04	1,37E-03	-0,26	6,34E-01	7,51E-01
Leucine-2TMS	-0,77	3,14E-07	6,72E-07	-0,87	2,80E-08	1,05E-07	-0,10	4,09E-01	6,29E-01
Lysine-4TMS	-0,48	5,54E-06	9,77E-06	-0,22	1,62E-02	1,87E-02	0,25	7,05E-03	1,63E-02
Methionine-2TMS	-1,94	5,56E-17	2,78E-16	-0,46	6,90E-04	1,09E-03	1,48	1,15E-13	6,90E-13
Ornithine-4TMS	1,58	1,75E-04	2,50E-04	1,36	9,59E-04	1,37E-03	-0,23	5,51E-01	7,51E-01
Phenylalanine-2TMS	-1,71	6,89E-19	4,13E-18	-0,53	2,59E-06	7,07E-06	1,18	3,07E-14	3,07E-13
Proline-2TMS	1,27	4,82E-14	2,07E-13	0,87	7,54E-10	3,77E-09	-0,40	3,86E-04	1,05E-03
Putrescine-4TMS	1,70	3,87E-07	7,74E-07	1,13	1,87E-04	3,51E-04	-0,57	4,30E-02	8,06E-02
Pyruvic acid-meto-TMS	-0,76	5,40E-03	6,23E-03	-0,64	1,79E-02	1,99E-02	0,12	6,30E-01	7,51E-01
Serine-3TMS	-1,30	5,00E-19	3,75E-18	-1,01	7,69E-16	1,15E-14	0,29	2,65E-04	7,95E-04
Succinic acid-2TMS	1,77	5,15E-11	1,72E-10	0,51	9,92E-03	1,24E-02	-1,26	9,22E-08	4,61E-07
Threonine-3TMS	-0,48	2,83E-06	5,30E-06	-0,41	3,16E-05	7,28E-05	0,07	4,20E-01	6,29E-01
Tryptophan-3TMS	-0,69	6,07E-04	7,29E-04	-0,68	6,78E-04	1,09E-03	0,01	9,69E-01	9,69E-01
Tyrosine-3TMS	-0,73	3,61E-08	8,34E-08	-0,45	1,17E-04	2,34E-04	0,28	9,35E-03	1,87E-02
Urea-2TMS	1,36	1,59E-04	2,39E-04	1,26	3,80E-04	6,70E-04	-0,10	7,63E-01	8,17E-01
Valine-2TMS	-0,69	6,14E-12	2,30E-11	-0,72	2,38E-12	1,43E-11	-0,03	7,00E-01	7,77E-01

Table A.28: Targeted GCMS metabolomics analysis of intracellular metabolites from *In vitro* cultures.

Metabolite	log2FC Tum-Ctrl	Pval Tum-Ctrl	adjPval Tum-Ctrl	log2FC Reg-Ctrl	Pval Reg-Ctrl	adjPval Reg-Ctrl	log2FC Reg-Tum	Pval Reg-Tum	adjPval Reg-Tum
2-Hydroxyglutaric acid-3TMS	-0,57	7,16E-04	1,19E-03	0,13	4,09E-01	4,58E-01	0,70	5,02E-05	2,12E-04
2-Ketoglutaric acid-meto-2TMS	-1,50	2,41E-05	5,09E-05	-0,57	8,08E-02	1,03E-01	0,93	5,89E-03	1,35E-02
3-Phosphoglyceric acid-4TMS	-0,01	9,70E-01	9,70E-01	-0,10	7,55E-01	7,69E-01	-0,09	7,84E-01	7,98E-01
4-Hydroxyproline-3TMS	0,11	4,16E-01	4,48E-01	0,07	5,97E-01	6,22E-01	-0,04	7,74E-01	7,98E-01
Adenine-2TMS	0,47	6,90E-03	9,48E-03	-0,09	5,99E-01	6,22E-01	-0,55	1,56E-03	4,51E-03
Adenosine monophosphate-5TMS	1,31	1,29E-04	2,44E-04	1,14	6,73E-04	1,16E-03	-0,17	6,02E-01	6,90E-01
Alanine-2TMS	0,31	1,22E-03	1,87E-03	-0,02	8,18E-01	8,18E-01	-0,33	6,08E-04	1,97E-03
Asparagine-3TMS	0,50	8,03E-04	1,26E-03	-0,42	4,28E-03	6,72E-03	-0,92	2,97E-08	3,26E-07
Aspartic acid-3TMS	-0,83	1,06E-04	2,10E-04	-1,44	1,82E-09	1,00E-08	-0,62	2,93E-03	7,33E-03
beta-alanine-3TMS	1,14	5,51E-15	7,58E-14	1,30	4,12E-17	1,13E-15	0,16	1,23E-01	1,87E-01
Cadaverine-4TMS	-0,80	1,48E-03	2,19E-03	-0,57	2,18E-02	3,08E-02	0,24	3,23E-01	3,94E-01
Cholesterol-TMS	-0,84	5,22E-08	1,51E-07	-0,18	1,70E-01	2,08E-01	0,66	7,16E-06	3,94E-05
Citric acid-4TMS	-0,21	2,71E-01	2,99E-01	0,32	9,04E-02	1,13E-01	0,53	6,54E-03	1,44E-02
Cysteine-3TMS	-0,08	5,47E-01	5,78E-01	-0,25	6,01E-02	7,88E-02	-0,17	1,94E-01	2,60E-01
Elaidic acid-TMS	-0,36	4,17E-02	5,21E-02	0,42	1,67E-02	2,41E-02	0,78	3,27E-05	1,50E-04
Fumaric acid-2TMS	0,36	3,95E-02	5,06E-02	0,79	2,05E-05	4,70E-05	0,44	1,25E-02	2,41E-02
Glucose-meto-5TMS(1)	-3,71	4,94E-19	9,05E-18	-2,70	6,62E-14	9,11E-13	1,01	3,42E-04	1,17E-03
Glutamic acid-3TMS	0,35	9,08E-07	2,27E-06	0,28	5,37E-05	1,18E-04	-0,07	2,41E-01	3,08E-01
Glutamine Pool	-0,98	1,36E-12	8,31E-12	-0,20	5,48E-02	7,35E-02	0,77	1,35E-09	1,86E-08
Glutamine/Glutamate Pool	-0,17	1,02E-02	1,37E-02	0,05	4,17E-01	4,58E-01	0,22	1,02E-03	3,13E-03
Glycerol 3-phosphate-4TMS	0,42	6,94E-02	8,49E-02	1,37	1,98E-07	7,24E-07	0,95	1,18E-04	4,64E-04
Glycerol-3TMS	-1,41	6,81E-06	1,50E-05	-0,90	2,42E-03	3,91E-03	0,51	7,29E-02	1,15E-01
Glycine-3TMS	0,34	4,61E-06	1,06E-05	0,17	1,46E-02	2,17E-02	-0,17	1,19E-02	2,41E-02
Histidine-3TMS	1,93	2,54E-10	9,31E-10	1,65	1,54E-08	6,53E-08	-0,28	2,56E-01	3,21E-01
Hypotaurine-3TMS	-0,30	7,15E-02	8,55E-02	0,21	1,91E-01	2,24E-01	0,51	2,64E-03	6,91E-03
Inositol phosphate-7TMS	-0,93	8,01E-04	1,26E-03	-0,14	5,90E-01	6,22E-01	0,79	3,89E-03	9,29E-03
Inositol-6TMS(1)	-2,32	3,77E-26	1,04E-24	-1,07	7,86E-13	8,64E-12	1,26	3,05E-15	1,68E-13
Isoleucine-2TMS	0,73	8,25E-09	2,67E-08	0,96	4,25E-12	3,90E-11	0,23	3,73E-02	6,08E-02
Lactic acid-2TMS	0,39	1,19E-01	1,37E-01	1,19	1,41E-05	3,60E-05	0,80	2,18E-03	5,99E-03

Metabolite	log2FC Tum-Ctrl	Pval Tum-Ctrl	adjPval Tum-Ctrl	log2FC Reg-Ctrl	Pval Reg-Ctrl	adjPval Reg-Ctrl	log2FC Reg-Tum	Pval Reg-Tum	adjPval Reg-Tum
Leucine-2TMS	0,84	8,33E-10	2,86E-09	0,81	2,44E-09	1,22E-08	-0,03	7,66E-01	7,98E-01
Lysine-4TMS	0,52	2,56E-06	6,12E-06	0,49	8,28E-06	2,28E-05	-0,03	7,36E-01	7,98E-01
Malic acid-3TMS	5,39	7,02E-04	1,19E-03	5,84	2,78E-04	5,27E-04	0,44	7,67E-01	7,98E-01
Methionine-2TMS	0,74	4,27E-11	1,81E-10	0,70	1,63E-10	1,02E-09	-0,03	7,06E-01	7,92E-01
Myristic acid-TMS	-0,04	8,35E-01	8,50E-01	1,11	8,14E-08	3,20E-07	1,15	3,84E-08	3,52E-07
N-Acetylaspartic acid-3TMS	0,67	2,47E-03	3,48E-03	1,15	1,73E-06	5,01E-06	0,47	3,01E-02	5,17E-02
Oleic acid-TMS	0,47	2,38E-03	3,45E-03	0,85	4,07E-07	1,32E-06	0,38	1,13E-02	2,39E-02
Ornithine-4TMS	0,92	2,94E-13	2,02E-12	0,45	1,73E-05	4,14E-05	-0,48	5,57E-06	3,41E-05
Palmitic acid-TMS	-1,12	2,64E-11	1,23E-10	-0,50	4,03E-04	7,15E-04	0,62	1,82E-05	9,12E-05
Pantothenic acid-3TMS	-0,48	1,96E-02	2,56E-02	-0,76	3,55E-04	6,52E-04	-0,28	1,61E-01	2,33E-01
Phenylalanine-2TMS	0,78	1,80E-10	7,06E-10	0,55	9,50E-07	2,90E-06	-0,23	2,02E-02	3,59E-02
Phosphoenolpyruvic acid-3TMS	-0,46	1,96E-01	2,20E-01	-0,47	1,82E-01	2,18E-01	-0,01	9,66E-01	9,66E-01
Proline-2TMS	1,72	7,57E-29	4,16E-27	1,12	8,19E-21	4,50E-19	-0,59	8,11E-11	2,23E-09
Putrescine-4TMS	-0,33	1,16E-01	1,36E-01	-0,85	1,37E-04	2,69E-04	-0,52	1,44E-02	2,65E-02
Pyruvic acid-meto-TMS	-1,18	1,07E-04	2,10E-04	-0,92	2,03E-03	3,38E-03	0,27	3,46E-01	4,13E-01
Serine-3TMS	-0,91	7,04E-15	7,74E-14	-0,69	4,41E-11	3,46E-10	0,21	1,27E-02	2,41E-02
Spermidine-5TMS	-0,79	5,44E-04	9,65E-04	-0,50	2,30E-02	3,16E-02	0,29	1,83E-01	2,51E-01
Stearic acid-TMS	-0,99	4,25E-07	1,11E-06	-0,74	7,46E-05	1,58E-04	0,26	1,40E-01	2,08E-01
Succinic acid-2TMS	1,93	2,51E-08	7,66E-08	2,34	1,67E-10	1,02E-09	0,41	1,67E-01	2,36E-01
Taurine-3TMS	-1,85	1,28E-07	3,51E-07	-2,05	1,22E-08	5,57E-08	-0,20	5,15E-01	6,03E-01
Threonine-3TMS	0,26	5,18E-04	9,49E-04	-0,29	1,37E-04	2,69E-04	-0,54	3,00E-10	5,51E-09
Tryptophan-3TMS	1,22	8,13E-14	7,45E-13	0,57	1,44E-05	3,60E-05	-0,65	1,76E-06	1,21E-05
Tyrosine-3TMS	0,95	2,23E-13	1,75E-12	0,57	2,11E-07	7,24E-07	-0,37	2,81E-04	1,03E-03
Uracil-2TMS	2,89	1,03E-11	5,68E-11	3,60	7,87E-15	1,44E-13	0,70	3,76E-02	6,08E-02
Urea-2TMS	-0,04	8,27E-01	8,50E-01	0,22	2,84E-01	3,26E-01	0,26	1,99E-01	2,61E-01
Valine-2TMS	0,67	2,69E-11	1,23E-10	0,21	8,90E-03	1,36E-02	-0,45	4,44E-07	3,49E-06

TABLE A.29. Significant reporter metabolites from the comparison of tumor cells with healthy cells. The table depicts a shortened version of the full list of reporter metabolites. Only reporter metabolites with an adjusted p-value < 0.01 are shown. The total number of genes annotated to a respective metabolite is displayed (#Genes annotated) and out of this the number of genes, which are higher (#Genes up) or lower (#Genes down) in the tumor cells than in the control cells. The different types of p-values are extensively reviewed in the vignette of the piano toolbox (https://bioconductor.org/packages/release/bioc/vignettes/piano/inst/doc/piano-vignette.pdf).

Metabolite	#Genes annotated	#Genes up	#Genes down	adjP non.dir	adjP dist.up	adjP dist.down	adjP mix.up	adjP mix.down
N-acetyl-D-mannosamine[c]	2	1	1	3,02E-05	7,78E-04	4,16E-03	2,44E-02	1,53E-02
UTP[c]	86	72	14	2,01E-04	3,81E-04	3,02E-01	1,92E-08	1,00E+00
H2O[l]	87	16	71	2,65E-04	6,12E-01	9,92E-06	1,00E+00	0,00E+00
heparan sulfate, precursor 1[g]	4	0	4	5,84E-04	NA	4,34E-04	1,00E+00	2,02E-09
N-acetyl-D-mannosamine[r]	1	1	0	6,38E-04	7,78E-04	NA	1,00E+00	9,76E-01
chondroitin sulfate D (GlcNAc6S-GlcA2S) precursor 2[g]	5	0	5	6,69E-04	NA	3,16E-04	1,00E+00	5,37E-09
sulfate[l]	15	3	12	7,12E-04	9,13E-01	3,78E-06	1,00E+00	6,76E-13
chondroitin sulfate D (GlcNAc6S-GlcA2S), precursor 3[g]	6	0	6	8,09E-04	NA	3,94E-04	1,00E+00	2,61E-05
chondroitin sulfate C (GalNAc6S-GlcA), precursor 2[g]	6	0	6	8,09E-04	NA	3,94E-04	1,00E+00	2,61E-05
chondroitin sulfate A (GalNAc4S-GlcA) and B (IdoA2S-GalNAc4S), precursor 2[g]	6	0	6	8,09E-04	NA	3,94E-04	1,00E+00	2,61E-05
chondroitin sulfate E (GalNAc4,6diS-GlcA), precursor 3[g]	6	0	6	8,09E-04	NA	3,94E-04	1,00E+00	2,61E-05
keratan sulfate I, degradation product 18[l]	8	0	8	1,43E-03	NA	8,15E-04	1,00E+00	3,28E-08
keratan sulfate I, degradation product 36[l]	8	0	8	1,43E-03	NA	8,15E-04	1,00E+00	3,28E-08
keratan sulfate I, degradation product 30[l]	8	0	8	1,43E-03	NA	8,15E-04	1,00E+00	3,28E-08
keratan sulfate I, degradation product 12[l]	8	0	8	1,43E-03	NA	8,15E-04	1,00E+00	3,28E-08
keratan sulfate I, degradation product 9[l]	8	0	8	1,43E-03	NA	8,15E-04	1,00E+00	3,28E-08
keratan sulfate II (core 2-linked), degradation product 3[l]	8	0	8	1,43E-03	NA	8,15E-04	1,00E+00	3,28E-08
keratan sulfate I, degradation product 27[l]	8	0	8	1,43E-03	NA	8,15E-04	1,00E+00	3,28E-08
keratan sulfate II (core 2-linked), degradation product 6[l]	8	0	8	1,43E-03	NA	8,15E-04	1,00E+00	3,28E-08
keratan sulfate II (core 4-linked), degradation product 3[l]	8	0	8	1,43E-03	NA	8,15E-04	1,00E+00	3,28E-08
keratan sulfate I, degradation product 33[l]	8	0	8	1,43E-03	NA	8,15E-04	1,00E+00	3,28E-08
keratan sulfate I, degradation product 21[l]	8	0	8	1,43E-03	NA	8,15E-04	1,00E+00	3,28E-08
keratan sulfate I, degradation product 15[l]	8	0	8	1,43E-03	NA	8,15E-04	1,00E+00	3,28E-08
keratan sulfate I, degradation product 24[l]	8	0	8	1,43E-03	NA	8,15E-04	1,00E+00	3,28E-08
keratan sulfate I, degradation product 6[l]	8	0	8	1,43E-03	NA	8,15E-04	1,00E+00	3,28E-08
fatty acid-LD-TG1 pool[l]	1	0	1	1,45E-03	NA	1,00E-03	9,93E-01	2,17E-07
tRNA(asp)[c]	3	2	1	1,50E-03	6,37E-03	4,68E-02	5,66E-02	8,73E-01
L-aspartyl-tRNA(asp)[c]	3	2	1	1,50E-03	6,37E-03	4,68E-02	5,66E-02	8,73E-01
guanidinoacetate[c]	2	1	1	1,84E-03	6,56E-03	4,26E-02	1,34E-01	5,38E-01
LTD4[c]	5	1	4	2,64E-03	2,52E-03	3,65E-02	5,92E-01	1,56E-02
chondroitin sulfate A (GalNAc4S-GlcA) and B (IdoA2S-GalNAc4S), precursor 3[g]	9	0	9	2,72E-03	NA	1,75E-03	1,00E+00	2,81E-03
3-hydroxyisobutyrate[m]	4	4	0	2,78E-03	4,01E-03	NA	3,85E-04	9,97E-01
PEP[c]	9	7	2	3,20E-03	2,11E-04	8,60E-01	2,73E-08	9,98E-01
heparan sulfate, degradation product 1[l]	2	0	2	3,21E-03	NA	2,15E-03	1,00E+00	5,48E-13
heparan sulfate, degradation product 6[l]	2	0	2	3,21E-03	NA	2,15E-03	1,00E+00	5,48E-13
heparan sulfate, degradation product 12[l]	2	0	2	3,21E-03	NA	2,15E-03	1,00E+00	5,48E-13
tRNA(lys)[c]	2	1	1	3,23E-03	1,17E-02	4,68E-02	1,91E-01	5,57E-01
L-lysyl-tRNA(lys)[c]	2	1	1	3,23E-03	1,17E-02	4,68E-02	1,91E-01	5,57E-01
2-phospho-D-glycerate[c]	6	3	3	3,39E-03	3,61E-05	5,84E-01	9,04E-05	9,46E-01
S-(3-methylbutanoyl)-dihydrolipoamide[m]	3	3	0	3,44E-03	4,01E-03	NA	1,67E-04	9,94E-01
S-(2-methylpropanoyl)-dihydrolipoamide[m]	3	3	0	3,44E-03	4,01E-03	NA	1,67E-04	9,94E-01
S-(2-methylbutanoyl)-dihydrolipoamide[m]	3	3	0	3,44E-03	4,01E-03	NA	1,67E-04	9,94E-01
GM2A[l]	21	0	21	3,58E-03	NA	1,62E-03	1,00E+00	3,16E-09
5-Phosphonooxy-L-lysine[c]	2	1	1	3,59E-03	9,82E-03	5,98E-02	1,31E-01	6,07E-01
sphingosine[l]	2	0	2	4,01E-03	NA	2,73E-03	9,90E-01	3,36E-05
glutamate[l]	19	0	19	4,13E-03	NA	2,29E-03	1,00E+00	1,99E-08
UDP-glucuronate[g]	10	0	10	4,14E-03	NA	2,70E-03	1,00E+00	3,96E-09
3-methyl-2-oxobutyrate[m]	3	3	0	4,43E-03	5,14E-03	NA	3,08E-04	9,94E-01
4-methyl-2-oxopentanoate[m]	3	3	0	4,43E-03	5,14E-03	NA	3,08E-04	9,94E-01

Metabolite	#Genes annotated	#Genes up	#Genes down	adjP non.dir	adjP dist.up	adjP dist.down	adjP mix.up	adjP mix.down
2-oxo-3-methylvalerate[m]	3	3	0	4,43E-03	5,14E-03	NA	3,08E-04	9,94E-01
H2S[c]	5	2	3	4,54E-03	2,25E-02	3,43E-02	4,43E-01	6,16E-01
heparan sulfate, degradation product 15[l]	2	0	2	4,70E-03	NA	3,24E-03	1,00E+00	5,48E-13
heparan sulfate, degradation product 21[l]	2	0	2	4,70E-03	NA	3,24E-03	1,00E+00	5,48E-13
UTP[n]	34	31	3	5,03E-03	5,79E-03	5,42E-01	4,64E-06	1,00E+00
galactose[l]	10	0	10	5,06E-03	NA	3,34E-03	1,00E+00	6,66E-05
glutamate[c]	66	41	25	5,32E-03	2,91E-03	3,12E-01	2,47E-03	9,23E-01
chondroitin sulfate A (GalNAc4S-GlcA), B (IdoA2S-GalNAc4S), and E (GalNAc4,6diS-GlcA), precursor 1[g]	9	0	9	5,74E-03	NA	3,87E-03	1,00E+00	8,81E-05
globotriaosylceramide[c]	6	0	6	5,80E-03	NA	3,45E-03	1,00E+00	2,26E-05
H2S2O3[c]	5	2	3	6,05E-03	3,23E-02	3,43E-02	5,17E-01	5,57E-01
nicotinamide D-ribonucleotide[m]	3	2	1	6,17E-03	3,20E-02	3,72E-02	3,06E-01	6,33E-01
chondroitin sulfate D (GlcNAc6S-GlcA2S), degradation product 1[l]	7	0	7	6,20E-03	NA	3,97E-03	1,00E+00	5,18E-05
keratan sulfate I, degradation product 11[l]	7	0	7	6,20E-03	NA	3,97E-03	1,00E+00	5,18E-05
F1,alpha[l]	7	0	7	6,20E-03	NA	3,97E-03	1,00E+00	5,18E-05
n2m2nnl[l]	7	0	7	6,20E-03	NA	3,97E-03	1,00E+00	5,18E-05
keratan sulfate I, degradation product 39[l]	7	0	7	6,20E-03	NA	3,97E-03	1,00E+00	5,18E-05
keratan sulfate I, degradation product 40[l]	7	0	7	6,20E-03	NA	3,97E-03	1,00E+00	5,18E-05
keratan sulfate I, degradation product 26[l]	7	0	7	6,20E-03	NA	3,97E-03	1,00E+00	5,18E-05
chondroitin sulfate C (GalNAc6S-GlcA), free chain[l]	7	0	7	6,20E-03	NA	3,97E-03	1,00E+00	5,18E-05
chondroitin sulfate D (GlcNAc6S-GlcA2S), degradation product 5[l]	7	0	7	6,20E-03	NA	3,97E-03	1,00E+00	5,18E-05
chondroitin sulfate E (GalNAc4,6diS-GlcA), degradation product 2[l]	7	0	7	6,20E-03	NA	3,97E-03	1,00E+00	5,18E-05
keratan sulfate I, degradation product 41[l]	7	0	7	6,20E-03	NA	3,97E-03	1,00E+00	5,18E-05
keratan sulfate I, degradation product 14[l]	7	0	7	6,20E-03	NA	3,97E-03	1,00E+00	5,18E-05
keratan sulfate I, degradation product 8[l]	7	0	7	6,20E-03	NA	3,97E-03	1,00E+00	5,18E-05
keratan sulfate I, degradation product 29[l]	7	0	7	6,20E-03	NA	3,97E-03	1,00E+00	5,18E-05
keratan sulfate II (core 2-linked), degradation product 9[l]	7	0	7	6,20E-03	NA	3,97E-03	1,00E+00	5,18E-05
keratan sulfate I, degradation product 35[l]	7	0	7	6,20E-03	NA	3,97E-03	1,00E+00	5,18E-05
keratan sulfate II (core 2-linked), degradation product 8[l]	7	0	7	6,20E-03	NA	3,97E-03	1,00E+00	5,18E-05
keratan sulfate I, degradation product 20[l]	7	0	7	6,20E-03	NA	3,97E-03	1,00E+00	5,18E-05
chondroitin sulfate C (GalNAc6S-GlcA), degradation product 1[l]	7	0	7	6,20E-03	NA	3,97E-03	1,00E+00	5,18E-05
keratan sulfate I, degradation product 32[l]	7	0	7	6,20E-03	NA	3,97E-03	1,00E+00	5,18E-05
chondroitin sulfate D (GlcNAc6S-GlcA2S), free chain[l]	7	0	7	6,20E-03	NA	3,97E-03	1,00E+00	5,18E-05
keratan sulfate II (core 2-linked), degradation product 5[l]	7	0	7	6,20E-03	NA	3,97E-03	1,00E+00	5,18E-05
chondroitin sulfate C (GalNAc6S-GlcA), degradation product 4[l]	7	0	7	6,20E-03	NA	3,97E-03	1,00E+00	5,18E-05
keratan sulfate I, degradation product 38[l]	7	0	7	6,20E-03	NA	3,97E-03	1,00E+00	5,18E-05
keratan sulfate I, degradation product 23[l]	7	0	7	6,20E-03	NA	3,97E-03	1,00E+00	5,18E-05
keratan sulfate I, degradation product 17[l]	7	0	7	6,20E-03	NA	3,97E-03	1,00E+00	5,18E-05
heparan sulfate, degradation product 2[l]	2	2	0	6,52E-03	NA	4,61E-03	9,99E-01	1,55E-06
heparan sulfate, degradation product 19[l]	2	2	0	6,52E-03	NA	4,61E-03	9,99E-01	1,55E-06

Metabolite	#Genes annotated	#Genes up	#Genes down	adjP non.dir	adjP dist.up	adjP dist.down	adjP mix.up	adjP mix.down
heparan sulfate, degradation product 13[l]	2	0	2	6,52E-03	NA	4,61E-03	9,99E-01	1,55E-06
heparan sulfate, degradation product 7[l]	2	0	2	6,52E-03	NA	4,61E-03	9,99E-01	1,55E-06
L-2-amino-3-oxobutanoic acid[m]	1	1	0	6,72E-03	7,73E-03	NA	7,91E-05	9,76E-01
tRNA(phe)[c]	4	3	1	6,77E-03	3,45E-02	4,68E-02	2,62E-01	7,53E-01
L-phenylalanyl-tRNA(phe)[c]	4	3	1	6,77E-03	3,45E-02	4,68E-02	2,62E-01	7,53E-01
6-deoxy-L-galactose[l]	2	0	2	7,09E-03	NA	5,04E-03	9,99E-01	3,12E-06
PA6[l]	2	0	2	7,09E-03	NA	5,04E-03	9,99E-01	3,12E-06
keratan sulfate I[l]	2	0	2	7,09E-03	NA	5,04E-03	9,99E-01	3,12E-06
choline[g]	4	0	4	7,26E-03	NA	5,95E-03	1,00E+00	4,69E-09
phosphatidate-LD-PC pool[g]	4	0	4	7,26E-03	NA	5,95E-03	1,00E+00	4,69E-09
choline[r]	4	0	4	7,26E-03	NA	5,95E-03	1,00E+00	4,69E-09
phosphatidate-LD-PC pool[r]	4	0	4	7,26E-03	NA	5,95E-03	1,00E+00	4,69E-09
2-acyl-1-(1-alkenyl)-sn-glycero-3-phosphate[c]	4	0	4	7,26E-03	NA	5,95E-03	1,00E+00	4,69E-09
chondroitin sulfate B (IdoA2S-GalNAc4s), precursor 5[g]	6	0	6	7,55E-03	NA	4,61E-03	1,00E+00	3,64E-05
3-methylglutaconyl-CoA[m]	3	3	0	7,60E-03	8,71E-03	NA	1,08E-03	9,95E-01
heparan sulfate, degradation product 4[l]	2	0	2	8,34E-03	NA	6,00E-03	9,99E-01	1,18E-06
beta-carboline[c]	72	63	9	8,37E-03	9,01E-03	6,28E-01	8,14E-07	1,00E+00
(R)-1,2-dimethyl-5,6-dihydroxy-tetrahydroisoquinoline[c]	72	63	9	8,37E-03	9,01E-03	6,28E-01	8,14E-07	1,00E+00
harman[c]	72	63	9	8,37E-03	9,01E-03	6,28E-01	8,14E-07	1,00E+00
tRNA(pro)[c]	3	2	1	8,88E-03	3,88E-02	4,68E-02	3,21E-01	6,99E-01
L-prolyl-tRNA(pro)[c]	3	2	1	8,88E-03	3,88E-02	4,68E-02	3,21E-01	6,99E-01
heparan sulfate, precursor 4[g]	4	0	4	8,99E-03	NA	7,43E-03	9,99E-01	2,39E-08
heparan sulfate, precursor 7[g]	4	0	4	8,99E-03	NA	7,43E-03	9,99E-01	2,39E-08
heparan sulfate, precursor 3[g]	4	0	4	8,99E-03	NA	7,43E-03	9,99E-01	2,39E-08
heparan sulfate, precursor 5[g]	4	0	4	8,99E-03	NA	7,43E-03	9,99E-01	2,39E-08
heparan sulfate, precursor 2[g]	4	0	4	8,99E-03	NA	7,43E-03	9,99E-01	2,39E-08
heparan sulfate, precursor 8[g]	4	0	4	8,99E-03	NA	7,43E-03	9,99E-01	2,39E-08
heparan sulfate, precursor 6[g]	4	0	4	8,99E-03	NA	7,43E-03	9,99E-01	2,39E-08
heparan sulfate, degradation product 20[l]	2	0	2	9,20E-03	NA	6,67E-03	9,99E-01	1,55E-06
heparan sulfate, degradation product 14[l]	2	0	2	9,20E-03	NA	6,67E-03	9,99E-01	1,55E-06
heparan sulfate, degradation product 3[l]	2	0	2	9,20E-03	NA	6,67E-03	9,99E-01	1,55E-06
heparan sulfate, degradation product 8[l]	2	0	2	9,20E-03	NA	6,67E-03	9,99E-01	1,55E-06
2-oxoglutaramate[m]	2	2	0	1,03E-02	1,11E-02	NA	7,04E-04	9,94E-01
heparan sulfate, degradation product 5[l]	2	0	2	1,03E-02	NA	7,57E-03	9,99E-01	1,18E-06
heparan sulfate, degradation product 22[l]	2	0	2	1,04E-02	NA	7,63E-03	9,99E-01	1,18E-06
chondroitin sulfate B - dermatan sulfate (IdoA2S-GalNAc4S), degradation product 3[l]	2	0	2	1,04E-02	NA	7,63E-03	9,99E-01	1,18E-06
heparan sulfate, degradation product 16[l]	2	0	2	1,04E-02	NA	7,63E-03	9,99E-01	1,18E-06
keratan sulfate I, degradation product 7[l]	4	0	4	1,11E-02	NA	9,22E-03	1,00E+00	1,43E-09
keratan sulfate I, degradation product 37[l]	4	0	4	1,11E-02	NA	9,22E-03	1,00E+00	1,43E-09
keratan sulfate I, degradation product 28[l]	4	0	4	1,11E-02	NA	9,22E-03	1,00E+00	1,43E-09
keratan sulfate I, degradation product 34[l]	4	0	4	1,11E-02	NA	9,22E-03	1,00E+00	1,43E-09
keratan sulfate I, degradation product 31[l]	4	0	4	1,11E-02	NA	9,22E-03	1,00E+00	1,43E-09
keratan sulfate I, degradation product 13[l]	4	0	4	1,11E-02	NA	9,22E-03	1,00E+00	1,43E-09
keratan sulfate II (core 2-linked), degradation product 7[l]	4	0	4	1,11E-02	NA	9,22E-03	1,00E+00	1,43E-09
keratan sulfate I, degradation product 22[l]	4	0	4	1,11E-02	NA	9,22E-03	1,00E+00	1,43E-09
keratan sulfate I, degradation product 16[l]	4	0	4	1,11E-02	NA	9,22E-03	1,00E+00	1,43E-09
keratan sulfate II (core 4-linked), degradation product 4[l]	4	0	4	1,11E-02	NA	9,22E-03	1,00E+00	1,43E-09
keratan sulfate II (core 2-linked), degradation product 4[l]	4	0	4	1,11E-02	NA	9,22E-03	1,00E+00	1,43E-09
keratan sulfate I, degradation product 19[l]	4	0	4	1,11E-02	NA	9,22E-03	1,00E+00	1,43E-09
keratan sulfate I, degradation product 25[l]	4	0	4	1,11E-02	NA	9,22E-03	1,00E+00	1,43E-09
keratan sulfate I, degradation product 10[l]	4	0	4	1,11E-02	NA	9,22E-03	1,00E+00	1,43E-09

Metabolite	#Genes annotated	#Genes up	#Genes down	adjP non.dir	adjP dist.up	adjP dist.down	adjP mix.up	adjP mix.down
chondroitin sulfate E (GalNAc4,6diS-GlcA), degradation product 1[l]	5	0	5	1,13E-02	NA	6,99E-03	9,96E-01	2,40E-02
alanine[l]	18	0	18	1,14E-02	NA	6,82E-03	1,00E+00	2,02E-06
tyrosine[l]	18	0	18	1,14E-02	NA	6,82E-03	1,00E+00	2,02E-06
lysine[l]	18	0	18	1,14E-02	NA	6,82E-03	1,00E+00	2,02E-06
valine[l]	18	0	18	1,14E-02	NA	6,82E-03	1,00E+00	2,02E-06
leucine[l]	18	0	18	1,14E-02	NA	6,82E-03	1,00E+00	2,02E-06
histidine[l]	18	0	18	1,14E-02	NA	6,82E-03	1,00E+00	2,02E-06
phenylalanine[l]	18	0	18	1,14E-02	NA	6,82E-03	1,00E+00	2,02E-06
methionine[l]	18	0	18	1,14E-02	NA	6,82E-03	1,00E+00	2,02E-06
arginine[l]	18	0	18	1,14E-02	NA	6,82E-03	1,00E+00	2,02E-06
tryptophan[l]	18	0	18	1,14E-02	NA	6,82E-03	1,00E+00	2,02E-06
isoleucine[l]	18	0	18	1,14E-02	NA	6,82E-03	1,00E+00	2,02E-06
glutamine[l]	18	0	18	1,14E-02	NA	6,82E-03	1,00E+00	2,02E-06
glycine[l]	18	0	18	1,14E-02	NA	6,82E-03	1,00E+00	2,02E-06
asparagine[l]	18	0	18	1,14E-02	NA	6,82E-03	1,00E+00	2,02E-06
threonine[l]	18	0	18	1,14E-02	NA	6,82E-03	1,00E+00	2,02E-06
cysteine[l]	18	0	18	1,14E-02	NA	6,82E-03	1,00E+00	2,02E-06
aspartate[l]	18	0	18	1,14E-02	NA	6,82E-03	1,00E+00	2,02E-06
proline[l]	18	0	18	1,14E-02	NA	6,82E-03	1,00E+00	2,02E-06
serine[l]	18	0	18	1,14E-02	NA	6,82E-03	1,00E+00	2,02E-06
tRNA-queuine[c]	2	2	0	1,15E-02	1,24E-02	NA	8,45E-04	9,64E-01
queuine[c]	2	2	0	1,15E-02	1,24E-02	NA	8,45E-04	9,64E-01
GM2A-GM2[l]	4	0	4	1,29E-02	NA	1,08E-02	1,00E+00	5,42E-06
nm4nasn[g]	3	0	3	1,29E-02	NA	8,21E-03	9,92E-01	1,83E-04
AIR[c]	2	2	0	1,37E-02	1,47E-02	NA	9,91E-01	1,44E-03
chondroitin sulfate C (GalNAc6S-GlcA) and D (GlcNAc6S-GlcA2S), precursor 1[g]	8	0	8	1,43E-02	NA	9,81E-03	1,00E+00	1,51E-06
N-acetylglucosamine[l]	7	1	6	1,45E-02	2,40E-01	1,23E-02	9,99E-01	1,15E-06
salsolinol[c]	74	64	10	1,51E-02	1,05E-02	7,08E-01	9,79E-07	1,00E+00
de-Fuc form of PA6[l]	3	0	3	1,52E-02	NA	9,82E-03	9,93E-01	1,61E-04
keratan sulfate I, degradation product 1[l]	3	0	3	1,52E-02	NA	9,82E-03	9,93E-01	1,61E-04
isoleucine[m]	1	1	0	1,59E-02	1,79E-02	NA	8,02E-04	9,76E-01
valine[m]	1	1	0	1,59E-02	1,79E-02	NA	8,02E-04	9,76E-01
leucine[m]	1	1	0	1,59E-02	1,79E-02	NA	8,02E-04	9,76E-01
LTD4[r]	4	1	3	1,63E-02	2,52E-03	1,89E-01	1,72E-01	5,15E-01
gamma-L-glutamyl-L-alanine[e]	4	1	3	1,63E-02	2,52E-03	1,89E-01	1,72E-01	5,15E-01
glutamate[r]	4	1	3	1,63E-02	2,52E-03	1,89E-01	1,72E-01	5,15E-01
leukotriene D5[c]	4	1	3	1,63E-02	2,52E-03	1,89E-01	1,72E-01	5,15E-01
chondroitin sulfate B - dermatan sulfate (IdoA2S-GalNAc4S) proteoglycan[g]	2	0	2	1,64E-02	NA	1,24E-02	1,00E+00	2,84E-06
chondroitin sulfate E (GalNAc4,6diS-GlcA), precursor 4[g]	12	0	12	1,64E-02	NA	1,10E-02	1,00E+00	6,52E-03
2-methylbutyryl-CoA[m]	5	4	1	1,65E-02	3,58E-03	7,73E-01	1,27E-03	9,87E-01
procollagen-5-hydroxy-L-lysine[c]	6	1	5	1,66E-02	7,83E-01	2,31E-03	9,99E-01	1,10E-02
UDP[g]	96	22	74	1,69E-02	5,24E-01	2,48E-03	1,00E+00	2,20E-07
LacCer pool[c]	56	18	38	1,73E-02	1,07E-01	3,38E-02	9,55E-01	1,08E-03
3-sulfopyruvate[m]	2	2	0	1,74E-02	1,86E-02	NA	2,57E-03	9,88E-01
heparan sulfate, degradation product 18[l]	1	0	1	1,76E-02	NA	1,40E-02	9,93E-01	2,17E-07
chondroitin sulfate E (GalNAc4,6diS-GlcA), precursor 2[g]	5	0	5	1,78E-02	NA	1,15E-02	9,95E-01	2,18E-04
guanine[c]	8	5	3	1,78E-02	7,88E-03	4,05E-01	3,05E-03	9,71E-01
globotriaosylceramide[l]	4	0	4	1,78E-02	NA	1,51E-02	1,00E+00	1,34E-05
D-galactosyl-N-acylsphingosine[l]	8	2	6	1,79E-02	7,50E-03	1,32E-01	4,66E-01	5,87E-01
heptaglutamyl-folate(DHF)[l]	1	0	1	1,80E-02	NA	1,44E-02	9,93E-01	2,17E-07
hexaglutamyl-folate(THF)[l]	1	0	1	1,80E-02	NA	1,44E-02	9,93E-01	2,17E-07

Metabolite	#Genes annotated	#Genes up	#Genes down	adjP non.dir	adjP dist.up	adjP dist.down	adjP mix.up	adjP mix.down
THF[l]	1	0	1	1,80E-02	NA	1,44E-02	9,93E-01	2,17E-07
hexaglutamyl-folate(DHF)[l]	1	0	1	1,80E-02	NA	1,44E-02	9,93E-01	2,17E-07
10-formyl-THF[l]	1	0	1	1,80E-02	NA	1,44E-02	9,93E-01	2,17E-07
pentaglutamyl-folate(THF)[l]	1	0	1	1,80E-02	NA	1,44E-02	9,93E-01	2,17E-07
heptaglutamyl-folate(THF)[l]	1	0	1	1,80E-02	NA	1,44E-02	9,93E-01	2,17E-07
pentaglutamyl-folate(DHF)[l]	1	0	1	1,80E-02	NA	1,44E-02	9,93E-01	2,17E-07
dihydrofolate[l]	1	0	1	1,80E-02	NA	1,44E-02	9,93E-01	2,17E-07
10-formyl-THF-glu(7)[l]	1	0	1	1,80E-02	NA	1,44E-02	9,93E-01	2,17E-07
10-formyl-THF-glu(5)[l]	1	0	1	1,80E-02	NA	1,44E-02	9,93E-01	2,17E-07
10-formyl-THF-glu(6)[l]	1	0	1	1,80E-02	NA	1,44E-02	9,93E-01	2,17E-07
N-acetylneuraminate[l]	8	2	6	1,81E-02	7,50E-03	1,34E-01	4,70E-01	5,84E-01
L-isoleucyl-tRNA(ile)[c]	2	2	0	1,88E-02	2,01E-02	NA	3,11E-03	9,89E-01
tRNA(ile)[c]	2	2	0	1,88E-02	2,01E-02	NA	3,11E-03	9,89E-01
prostaglandin D2[c]	6	0	6	1,92E-02	NA	1,29E-02	9,96E-01	5,71E-04
deoxyadenosine[l]	1	0	1	1,93E-02	NA	1,55E-02	9,93E-01	2,17E-07
dAMP[l]	1	0	1	1,93E-02	NA	1,55E-02	9,93E-01	2,17E-07
dCMP[l]	1	0	1	1,93E-02	NA	1,55E-02	9,93E-01	2,17E-07
deoxyguanosine[l]	1	0	1	1,93E-02	NA	1,55E-02	9,93E-01	2,17E-07
deoxycytidine[l]	1	0	1	1,93E-02	NA	1,55E-02	9,93E-01	2,17E-07
dGMP[l]	1	0	1	1,93E-02	NA	1,55E-02	9,93E-01	2,17E-07
dephospho-CoA[l]	1	0	1	1,93E-02	NA	1,55E-02	9,93E-01	2,17E-07
CoA[l]	1	0	1	1,93E-02	NA	1,55E-02	9,93E-01	2,17E-07
prostaglandin F2beta[c]	1	0	1	1,98E-02	NA	1,60E-02	9,93E-01	2,17E-07
prostaglandin B2[c]	1	0	1	1,98E-02	NA	1,60E-02	9,93E-01	2,17E-07
prostaglandin B1[c]	1	0	1	1,98E-02	NA	1,60E-02	9,93E-01	2,17E-07
prostaglandin C1[c]	1	0	1	1,98E-02	NA	1,60E-02	9,93E-01	2,17E-07
leukotriene F4[c]	1	0	1	1,98E-02	NA	1,60E-02	9,93E-01	2,17E-07
prostaglandin C2[c]	1	0	1	1,98E-02	NA	1,60E-02	9,93E-01	2,17E-07
prostaglandin D1[c]	1	0	1	1,98E-02	NA	1,60E-02	9,93E-01	2,17E-07
prostaglandin D3[c]	1	0	1	1,98E-02	NA	1,60E-02	9,93E-01	2,17E-07
prostaglandin F1alpha[c]	1	0	1	1,98E-02	NA	1,60E-02	9,93E-01	2,17E-07
prostaglandin G2[c]	1	0	1	1,98E-02	NA	1,60E-02	9,93E-01	2,17E-07
prostaglandin I2[c]	1	0	1	1,98E-02	NA	1,60E-02	9,93E-01	2,17E-07
(alpha-D-mannosyl)2-beta-D-mannosyl-N-acetylglucosamine[l]	6	0	6	1,99E-02	NA	1,35E-02	1,00E+00	7,03E-08
dynorphin A-(1-8)[c]	1	1	0	2,04E-02	2,28E-02	NA	1,52E-03	9,76E-01
dynorphin A-(6-8)[c]	1	1	0	2,04E-02	2,28E-02	NA	1,52E-03	9,76E-01
dynorphin A-(1-5)[c]	1	1	0	2,04E-02	2,28E-02	NA	1,52E-03	9,76E-01
L-cystathionine[c]	2	2	0	2,10E-02	2,25E-02	NA	4,07E-03	9,89E-01
selenocystathionine[c]	2	2	0	2,10E-02	2,25E-02	NA	4,07E-03	9,89E-01
thiamin-PPP[c]	3	3	0	2,11E-02	2,37E-02	NA	9,46E-03	9,67E-01
biotin[n]	1	0	1	2,12E-02	NA	1,72E-02	9,93E-01	2,17E-07
biocytin[n]	1	0	1	2,12E-02	NA	1,72E-02	9,93E-01	2,17E-07
biocytin[c]	1	0	1	2,12E-02	NA	1,72E-02	9,93E-01	2,17E-07
lysine[n]	1	0	1	2,12E-02	NA	1,72E-02	9,93E-01	2,17E-07
reduced vitamin K[c]	2	0	2	2,12E-02	NA	1,64E-02	9,94E-01	1,56E-05
vitamin K[c]	2	0	2	2,12E-02	NA	1,64E-02	9,94E-01	1,56E-05
Pi[l]	21	1	20	2,25E-02	2,38E-01	1,81E-02	1,00E+00	6,05E-07
dihydrolipoamide[m]	7	7	0	2,27E-02	2,91E-02	NA	9,36E-04	9,92E-01
peptidylglycine[c]	1	0	1	2,34E-02	NA	1,91E-02	9,93E-01	2,17E-07
peptidylamidoglycolate[c]	1	0	1	2,34E-02	NA	1,91E-02	9,93E-01	2,17E-07
3,5,3-triiodothyronine-4-sulfate[c]	1	0	1	2,35E-02	NA	1,91E-02	9,93E-01	2,17E-07

Metabolite	#Genes annotated	#Genes up	#Genes down	adjP non.dir	adjP dist.up	adjP dist.down	adjP mix.up	adjP mix.down
4-nitrophenyl-sulfate[c]	1	0	1	2,35E-02	NA	1,91E-02	9,93E-01	2,17E-07
dopamine-3-O-sulfate[c]	1	0	1	2,35E-02	NA	1,91E-02	9,93E-01	2,17E-07
tyramine-O-sulfate[c]	1	0	1	2,35E-02	NA	1,91E-02	9,93E-01	2,17E-07
chondroitin sulfate B - dermatan sulfate (IdoA2S-GalNAc4S), degradation product 1[l]	4	0	4	2,41E-02	NA	2,07E-02	9,99E-01	3,06E-05
chondroitin sulfate A (GalNAc4S-GlcA), degradation product 1[l]	4	0	4	2,41E-02	NA	2,07E-02	9,99E-01	3,06E-05
cytosine[c]	1	1	0	2,42E-02	2,70E-02	NA	2,37E-03	9,76E-01
xanthurenate[c]	2	2	0	2,52E-02	2,68E-02	NA	5,99E-03	9,74E-01
4-(2-amino-3-hydroxyphenyl)-2,4-dioxobutanoate[c]	2	2	0	2,52E-02	2,68E-02	NA	5,99E-03	9,74E-01
4-(2-aminophenyl)-2,4-dioxobutanoate[c]	2	2	0	2,52E-02	2,68E-02	NA	5,99E-03	9,74E-01
4-hydroxy-2-quinolinecarboxylic acid[c]	2	2	0	2,52E-02	2,68E-02	NA	5,99E-03	9,74E-01
5-phosphoribosylamine[c]	2	2	0	2,53E-02	2,70E-02	NA	6,28E-03	9,84E-01
mercaptopyruvate[c]	7	5	2	2,63E-02	1,54E-02	4,72E-01	9,83E-01	9,76E-01
tRNA-guanine[c]	6	6	0	2,67E-02	3,56E-02	NA	5,59E-04	9,79E-01
plasminogen[l]	17	0	17	2,68E-02	NA	1,72E-02	1,00E+00	8,91E-06
fibrinogen[l]	17	0	17	2,68E-02	NA	1,72E-02	1,00E+00	8,91E-06
apoB48[l]	17	0	17	2,68E-02	NA	1,72E-02	1,00E+00	8,91E-06
albumin[l]	17	0	17	2,68E-02	NA	1,72E-02	1,00E+00	8,91E-06
haptoglobin[l]	17	0	17	2,68E-02	NA	1,72E-02	1,00E+00	8,91E-06
STAR[l]	17	0	17	2,68E-02	NA	1,72E-02	1,00E+00	8,91E-06
apocytochrome-C[l]	17	0	17	2,68E-02	NA	1,72E-02	1,00E+00	8,91E-06
ADP[l]	17	0	17	2,68E-02	NA	1,72E-02	1,00E+00	8,91E-06
prothrombin[l]	17	0	17	2,68E-02	NA	1,72E-02	1,00E+00	8,91E-06
apoE[l]	17	0	17	2,68E-02	NA	1,72E-02	1,00E+00	8,91E-06
ATP[l]	17	0	17	2,68E-02	NA	1,72E-02	1,00E+00	8,91E-06
antitrypsin[l]	17	0	17	2,68E-02	NA	1,72E-02	1,00E+00	8,91E-06
apoB100[l]	17	0	17	2,68E-02	NA	1,72E-02	1,00E+00	8,91E-06
antichymotrypsin[l]	17	0	17	2,68E-02	NA	1,72E-02	1,00E+00	8,91E-06
PPARA[l]	17	0	17	2,68E-02	NA	1,72E-02	1,00E+00	8,91E-06
apoA1[l]	17	0	17	2,68E-02	NA	1,72E-02	1,00E+00	8,91E-06
heparan sulfate, degradation product 25[l]	1	0	1	2,69E-02	NA	2,21E-02	9,93E-01	2,17E-07
heparan sulfate, degradation product 24[l]	1	0	1	2,69E-02	NA	2,21E-02	9,93E-01	2,17E-07
THF-hexaglutamate[c]	2	1	1	2,71E-02	2,60E-01	1,44E-02	9,24E-01	5,66E-04
phylloquinol[c]	1	0	1	2,76E-02	NA	2,27E-02	9,93E-01	2,17E-07
phylloquinone[c]	1	0	1	2,76E-02	NA	2,27E-02	9,93E-01	2,17E-07
heparan sulfate, precursor 9[g]	8	0	8	2,81E-02	NA	2,03E-02	9,99E-01	2,02E-06
dTTP[c]	32	28	4	2,85E-02	1,61E-02	7,52E-01	5,87E-05	1,00E+00
thiocyanate[m]	2	2	0	3,03E-02	3,23E-02	NA	9,51E-03	9,79E-01
hydrogen-cyanide[e]	2	2	0	3,03E-02	3,23E-02	NA	9,51E-03	9,79E-01
hydrogen-cyanide[m]	2	2	0	3,03E-02	3,23E-02	NA	9,51E-03	9,79E-01
L-glutaminyl-peptide[c]	1	1	1	3,08E-02	NA	2,55E-02	9,93E-01	2,17E-07
5-oxoprolyl-peptide[c]	1	0	1	3,08E-02	NA	2,55E-02	9,93E-01	2,17E-07
5-phosphoribosyl-4-carboxy-5-aminoimidazole[c]	1	1	0	3,13E-02	3,47E-02	NA	4,49E-03	9,76E-01
pseudouridine-5-phosphate[c]	1	1	0	3,15E-02	3,48E-02	NA	4,55E-03	9,76E-01
L-cysteate[m]	1	1	0	3,26E-02	3,60E-02	NA	4,94E-03	9,76E-01
mercaptopyruvate[m]	1	1	0	3,26E-02	3,60E-02	NA	4,94E-03	9,76E-01
3-sulfinylpyruvic acid[m]	1	1	0	3,26E-02	3,60E-02	NA	4,94E-03	9,76E-01
(alpha-D-mannosyl)4-beta-D-mannosyl-diacetylchitobiosyl-L-asparagine (protein)[g]	5	0	5	3,28E-02	NA	2,25E-02	9,99E-01	1,12E-07
N-acetylmethionine[c]	1	1	0	3,41E-02	3,77E-02	NA	5,54E-03	9,76E-01
N-acetylornithine[c]	1	1	0	3,41E-02	3,77E-02	NA	5,54E-03	9,76E-01
N-acetyl-L-alaninel[c]	1	1	0	3,41E-02	3,77E-02	NA	5,54E-03	9,76E-01
heparan sulfate, degradation product 11[l]	1	0	1	3,49E-02	NA	2,91E-02	9,93E-01	2,17E-07

Metabolite	#Genes annotated	#Genes up	#Genes down	adjP non.dir	adjP dist.up	adjP dist.down	adjP mix.up	adjP mix.down
GA1[c]	8	1	7	3,92E-02	7,83E-01	1,05E-02	9,99E-01	2,91E-04
tRNA containing 6-isopentenyladenosine[c]	1	1	0	3,93E-02	4,33E-02	NA	7,83E-03	9,76E-01
GM4[l]	4	2	2	3,95E-02	7,50E-03	5,08E-01	1,88E-02	9,61E-01
dGTP[c]	38	33	5	4,00E-02	1,91E-02	8,18E-01	5,77E-05	1,00E+00
3-UMP[c]	1	0	1	4,04E-02	NA	3,40E-02	9,93E-01	2,17E-07
2,3-cyclic-UMP[c]	1	0	1	4,04E-02	NA	3,40E-02	9,93E-01	2,17E-07
GM3[c]	9	3	6	4,05E-02	4,78E-01	1,29E-02	9,72E-01	3,98E-04
UDP-N-acetylglucosamine[g]	31	7	24	4,09E-02	8,29E-01	4,14E-03	1,00E+00	1,72E-05
trans-2-methyl-5-isopropylhexa-2,5-dienoyl-CoA[m]	1	1	0	4,17E-02	4,58E-02	NA	9,04E-03	9,76E-01
3-hydroxy-2,6-dimethyl-5-methylene-heptanoyl-CoA[m]	1	1	0	4,17E-02	4,58E-02	NA	9,04E-03	9,76E-01
cis-2-methyl-5-isopropylhexa-2,5-dienoyl-CoA[m]	1	1	0	4,17E-02	4,58E-02	NA	9,04E-03	9,76E-01
chondroitin sulfate D (GlcNAc6S-GlcA2S) proteoglycan[g]	1	0	1	4,23E-02	NA	3,56E-02	9,93E-01	2,17E-07
2-hydroxy-3-phenylpropenoate[c]	1	1	0	4,30E-02	4,72E-02	NA	9,72E-03	9,76E-01
2-hydroxy-3-(4-hydroxyphenyl)propenoate[c]	1	1	0	4,30E-02	4,72E-02	NA	9,72E-03	9,76E-01
N-acetylmannosamine-6-phosphate[c]	2	2	0	4,42E-02	4,68E-02	NA	1,28E-04	9,21E-01
sphinganine-1-phosphate[c]	10	3	7	4,53E-02	7,38E-01	5,98E-03	9,98E-01	1,12E-03
sphingosine-1-phosphate[c]	10	3	7	4,53E-02	7,38E-01	5,98E-03	9,98E-01	1,12E-03
CTP[c]	63	48	15	4,54E-02	3,76E-02	4,82E-01	7,71E-04	9,97E-01
isobutyryl-CoA[m]	6	5	1	4,84E-02	2,13E-02	7,73E-01	3,13E-03	9,80E-01
phosphatidate-LD-PE pool[c]	23	6	17	5,04E-02	6,21E-01	1,27E-02	9,99E-01	1,38E-06
phosphatidate-LD-PS pool[c]	23	6	17	5,04E-02	6,21E-01	1,27E-02	9,99E-01	1,38E-06
L-hydroxylysine[c]	4	1	3	5,10E-02	7,83E-01	7,35E-03	9,96E-01	2,16E-02
L-xylulose[c]	3	3	0	5,69E-02	6,23E-02	NA	2,79E-03	9,72E-01
cGMP[c]	40	9	31	6,01E-02	8,22E-01	6,68E-03	1,00E+00	9,83E-05
cAMP[c]	40	9	31	6,01E-02	8,22E-01	6,68E-03	1,00E+00	9,83E-05
chondroitin sulfate C (GalNAc6S-GlcA), degradation product 5[l]	3	0	3	6,20E-02	NA	4,63E-02	9,98E-01	4,84E-05
chitobiose[l]	3	0	3	6,20E-02	NA	4,63E-02	9,98E-01	4,84E-05
chondroitin sulfate D (GlcNAc6S-GlcA2S), degradation product 6[l]	3	0	3	6,20E-02	NA	4,63E-02	9,98E-01	4,84E-05
chondroitin sulfate D (GlcNAc6S-GlcA2S), degradation product 2[l]	3	0	3	6,20E-02	NA	4,63E-02	9,98E-01	4,84E-05
chondroitin sulfate E (GalNAc4,6diS-GlcA), degradation product 7[l]	3	0	3	6,20E-02	NA	4,63E-02	9,98E-01	4,84E-05
3-sulfinoalanine[m]	3	3	0	6,29E-02	6,87E-02	NA	3,76E-03	9,86E-01
prostaglandin F2alpha[c]	8	2	6	6,38E-02	8,64E-01	4,93E-03	9,98E-01	5,32E-04
globoside[l]	5	1	4	6,64E-02	7,83E-01	1,51E-02	9,99E-01	1,21E-04
RNA[c]	43	36	7	6,69E-02	1,05E-01	3,07E-01	1,20E-03	9,93E-01
isocitrate[m]	8	7	1	6,74E-02	3,76E-02	7,73E-01	1,92E-03	9,91E-01
sphinganine[c]	21	7	14	6,87E-02	8,09E-01	4,45E-03	9,96E-01	7,91E-04
phosphatidate-LD-PC pool[c]	24	7	17	7,14E-02	7,23E-01	1,27E-02	9,99E-01	1,63E-06
4-hydroxyphenylpyruvate[c]	5	4	1	7,54E-02	2,76E-02	7,73E-01	3,38E-03	9,89E-01
isovaleryl-CoA[m]	5	4	1	7,65E-02	2,82E-02	7,73E-01	3,49E-03	9,76E-01
sphingosine[g]	4	2	2	7,90E-02	8,64E-01	8,19E-04	9,85E-01	7,85E-04
acyl-CoA-LD-SM pool[g]	4	2	2	7,90E-02	8,64E-01	8,19E-04	9,85E-01	7,85E-04
SAH[c]	131	104	27	8,10E-02	4,39E-02	7,89E-01	5,67E-07	1,00E+00
CO2[m]	35	24	11	8,39E-02	3,63E-02	6,23E-01	6,56E-03	9,91E-01
PC-LD pool[g]	6	0	6	8,67E-02	NA	6,82E-02	9,98E-01	1,94E-06
pyruvate[c]	31	19	12	8,81E-02	1,17E-02	8,06E-01	1,08E-03	9,80E-01
dCTP[c]	36	31	5	9,11E-02	4,79E-02	8,18E-01	3,89E-04	9,99E-01
CDP[c]	17	14	3	9,29E-02	6,04E-02	6,74E-01	6,47E-03	9,88E-01
dATP[c]	42	34	8	9,51E-02	2,12E-02	9,38E-01	8,74E-05	1,00E+00
chondroitin sulfate E (GalNAc4,6diS-GlcA), degradation product 6[l]	9	3	6	1,11E-01	9,13E-01	4,35E-03	9,99E-01	6,95E-04
DNA[c]	34	26	8	1,12E-01	3,59E-02	8,53E-01	6,31E-04	9,99E-01
DHAP[c]	9	8	1	1,13E-01	7,43E-02	7,73E-01	4,76E-03	9,90E-01

Metabolite	#Genes annotated	#Genes up	#Genes down	adjP non.dir	adjP dist.up	adjP dist.down	adjP mix.up	adjP mix.down
ceramide pool[l]	8	2	6	1,17E-01	8,64E-01	1,47E-02	9,93E-01	1,91E-03
H2O[g]	41	9	32	1,27E-01	9,17E-01	1,21E-02	1,00E+00	5,82E-06
CMP-N-acetylneuraminate[c]	15	4	11	1,36E-01	9,43E-01	8,66E-03	9,99E-01	1,45E-03
SAM[c]	132	104	28	1,46E-01	5,90E-02	8,84E-01	6,33E-07	1,00E+00
phenylpyruvate[c]	4	3	1	1,52E-01	6,28E-02	7,73E-01	9,13E-03	9,76E-01
formate[m]	4	4	0	1,53E-01	1,76E-01	NA	9,32E-03	9,72E-01
lc3Cer[g]	3	2	1	1,55E-01	3,90E-02	7,73E-01	1,25E-03	8,73E-01
1D-myo-inositol-3-phosphate[c]	6	3	3	1,65E-01	4,71E-03	9,02E-01	9,07E-03	9,80E-01
phytosphingosine[c]	5	3	2	1,86E-01	9,13E-01	8,19E-04	9,74E-01	2,89E-03
CoA[g]	5	2	3	1,86E-01	8,64E-01	1,47E-02	9,74E-01	2,89E-03
chondroitin sulfate B - dermatan sulfate (ddoA2S-GalNAc4S), degradation product 2[l]	7	3	4	2,00E-01	9,13E-01	9,27E-03	9,98E-01	4,02E-06
ubiquinol[m]	72	67	5	2,27E-01	1,69E-01	9,52E-01	1,61E-04	1,00E+00
inositol-1-phosphate[c]	21	10	11	2,33E-01	8,69E-01	1,58E-02	9,71E-01	5,59E-03
ubiquinone[m]	71	66	5	2,53E-01	1,83E-01	9,52E-01	1,74E-04	1,00E+00
ribose-5-phosphate[c]	14	11	3	2,82E-01	1,12E-01	9,02E-01	4,83E-03	9,86E-01
succinate[m]	18	13	5	2,85E-01	5,80E-02	9,52E-01	4,87E-03	9,88E-01
IDP[c]	15	11	4	2,89E-01	7,11E-02	9,36E-01	9,93E-03	9,87E-01
phytoceramide pool[c]	6	4	2	3,01E-01	9,43E-01	8,19E-04	9,65E-01	5,62E-03
GM3[g]	3	2	1	3,18E-01	8,64E-01	6,38E-03	9,31E-01	2,55E-03
NAD+[m]	146	108	38	3,45E-01	1,82E-01	8,74E-01	2,76E-04	1,00E+00
H+[g]	7	4	3	3,61E-01	6,29E-02	9,02E-01	5,26E-03	9,11E-01
FADH2[m]	30	24	6	3,69E-01	1,25E-01	9,70E-01	8,21E-03	9,92E-01
FAD[m]	30	24	6	3,69E-01	1,25E-01	9,70E-01	8,21E-03	9,92E-01
ADP[m]	72	55	17	3,73E-01	1,33E-01	9,55E-01	4,26E-04	9,99E-01
AKG[m]	28	17	11	3,80E-01	6,04E-02	9,37E-01	3,53E-03	9,90E-01
serine[c]	44	23	21	3,96E-01	9,72E-01	7,00E-03	9,96E-01	2,20E-04
SAM[n]	33	28	5	4,86E-01	3,71E-01	8,53E-01	3,15E-03	9,95E-01
SAH[n]	33	28	5	4,86E-01	3,71E-01	8,53E-01	3,15E-03	9,95E-01
Pi[m]	46	37	9	4,98E-01	1,76E-01	9,88E-01	1,20E-03	9,98E-01
1D-myo-inositol-1,4-bisphosphate[c]	19	10	9	5,42E-01	9,94E-01	5,60E-03	9,94E-01	8,51E-03
NADH[m]	141	105	36	5,50E-01	3,45E-01	9,14E-01	1,09E-03	1,00E+00
histone-N6-methyl-L-lysine[n]	27	26	1	5,77E-01	5,77E-01	7,73E-01	7,24E-03	9,89E-01
histone-L-lysine[n]	27	26	1	5,77E-01	5,77E-01	7,73E-01	7,24E-03	9,89E-01
PPi[c]	391	262	129	6,16E-01	3,01E-01	9,49E-01	2,33E-05	1,00E+00
H+[m]	294	203	91	8,25E-01	6,58E-01	9,25E-01	2,97E-03	9,99E-01
ATP[m]	115	81	34	8,41E-01	4,28E-01	9,93E-01	1,02E-03	9,99E-01
CoA[m]	93	62	31	8,55E-01	4,56E-01	9,87E-01	2,02E-03	9,92E-01
AMP[c]	335	211	124	9,94E-01	8,28E-01	9,99E-01	1,61E-03	1,00E+00
PNP[s]	9	4	5	1,25E-03	1,57E-03	7,20E-02	2,26E-01	3,17E-01
4-nitrophenyl-phosphate[s]	9	4	5	1,25E-03	1,57E-03	7,20E-02	2,26E-01	3,17E-01
THF[s]	2	1	1	2,52E-03	2,93E-02	1,44E-02	4,11E-01	1,53E-02
sphingosine[s]	1	0	1	2,95E-03	NA	2,12E-03	9,93E-01	2,17E-07
sphingosine-1-phosphate[s]	1	0	1	2,95E-03	NA	2,12E-03	9,93E-01	2,17E-07
Pi[s]	41	19	22	4,88E-03	6,84E-03	1,13E-01	2,50E-01	2,32E-01
keratan sulfate I, degradation product 1[s]	2	0	2	7,09E-03	NA	5,04E-03	9,99E-01	3,12E-06
6-deoxy-L-galactose[s]	2	0	2	7,09E-03	NA	5,04E-03	9,99E-01	3,12E-06
PA6[s]	2	0	2	7,09E-03	NA	5,04E-03	9,99E-01	3,12E-06
de-Fuc form of PA6[s]	2	0	2	7,09E-03	NA	5,04E-03	9,99E-01	3,12E-06
keratan sulfate II[s]	2	0	2	7,09E-03	NA	5,04E-03	9,99E-01	3,12E-06
adenine[s]	2	0	2	1,04E-02	1,12E-02	NA	7,23E-04	9,92E-01
5-L-gamma-glutamyl[s]	4	1	3	1,63E-02	2,52E-03	1,89E-01	1,72E-01	5,15E-01

Metabolite	#Genes annotated	#Genes up	#Genes down	adjP non.dir	adjP dist.up	adjP dist.down	adjP mix.up	adjP mix.down
gamma-glutamyl-3-aminopropiononitrile[s]	4	1	3	1,63E-02	2,52E-03	1,89E-01	1,72E-01	5,15E-01
L-3-cyanoalanine[s]	4	1	3	1,63E-02	2,52E-03	1,89E-01	1,72E-01	5,15E-01
gamma-glutamyl-beta-cyanoalanine[s]	4	1	3	1,63E-02	2,52E-03	1,89E-01	1,72E-01	5,15E-01
leukotriene C4[s]	4	1	3	1,63E-02	2,52E-03	1,89E-01	1,72E-01	5,15E-01
10-formyl-THF[s]	1	0	1	1,80E-02	NA	1,44E-02	9,93E-01	2,17E-07
heptaglutamyl-folate(DHF)[s]	1	0	1	1,80E-02	NA	1,44E-02	9,93E-01	2,17E-07
heptaglutamyl-folate(THF)[s]	1	0	1	1,80E-02	NA	1,44E-02	9,93E-01	2,17E-07
hexaglutamyl-folate(THF)[s]	1	0	1	1,80E-02	NA	1,44E-02	9,93E-01	2,17E-07
10-formyl-THF-glu(6)[s]	1	0	1	1,80E-02	NA	1,44E-02	9,93E-01	2,17E-07
dihydrofolate[s]	1	0	1	1,80E-02	NA	1,44E-02	9,93E-01	2,17E-07
10-formyl-THF-glu(5)[s]	1	0	1	1,80E-02	NA	1,44E-02	9,93E-01	2,17E-07
hexaglutamyl-folate(DHF)[s]	1	0	1	1,80E-02	NA	1,44E-02	9,93E-01	2,17E-07
pentaglutamyl-folate(DHF)[s]	1	0	1	1,80E-02	NA	1,44E-02	9,93E-01	2,17E-07
pentaglutamyl-folate(THF)[s]	1	0	1	1,80E-02	NA	1,44E-02	9,93E-01	2,17E-07
10-formyl-THF-glu(7)[s]	1	0	1	1,80E-02	NA	1,44E-02	9,93E-01	2,17E-07
prostaglandin F2alpha[s]	1	0	1	1,98E-02	NA	1,60E-02	9,93E-01	2,17E-07
prostaglandin C1[s]	1	0	1	1,98E-02	NA	1,60E-02	9,93E-01	2,17E-07
prostaglandin C2[s]	1	0	1	1,98E-02	NA	1,60E-02	9,93E-01	2,17E-07
prostaglandin B1[s]	1	0	1	1,98E-02	NA	1,60E-02	9,93E-01	2,17E-07
prostaglandin D1[s]	1	0	1	1,98E-02	NA	1,60E-02	9,93E-01	2,17E-07
prostaglandin A2[s]	1	0	1	1,98E-02	NA	1,60E-02	9,93E-01	2,17E-07
prostaglandin E3[s]	1	0	1	1,98E-02	NA	1,60E-02	9,93E-01	2,17E-07
prostaglandin B2[s]	1	0	1	1,98E-02	NA	1,60E-02	9,93E-01	2,17E-07
prostaglandin D2[s]	1	0	1	1,98E-02	NA	1,60E-02	9,93E-01	2,17E-07
prostaglandin F2beta[s]	1	0	1	1,98E-02	NA	1,60E-02	9,93E-01	2,17E-07
prostaglandin F1alpha[s]	1	0	1	1,98E-02	NA	1,60E-02	9,93E-01	2,17E-07
prostaglandin H2[s]	1	0	1	1,98E-02	NA	1,60E-02	9,93E-01	2,17E-07
leukotriene B4[s]	1	0	1	1,98E-02	NA	1,60E-02	9,93E-01	2,17E-07
leukotriene F4[s]	1	0	1	1,98E-02	NA	1,60E-02	9,93E-01	2,17E-07
prostaglandin I2[s]	1	0	1	1,98E-02	NA	1,60E-02	9,93E-01	2,17E-07
prostaglandin D3[s]	1	0	1	1,98E-02	NA	1,60E-02	9,93E-01	2,17E-07
20-hydroxy-arachidonate[s]	1	0	1	1,98E-02	NA	1,60E-02	9,93E-01	2,17E-07
prostaglandin A1[s]	1	0	1	1,98E-02	NA	1,60E-02	9,93E-01	2,17E-07
prostaglandin G2[s]	1	0	1	1,98E-02	NA	1,60E-02	9,93E-01	2,17E-07
leukotriene A4[s]	1	0	1	1,98E-02	NA	1,60E-02	9,93E-01	2,17E-07
biocytin[s]	1	0	1	2,12E-02	NA	1,72E-02	9,93E-01	2,17E-07
prostaglandin E1[s]	3	0	3	2,18E-02	NA	1,46E-02	9,86E-01	3,65E-04
guanine[s]	1	1	0	2,42E-02	2,70E-02	NA	2,37E-03	9,76E-01
thymine[s]	1	1	0	2,42E-02	2,70E-02	NA	2,37E-03	9,76E-01
uracil[s]	1	1	0	2,42E-02	2,70E-02	NA	2,37E-03	9,76E-01
cytosine[s]	1	1	0	2,42E-02	2,70E-02	NA	2,37E-03	9,76E-01
hypoxanthine[s]	1	1	0	2,42E-02	2,70E-02	NA	2,37E-03	9,76E-01
chondroitin sulfate A (GalNAc4S-GlcA) proteoglycan[s]	1	1	0	2,42E-02	2,70E-02	NA	2,37E-03	9,76E-01
thiamin-P[s]	1	1	0	2,64E-02	2,93E-02	NA	2,93E-03	9,76E-01
5-formyl-THF[s]	1	1	0	2,64E-02	2,93E-02	NA	2,93E-03	9,76E-01
folate[s]	1	1	0	2,64E-02	2,93E-02	NA	2,93E-03	9,76E-01
thiamin-PPP[s]	1	1	0	2,64E-02	2,93E-02	NA	2,93E-03	9,76E-01
Fe3+[s]	5	1	4	4,49E-02	7,83E-01	8,46E-03	9,99E-01	1,75E-07
LTD4[s]	8	1	7	8,07E-02	2,52E-03	3,05E-01	6,00E-01	4,35E-02
H+[s]	56	25	31	2,27E-01	9,78E-01	1,52E-03	1,00E+00	4,82E-06
proline[s]	19	8	11	2,51E-01	9,42E-01	1,05E-02	9,94E-01	8,17E-03

TABLE A.30. Significant reporter metabolites from the comparison of regressed cells with healthy cells. The table depicts a shortened version of the full list of reporter metabolites. Only reporter metabolites with an adjusted p-value < 0.01 are shown. The total number of genes annotated to a respective metabolite is displayed (#Genes annotated) and out of this the number of genes, which are higher (#Genes up) or lower (#Genes down) in the regressed cells than in the control cells. The different types of p-values are extensively reviewed in the vignette of the piano toolbox (https://bioconductor.org/packages/release/bioc/vignettes/piano/inst/doc/piano-vignette.pdf).

Metabolite	#Genes annotated	#Genes up	#Genes down	adjP non.dir	adjP dist.up	adjP dist.down	adjP mix.up	adjP mix.down
reduced vitamin K[c]	2	0	2	1,06E-08	NA	2,50E-09	1,00E+00	0,00E+00
vitamin K[c]	2	0	2	1,06E-08	NA	2,50E-09	1,00E+00	0,00E+00
phylloquinol[c]	1	0	1	1,55E-08	NA	1,73E-09	1,00E+00	0,00E+00
phylloquinone[c]	1	0	1	1,55E-08	NA	1,73E-09	1,00E+00	0,00E+00
G00077[g]	2	2	0	1,07E-07	1,33E-06	NA	4,43E-13	1,00E+00
G00077[c]	2	2	0	1,07E-07	1,33E-06	NA	4,43E-13	1,00E+00
glucose-6-phosphate[c]	13	6	7	1,21E-06	2,96E-10	3,64E-01	4,13E-04	9,99E-01
nLc8Cer[g]	2	1	1	1,75E-06	1,94E-03	1,48E-04	6,34E-01	3,86E-01
tagatose-1,6-bisphosphate[c]	3	2	1	9,39E-06	3,74E-07	6,34E-01	3,17E-10	1,00E+00
G00077[c]	1	1	0	1,61E-05	8,81E-05	NA	1,21E-10	1,00E+00
nLc6Cer[c]	14	7	7	2,09E-05	2,61E-03	2,10E-03	2,04E-01	7,87E-01
sedoheptulose-1,7-bisphosphate[c]	6	5	1	2,60E-05	8,50E-06	6,34E-01	1,72E-10	1,00E+00
sarcosine[m]	1	0	1	2,63E-05	NA	7,67E-06	1,00E+00	8,52E-09
NO[c]	3	1	2	4,80E-05	6,66E-04	9,13E-03	4,96E-01	5,10E-01
N-(omega)-hydroxyarginine[c]	3	1	2	4,80E-05	6,66E-04	9,13E-03	4,96E-01	5,10E-01
glucosamine[c]	7	5	2	5,19E-05	2,39E-06	6,86E-01	1,10E-05	1,00E+00
beta-D-glucose-6-phosphate[c]	7	4	3	7,08E-05	1,15E-07	7,24E-01	2,76E-05	1,00E+00
mannose[c]	7	5	2	9,82E-05	5,49E-06	6,86E-01	6,29E-05	1,00E+00
keratan sulfate II (core 2-linked)[g]	3	0	3	1,04E-04	NA	3,89E-05	1,00E+00	0,00E+00
keratan sulfate II (core 4-linked)[g]	3	0	3	1,04E-04	NA	3,89E-05	1,00E+00	0,00E+00
keratan sulfate I[g]	3	0	3	1,04E-04	NA	3,89E-05	1,00E+00	0,00E+00
carbonate[c]	11	6	5	1,28E-04	5,37E-05	1,80E-01	1,28E-04	9,99E-01
D-tagatose-6-phosphate[c]	7	6	1	1,38E-04	7,95E-05	6,34E-01	2,62E-09	1,00E+00
choline[m]	1	0	1	1,70E-04	NA	6,31E-05	1,00E+00	4,78E-06
ADP[c]	674	338	336	1,70E-04	5,41E-06	4,16E-01	1,46E-05	1,00E+00
glycogen[c]	3	2	1	2,58E-04	3,82E-02	3,48E-04	4,91E-01	5,15E-01
nLc6Cer[g]	6	3	3	2,60E-04	3,86E-02	5,45E-04	3,53E-01	6,44E-01
PEP[c]	9	8	1	2,93E-04	3,61E-04	6,34E-01	2,50E-10	1,00E+00
dimethylglycine[c]	3	1	2	3,22E-04	2,41E-02	3,18E-03	9,97E-01	5,47E-03
sarcosine[c]	3	2	1	3,22E-04	1,28E-01	7,67E-06	9,97E-01	5,47E-03
fucgalacglc13galacglcgal14acglcgalgluside heparan sulfate[g]	1	0	1	3,61E-04	NA	1,48E-04	1,00E+00	4,82E-05
III3Fuc-nLc6Cer[g]	1	0	1	3,61E-04	NA	1,48E-04	1,00E+00	4,82E-05
IV3NeuAc,III3Fuc-nLc4Cer[g]	1	0	1	3,61E-04	NA	1,48E-04	1,00E+00	4,82E-05
fucfucgalacglc13galacglcgal14acglcgalgluside heparan sulfate[g]	1	0	1	3,61E-04	NA	1,48E-04	1,00E+00	4,82E-05
fucfuc132galacglcgal14acglcgalgluside heparan sulfate[g]	1	0	1	3,61E-04	NA	1,48E-04	1,00E+00	4,82E-05
V3Fuc-nLc6Cer[g]	1	0	1	3,61E-04	NA	1,48E-04	1,00E+00	4,82E-05
lacto-N-fucopentaosyl-III-ceramide[g]	1	0	1	3,61E-04	NA	1,48E-04	1,00E+00	4,82E-05
fucfucfucgalacglc13galacglcgal14acglcgalgluside heparan sulfate[g]	1	0	1	3,61E-04	NA	1,48E-04	1,00E+00	4,82E-05
fucfucgalacglcgal14acglcgalgluside heparan sulfate[g]	1	0	1	3,61E-04	NA	1,48E-04	1,00E+00	4,82E-05

Metabolite	#Genes annotated	#Genes up	#Genes down	adjP non.dir	adjP dist.up	adjP dist.down	adjP mix.up	adjP mix.down
fucfucfucgalacglcgal14acglcgalgluside heparan sulfate[g]	1	0	1	3,61E-04	NA	1,48E-04	1,00E+00	4,82E-05
glycolipid[g]	1	0	1	3,61E-04	NA	1,48E-04	1,00E+00	4,82E-05
L-glutamate 5-semialdehyde[c]	1	0	1	4,23E-04	NA	1,77E-04	1,00E+00	7,65E-05
L-4-hydroxyglutamate semialdehyde[m]	1	0	1	4,23E-04	NA	1,77E-04	1,00E+00	7,65E-05
2-hydroxy-3-phenylpropenoate[c]	1	1	0	5,44E-04	1,66E-03	NA	6,38E-05	1,00E+00
2-hydroxy-3-(4-hydroxyphenyl)propenoate[c]	1	1	0	5,44E-04	1,66E-03	NA	6,38E-05	1,00E+00
cGMP[c]	39	10	29	6,31E-04	6,16E-01	8,51E-06	9,99E-01	3,65E-03
cAMP[c]	39	10	29	6,31E-04	6,16E-01	8,51E-06	9,99E-01	3,65E-03
acgalfuc12gal14acglcgalgluside heparan sulfate[g]	1	1	0	6,56E-04	1,94E-03	NA	1,15E-04	1,00E+00
acgalfucgalacglcgal14acglcgalgluside heparan sulfate[g]	1	1	0	6,56E-04	1,94E-03	NA	1,15E-04	1,00E+00
galgalgalthcrm heparan sulfate[g]	1	1	0	6,56E-04	1,94E-03	NA	1,15E-04	1,00E+00
glcnac-gal-globoside[g]	1	1	0	6,56E-04	1,94E-03	NA	1,15E-04	1,00E+00
galgalthcrm heparan sulfate[g]	1	1	0	6,56E-04	1,94E-03	NA	1,15E-04	1,00E+00
gal-glcnac-gal-globoside[g]	1	1	0	6,56E-04	1,94E-03	NA	1,15E-04	1,00E+00
galthcrm heparan sulfate[g]	1	1	0	6,56E-04	1,94E-03	NA	1,15E-04	1,00E+00
beta-GalNAc-globoside[g]	1	1	0	6,56E-04	1,94E-03	NA	1,15E-04	1,00E+00
N-acetylgalactosamine[g]	1	1	0	6,56E-04	1,94E-03	NA	1,15E-04	1,00E+00
3-mercaptolactate[c]	3	1	2	6,78E-04	1,45E-03	4,82E-02	1,41E-01	8,42E-01
1D-myo-inositol-3,4,5,6-tetrakisphosphate[c]	1	1	0	7,50E-04	2,17E-03	NA	1,75E-04	1,00E+00
guanosine[m]	1	0	1	8,41E-04	NA	3,83E-04	1,00E+00	5,23E-04
cytidine[m]	1	0	1	8,41E-04	NA	3,83E-04	1,00E+00	5,23E-04
inosine[m]	1	0	1	8,41E-04	NA	3,83E-04	1,00E+00	5,23E-04
ceramide-1P pool[c]	11	4	7	9,59E-04	1,56E-01	5,36E-04	9,62E-01	5,60E-06
lactoneotetraosylceramide[g]	6	3	3	9,87E-04	1,03E-01	5,45E-04	7,55E-01	2,72E-01
IDP[c]	15	8	7	1,09E-03	7,27E-05	4,63E-01	4,71E-05	1,00E+00
2-hydroxybutyrate[c]	9	4	5	1,09E-03	5,26E-03	3,89E-02	7,06E-02	9,16E-01
glycogenin G11[c]	3	2	1	1,10E-03	1,69E-04	6,34E-01	1,66E-03	9,97E-01
sialyl-3-paragloboside[g]	3	1	2	1,12E-03	6,45E-01	1,62E-05	9,99E-01	2,94E-03
fructose-1,6-bisphosphate[c]	9	6	3	1,27E-03	7,95E-05	7,24E-01	2,16E-07	1,00E+00
paragloboside[c]	13	6	7	1,28E-03	7,29E-02	2,10E-03	7,97E-01	2,33E-01
S-farnesyl-protein[c]	2	1	1	1,44E-03	1,70E-05	6,34E-01	3,71E-08	1,00E+00
5-oxo-6-trans-LTB4[p]	24	7	17	1,52E-03	7,94E-03	1,60E-02	4,36E-01	5,78E-01
5-oxo-6-trans-LTB4[c]	24	7	17	1,52E-03	7,94E-03	1,60E-02	4,36E-01	5,78E-01
5-oxo-6-trans-LTB4[m]	24	7	17	1,52E-03	7,94E-03	1,60E-02	4,36E-01	5,78E-01
5-oxo-(6E)-12-epi-LTB4[c]	24	7	17	1,52E-03	7,94E-03	1,60E-02	4,36E-01	5,78E-01
5-oxo-(6E)-12-epi-LTB4[m]	24	7	17	1,52E-03	7,94E-03	1,60E-02	4,36E-01	5,78E-01
5-oxo-(6E)-12-epi-LTB4[p]	24	7	17	1,52E-03	7,94E-03	1,60E-02	4,36E-01	5,78E-01
L-glutaminyl-peptide[c]	1	0	1	1,76E-03	NA	8,81E-04	9,98E-01	3,41E-03
5-oxoprolyl-peptide[c]	1	0	1	1,76E-03	NA	8,81E-04	9,98E-01	3,41E-03
ITP[c]	16	8	8	1,87E-03	7,27E-05	5,19E-01	6,97E-05	1,00E+00

Metabolite	#Genes annotated	#Genes up	#Genes down	adjP non.dir	adjP dist.up	adjP dist.down	adjP mix.up	adjP mix.down
N-acetyl-O-acetylneuraminate[c]	1	1	0	2,14E-03	5,22E-03	NA	3,43E-03	9,94E-01
keratan sulfate I biosynthesis, precursor 1[g]	9	5	4	2,29E-03	3,13E-03	1,56E-01	2,67E-03	9,88E-01
H2S[c]	5	0	5	2,42E-03	NA	1,02E-03	1,00E+00	1,81E-05
pyruvate[p]	10	5	5	2,43E-03	1,64E-02	3,89E-02	8,31E-02	9,02E-01
keratan sulfate I biosynthesis, precursor 36[g]	7	2	5	2,43E-03	1,21E-01	2,73E-03	9,89E-01	7,37E-09
keratan sulfate II biosynthesis, precursor 10[g]	7	2	5	2,43E-03	1,21E-01	2,73E-03	9,89E-01	7,37E-09
keratan sulfate II (core 4-linked), biosynthesis, precursor 10[g]	7	2	5	2,43E-03	1,21E-01	2,73E-03	9,89E-01	7,37E-09
2-phospho-D-glycerate[c]	6	5	1	2,48E-03	1,32E-03	6,34E-01	5,38E-08	1,00E+00
heptaglutamyl-folate(DHF)[l]	1	0	1	2,72E-03	NA	1,44E-03	9,94E-01	9,31E-03
hexaglutamyl-folate(THF)[l]	1	0	1	2,72E-03	NA	1,44E-03	9,94E-01	9,31E-03
THF[l]	1	0	1	2,72E-03	NA	1,44E-03	9,94E-01	9,31E-03
hexaglutamyl-folate(DHF)[l]	1	0	1	2,72E-03	NA	1,44E-03	9,94E-01	9,31E-03
10-formyl-THF[l]	1	0	1	2,72E-03	NA	1,44E-03	9,94E-01	9,31E-03
pentaglutamyl-folate(THF)[l]	1	0	1	2,72E-03	NA	1,44E-03	9,94E-01	9,31E-03
heptaglutamyl-folate(THF)[l]	1	0	1	2,72E-03	NA	1,44E-03	9,94E-01	9,31E-03
pentaglutamyl-folate(DHF)[l]	1	0	1	2,72E-03	NA	1,44E-03	9,94E-01	9,31E-03
dihydrofolate[l]	1	0	1	2,72E-03	NA	1,44E-03	9,94E-01	9,31E-03
10-formyl-THF-glu(7)[l]	1	0	1	2,72E-03	NA	1,44E-03	9,94E-01	9,31E-03
10-formyl-THF-glu(5)[l]	1	0	1	2,72E-03	NA	1,44E-03	9,94E-01	9,31E-03
10-formyl-THF-glu(6)[l]	1	0	1	2,72E-03	NA	1,44E-03	9,94E-01	9,31E-03
CDP[c]	17	8	9	2,81E-03	8,44E-04	2,35E-01	1,73E-04	9,99E-01
dehydroascorbic acid[c]	6	4	2	2,83E-03	1,75E-02	4,76E-02	1,36E-01	8,48E-01
L-cystathionine[c]	2	0	2	3,31E-03	NA	2,17E-03	1,00E+00	1,78E-05
selenocystathionine[c]	2	0	2	3,31E-03	NA	2,17E-03	1,00E+00	1,78E-05
keratan sulfate I biosynthesis, precursor 28[g]	9	6	3	3,48E-03	3,23E-04	7,24E-01	1,29E-05	1,00E+00
keratan sulfate II biosynthesis, precursor 8[g]	9	6	3	3,48E-03	3,23E-04	7,24E-01	1,29E-05	1,00E+00
keratan sulfate I biosynthesis, precursor 16[g]	9	6	3	3,48E-03	3,23E-04	7,24E-01	1,29E-05	1,00E+00
keratan sulfate I biosynthesis, precursor 25[g]	9	6	3	3,48E-03	3,23E-04	7,24E-01	1,29E-05	1,00E+00
keratan sulfate I biosynthesis, precursor 13[g]	9	6	3	3,48E-03	3,23E-04	7,24E-01	1,29E-05	1,00E+00
keratan sulfate I biosynthesis, precursor 22[g]	9	6	3	3,48E-03	3,23E-04	7,24E-01	1,29E-05	1,00E+00
keratan sulfate I biosynthesis, precursor 4[g]	9	6	3	3,48E-03	3,23E-04	7,24E-01	1,29E-05	1,00E+00
keratan sulfate II biosynthesis, precursor 5[g]	9	6	3	3,48E-03	3,23E-04	7,24E-01	1,29E-05	1,00E+00
keratan sulfate I biosynthesis, precursor 7[g]	9	6	3	3,48E-03	3,23E-04	7,24E-01	1,29E-05	1,00E+00
keratan sulfate I biosynthesis, precursor 34[g]	9	6	3	3,48E-03	3,23E-04	7,24E-01	1,29E-05	1,00E+00
keratan sulfate II (core 4-linked), biosynthesis, precursor 8[g]	9	6	3	3,48E-03	3,23E-04	7,24E-01	1,29E-05	1,00E+00
keratan sulfate II (core 4-linked), biosynthesis, precursor 5[g]	9	6	3	3,48E-03	3,23E-04	7,24E-01	1,29E-05	1,00E+00
keratan sulfate I biosynthesis, precursor 10[g]	9	6	3	3,48E-03	3,23E-04	7,24E-01	1,29E-05	1,00E+00
keratan sulfate I biosynthesis, precursor 19[g]	9	6	3	3,48E-03	3,23E-04	7,24E-01	1,29E-05	1,00E+00
keratan sulfate I biosynthesis, precursor 31[g]	9	6	3	3,48E-03	3,23E-04	7,24E-01	1,29E-05	1,00E+00
1D-myo-inositol-1,4-bisphosphate[c]	19	7	12	3,49E-03	1,18E-01	4,13E-03	9,17E-01	1,15E-01
apppA[c]	1	0	1	3,57E-03	NA	1,96E-03	9,89E-01	1,66E-02
ADP-ribose-2-phosphate[c]	2	1	1	3,61E-03	8,31E-05	6,34E-01	2,76E-06	1,00E+00
fructose-6-phosphate[c]	24	12	12	3,61E-03	2,69E-06	8,83E-01	1,02E-06	1,00E+00
UDP[c]	96	36	60	3,78E-03	7,00E-04	2,25E-01	2,33E-02	9,64E-01
beta-alanine[m]	1	0	1	3,82E-03	NA	2,11E-03	9,87E-01	1,90E-02
L-3-amino-isobutanoate[m]	1	0	1	3,82E-03	NA	2,11E-03	9,87E-01	1,90E-02
FAD[c]	41	13	28	3,89E-03	1,89E-02	2,64E-02	6,98E-01	3,08E-02
NADPH[p]	33	10	23	4,16E-03	4,95E-02	1,42E-02	7,23E-01	3,15E-01
NADP+[p]	33	10	23	4,16E-03	4,95E-02	1,42E-02	7,23E-01	3,15E-01
dUMP[n]	1	0	1	4,57E-03	NA	2,58E-03	9,81E-01	2,72E-02

Metabolite	#Genes annotated	#Genes up	#Genes down	adjP non.dir	adjP dist.up	adjP dist.down	adjP mix.up	adjP mix.down
formaldehyde[p]	2	0	2	4,72E-03	NA	3,18E-03	1,00E+00	6,62E-05
sarcosine[p]	2	0	2	4,72E-03	NA	3,18E-03	1,00E+00	6,62E-05
peptidylglycine[c]	1	0	1	4,73E-03	NA	2,68E-03	9,79E-01	2,90E-02
peptidylamidoglycolate[c]	1	0	1	4,73E-03	NA	2,68E-03	9,79E-01	2,90E-02
H+[p]	69	21	48	4,77E-03	7,30E-03	5,54E-02	4,11E-01	6,15E-01
12-hydroxy-arachidonate[r]	1	0	1	4,78E-03	NA	2,72E-03	9,79E-01	2,97E-02
beta-D-glucose[c]	7	3	4	4,96E-03	5,06E-06	7,51E-01	1,73E-03	9,96E-01
L-lactate[p]	4	2	2	5,13E-03	3,25E-02	4,82E-02	1,77E-01	8,05E-01
1-(1-alkenyl)-sn-glycero-3-phosphate[c]	1	0	1	5,35E-03	NA	3,09E-03	9,73E-01	3,67E-02
5-hydroxy-L-tryptophan[c]	5	1	4	5,37E-03	6,45E-01	5,01E-04	1,00E+00	2,61E-04
tRNA containing N7-methylguanine[c]	1	0	1	5,56E-03	NA	3,22E-03	9,71E-01	3,94E-02
sedoheptulose-7-phosphate[c]	6	3	3	5,94E-03	5,20E-05	7,24E-01	3,81E-06	1,00E+00
sphinganine-1-phosphate[c]	10	5	5	6,06E-03	2,29E-01	1,98E-03	9,17E-01	1,46E-05
sphingosine-1-phosphate[c]	10	5	5	6,06E-03	2,29E-01	1,98E-03	9,17E-01	1,46E-05
1-lyso-2-arachidonoyl-phosphatidate[c]	10	4	6	6,06E-03	1,56E-01	6,31E-03	9,17E-01	1,46E-05
2-acyl-1-alkyl-sn-glycero-3-phosphate[c]	10	4	6	6,06E-03	1,56E-01	6,31E-03	9,17E-01	1,46E-05
phosphatidate-bile-PC pool[c]	19	9	10	6,27E-03	1,99E-01	2,58E-03	9,67E-01	8,30E-05
phosphatidate-LD-SM pool[c]	19	9	10	6,27E-03	1,99E-01	2,58E-03	9,67E-01	8,30E-05
alkylamine[c]	6	2	4	6,84E-03	5,55E-02	2,31E-02	4,28E-01	5,75E-01
glucose-1-phosphate[c]	15	8	7	7,19E-03	1,29E-01	8,28E-03	4,36E-01	5,74E-01
sialyl-3-paragloboside[c]	4	0	4	7,31E-03	NA	3,78E-03	9,96E-01	8,93E-03
1,2-diacylglycerol-LD-PI pool[c]	35	16	19	7,36E-03	2,02E-01	3,84E-03	9,02E-01	3,42E-03
phosphatidate-LD-PE pool[c]	23	11	12	8,41E-03	2,89E-01	1,65E-03	9,57E-01	2,61E-04
phosphatidate-LD-PS pool[c]	23	11	12	8,41E-03	2,89E-01	1,65E-03	9,57E-01	2,61E-04
dADP[c]	29	15	14	8,94E-03	1,67E-03	4,51E-01	7,61E-04	9,98E-01
2-oxobutyrate[c]	12	6	6	9,80E-03	3,54E-02	7,03E-02	1,02E-01	8,82E-01
3-phospho-D-glycerate[c]	11	4	7	9,82E-03	1,42E-01	1,41E-02	4,39E-01	5,69E-01
17-HETE[c]	20	7	13	1,01E-02	7,94E-03	1,33E-01	1,59E-01	8,32E-01
11,14,15-THETA[c]	20	7	13	1,01E-02	7,94E-03	1,33E-01	1,59E-01	8,32E-01
14,15-EET[r]	20	7	13	1,01E-02	7,94E-03	1,33E-01	1,59E-01	8,32E-01
6,7-dihydro-LTB4[p]	20	7	13	1,01E-02	7,94E-03	1,33E-01	1,59E-01	8,32E-01
5-oxo-(6E)-12-epi-LTB4[r]	20	7	13	1,01E-02	7,94E-03	1,33E-01	1,59E-01	8,32E-01
2-hydroxyestradiol-17beta[r]	20	7	13	1,01E-02	7,94E-03	1,33E-01	1,59E-01	8,32E-01
19-oxo-testosterone[c]	20	7	13	1,01E-02	7,94E-03	1,33E-01	1,59E-01	8,32E-01
10-HETE[c]	20	7	13	1,01E-02	7,94E-03	1,33E-01	1,59E-01	8,32E-01
11-HETE[c]	20	7	13	1,01E-02	7,94E-03	1,33E-01	1,59E-01	8,32E-01
18-HETE[c]	20	7	13	1,01E-02	7,94E-03	1,33E-01	1,59E-01	8,32E-01
16(R)-HETE[c]	20	7	13	1,01E-02	7,94E-03	1,33E-01	1,59E-01	8,32E-01
6,7-dihydro-LTB4[c]	20	7	13	1,01E-02	7,94E-03	1,33E-01	1,59E-01	8,32E-01
15H-11,12-EETA[c]	20	7	13	1,01E-02	7,94E-03	1,33E-01	1,59E-01	8,32E-01
FAD[r]	20	7	13	1,01E-02	7,94E-03	1,33E-01	1,59E-01	8,32E-01
11h-14,15-EETA[c]	20	7	13	1,01E-02	7,94E-03	1,33E-01	1,59E-01	8,32E-01
16alpha-hydroxyestrone[r]	20	7	13	1,01E-02	7,94E-03	1,33E-01	1,59E-01	8,32E-01
7-HETE[c]	20	7	13	1,01E-02	7,94E-03	1,33E-01	1,59E-01	8,32E-01
5-oxo-6-trans-LTB4[r]	20	7	13	1,01E-02	7,94E-03	1,33E-01	1,59E-01	8,32E-01
18-hydroxy-all-trans-retinoate[r]	20	7	13	1,01E-02	7,94E-03	1,33E-01	1,59E-01	8,32E-01
8,9-EET[r]	20	7	13	1,01E-02	7,94E-03	1,33E-01	1,59E-01	8,32E-01
16alpha-hydroxyestrone[c]	20	7	13	1,01E-02	7,94E-03	1,33E-01	1,59E-01	8,32E-01
19-hydroxyandrostenedione[c]	20	7	13	1,01E-02	7,94E-03	1,33E-01	1,59E-01	8,32E-01
8-HETE[c]	20	7	13	1,01E-02	7,94E-03	1,33E-01	1,59E-01	8,32E-01

Metabolite	#Genes annotated	#Genes up	#Genes down	adjP non.dir	adjP dist.up	adjP dist.down	adjP mix.up	adjP mix.down
11,12,15-THETA[c]	20	7	13	1,01E-02	7,94E-03	1,33E-01	1,59E-01	8,32E-01
19-hydroxytestosterone[c]	20	7	13	1,01E-02	7,94E-03	1,33E-01	1,59E-01	8,32E-01
FADH2[r]	20	7	13	1,01E-02	7,94E-03	1,33E-01	1,59E-01	8,32E-01
6,7-dihydro-LTB4[m]	20	7	13	1,01E-02	7,94E-03	1,33E-01	1,59E-01	8,32E-01
18-hydroxy-all-trans-retinoate[c]	20	7	13	1,01E-02	7,94E-03	1,33E-01	1,59E-01	8,32E-01
13-HETE[c]	20	7	13	1,01E-02	7,94E-03	1,33E-01	1,59E-01	8,32E-01
19-oxoandrostenedione[c]	20	7	13	1,01E-02	7,94E-03	1,33E-01	1,59E-01	8,32E-01
9-HETE[c]	20	7	13	1,01E-02	7,94E-03	1,33E-01	1,59E-01	8,32E-01
19(S)-HETE[c]	20	7	13	1,01E-02	7,94E-03	1,33E-01	1,59E-01	8,32E-01
5,6-EET[r]	20	7	13	1,01E-02	7,94E-03	1,33E-01	1,59E-01	8,32E-01
6,7-dihydro-LTB4[r]	20	7	13	1,01E-02	7,94E-03	1,33E-01	1,59E-01	8,32E-01
phosphatidate-LD-PC pool[c]	24	11	13	1,16E-02	2,89E-01	9,55E-01	3,16E-04	8,32E-01
betaine_aldehyde[c]	2	0	2	1,16E-02	NA	8,40E-03	1,00E+00	1,36E-03
betaine_aldehyde[m]	2	0	2	1,16E-02	NA	8,40E-03	1,00E+00	1,36E-03
VI3NeuAc-nLc6Cer[g]	1	0	1	1,17E-02	NA	7,42E-03	8,87E-01	1,31E-01
VI3NeuAc-nLc6Cer[e]	1	0	1	1,17E-02	NA	7,42E-03	8,87E-01	1,31E-01
4-aminobutyrate[m]	7	1	6	1,18E-02	6,45E-01	1,92E-03	9,92E-01	1,48E-02
prostaglandin F2alpha[c]	8	0	8	1,24E-02	NA	6,71E-03	9,96E-01	8,72E-03
phosphatidate-LD-P1 pool[c]	21	11	10	1,34E-02	2,89E-01	2,58E-03	9,60E-01	1,40E-04
keratan sulfate I biosynthesis, precursor 21[g]	11	6	5	1,47E-02	4,10E-04	7,76E-01	1,44E-04	9,99E-01
keratan sulfate I biosynthesis, precursor 2[g]	11	6	5	1,47E-02	4,10E-04	7,76E-01	1,44E-04	9,99E-01
keratan sulfate I biosynthesis, precursor 12[g]	11	6	5	1,47E-02	4,10E-04	7,76E-01	1,44E-04	9,99E-01
keratan sulfate II (core 4-linked), biosynthesis, precursor 3[g]	11	6	5	1,47E-02	4,10E-04	7,76E-01	1,44E-04	9,99E-01
keratan sulfate I biosynthesis, precursor 9[g]	11	6	5	1,47E-02	4,10E-04	7,76E-01	1,44E-04	9,99E-01
keratan sulfate II biosynthesis, precursor 27[g]	11	6	5	1,47E-02	4,10E-04	7,76E-01	1,44E-04	9,99E-01
keratan sulfate II biosynthesis, precursor 4[g]	11	6	5	1,47E-02	4,10E-04	7,76E-01	1,44E-04	9,99E-01
keratan sulfate I biosynthesis, precursor 3[g]	11	6	5	1,47E-02	4,10E-04	7,76E-01	1,44E-04	9,99E-01
keratan sulfate II (core 4-linked), biosynthesis, precursor 4[g]	11	6	5	1,47E-02	4,10E-04	7,76E-01	1,44E-04	9,99E-01
keratan sulfate I biosynthesis, precursor 18[g]	11	6	5	1,47E-02	4,10E-04	7,76E-01	1,44E-04	9,99E-01
keratan sulfate I biosynthesis, precursor 24[g]	11	6	5	1,47E-02	4,10E-04	7,76E-01	1,44E-04	9,99E-01
keratan sulfate II (core 4-linked), biosynthesis, precursor 7[g]	11	6	5	1,47E-02	4,10E-04	7,76E-01	1,44E-04	9,99E-01
keratan sulfate II biosynthesis, precursor 15[g]	11	6	5	1,47E-02	4,10E-04	7,76E-01	1,44E-04	9,99E-01
keratan sulfate II biosynthesis, precursor 7[g]	11	6	5	1,47E-02	4,10E-04	7,76E-01	1,44E-04	9,99E-01
keratan sulfate I biosynthesis, precursor 33[g]	11	6	5	1,47E-02	4,10E-04	7,76E-01	1,44E-04	9,99E-01
keratan sulfate II biosynthesis, precursor 3[g]	11	6	5	1,47E-02	4,10E-04	7,76E-01	1,44E-04	9,99E-01
keratan sulfate II biosynthesis, precursor 2[g]	11	6	5	1,47E-02	4,10E-04	7,76E-01	1,44E-04	9,99E-01
keratan sulfate I biosynthesis, precursor 30[g]	11	6	5	1,47E-02	4,10E-04	7,76E-01	1,44E-04	9,99E-01
keratan sulfate I biosynthesis, precursor 6[g]	11	6	5	1,47E-02	4,10E-04	7,76E-01	1,44E-04	9,99E-01
chondroitin sulfate D (GlcNAc6S-GlcA2S) proteoglycan[g]	1	0	1	1,48E-02	NA	9,66E-03	8,42E-01	1,77E-01
FADH2[c]	27	9	18	1,48E-02	1,60E-03	2,97E-01	6,46E-02	9,23E-01
formate[r]	21	7	14	1,54E-02	7,94E-03	1,64E-01	1,65E-01	8,26E-01
6-trans-12-epi-LTB4[c]	4	0	4	1,59E-02	NA	9,16E-03	9,67E-01	5,06E-02
10,11-dihydro-12-epi-LTB4[p]	4	0	4	1,59E-02	NA	9,16E-03	9,67E-01	5,06E-02
12-oxo-10,11-dihydro-20-COOH-LTB4[r]	4	0	4	1,59E-02	NA	9,16E-03	9,67E-01	5,06E-02
12-oxo-20-carboxy-LTB4[c]	4	0	4	1,59E-02	NA	9,16E-03	9,67E-01	5,06E-02
6-trans-12-epi-LTB4[p]	4	0	4	1,59E-02	NA	9,16E-03	9,67E-01	5,06E-02
12-oxo-20-carboxy-LTB4[r]	4	0	4	1,59E-02	NA	9,16E-03	9,67E-01	5,06E-02
5-oxo-EPE[c]	4	0	4	1,59E-02	NA	9,16E-03	9,67E-01	5,06E-02
10,11-dihydro-12-epi-LTB4[c]	4	0	4	1,59E-02	NA	9,16E-03	9,67E-01	5,06E-02
10,11-dihydro-12R-hydroxy-LTC4[m]	4	0	4	1,59E-02	NA	9,16E-03	9,67E-01	5,06E-02
10,11-dihydro-12R-hydroxy-LTC4[c]	4	0	4	1,59E-02	NA	9,16E-03	9,67E-01	5,06E-02

Metabolite	#Genes annotated	#Genes up	#Genes down	adjP non.dir	adjP dist.up	adjP dist.down	adjP mix.up	adjP mix.down
6-trans-LTB4[c]	4	0	4	1,59E-02	NA	9,16E-03	9,67E-01	5,06E-02
20-COOH-10,11-dihydro-LTB4[m]	4	0	4	1,59E-02	NA	9,16E-03	9,67E-01	5,06E-02
20-COOH-10,11-dihydro-LTB4[c]	4	0	4	1,59E-02	NA	9,16E-03	9,67E-01	5,06E-02
5(S)-HEPE[p]	4	0	4	1,59E-02	NA	9,16E-03	9,67E-01	5,06E-02
6-trans-12-epi-LTB4[m]	4	0	4	1,59E-02	NA	9,16E-03	9,67E-01	5,06E-02
20-COOH-10,11-dihydro-LTB4[p]	4	0	4	1,59E-02	NA	9,16E-03	9,67E-01	5,06E-02
12-oxo-10,11-dihydro-20-COOH-LTB4[c]	4	0	4	1,59E-02	NA	9,16E-03	9,67E-01	5,06E-02
6-trans-LTB4[m]	4	0	4	1,59E-02	NA	9,16E-03	9,67E-01	5,06E-02
5-oxo-EPE[p]	4	0	4	1,59E-02	NA	9,16E-03	9,67E-01	5,06E-02
5(S)-HEPE[c]	4	0	4	1,59E-02	NA	9,16E-03	9,67E-01	5,06E-02
10,11-dihydro-12-epi-LTB4[m]	4	0	4	1,59E-02	NA	9,16E-03	9,67E-01	5,06E-02
leukotriene B4[p]	4	0	4	1,59E-02	NA	9,16E-03	9,67E-01	5,06E-02
10,11-dihydro-12R-hydroxy-LTC4[p]	4	0	4	1,59E-02	NA	9,16E-03	9,67E-01	5,06E-02
6-trans-LTB4[p]	4	0	4	1,59E-02	NA	9,16E-03	9,67E-01	5,06E-02
oxalosuccinate[p]	2	1	1	1,64E-02	6,45E-01	1,42E-04	9,99E-01	3,96E-03
oxalosuccinate[m]	2	1	1	1,64E-02	6,45E-01	1,42E-04	9,99E-01	3,96E-03
oxalosuccinate[c]	2	1	1	1,64E-02	6,45E-01	1,42E-04	9,99E-01	3,96E-03
V3Fuc-nLc6Cer[c]	2	0	2	1,67E-02	NA	1,24E-02	9,99E-01	4,16E-03
V3Fuc,III3Fuc-nLc6Cer[c]	2	0	2	1,67E-02	NA	1,24E-02	9,99E-01	4,16E-03
G00086[c]	2	0	2	1,67E-02	NA	1,24E-02	9,99E-01	4,16E-03
G00082[c]	2	0	2	1,67E-02	NA	1,24E-02	9,99E-01	4,16E-03
G00084[c]	2	0	2	1,67E-02	NA	1,24E-02	9,99E-01	4,16E-03
G00085[c]	2	0	2	1,67E-02	NA	1,24E-02	9,99E-01	4,16E-03
nLc8Cer[c]	2	0	2	1,67E-02	NA	1,24E-02	9,99E-01	4,16E-03
IV3NeuAc,III3Fuc-nLc4Cer[c]	2	0	2	1,67E-02	NA	1,24E-02	9,99E-01	4,16E-03
G00081[c]	2	0	2	1,67E-02	NA	1,24E-02	9,99E-01	4,16E-03
III3Fuc-nLc6Cer[c]	2	0	2	1,67E-02	NA	1,24E-02	9,99E-01	4,16E-03
III3Fuc-nLc4Cer[c]	2	0	2	1,67E-02	NA	1,24E-02	9,99E-01	4,16E-03
III3,IV2Fuc-nLc4Cer[c]	2	0	2	1,67E-02	NA	1,24E-02	9,99E-01	4,16E-03
phosphatidate-LD-TAG pool[c]	28	15	13	1,75E-02	1,86E-01	1,53E-02	8,27E-01	4,37E-03
ferrocytochrome B5[c]	5	1	4	1,79E-02	8,06E-03	1,25E-01	7,15E-01	3,08E-01
ferricytochrome B5[c]	5	1	4	1,79E-02	8,06E-03	1,25E-01	7,15E-01	3,08E-01
melatonin[c]	4	2	2	1,84E-02	7,00E-01	1,39E-04	9,55E-01	6,57E-02
9(10)-EpOME[c]	22	7	15	1,87E-02	7,94E-03	2,06E-01	1,72E-01	8,20E-01
8,9-EET[c]	22	7	15	1,87E-02	7,94E-03	2,06E-01	1,72E-01	8,20E-01
12(13)-EpOME[r]	22	7	15	1,87E-02	7,94E-03	2,06E-01	1,72E-01	8,20E-01
12(13)-EpOME[c]	22	7	15	1,87E-02	7,94E-03	2,06E-01	1,72E-01	8,20E-01
5,6-EET[c]	22	7	15	1,87E-02	7,94E-03	2,06E-01	1,72E-01	8,20E-01
9(10)-EpOME[r]	22	7	15	1,87E-02	7,94E-03	2,06E-01	1,72E-01	8,20E-01
1,2-diacylglycerol-bile-PC pool[c]	12	6	6	1,99E-02	2,94E-01	6,31E-03	8,97E-01	7,85E-05
dUTP[n]	7	1	6	2,22E-02	6,45E-01	4,67E-03	9,31E-01	9,22E-02
nLc5Cer[g]	2	2	0	2,22E-02	3,75E-02	NA	4,32E-03	9,91E-01
nLc7Cer[g]	2	2	0	2,22E-02	3,75E-02	NA	4,32E-03	9,91E-01
GM1alpha[g]	2	2	0	2,22E-02	3,75E-02	NA	4,32E-03	9,91E-01
glucosylceramide pool[g]	2	1	1	2,22E-02	1,94E-03	6,34E-01	4,32E-03	9,91E-01
GM2alpha[g]	2	2	0	2,22E-02	3,75E-02	NA	4,32E-03	9,91E-01
tetrahydrobiopterin[c]	3	1	2	2,26E-02	6,45E-01	2,39E-03	1,00E+00	5,21E-04
4alpha-hydroxytetrahydrobiopterin[c]	3	1	2	2,26E-02	6,45E-01	2,39E-03	1,00E+00	5,21E-04
glycogenin G8[c]	2	1	1	2,27E-02	2,02E-03	6,34E-01	4,67E-03	9,90E-01
1D-myo-inositol-1,3,4,6-tetrakisphosphate[c]	2	1	1	2,37E-02	2,17E-03	6,34E-01	5,40E-03	9,89E-01
guanidinoacetate[c]	2	1	1	2,43E-02	6,45E-01	3,57E-04	9,94E-01	1,23E-02

Metabolite	#Genes annotated	#Genes up	#Genes down	adjP non.dir	adjP dist.up	adjP dist.down	adjP mix.up	adjP mix.down
deoxycytidine[m]	2	1	1	2,50E-02	6,45E-01	3,83E-04	9,94E-01	1,33E-02
ribose-1-phosphate[c]	6	4	2	2,98E-02	7,18E-03	6,86E-01	3,59E-03	9,93E-01
ADP-ribose[c]	7	4	3	2,99E-02	2,72E-03	7,24E-01	5,67E-04	9,99E-01
1-alkyl-2-acylglycerol[c]	13	6	7	3,05E-02	2,94E-01	1,53E-02	8,86E-01	1,20E-04
2-arachidonoylglycerol[c]	13	6	7	3,05E-02	2,94E-01	1,53E-02	8,86E-01	1,20E-04
ATP[c]	999	505	494	3,69E-02	3,12E-03	7,26E-01	4,31E-04	9,99E-01
6-hydroxymelatonin[c]	21	9	12	3,73E-02	5,94E-01	2,81E-03	8,57E-01	1,73E-01
4-hydroxy-4-(methylnitrosoamino)-1-(3-pyridinyl)-1-butanone[c]	5	3	2	3,89E-02	7,55E-03	6,86E-01	3,03E-02	9,59E-01
acngalac6glcga1gluside heparan sulfate[g]	2	1	1	3,95E-02	6,45E-01	1,11E-03	9,74E-01	4,32E-02
3-isoLM1[c]	2	1	1	3,95E-02	6,45E-01	1,11E-03	9,74E-01	4,32E-02
sphingosine[c]	19	6	13	3,97E-02	4,28E-02	1,53E-01	6,86E-01	5,56E-03
3,3-diodo-L-thyronine[c]	26	8	18	4,03E-02	5,53E-01	8,05E-03	8,76E-01	1,58E-01
LTD4[r]	4	1	3	4,17E-02	1,86E-05	7,24E-01	1,53E-04	9,98E-01
gamma-L-glutamyl-L-alanine[c]	4	1	3	4,17E-02	1,86E-05	7,24E-01	1,53E-04	9,98E-01
glutamate[r]	4	1	3	4,17E-02	1,86E-05	7,24E-01	1,53E-04	9,98E-01
leukotriene D5[c]	4	1	3	4,17E-02	1,86E-05	7,24E-01	1,53E-04	9,98E-01
cys-gly[c]	9	5	4	4,33E-02	3,92E-03	7,51E-01	2,23E-04	9,99E-01
3-sulfinoalanine[m]	3	1	2	4,36E-02	4,82E-04	6,86E-01	3,09E-03	9,94E-01
Fe3+[c]	3	0	3	4,68E-02	NA	3,49E-02	9,97E-01	6,79E-03
glucosamine-6-phosphate[c]	11	6	5	4,77E-02	3,49E-03	7,76E-01	1,25E-02	9,81E-01
formyl-5-hydroxykynurenamine[c]	2	1	1	5,34E-02	6,45E-01	2,24E-03	9,40E-01	8,58E-02
formyl-N-acetyl-5-methoxykynurenamine[c]	2	1	1	5,34E-02	6,45E-01	2,24E-03	9,40E-01	8,58E-02
keratan sulfate II (core 4-linked), biosynthesis, precursor 2[g]	10	5	5	5,68E-02	3,13E-03	7,76E-01	2,63E-04	9,98E-01
isocitrate[p]	3	2	1	6,04E-02	7,00E-01	1,42E-04	9,91E-01	1,55E-02
sphinganine[c]	21	10	11	6,54E-02	1,97E-01	9,53E-02	6,81E-01	7,04E-03
heparan sulfate, degradation product 15[l]	2	1	1	6,86E-02	6,45E-01	4,00E-03	8,88E-01	1,42E-01
heparan sulfate, degradation product 22[l]	2	1	1	6,86E-02	6,45E-01	4,00E-03	8,88E-01	1,42E-01
heparan sulfate, degradation product 21[l]	2	1	1	6,86E-02	6,45E-01	4,00E-03	8,88E-01	1,42E-01
chondroitin sulfate B - dermatan sulfate (IdoA2S-GalNAc4S), degradation product 3[l]	2	1	1	6,86E-02	6,45E-01	4,00E-03	8,88E-01	1,42E-01
heparan sulfate, degradation product 16[l]	2	1	1	6,86E-02	6,45E-01	4,00E-03	8,88E-01	1,42E-01
GAP[c]	9	7	2	6,87E-02	4,13E-02	6,86E-01	2,05E-03	9,96E-01
DHAP[c]	9	6	3	6,87E-02	2,16E-02	7,24E-01	2,05E-03	9,96E-01
glycine[p]	4	2	2	7,05E-02	7,00E-01	3,18E-03	9,98E-01	3,88E-03
tryptophan[c]	24	7	17	7,16E-02	8,31E-01	3,52E-03	9,98E-01	5,75E-03
globotriaosylceramide[g]	3	1	2	7,37E-02	1,94E-03	6,86E-01	2,10E-02	9,70E-01
UDP-N-acetylglucosamine[g]	31	10	21	7,63E-02	3,93E-03	5,47E-01	1,59E-02	9,67E-01
deoxyguanosine[m]	3	2	1	7,97E-02	7,00E-01	3,83E-04	9,76E-01	3,58E-02
leukotriene C5[c]	5	1	4	8,16E-02	1,86E-05	7,51E-01	6,22E-04	9,96E-01
leukotriene C4[c]	5	1	4	8,16E-02	1,86E-05	7,51E-01	6,22E-04	9,96E-01
LTD4[c]	5	1	4	8,16E-02	1,86E-05	7,51E-01	6,22E-04	9,96E-01
leukotriene C4[r]	5	1	4	8,16E-02	1,86E-05	7,51E-01	6,22E-04	9,96E-01
glucose-6-phosphate[r]	6	3	3	8,44E-02	9,30E-03	7,24E-01	8,20E-02	9,03E-01
butyryl-CoA[c]	22	7	15	1,03E-01	8,31E-01	9,00E-03	9,99E-01	3,74E-03
glucose[c]	32	17	15	1,11E-01	4,07E-03	9,06E-01	8,98E-03	9,87E-01
5-hydroxy-N-formylkynurenine[c]	3	2	1	1,31E-01	7,00E-01	2,24E-03	8,92E-01	1,32E-01
L-formylkynureninel[c]	3	2	1	1,31E-01	7,00E-01	2,24E-03	8,92E-01	1,32E-01
glycine[m]	12	2	10	1,31E-01	7,00E-01	4,72E-02	9,99E-01	3,79E-03
PAP[g]	26	8	18	1,34E-01	5,53E-01	5,70E-02	9,19E-01	1,12E-03
phenylpyruvate[c]	4	1	3	1,39E-01	1,66E-03	7,24E-01	3,33E-02	9,54E-01
mannose-6-phosphate[c]	9	2	7	1,46E-01	1,56E-04	8,19E-01	4,08E-02	9,48E-01
PAPS[g]	27	8	19	1,54E-01	5,53E-01	6,97E-02	9,18E-01	1,40E-03

Metabolite	#Genes annotated	#Genes up	#Genes down	adjP non.dir	adjP dist.up	adjP dist.down	adjP mix.up	adjP mix.down
1,2-diacylglycerol-LD-SM pool[c]	20	12	8	1,68E-01	6,05E-01	3,06E-02	8,43E-01	1,38E-03
selenohomocysteine[c]	6	1	5	1,68E-01	6,45E-01	8,06E-02	9,96E-01	8,19E-03
farnesyl-PP[c]	7	3	4	1,86E-01	2,29E-02	7,51E-01	2,44E-03	9,88E-01
GTP[c]	90	36	54	1,97E-01	8,41E-01	1,68E-02	9,59E-01	6,41E-03
1,2-diacylglycerol-LD-PC pool[c]	22	14	8	2,20E-01	6,74E-01	3,06E-02	8,40E-01	1,91E-03
1,2-diacylglycerol-LD-PE pool[c]	22	13	9	2,20E-01	6,39E-01	4,61E-02	8,40E-01	1,91E-03
1,2-diacylglycerol-LD-PS pool[c]	22	13	9	2,20E-01	6,39E-01	4,61E-02	8,40E-01	1,91E-03
ubiquitin C terminal thiolester[c]	49	35	14	2,35E-01	8,27E-02	9,02E-01	2,05E-04	9,99E-01
thiol[c]	49	35	14	2,35E-01	8,27E-02	9,02E-01	2,05E-04	9,99E-01
NADH[c]	140	43	97	4,16E-01	9,31E-01	6,08E-02	9,93E-01	1,55E-03
Na+[c]	83	24	59	4,25E-01	9,14E-01	8,90E-02	9,98E-01	6,29E-03
ubiquitin[c]	223	139	84	5,83E-01	3,18E-01	9,19E-01	4,36E-03	9,95E-01
sphingosine[s]	1	0	1	5,18E-06	NA	1,23E-06	1,00E+00	0,00E+00
sphingosine-1-phosphate[s]	1	0	1	5,18E-06	NA	1,23E-06	1,00E+00	0,00E+00
CO2[s]	16	7	9	6,95E-05	1,16E-07	4,16E-01	4,19E-07	1,00E+00
carbonate[s]	11	6	5	1,28E-04	5,37E-05	1,80E-01	1,28E-04	9,99E-01
cAMP[s]	2	0	2	5,99E-04	NA	3,42E-04	9,68E-01	5,13E-02
cGMP[s]	2	0	2	5,99E-04	NA	3,42E-04	9,68E-01	5,13E-02
mannose[s]	3	3	0	1,64E-03	4,11E-03	NA	4,14E-03	9,93E-01
10-formyl-THF[s]	1	0	1	2,72E-03	NA	1,44E-03	9,94E-01	9,31E-03
heptaglutamyl-folate(DHF)[s]	1	0	1	2,72E-03	NA	1,44E-03	9,94E-01	9,31E-03
heptaglutamyl-folate(THF)[s]	1	0	1	2,72E-03	NA	1,44E-03	9,94E-01	9,31E-03
hexaglutamyl-folate(THF)[s]	1	0	1	2,72E-03	NA	1,44E-03	9,94E-01	9,31E-03
10-formyl-THF-glu(6)[s]	1	0	1	2,72E-03	NA	1,44E-03	9,94E-01	9,31E-03
dihydrofolate[s]	1	0	1	2,72E-03	NA	1,44E-03	9,94E-01	9,31E-03
10-formyl-THF-glu(5)[s]	1	0	1	2,72E-03	NA	1,44E-03	9,94E-01	9,31E-03
hexaglutamyl-folate(DHF)[s]	1	0	1	2,72E-03	NA	1,44E-03	9,94E-01	9,31E-03
pentaglutamyl-folate(DHF)[s]	1	0	1	2,72E-03	NA	1,44E-03	9,94E-01	9,31E-03
pentaglutamyl-folate(THF)[s]	1	0	1	2,72E-03	NA	1,44E-03	9,94E-01	9,31E-03
10-formyl-THF-glu(7)[s]	1	0	1	2,72E-03	NA	1,44E-03	9,94E-01	9,31E-03
NADP+[s]	2	1	1	3,61E-03	8,31E-05	6,34E-01	2,76E-06	1,00E+00
NAD+[s]	2	1	1	3,61E-03	8,31E-05	6,34E-01	2,76E-06	1,00E+00
ADP-ribose-2-phosphate[s]	2	1	1	3,61E-03	8,31E-05	6,34E-01	2,76E-06	1,00E+00
ADP-ribose[s]	2	1	1	3,61E-03	8,31E-05	6,34E-01	2,76E-06	1,00E+00
nicotinamide[s]	2	1	1	3,61E-03	8,31E-05	6,34E-01	2,76E-06	1,00E+00
lauric acid[s]	21	9	12	5,29E-03	2,73E-03	1,84E-01	2,45E-02	9,48E-01
dehydroascorbic acid[s]	4	3	1	9,60E-03	4,11E-03	6,34E-01	1,10E-02	9,82E-01
glucosamine[s]	2	2	0	2,49E-02	4,13E-02	NA	6,41E-03	9,87E-01
CDP[s]	2	1	1	2,91E-02	3,10E-03	6,34E-01	1,06E-02	9,81E-01
CTP[s]	2	1	1	2,91E-02	3,10E-03	6,34E-01	1,06E-02	9,81E-01
ITP[s]	2	1	1	2,91E-02	3,10E-03	6,34E-01	1,06E-02	9,81E-01
glutamate[s]	16	4	12	3,90E-02	4,21E-03	3,14E-01	1,23E-01	8,13E-01
5-L-gamma-glutamyl[s]	4	1	3	4,17E-02	1,86E-05	7,24E-01	1,53E-04	9,98E-01
gamma-glutamyl-3-aminopropiononitrile[s]	4	1	3	4,17E-02	1,86E-05	7,24E-01	1,53E-04	9,98E-01
L-3-cyanoalanine[s]	4	1	3	4,17E-02	1,86E-05	7,24E-01	1,53E-04	9,98E-01
gamma-glutamyl-beta-cyanoalanine[s]	4	1	3	4,17E-02	1,86E-05	7,24E-01	1,53E-04	9,98E-01
leukotriene C4[s]	4	1	3	4,17E-02	1,86E-05	7,24E-01	1,53E-04	9,98E-01
cys-gly[s]	9	5	4	4,33E-02	3,92E-03	7,51E-01	2,23E-04	9,99E-01
UTP[s]	3	1	2	8,79E-02	3,10E-03	6,86E-01	3,74E-02	9,51E-01
ADP[s]	3	1	2	8,79E-02	3,10E-03	6,86E-01	3,74E-02	9,51E-01
FAD[s]	11	3	8	1,28E-01	7,40E-01	3,06E-02	9,95E-01	1,56E-07
(5-L-glutamyl)-L-amino acid[s]	6	1	5	1,35E-01	1,86E-05	7,76E-01	1,31E-03	9,93E-01
LTD4[s]	7	1	6	1,88E-01	1,86E-05	7,96E-01	2,63E-03	9,88E-01
Na+[s]	81	24	57	3,95E-01	9,14E-01	7,34E-02	9,98E-01	6,17E-03
Pi[s]	41	15	26	4,21E-01	5,31E-01	3,44E-01	8,59E-01	8,74E-03

TABLE A.31. Flux Predictions, regressed vs control.

Reaction ID	Control Flux	Deregulated Flux	Reaction equation	Compartment	Pathway
HMR_4141	0,972	0,46	H+[m] + NADH[m] + OAA[m] <=> NAD+[m] + malate[m]	m	TCA cycle and glyoxylate /dicarboxylate metabolism
HMR_4139	-2,04	-1,53	H+[c] + NADH[c] + OAA[c] <=> NAD+[c] + malate[c]	c	TCA cycle and glyoxylate /dicarboxylate metabolism
HMR_3949	0,471	0	OAA[c] + malate[m] => OAA[m] + malate[c]	m	Transport, mitochondrial
HMR_3859	0,284	0	D-lactate[c] + 2 ferricytochrome C[m] => 2 H+[c] + 2 ferrocytochrome C[m] + pyruvate[c]	m	Pyruvate metabolism
HMR_8512	-0,284	0	D-lactate[c] + NAD+[c] <=> H+[c] + NADH[c] + pyruvate[c]	c	Pyruvate metabolism
HMR_4926	0,469	0,745	H+[c] + pyruvate[c] => H+[m] + pyruvate[m]	m	Transport, mitochondrial
HMR_3911	1,29	1,03	H+[c] + NADH[c] + taurine[c] <=> H2O[c] + NAD+[c] + hypotaurine[c]	c	Bile acid biosynthesis
HMR_8514	1,06	1,31	L-lactate[c] + 2 ferricytochrome C[m] => 2 H+[c] + 2 ferrocytochrome C[m] + pyruvate[c]	m	Pyruvate metabolism
HMR_4152	0,919	0,703	ADP[m] + Pi[m] + succinyl-CoA[m] <=> ATP[m] + CoA[m] + succinate[m]	m	TCA cycle and glyoxylate /dicarboxylate metabolism
HMR_4888	-3,2	-3,4	H2O[c] <=> H2O[m]	m	Transport, mitochondrial
HMR_4147	-0,0439	-0,232	CoA[m] + GTP[m] + succinate[m] <=> GDP[m] + Pi[m] + succinyl-CoA[m]	m	TCA cycle and glyoxylate /dicarboxylate metabolism
HMR_4843	0,0439	0,232	GDP[c] + GTP[m] <=> GDP[m] + GTP[c]	m	Transport, mitochondrial
HMR_7800	0	-0,162	ADP[c] + GDP[c] <=> AMP[c] + GTP[c]	c	Nucleotide metabolism
HMR_4002	-0,159	0	2 ADP[c] <=> AMP[c] + ATP[c]	c	Purine metabolism
HMR_8759	0,642	0,514	O2[c] + 2 hypotaurine[c] => 2 taurine[c]	c	Bile acid biosynthesis
HMR_0731	0,123	0	ceramide pool[c] => ceramide pool[g]	g	Transport, Golgi apparatus
HMR_0795	0,123	0	H2O[c] + SM pool[c] => ceramide pool[c] + phosphocholine[c]	c	Sphingolipid metabolism
HMR_8241	-0,123	0	SM pool[c] <=> SM pool[g]	g	Transport, Golgi apparatus
HMR_4892	0	0,121	H2O[c] <=> H2O[g]	g	Transport, Golgi apparatus
HMR_8242	0	0,121	H2O[g] + SM pool[g] => ceramide pool[g] + phosphocholine[g]	g	Sphingolipid metabolism
HMR_8243	0	-0,121	phosphocholine[c] <=> phosphocholine[g]	g	Transport, Golgi apparatus
HMR_6328	2,68	2,56	ADP[c] + ATP[m] <=> ADP[m] + ATP[c]	m	Transport, mitochondrial
HMR_4388	0	0,362	H+[c] + NADH[c] + pyruvate[c] <=> L-lactate[c] + NAD+[c]	c	Glycolysis / Gluconeogenesis
HMR_4885	0,273	0,163	H2O[c] <=> H2O[s]	s	Transport, extracellular
HMR_9047	-0,411	-0,301	H2O[x] <=> H2O[s]	x	Exchange reactions
HMR_5043	2,23	2,33	H+[c] + Pi[c] <=> H+[m] + Pi[m]	m	Transport, mitochondrial
HMR_6028	0,641	0,537	AKG[c] + retinoate[s] <=> AKG[s] + retinoate[c]	s	Transport, extracellular
HMR_9259	-0,641	-0,537	AKG[x] <=> AKG[s]	x	Exchange reactions
HMR_8721	0,696	0,596	retinoate[c] <=> retinoate[s]	s	Transport, extracellular

TABLE A.32. List of plasmids.

name	**description**	**source**
pSP-GM1	2μ; Ptef1-Ppgk; AmpR/KI.URA3	Partow et al., 2010
pcfb2223	Integrative X3; USER cassette; AmpR/KanMx	Stovicek et al., 2015a
pCfB2195	Integrative XI3; USER cassette; AmpR/KanMx	Stovicek et al., 2015a
pCfB2311	2μ; Template for gRNA plasmids; AmpR/NatMX	Stovicek et al., 2015b
pCfB2312	CEN/ARS; Ptef1-Cas9; AmpR/KanMX	Stovicek et al., 2015b
pTAJAK71	2μ; USER cassette; AmpR/NatMX	Jakociunas et al. 2015
pTS1	X3::TEF1::nox; AmpR/KanMX	This study
pTS53	2μ; gRNA-gut1_1; AmpR/KanMX	This study
PTS54	2μ; gRNA-hog1_1; AmpR/KanMX	This study
pTS56	2μ; gRNA-kgd1; AmpR/KanMX	This study
pTS58	2μ; gRNA-gut1_3; AmpR/KanMX	This study
pTS59	2μ; gRNA-hog1_2; AmpR/KanMX	This study
pTS61	2μ; gRNA-pbs2; AmpR/KanMX	This study
pTS63	2μ; gRNA-tea1; AmpR/KanMX	This study
pTS64	2μ; gRNA-ppz2; AmpR/KanMX	This study
pTS66	2μ; gRNA-gut1_2; AmpR/KanMX	This study
pTS68	2μ; gRNA-ino80; AmpR/KanMX	This study
pTS70	2μ; gRNA-ubc13; AmpR/KanMX	This study
pTS71	2μ; gRNA-cym1; AmpR/KanMX	This study
pTS72	2μ; gRNA-ret1; AmpR/KanMX	This study
pTS74	2μ; gRNA-ymr206w; AmpR/KanMX	This study
pTS81	2μ; gRNA-gut1-kgd1-ino80; AmpR/KanMX	This study
pTS83	2μ; gRNA-gut1-kgd1-ubc13; AmpR/KanMX	This study

TABLE A.33. Permission for the reproduction of figures. The figures that are reproduced from other sources are listed below with their corresponding permission

Figure No.	Title	Author	Year	License No.	Publisher	Reference
1.1	Schematic representation of plasticity and redundancy synthetic lethality subtypes in metabolic networks.	Güell et al	2014	CC BY 4.0	PLOS Computational Biology	(Güell 2014)
1.2	Fundamentals of the genome-scale metabolic genotype-phenotype relationship.	Lewis et al	2012		4447770477248 Nature Reviews Microbiology	(Lewis 2012)
1.2	Formulation of an FBA problem	Orth et al	2010		4447781440475 Nature Biotechnology	(Orth 2010)
1.4	The multiple uses of high-throughput data in constraint-based models.	Bordbar et al	2014		4447771500547 Nature Review Genetic	(Bordbar 2014)
2.1; 2.3-2.5;2.7-2.10;S2.6-S2.12	Fig.1-Fig.3; SupFig.1-8; SupTable 1-10	Strucko et al.	2018	CC BY 4.0	Elsevier	(Strucko 2018)
2.2	Methods used for studying microbial evolution in vivo.	Mozhayskiy & Tagkopoulos	2013		Royal Society of chemistry	(Mozhayskiy 2013)
3.1	Formulation of a Computational Model	O'Brien	2015		4447740789115 Elsevier	(O'Brien 2015)
4.1	Identifying temporally deregulated genes in a breast cancer model.	Havas et al.	2017		4447750363760 American Society for Clinical Investigation	(Havas 2017)
4.2	SupFig.1, SupFig5	Havas et al.	2017		4447750363760 American Society for Clinical Investigation	(Havas 2017)
4.9	Primary Mammary Epithelial Cells.	Oatley et al.	2018	CC BY-NC-ND 4.0*	BioRxiv	(Oatley 2018)

*https://creativecommons.org/licenses/by-nc-nd/4.0/

BIBLIOGRAPHY

[1] N. AFRATIS, C. GIALELI, D. NIKITOVIC, T. TSEGENIDIS, E. KAROUSOU, A. D. THEOCHARIS, M. S. PAVÃO, G. N. TZANAKAKIS, AND N. K. KARAMANOS, *Glycosaminoglycans: Key players in cancer cell biology and treatment*, 2012.

[2] R. AGREN, L. LIU, S. SHOAIE, W. VONGSANGNAK, I. NOOKAEW, AND J. NIELSEN, *The RAVEN Toolbox and Its Use for Generating a Genome-scale Metabolic Model for Penicillium chrysogenum*, PLoS Computational Biology, (2013).

[3] S. ANDERS AND W. HUBER, *Differential expression analysis for sequence count data*, Genome Biology, (2010).

[4] S. ANDERS, P. T. PYL, AND W. HUBER, *HTSeq-A Python framework to work with high-throughput sequencing data*, Bioinformatics, (2015).

[5] V. ANDRE, H. ROSEANNE, T. COLLEEN, P. CECILE, AND W. CYNTHIA, *Molecular insights into polyubiquitin chain assembly*, Trends In Biotechnology, (2001).

[6] S. ANDREWS, J. GILLEY, AND M. P. COLEMAN, *Difference Tracker: ImageJ plugins for fully automated analysis of multiple axonal transport parameters*, Journal of Neuroscience Methods, (2010).

[7] K. ARAKAWA, Y. YAMADA, K. SHINODA, Y. NAKAYAMA, AND M. TOMITA, *GEM system: Automatic prototyping of cell-wide metabolic pathway models from genomes*, BMC Bioinformatics, (2006).

[8] R. ARGELAGUET, B. VELTEN, D. ARNOL, S. DIETRICH, T. ZENZ, J. C. MARIONI, F. BUETTNER, W. HUBER, AND O. STEGLE, *Multi-Omics factor analysis disentangles heterogeneity in blood cancer*, bioRxiv, (2017).

[9] H. ASHTIANI, A. BAKHSHANDI, M. RAHBAR, A. MIRZAEI, A. POUR, AND H. RASTEGAR, *Glutathione, cell proliferation and differentiation*, African Journal of Biotechnology, (2011).

[10] S. ATSUMI, T.-Y. WU, I. M. P. MACHADO, W.-C. HUANG, P.-Y. CHEN, M. PELLEGRINI, AND J. C. LIAO, *Evolution, genomic analysis, and reconstruction of isobutanol tolerance in Escherichia coli*, Molecular Systems Biology, (2010).

[11] G. J. BAART, J. WILLEMSEN, AND D. E. MARTENS, *Genome-scale metabolic models: reconstruction and analysis.*, Methods Mol Biol, (2012).

[12] G. J. BAART, M. WILLEMSEN, E. KHATAMI, A. DE HAAN, B. ZOMER, E. C. BEUVERY, J. TRAMPER, AND D. E. MARTENS, *Modeling Neisseria meningitidis B metabolism at different specific growth rates*, Biotechnology and Bioengineering, (2008).

[13] M. D. BAART GJ1, ZOMER B, *Modeling Neisseria meningitidis metabolism: from genome to metabolic fluxes.*, Methods Mol Biol, (2007).

[14] J. H. BAEK, J. E. JANG, C. M. KANG, H. Y. CHUNG, N. D. KIM, AND K. W. KIM, *Hypoxia-induced VEGF enhances tumor survivability via suppression of serum deprivation-induced apoptosis*, Oncogene, (2000).

[15] T. BARRETT, S. E. WILHITE, P. LEDOUX, C. EVANGELISTA, I. F. KIM, M. TOMASHEVSKY, K. A. MARSHALL, K. H. PHILLIPPY, P. M. SHERMAN, M. HOLKO, A. YEFANOV, H. LEE, N. ZHANG, C. L. ROBERTSON, N. SEROVA, S. DAVIS, AND A. SOBOLEVA, *NCBI GEO: Archive for functional genomics data sets - Update*, Nucleic Acids Research, (2013).

[16] J. E. BARRICK AND R. E. LENSKI, *Genome dynamics during experimental evolution*, 2013.

[17] G. BELLOT, R. GARCIA-MEDINA, P. GOUNON, J. CHICHE, D. ROUX, J. POUYSSEGUR, AND N. M. MAZURE, *Hypoxia-Induced Autophagy Is Mediated through Hypoxia-Inducible Factor Induction of BNIP3 and BNIP3L via Their BH3 Domains*, Molecular and Cellular Biology, (2009).

[18] B. BENJAMIN, K. SARAH, A. JOURAKU, AND H. MICHAEL, *LibSBML: An API Library for SBML.*, Methods Mol Biol, (2008).

[19] R. BLUM, J. JACOB-HIRSCH, N. AMARIGLIO, G. RECHAVI, AND Y. KLOOG, *Ras inhibition in glioblastoma down-regulates hypoxia-inducible factor-1α, causing glycolysis shutdown and cell death*, Cancer Research, (2005).

[20] A. BORDBAR, J. M. MONK, Z. A. KING, AND B. O. PALSSON, *Constraint-based models predict metabolic and associated cellular functions*, 2014.

[21] J. L. BREWSTER AND M. C. GUSTIN, *Hog1: 20 years of discovery and impact*, 2014.

[22] A. R. BROCHADO, C. MATOS, B. L. MØLLER, J. HANSEN, U. H. MORTENSEN, AND K. R. PATIL, *Improved vanillin production in baker's yeast through in silico design*, Microbial Cell Factories, (2010).

[23] E. BRUNK, S. SAHOO, D. C. ZIELINSKI, A. ALTUNKAYA, A. DRÄGER, N. MIH, F. GATTO, A. NILSSON, G. A. PRECIAT GONZALEZ, M. K. AURICH, A. PRLIC, A. SASTRY, A. D. DANIELSDOTTIR, A. HEINKEN, A. NORONHA, P. W. ROSE, S. K. BURLEY, R. M. FLEMING, J. NIELSEN, I. THIELE, AND B. O. PALSSON, *Recon3D enables a three-dimensional view of gene variation in human metabolism*, Nature Biotechnology, (2018).

[24] J. BRUSKY, Y. ZHU, AND W. XIAO, *UBC13, a DNA-damage-inducible gene, is a member of the error-free postreplication repair pathway in Saccharomyces cerevisiae*, Current Genetics, (2000).

[25] A. CADIÈRE, A. ORTIZ-JULIEN, C. CAMARASA, AND S. DEQUIN, *Evolutionary engineered Saccharomyces cerevisiae wine yeast strains with increased in vivo flux through the pentose phosphate pathway*, Metabolic Engineering, (2011).

[26] Z. P. ÇAKAR, U. O. SEKER, C. TAMERLER, M. SONDEREGGER, AND U. SAUER, *Evolutionary engineering of multiple-stress resistant Saccharomyces cerevisiae*, in FEMS Yeast Research, 2005.

[27] Z. P. ÇAKAR, B. TURANLI-YILDIZ, C. ALKIM, AND Ü. YILMAZ, *Evolutionary engineering of Saccharomyces cerevisiae for improved industrially important properties*, 2012.

[28] N. L. CHAN AND C. P. HILL, *Defining polyubiquitin chain topology*, 2001.

[29] S. CHANDRASEKARAN AND N. D. PRICE, *Probabilistic integrative modeling of genome-scale metabolic and regulatory networks in Escherichia coli and Mycobacterium tuberculosis.*, Proceedings of the National Academy of Sciences of the United States of America, (2010).

[30] P. CHARUSANTI, T. M. CONRAD, E. M. KNIGHT, K. VENKATARAMAN, N. L. FONG, B. XIE, Y. GAO, AND B. PALSSON, *Genetic basis of growth adaptation of Escherichia coli after deletion of pgi, a major metabolic gene*, PLoS Genetics, (2010).

[31] L. CHENG, M. D. SWARTZ, H. ZHAO, A. S. KAPADIA, D. LAI, P. J. ROWAN, T. A. BUCHHOLZ, AND S. H. GIORDANO, *Hazard of Recurrence among Women after Primary Breast Cancer Treatment–A 10-Year Follow-up Using Data from SEER-Medicare*, Cancer Epidemiology Biomarkers & Prevention, (2012).

[32] T. M. CONRAD, N. E. LEWIS, AND B. O. PALSSON, *Microbial laboratory evolution in the era of genome-scale science*, 2011.

[33] D. CUNCAN AND L. GUIHUA, *The PI3K/Akt Signalling Pathway Plays Essential Roles in Mesenchymal Stem Cells*, Methods Mol Biol, (2017).

[34] X. DAI, T. LI, Z. BAI, Y. YANG, X. LIU, J. ZHAN, AND B. SHI, *Breast cancer intrinsic subtype classification, clinical use and future trends*, Am J Cancer Res, (2015).

[35] C. V. DANG, J. W. KIM, P. GAO, AND J. YUSTEIN, *The interplay between MYC and HIF in cancer*, 2008.

[36] L. DAVID, W. HUBER, M. GRANOVSKAIA, J. TOEDLING, C. J. PALM, L. BOFKIN, T. JONES, R. W. DAVIS, AND L. M. STEINMETZ, *A high-resolution map of transcription in the yeast genome*, Proceedings of the National Academy of Sciences, (2006).

[37] R. M. DAY AND Y. J. SUZUKI, *Cell proliferation, reactive oxygen and cellular glutathione.*, Dose-response : a publication of International Hormesis Society, (2005).

[38] M. A. DEPRISTO, E. BANKS, R. POPLIN, K. V. GARIMELLA, J. R. MAGUIRE, C. HARTL, A. A. PHILIPPAKIS, G. DEL ANGEL, M. A. RIVAS, M. HANNA, A. MCKENNA, T. J. FENNELL, A. M. KERNYTSKY, A. Y. SIVACHENKO, K. CIBULSKIS, S. B. GABRIEL, D. ALTSHULER, AND M. J. DALY, *A framework for variation discovery and genotyping using next-generation DNA sequencing data*, Nature Genetics, (2011).

[39] O. DIAS, M. ROCHA, E. C. FERREIRA, AND I. ROCHA, *Reconstructing genome-scale metabolic models with merlin*, Nucleic Acids Research, (2015).

[40] M. DRAGOSITS AND D. MATTANOVICH, *Adaptive laboratory evolution - principles and applications for biotechnology*, 2013.

[41] N. C. DUARTE, S. A. BECKER, N. JAMSHIDI, I. THIELE, M. L. MO, T. D. VO, R. SRIVAS, AND B. O. PALSSON, *Global reconstruction of the human metabolic network based on genomic and bibliomic data*, Proceedings of the National Academy of Sciences, (2007).

[42] W. F. EANES, T. J. S. MERRITT, J. M. FLOWERS, S. KUMAGAI, E. SEZGIN, AND C.-T. ZHU, *Flux control and excess capacity in the enzymes of glycolysis and their relationship to flight metabolism in Drosophila melanogaster.*, Proceedings of the National Academy of Sciences of the United States of America, (2006).

[43] J. S. EDWARDS AND B. O. PALSSON, *Systems properties of the Haemophilus influenzae Rd metabolic genotype*, Journal of Biological Chemistry, (1999).

[44] S. R. ENGEL, F. S. DIETRICH, D. G. FISK, G. BINKLEY, R. BALAKRISHNAN, M. C. COSTANZO, S. S. DWIGHT, B. C. HITZ, K. KARRA, R. S. NASH, S. WENG, E. D. WONG, P. LLOYD, M. S. SKRZYPEK, S. R. MIYASATO, M. SIMISON, AND J. M. CHERRY, *The reference genome sequence of Saccharomyces cerevisiae: then and now.*, G3 (Bethesda, Md.), (2014).

[45] J. A. ENGELMAN, *Targeting PI3K signalling in cancer: Opportunities, challenges and limitations*, 2009.

[46] Y. FALLAH, J. BRUNDAGE, P. ALLEGAKOEN, AND A. N. SHAJAHAN-HAQ, *MYC-Driven pathways in breast cancer subtypes*, 2017.

[47] X. FANG, A. WALLQVIST, AND J. REIFMAN, *Modeling Phenotypic Metabolic Adaptations of Mycobacterium tuberculosis H37Rv under Hypoxia*, PLoS Computational Biology, (2012).

[48] J. D. FEALA, L. COQUIN, D. ZHOU, G. G. HADDAD, G. PATERNOSTRO, AND A. D. MCCULLOCH, *Metabolism as means for hypoxia adaptation: Metabolic profiling and flux balance analysis*, BMC Systems Biology, (2009).

[49] D. FINLEY, H. D. ULRICH, T. SOMMER, AND P. KAISER, *The ubiquitin-proteasome system of Saccharomyces cerevisiae*, Genetics, (2012).

[50] L. FLAMANT, A. NOTTE, N. NINANE, M. RAES, AND C. MICHIELS, *Anti-apoptotic role of HIF-1 and AP-1 in paclitaxel exposed breast cancer cells under hypoxia*, Molecular Cancer, (2010).

[51] A. FLAMHOLZ, E. NOOR, A. BAR-EVEN, AND R. MILO, *EQuilibrator - The biochemical thermodynamics calculator*, Nucleic Acids Research, (2012).

[52] O. FOLGER, L. JERBY, C. FREZZA, E. GOTTLIEB, E. RUPPIN, AND T. SHLOMI, *Predicting selective drug targets in cancer through metabolic networks*, Molecular Systems Biology, (2011).

[53] S. S. FONG AND B. PALSSON, *Metabolic gene-deletion strains of Escherichia coli evolve to computationally predicted growth phenotypes*, Nature Genetics, (2004).

[54] J. FÖRSTER, I. FAMILI, P. FU, B. PALSSON, AND J. NIELSEN, *Genome-scale reconstruction of the Saccharomyces cerevisiae metabolic network*, Genome Research, (2003).

[55] S. FREILICH, R. ZARECKI, O. EILAM, E. S. SEGAL, C. S. HENRY, M. KUPIEC, U. GOPHNA, R. SHARAN, AND E. RUPPIN, *Competitive and cooperative metabolic interactions in bacterial communities*, Nature Communications, (2011).

[56] C. FREZZA, *Mitochondrial metabolites: undercover signalling molecules.*, Interface Focus, (2017).

[57] C. FREZZA, L. ZHENG, O. FOLGER, K. N. RAJAGOPALAN, E. D. MACKENZIE, L. JERBY, M. MICARONI, B. CHANETON, J. ADAM, A. HEDLEY, G. KALNA, I. P. TOMLINSON, P. J. POLLARD, D. G. WATSON, R. J. DEBERARDINIS, T. SHLOMI, E. RUPPIN, AND

E. GOTTLIEB, *Haem oxygenase is synthetically lethal with the tumour suppressor fumarate hydratase*, Nature, (2011).

[58] S. FULDA AND K. DEBATIN, *HIF-1-regulated glucose metabolism: a key to apoptosis resistance?*, Methods Mol Biol, (2007).

[59] C. GANCEDO, J. M. GANCEDO, AND A. SOLS, *Glycerol Metabolism in Yeasts: Pathways of Utilization and Production*, European Journal of Biochemistry, (1968).

[60] S. GAYATHRI AND R. KARTHIK, *Understanding the evolution of functional redundancy in metabolic networks*, Bioinformatics, (2018).

[61] F. GEU-FLORES, H. H. NOUR-ELDIN, M. T. NIELSEN, AND B. A. HALKIER, *USER fusion: A rapid and efficient method for simultaneous fusion and cloning of multiple PCR products*, Nucleic Acids Research, (2007).

[62] G. GIAEVER, A. M. CHU, L. NI, C. CONNELLY, L. RILES, S. VÉRONNEAU, S. DOW, A. LUCAU-DANILA, K. ANDERSON, B. ANDRÉ, A. P. ARKIN, A. ASTROMOFF, M. EL BAKKOURY, R. BANGHAM, R. BENITO, S. BRACHAT, S. CAMPANARO, M. CURTISS, K. DAVIS, A. DEUTSCHBAUER, K. D. ENTIAN, P. FLAHERTY, F. FOURY, D. J. GARFINKEL, M. GERSTEIN, D. GOTTE, U. GÜLDENER, J. H. HEGEMANN, S. HEMPEL, Z. HERMAN, D. F. JARAMILLO, D. E. KELLY, S. L. KELLY, P. KÖTTER, D. LABONTE, D. C. LAMB, N. LAN, H. LIANG, H. LIAO, L. LIU, C. LUO, M. LUSSIER, R. MAO, P. MENARD, S. L. OOI, J. L. REVUELTA, C. J. ROBERTS, M. ROSE, P. ROSS-MACDONALD, B. SCHERENS, G. SCHIMMACK, B. SHAFER, D. D. SHOEMAKER, S. SOOKHAI-MAHADEO, R. K. STORMS, J. N. STRATHERN, G. VALLE, M. VOET, G. VOLCKAERT, C. YUN WANG, T. R. WARD, J. WILHELMY, E. A. WINZELER, Y. YANG, G. YEN, E. YOUNGMAN, K. YU, H. BUSSEY, J. D. BOEKE, M. SNYDER, P. PHILIPPSEN, R. W. DAVIS, AND M. JOHNSTON, *Functional profiling of the Saccharomyces cerevisiae genome*, Nature, (2002).

[63] H. GOGAS, V. KOTOULA, Z. ALEXOPOULOU, C. CHRISTODOULOU, I. KOSTOPOULOS, M. BOBOS, G. RAPTOU, E. CHARALAMBOUS, E. TSOLAKI, I. XANTHAKIS, G. PENTHEROUDAKIS, A. KOUTRAS, D. BAFALOUKOS, P. PAPAKOSTAS, G. ARAVANTINOS, A. PSYRRI, K. PETRAKI, K. T. KALOGERAS, D. PECTASIDES, AND G. FOUNTZILAS, *MYC copy gain, chromosomal instability and PI3K activation as potential markers of unfavourable outcome in trastuzumab-treated patients with metastatic breast cancer*, Journal of Translational Medicine, (2016).

[64] A. M. GONZALEZ-ANGULO, T. IWAMOTO, S. LIU, H. CHEN, K.-A. DO, G. N. HORTOBAGYI, G. B. MILLS, F. MERIC-BERNSTAM, W. F. SYMMANS, AND L. PUSZTAI, *Gene expression, molecular class changes, and pathway analysis after neoadjuvant systemic therapy for*

breast cancer., Clinical cancer research : an official journal of the American Association for Cancer Research, (2012).

[65] O. GÜELL, F. SAGUÉS, AND M. Á. SERRANO, *Essential Plasticity and Redundancy of Metabolism Unveiled by Synthetic Lethality Analysis*, PLoS Computational Biology, (2014).

[66] W. HADLEY, *Elegant Graphics for Data Analysis*, Springer Verlag, 2009.

[67] R. HARRISON, B. PAPP, C. PAL, S. G. OLIVER, AND D. DELNERI, *Plasticity of genetic interactions in metabolic networks of yeast*, Proceedings of the National Academy of Sciences, (2007).

[68] Y. HASIN, M. SELDIN, AND A. LUSIS, *Multi-omics approaches to disease*, 2017.

[69] K. M. HAVAS, V. MILCHEVSKAYA, K. RADIC, A. ALLADIN, E. KAFKIA, M. GARCIA, J. STOLTE, B. KLAUS, N. ROTMENSZ, T. J. GIBSON, B. BURWINKEL, A. SCHNEEWEISS, G. PRUNERI, K. R. PATIL, R. SOTILLO, AND M. JECHLINGER, *Metabolic shifts in residual breast cancer drive tumor recurrence*, Journal of Clinical Investigation, (2017).

[70] C. S. HENRY, M. DEJONGH, A. A. BEST, P. M. FRYBARGER, B. LINSAY, AND R. L. STEVENS, *High-throughput generation, optimization and analysis of genome-scale metabolic models*, Nature Biotechnology, (2010).

[71] M. J. HERRGÅRD, B.-S. LEE, V. PORTNOY, AND B. Ø. PALSSON, *Integrated analysis of regulatory and metabolic networks reveals novel regulatory mechanisms in Saccharomyces cerevisiae.*, Genome research, (2006).

[72] J. K. HILTUNEN, K. J. AUTIO, M. S. SCHONAUER, V. S. KURSU, C. L. DIECKMANN, AND A. J. KASTANIOTIS, *Mitochondrial fatty acid synthesis and respiration*, Biochimica et Biophysica Acta (BBA) - Bioenergetics, (2010).

[73] J. K. HILTUNEN, A. M. MURSULA, H. ROTTENSTEINER, R. K. WIERENGA, A. J. KASTANIOTIS, AND A. GURVITZ, *The biochemistry of peroxisomal β-oxidation in the yeast Saccharomyces cerevisiae*, 2003.

[74] P. W. HO, S. SWINNEN, J. DUITAMA, AND E. NEVOIGT, *The sole introduction of two single-point mutations establishes glycerol utilization in Saccharomyces cerevisiae CEN.PK derivatives*, Biotechnology for Biofuels, (2017).

[75] T. HORINOUCHI, K. TAMAOKA, C. FURUSAWA, N. ONO, S. SUZUKI, T. HIRASAWA, T. YOMO, AND H. SHIMIZU, *Transcriptome analysis of parallel-evolved Escherichia coli strains under ethanol stress*, BMC Genomics, (2010).

[76] S.-W. HUANG, J.-K. KAO, C.-Y. WU, S.-T. WANG, H.-C. LEE, S.-M. LIANG, Y.-J. CHEN, J.-J. SHIEH, S.-W. HUANG, J.-K. KAO, C.-Y. WU, S.-T. WANG, H.-C. LEE, S.-M. LIANG, Y.-J. CHEN, AND J.-J. SHIEH, *Targeting Aerobic Glycolysis and HIF-1α Expression Enhance Imiquimod-induced Apoptosis in Cancer Cells*, Oncotarget, (2014).

[77] D. R. HYDUKE, N. E. LEWIS, AND B. O. PALSSON, *Analysis of omics data with genome-scale models of metabolism*, 2013.

[78] C. ILLUXLEY, E. D. GREEN, AND I. DUNBAM, *Rapid assessment of S. cerevisiae mating type by PCR*, Trends in Genetics, (1990).

[79] M. IMIELINSKI AND C. BELTA, *Exploiting the pathway structure of metabolism to reveal high-order epistasis*, BMC Systems Biology, (2008).

[80] M. JAIN, R. NILSSON, S. SHARMA, N. MADHUSUDHAN, T. KITAMI, A. SOUZA, R. KAFRI, M. KIRSCHNER, C. CLISH, AND V. MOOTHA, *Metabolite profiling identifies a key role for glycine in rapid cancer cell proliferation.* , Science, (2012).

[81] T. JAKOCIUNAS, I. BONDE, M. HERRGARD, AND J. KEASLING, *Multiplex metabolic pathway engineering using CRISPR/Cas9 in Saccharomyces cerevisiae.*, Metab. Eng., (2015).

[82] G. JANSEN, C. BARBOSA, AND H. SCHULENBURG, *Experimental evolution as an efficient tool to dissect adaptive paths to antibiotic resistance*, Drug Resistance Updates, (2013).

[83] A. JEMAL, F. BRAY, M. M. CENTER, J. FERLAY, E. WARD, AND D. FORMAN, *Global cancer statistics.*, CA: a cancer journal for clinicians, (2017).

[84] B. JIANG, *Aerobic glycolysis and high level of lactate in cancer metabolism and microenvironment*, 2017.

[85] P. JOUHTEN, O. PONOMAROVA, R. GONZALEZ, AND K. R. PATIL, *Saccharomyces cerevisiae metabolism in ecological context*, 2016.

[86] P. D. KARP, S. PALEY, AND P. ROMERO, *The pathway tools software*, in Bioinformatics, 2002.

[87] M. KILIC, H. KASPERCZYK, S. FULDA, AND K.-M. DEBATIN, *Role of hypoxia inducible factor-1 alpha in modulation of apoptosis resistance*, Oncogene, (2007).

[88] J.-W. KIM, P. GAO, Y.-C. LIU, G. L. SEMENZA, AND C. V. DANG, *Hypoxia-Inducible Factor 1 and Dysregulated c-Myc Cooperatively Induce Vascular Endothelial Growth Factor and Metabolic Switches Hexokinase 2 and Pyruvate Dehydrogenase Kinase 1*, Molecular and Cellular Biology, (2007).

[89] M. KIM AND D. LUN, *Methods for integration of transcriptomic data in genome-scale metabolic models.*, Compute Structure Biotechnology, (2014).

[90] S. KIM, D. Y. LEE, G. WOHLGEMUTH, H. S. PARK, O. FIEHN, AND K. H. KIM, *Evaluation and optimization of metabolome sample preparation methods for Saccharomyces cerevisiae*, Analytical Chemistry, (2013).

[91] T. Y. KIM, H. U. KIM, AND S. Y. LEE, *Metabolite-centric approaches for the discovery of antibacterials using genome-scale metabolic networks*, Metabolic Engineering, (2010).

[92] M. KLEIN, S. SWINNEN, J. M. THEVELEIN, AND E. NEVOIGT, *Glycerol metabolism and transport in yeast and fungi: established knowledge and ambiguities*, 2017.

[93] N. KLITGORD AND D. SEGRÈ, *Environments that induce synthetic microbial ecosystems*, PLoS Computational Biology, (2010).

[94] E. V. KOONIN, *Comparative genomics, minimal gene-sets and the last universal common ancestor*, Nature Reviews Microbiology, (2003).

[95] M. KUYPER, M. J. TOIRKENS, J. A. DIDERICH, A. A. WINKLER, J. P. VAN DIJKEN, AND J. T. PRONK, *Evolutionary engineering of mixed-sugar utilization by a xylose-fermenting Saccharomyces cerevisiae strain*, FEMS Yeast Research, (2005).

[96] R. A. LACROIX, B. O. PALSSON, AND A. M. FEIST, *A model for designing adaptive laboratory evolution experiments*, Applied and Environmental Microbiology, (2017).

[97] R. A. LACROIX, T. E. SANDBERG, E. J. O'BRIEN, J. UTRILLA, A. EBRAHIM, G. I. GUZMAN, R. SZUBIN, B. O. PALSSON, AND A. M. FEIST, *Use of adaptive laboratory evolution to discover key mutations enabling rapid growth of Escherichia coli K-12 MG1655 on glucose minimal medium*, Applied and Environmental Microbiology, (2015).

[98] F. LAGES, M. SILVA-GRAÇA, AND C. LUCAS, *Active glycerol uptake is a mechanism underlying halotolerance in yeasts: A study of 42 species*, Microbiology, (1999).

[99] G. I. LANG AND A. W. MURRAY, *Estimating the per-base-pair mutation rate in the yeast Saccharomyces cerevisiae*, Genetics, (2008).

[100] T. LAUKKA, C. J. MARIANI, T. IHANTOLA, J. Z. CAO, J. HOKKANEN, W. G. KAELIN, L. A. GODLEY, AND P. KOIVUNEN, *Fumarate and succinate regulate expression of hypoxia-inducible genes via TET enzymes*, Journal of Biological Chemistry, (2016).

[101] E. LETOUZÉ, C. MARTINELLI, C. LORIOT, N. BURNICHON, N. ABERMIL, C. OTTOLENGHI, M. JANIN, M. MENARA, A. T. NGUYEN, P. BENIT, A. BUFFET, C. MARCAILLOU, J. Ô. BERTHERAT, L. AMAR, P. RUSTIN, A. DEREYNIÈS, A. P. GIMENEZ-ROQUEPLO, AND

J. FAVIER, *SDH Mutations Establish a Hypermethylator Phenotype in Paraganglioma*, Cancer Cell, (2013).

[102] N. E. LEWIS, H. NAGARAJAN, AND B. O. PALSSON, *Constraining the metabolic genotype-phenotype relationship using a phylogeny of in silico methods*, 2012.

[103] H. LI, B. YU, J. LI, L. SU, M. YAN, J. ZHANG, C. LI, Z. ZHU, AND B. LI, *Characterization of differentially expressed genes involved in pathways associated with gastric cancer*, PLoS ONE, (2015).

[104] J. LI, R. HOU, X. NIU, R. LIU, Q. WANG, C. WANG, X. LI, Z. HAO, G. YIN, AND K. ZHANG, *Comparison of microarray and RNA-Seq analysis of mRNA expression in dermal mesenchymal stem cells*, Biotechnology Letters, (2016).

[105] M. V. LIBERTI AND J. W. LOCASALE, *Correction to: 'The Warburg Effect: How Does it Benefit Cancer Cells?'. [Trends in Biochemical Sciences, 41 (2016) 211].*, 2016.

[106] O. LISBETH AND N. JENS, *On-line and in situ monitoring of biomass in submerged cultivations*, Trends In Biotechnology, (2012).

[107] Z. LIU AND R. A. BUTOW, *A transcriptional switch in the expression of yeast tricarboxylic acid cycle genes in response to a reduction or loss of respiratory function.*, Molecular and cellular biology, (1999).

[108] L. LOBEL, N. SIGAL, I. BOROVOK, E. RUPPIN, AND A. A. HERSKOVITS, *Integrative Genomic Analysis Identifies Isoleucine and CodY as Regulators of Listeria monocytogenes Virulence*, PLoS Genetics, (2012).

[109] M. I. LOVE, W. HUBER, AND S. ANDERS, *Moderated estimation of fold change and dispersion for RNA-seq data with DESeq2*, Genome Biology, (2014).

[110] D. MACHADO, S. ANDREJEV, M. TRAMONTANO, AND K. R. PATIL, *Fast automated reconstruction of genome-scale metabolic models for microbial species and communities*, Nucleic Acids Research, (2018).

[111] D. MACHADO AND M. J. HERRGÅRD, *Co-evolution of strain design methods based on flux balance and elementary mode analysis*, 2015.

[112] D. MACHADO, M. J. HERRGÅRD, AND I. ROCHA, *Stoichiometric representation of gene–protein–reaction associations leverages constraint-based analysis from reaction to gene-level phenotype prediction*, PLoS Computational Biology, 12 (2016), p. e1005140.

[113] R. MAHADEVAN AND C. H. SCHILLING, *The effects of alternate optimal solutions in constraint-based genome-scale metabolic models*, Metabolic Engineering, (2003).

[114] V. MAIRE, F. NÉMATI, M. RICHARDSON, A. VINCENT-SALOMON, B. TESSON, G. RIGAILL, E. GRAVIER, B. MARTY-PROUVOST, L. DE KONING, G. LANG, D. GENTIEN, A. DUMONT, E. BARILLOT, E. MARANGONI, D. DECAUDIN, S. ROMAN-ROMAN, A. PIERRÉ, F. CRUZALEGUI, S. DEPIL, G. C. TUCKER, AND T. DUBOIS, *Polo-like kinase 1: A potential therapeutic option in combination with conventional chemotherapy for the management of patients with triple-negative breast cancer*, Cancer Research, (2013).

[115] A. MARDINOGLU, R. AGREN, C. KAMPF, A. ASPLUND, I. NOOKAEW, P. JACOBSON, A. J. WALLEY, P. FROGUEL, L. M. CARLSSON, M. UHLEN, AND J. NIELSEN, *Integration of clinical data with a genome-scale metabolic model of the human adipocyte*, Molecular Systems Biology, (2013).

[116] A. MARDINOGLU, R. AGREN, C. KAMPF, A. ASPLUND, M. UHLEN, AND J. NIELSEN, *Genome-scale metabolic modelling of hepatocytes reveals serine deficiency in patients with non-alcoholic fatty liver disease*, Nature Communications, (2014).

[117] M. MARTIN, *Cutadapt removes adapter sequences from high-throughput sequencing reads*, EMBnet.journal, (2011).

[118] T. MCFATE, A. MOHYELDIN, H. LU, J. THAKAR, J. HENRIQUES, N. D. HALIM, H. WU, M. J. SCHELL, T. M. TSANG, O. TEAHAN, S. ZHOU, J. A. CALIFANO, N. H. JEOUNG, R. A. HARRIS, AND A. VERMA, *Pyruvate dehydrogenase complex activity controls metabolic and malignant phenotype in cancer cells.*, The Journal of biological chemistry, (2008).

[119] A. MCKENNA, M. HANNA, E. BANKS, A. SIVACHENKO, K. CIBULSKIS, A. KERNYTSKY, K. GARIMELLA, D. ALTSHULER, S. GABRIEL, M. DALY, AND M. A. DEPRISTO, *The genome analysis toolkit: A MapReduce framework for analyzing next-generation DNA sequencing data*, Genome Research, (2010).

[120] A. MERICO, E. RAGNI, S. GALAFASSI, L. POPOLO, AND C. COMPAGNO, *Generation of an evolved Saccharomyces cerevisiae strain with a high freeze tolerance and an improved ability to grow on glycerol*, Journal of Industrial Microbiology and Biotechnology, (2011).

[121] M. D. MIKKELSEN, L. D. BURON, B. SALOMONSEN, C. E. OLSEN, B. G. HANSEN, U. H. MORTENSEN, AND B. A. HALKIER, *Microbial production of indolylglucosinolate through engineering of a multi-gene pathway in a versatile yeast expression platform*, Metabolic Engineering, (2012).

[122] V. MOZHAYSKIY AND I. TAGKOPOULOS, *Microbial evolution in vivo and in silico: Methods and applications*, 2013.

[123] M. P. MURPHY AND L. A. O'NEILL, *Krebs Cycle Reimagined: The Emerging Roles of Succinate and Itaconate as Signal Transducers*, 2018.

[124] Y. NAITO, H. KIMIHIRO, B. HIDEMASA, AND U.-T. KUMIKO, *Crisprdirect: software for designing crispr/cas guide rna with reduced off-target sites*, Trends In Biotechnology, (2015).

[125] J. F. NIJKAMP, M. VAN DEN BROEK, E. DATEMA, S. DE KOK, L. BOSMAN, M. A. LUTTIK, P. DARAN-LAPUJADE, W. VONGSANGNAK, J. NIELSEN, W. H. HEIJNE, P. KLAASSEN, C. J. PADDON, D. PLATT, P. KÖTTER, R. C. VAN HAM, M. J. REINDERS, J. T. PRONK, D. DE RIDDER, AND J. M. DARAN, *De novo sequencing, assembly and analysis of the genome of the laboratory strain Saccharomyces cerevisiae CEN.PK113-7D, a model for modern industrial biotechnology*, Microbial Cell Factories, (2012).

[126] K. T. NISHANT, W. WEI, E. MANCERA, J. L. ARGUESO, A. SCHLATTL, N. DELHOMME, X. MA, C. D. BUSTAMANTE, J. O. KORBEL, Z. GU, L. M. STEINMETZ, AND E. ALANI, *The Baker's yeast diploid genome is remarkably stable in vegetative growth and meiosis*, PLoS Genetics, (2010).

[127] M. H. H. NØRHOLM, *A mutant Pfu DNA polymerase designed for advanced uracil-excision DNA engineering*, BMC Biotechnology, (2010).

[128] M. OATLEY, O. V. BOLUKBASI, V. SVENSSON, M. SHVARTSMAN, K. GANTER, K. ZIRNGIBL, P. V. PAVLOVICH, V. MILCHEVSKAYA, V. FOTEVA, K. N. NATARAJAN, B. BAYING, V. BENES, K. R. PATIL, S. A. TEICHMANN, AND C. LANCRIN, *Single-cell transcriptomics identifies CD44 as a new marker and regulator of haematopoietic stem cells development*, bioRxiv, (2018).

[129] M. A. OBERHARDT, B. PALSSON, AND J. A. PAPIN, *Applications of genome-scale metabolic reconstructions*, 2009.

[130] E. J. O'BRIEN, J. M. MONK, AND B. O. PALSSON, *Using genome-scale models to predict biological capabilities*, Cell, (2015).

[131] S. OPDAM, A. RICHELLE, B. KELLMAN, S. LI, D. C. ZIELINSKI, AND N. E. LEWIS, *A Systematic Evaluation of Methods for Tailoring Genome-Scale Metabolic Models*, Cell Systems, (2017).

[132] J. D. ORTH, T. M. CONRAD, J. NA, J. A. LERMAN, H. NAM, A. M. FEIST, AND B. PALSSON, *A comprehensive genome-scale reconstruction of Escherichia coli metabolism-2011*, Molecular Systems Biology, (2011).

[133] J. D. ORTH, I. THIELE, AND B. Ø PALSSON, *What is flux balance analysis?*, Nature Publishing Group, (2010).

[134] T. Österlund, I. Nookaew, S. Bordel, and J. Nielsen, *Mapping condition-dependent regulation of metabolism in yeast through genome-scale modeling*, BMC Systems Biology, (2013).

[135] Y. Pan, G. Liu, Y. Yuan, J. Zhao, Y. Yang, and Y. Li, *Analysis of differential gene expression profile identifies novel biomarkers for breast cancer*, Oncotarget, (2017).

[136] B. Papp, B. Teusink, and R. A. Notebaart, *A critical view of metabolic network adaptations*, HFSP Journal, (2009).

[137] J. H. Park and S. Y. Lee, *Towards systems metabolic engineering of microorganisms for amino acid production*, 2008.

[138] J. Parrilla, C. Gaillard, J. Verbeke, M. Maucourt, R. A. Aleksandrov, F. Thibault, P. Fleurat-Lessard, Y. Gibon, D. Rolin, and R. Atanassova, *Comparative metabolomics and glycolysis enzyme profiling of embryogenic and nonembryogenic grape cells*, FEBS Open Bio, (2018).

[139] S. Partow, V. Siewers, S. Bjørn, J. Nielsen, and J. Maury, *Characterization of different promoters for designing a new expression vector in Saccharomyces cerevisiae*, Yeast, (2010).

[140] J. Paula and P. Kiran, *WO2018007522A1*, Interface Focus, (2017).

[141] N. N. Pavlova and C. B. Thompson, *The Emerging Hallmarks of Cancer Metabolism*, 2016.

[142] J. P. Piret, C. Lecocq, S. Toffoli, N. Ninane, M. Raes, and C. Michiels, *Hypoxia and CoCl2protect HepG2 cells against serum deprivation- and t-BHP-induced apoptosis: A possible anti-apoptotic role for HIF-1*, Experimental Cell Research, (2004).

[143] J. P. Piret, D. Mottet, M. Raes, and C. Michiels, *Is HIF-1α a pro- or an anti-apoptotic protein?*, Biochemical Pharmacology, (2002).

[144] E. Pitkänen, P. Jouhten, J. Hou, M. F. Syed, P. Blomberg, J. Kludas, M. Oja, L. Holm, M. Penttilä, J. Rousu, and M. Arvas, *Comparative Genome-Scale Reconstruction of Gapless Metabolic Networks for Present and Ancestral Species*, PLoS Computational Biology, (2014).

[145] L. Poillet-Perez, G. Despouy, R. Delage-Mourroux, and M. Boyer-Guittaut, *Interplay between ROS and autophagy in cancer cells, from tumor initiation to cancer therapy*, 2015.

[146] Y. Poirier, V. D. Antonenkov, T. Glumoff, and J. K. Hiltunen, *Peroxisomal β-oxidation-A metabolic pathway with multiple functions*, 2006.

[147] O. PONOMAROVA, N. GABRIELLI, D. C. SÉVIN, M. MÜLLEDER, K. ZIRNGIBL, K. BULYHA, S. ANDREJEV, E. KAFKIA, A. TYPAS, U. SAUER, M. RALSER, AND K. R. PATIL, *Yeast Creates a Niche for Symbiotic Lactic Acid Bacteria through Nitrogen Overflow*, Cell Systems, (2017).

[148] V. A. PORTNOY, D. BEZDAN, AND K. ZENGLER, *Adaptive laboratory evolution-harnessing the power of biology for metabolic engineering*, 2011.

[149] N. D. PRICE, J. A. PAPIN, C. H. SCHILLING, AND B. O. PALSSON, *Genome-scale microbial in silico models: The constraints-based approach*, 2003.

[150] S. PRINZ, I. AVILA-CAMPILLO, C. ALDRIDGE, A. SRINIVASAN, K. DIMITROV, A. F. SIEGEL, AND T. GALITSKI, *Control of yeast filamentous-form growth by modules in an integrated molecular network*, 2004.

[151] L. E. QUEK, S. DIETMAIR, M. HANSCHO, V. S. MARTÍNEZ, N. BORTH, AND L. K. NIELSEN, *Reducing Recon 2 for steady-state flux analysis of HEK cell culture*, Journal of Biotechnology, (2014).

[152] T. RAUSCH, T. ZICHNER, A. SCHLATTL, A. M. STÜTZ, V. BENES, AND J. O. KORBEL, *DELLY: Structural variant discovery by integrated paired-end and split-read analysis*, Bioinformatics, (2012).

[153] M. REBHAN, V. CHALIFA-CASPI, J. PRILUSKY, AND D. LANCET, *GeneCards: Integrating information about genes, proteins and diseases*, Trends in Genetics, (1997).

[154] B. REPETTO AND A. TZAGOLOFF, *Structure and regulation of KGD1, the structural gene for yeast alpha-ketoglutarate dehydrogenase.*, Molecular and cellular biology, (1989).

[155] L. H. REYES, M. P. ALMARIO, J. WINKLER, M. M. OROZCO, AND K. C. KAO, *Visualizing evolution in real time to determine the molecular mechanisms of n-butanol tolerance in Escherichia coli*, Metabolic Engineering, (2012).

[156] L. H. REYES, J. M. GOMEZ, AND K. C. KAO, *Improving carotenoids production in yeast via adaptive laboratory evolution*, Metabolic Engineering, (2014).

[157] C. ROODVELDT, A. AHARONI, AND D. S. TAWFIK, *Directed evolution of proteins for heterologous expression and stability*, 2005.

[158] J. Y. RYU, H. U. KIM, AND S. Y. LEE, *Framework and resource for more than 11,000 gene-transcript-protein-reaction associations in human metabolism*, Proceedings of the National Academy of Sciences, (2017).

[159] S. SAHOO, M. K. AURICH, J. J. JONSSON, AND I. THIELE, *Membrane transporters in a human genome-scale metabolic knowledgebase and their implications for disease*, 2014.

[160] S. SAHOO, H. S. HARALDSDÓTTIR, R. M. T. FLEMING, AND I. THIELE, *Modeling the effects of commonly used drugs on human metabolism*, The FEBS Journal, (2015).

[161] H. SAITO AND F. POSAS, *Response to hyperosmotic stress*, 2012.

[162] F. SALIMI, K. ZHUANG, AND R. MAHADEVAN, *Genome-scale metabolic modeling of a clostridial co-culture for consolidated bioprocessing*, Biotechnology Journal, (2010).

[163] A. SAMAL, *Conservation of high-flux backbone in alternate optimal and near-optimal flux distributions of metabolic networks*, Systems and Synthetic Biology, (2008).

[164] T. E. SANDBERG, M. PEDERSEN, R. A. LACROIX, A. EBRAHIM, M. BONDE, M. J. HERRGARD, B. O. PALSSON, M. SOMMER, AND A. M. FEIST, *Evolution of escherichia coli to 42 °c and subsequent genetic engineering reveals adaptive mechanisms and novel mutations*, Molecular Biology and Evolution, (2014).

[165] E. SASABE, Y. TATEMOTO, D. LI, T. YAMAMOTO, AND T. OSAKI, *Mechanism of HIF-1alpha-dependent suppression of hypoxia-induced apoptosis in squamous cell carcinoma cells*, Cancer Science, (2005).

[166] C. H. SCHILLING AND B. PALSSON, *Assessment of the metabolic capabilities of Haemophilus influenzae Rd through a genome-scale pathway analysis*, Journal of Theoretical Biology, (2000).

[167] M. SCIACOVELLI, E. GAUDE, M. HILVO, AND C. FREZZA, *The metabolic alterations of cancer cells*, Methods in Enzymology, (2014).

[168] B. SÉGUI, N. ANDRIEU-ABADIE, J.-P. JAFFRÉZOU, H. BENOIST, AND T. LEVADE, *Sphingolipids as modulators of cancer cell death: potential therapeutic targets.*, Biochimica et biophysica acta, (2006).

[169] A. M. SELMECKI, Y. E. MARUVKA, P. A. RICHMOND, M. GUILLET, N. SHORESH, A. L. SORENSON, S. DE, R. KISHONY, F. MICHOR, R. DOWELL, AND D. PELLMAN, *Polyploidy can drive rapid adaptation in yeast*, Nature, (2015).

[170] G. L. SEMENZA, *HIF-1: upstream and downstream of cancer metabolism*, 2010.

[171] P. SHANNON, A. MARKIEL, O. OZIER, N. S. BALIGA, J. T. WANG, D. RAMAGE, N. AMIN, B. SCHWIKOWSKI, AND T. IDEKER, *Cytoscape: A software Environment for integrated models of biomolecular interaction networks*, Genome Research, (2003).

[172] F. SHERMAN, *Getting Started with Yeast • Contents •*, Methods in Enzymology, (2002).

[173] T. SHLOMI, M. N. CABILI, M. J. HERRGÅRD, B. PALSSON, AND E. RUPPIN, *Network-based prediction of human tissue-specific metabolism*, 2008.

[174] T. SHLOMI, Y. EISENBERG, R. SHARAN, AND E. RUPPIN, *A genome-scale computational study of the interplay between transcriptional regulation and metabolism*, Molecular Systems Biology, (2007).

[175] M. I. SIGURDSSON, N. JAMSHIDI, E. STEINGRIMSSON, I. THIELE, AND B. T. PALSSON, *A detailed genome-wide reconstruction of mouse metabolism based on human Recon 1*, BMC Systems Biology, (2010).

[176] V. STOVICEK, I. BORODINA, AND J. FORSTER, *CRISPR-Cas system enables fast and simple genome editing of industrial Saccharomyces cerevisiae strains*, Metabolic Engineering Communications, (2015).

[177] K. STRIMMER, *A unified approach to false discovery rate estimation*, BMC Bioinformatics, (2008).

[178] T. STRUCKO, K. ZIRNGIBL, F. PEREIRA, E. KAFKIA, E. T. MOHAMED, M. RETTEL, F. STEIN, A. M. FEIST, P. JOUHTEN, K. R. PATIL, AND J. FORSTER, *Laboratory evolution reveals regulatory and metabolic trade-offs of glycerol utilization in Saccharomyces cerevisiae*, Metabolic Engineering, (2018).

[179] N. SWAINSTON, K. SMALLBONE, H. HEFZI, P. D. DOBSON, J. BREWER, M. HANSCHO, D. C. ZIELINSKI, K. S. ANG, N. J. GARDINER, J. M. GUTIERREZ, S. KYRIAKOPOULOS, M. LAKSHMANAN, S. LI, J. K. LIU, V. S. MARTÍNEZ, C. A. ORELLANA, L. E. QUEK, A. THOMAS, J. ZANGHELLINI, N. BORTH, D. Y. LEE, L. K. NIELSEN, D. B. KELL, N. E. LEWIS, AND P. MENDES, *Recon 2.2: from reconstruction to model of human metabolism*, Metabolomics, (2016).

[180] S. SWINNEN, P. W. HO, M. KLEIN, AND E. NEVOIGT, *Genetic determinants for enhanced glycerol growth of Saccharomyces cerevisiae*, Metabolic Engineering, (2016).

[181] S. SWINNEN, M. KLEIN, M. CARRILLO, J. MCINNES, H. T. T. NGUYEN, AND E. NEVOIGT, *Re-evaluation of glycerol utilization in Saccharomyces cerevisiae: Characterization of an isolate that grows on glycerol without supporting supplements*, Biotechnology for Biofuels, (2013).

[182] A. TACHTSIDIS, L. M. MCINNES, N. JACOBSEN, E. W. THOMPSON, AND C. M. SAUNDERS, *Minimal residual disease in breast cancer: an overview of circulating and disseminated tumour cells*, Clinical & Experimental Metastasis, (2016).

[183] O. TENAILLON, A. RODRÍGUEZ-VERDUGO, R. L. GAUT, P. MCDONALD, A. F. BENNETT, A. D. LONG, AND B. S. GAUT, *The molecular diversity of adaptive convergence*, Science, (2012).

[184] B. TEUSINK, F. H. VAN ENCKEVORT, C. FRANCKE, A. WIERSMA, A. WEGKAMP, E. J. SMID, AND R. J. SIEZEN, *In silico reconstruction of the metabolic pathways of Lactobacillus plantarum: Comparing predictions of nutrient requirements with those from growth experiments*, Applied and Environmental Microbiology, (2005).

[185] B. TEUSINK, A. WIERSMA, L. JACOBS, R. A. NOTEBAART, AND E. J. SMID, *Understanding the adaptive growth strategy of Lactobacillus plantarumby in silico optimisation*, PLoS Computational Biology, (2009).

[186] A. D. THEOCHARIS, I. TSOLAKIS, G. N. TZANAKAKIS, AND N. K. KARAMANOS, *Chondroitin Sulfate as a Key Molecule in the Development of Atherosclerosis and Cancer Progression*, 2006.

[187] I. THIELE, N. SWAINSTON, R. M. FLEMING, A. HOPPE, S. SAHOO, M. K. AURICH, H. HARALDSDOTTIR, M. L. MO, O. ROLFSSON, M. D. STOBBE, S. G. THORLEIFSSON, R. AGREN, C. BÖLLING, S. BORDEL, A. K. CHAVALI, P. DOBSON, W. B. DUNN, L. ENDLER, D. HALA, M. HUCKA, D. HULL, D. JAMESON, N. JAMSHIDI, J. J. JONSSON, N. JUTY, S. KEATING, I. NOOKAEW, N. LE NOVÈRE, N. MALYS, A. MAZEIN, J. A. PAPIN, N. D. PRICE, E. SELKOV, M. I. SIGURDSSON, E. SIMEONIDIS, N. SONNENSCHEIN, K. SMALLBONE, A. SOROKIN, J. H. VAN BEEK, D. WEICHART, I. GORYANIN, J. NIELSEN, H. V. WESTERHOFF, D. B. KELL, P. MENDES, AND B. O. PALSSON, *A community-driven global reconstruction of human metabolism*, Nature Biotechnology, (2013).

[188] L. VÄREMO, J. NIELSEN, AND I. NOOKAEW, *Enriching the gene set analysis of genome-wide data by incorporating directionality of gene expression and combining statistical hypotheses and methods*, Nucleic Acids Research, (2013).

[189] C. VERDUYN, E. POSTMA, W. A. SCHEFFERS, AND J. P. VAN DIJKEN, *Effect of benzoic acid on metabolic fluxes in yeasts: A continuous???culture study on the regulation of respiration and alcoholic fermentation*, Yeast, (1992).

[190] R. P. VIVEK-ANANTH AND A. SAMAL, *Advances in the integration of transcriptional regulatory information into genome-scale metabolic models*, 2016.

[191] C. WANG, B. GONG, P. R. BUSHEL, J. THIERRY-MIEG, D. THIERRY-MIEG, J. XU, H. FANG, H. HONG, J. SHEN, Z. SU, J. MEEHAN, X. LI, L. YANG, H. LI, P. P. ŁABAJ, D. P. KREIL, D. MEGHERBI, S. GAJ, F. CAIMENT, J. VAN DELFT, J. KLEINJANS, A. SCHERER, V. DEVANARAYAN, J. WANG, Y. YANG, H. R. QIAN, L. J. LANCASHIRE, M. BESSARABOVA, Y. NIKOLSKY, C. FURLANELLO, M. CHIERICI, D. ALBANESE, G. JURMAN, S. RICCADONNA, M. FILOSI, R. VISINTAINER, K. K. ZHANG, J. LI, J. H. HSIEH, D. L. SVOBODA, J. C. FUSCOE, Y. DENG, L. SHI, R. S. PAULES, S. S. AUERBACH, AND

W. TONG, *The concordance between RNA-seq and microarray data depends on chemical treatment and transcript abundance*, Nature Biotechnology, (2014).

[192] T. WANG, K. BIRSOY, N. W. HUGHES, K. M. KRUPCZAK, Y. POST, J. J. WEI, E. S. LANDER, AND D. M. SABATINI, *Identification and characterization of essential genes in the human genome*, Science, (2015).

[193] F. WESSELY, M. BARTL, R. GUTHKE, P. LI, S. SCHUSTER, AND C. KALETA, *Optimal regulatory strategies for metabolic pathways in Escherichia coli depending on protein costs*, Molecular Systems Biology, (2011).

[194] L. WILSON, Y. H. CHING, M. FARIAS, S. A. HARTFORD, G. HOWELL, H. SHAO, M. BUCAN, AND J. C. SCHIMENTI, *Random mutagenesis of proximal mouse chromosome 5 uncovers predominantly embryonic lethal mutations*, Genome Research, (2005).

[195] J. WINKLER, L. H. REYES, AND K. C. KAO, *Adaptive laboratory evolution for strain engineering*, Methods in Molecular Biology, (2013).

[196] M. J. WISER, N. RIBECK, AND R. E. LENSKI, *Long-term dynamics of adaptation in asexual populations*, Science, (2013).

[197] D. S. WISHART, T. JEWISON, A. C. GUO, M. WILSON, C. KNOX, Y. LIU, Y. DJOUMBOU, R. MANDAL, F. AZIAT, E. DONG, S. BOUATRA, I. SINELNIKOV, D. ARNDT, J. XIA, P. LIU, F. YALLOU, T. BJORNDAHL, R. PEREZ-PINEIRO, R. EISNER, F. ALLEN, V. NEVEU, R. GREINER, AND A. SCALBERT, *HMDB 3.0-The Human Metabolome Database in 2013*, Nucleic Acids Research, (2013).

[198] M. XIAO, H. YANG, W. XU, S. MA, H. LIN, H. ZHU, L. LIU, Y. LIU, C. YANG, Y. XU, S. ZHAO, D. YE, Y. XIONG, AND K. L. GUAN, *Inhibition of α-KG-dependent histone and DNA demethylases by fumarate and succinate that are accumulated in mutations of FH and SDH tumor suppressors*, Genes and Development, (2012).

[199] J. XU, Y. CHEN, AND O. I. OLOPADE, *MYC and Breast Cancer*, Genes & Cancer, (2010).

[200] M. YEUNG, I. THIELE, AND B. O. PALSSON, *Estimation of the number of extreme pathways for metabolic networks*, BMC Bioinformatics, (2007).

[201] K. ZAMAN, H. RYU, D. HALL, K. O'DONOVAN, AND R. RATA, *Protection from oxidative stress-induced apoptosis in cortical neuronal cultures by iron chelators is associated with enhanced DNA binding of hypoxia-inducible factor-1 and ATF-1/CREB and increased expression of glycolytic enzymes, p21(waf1/cip1), and erythropoietin.*, Methods Mol Biol, (1999).

[202] A. ZELEZNIAK, S. ANDREJEV, O. PONOMAROVA, D. R. MENDE, P. BORK, AND K. R. PATIL, *Metabolic dependencies drive species co-occurrence in diverse microbial communities*, Proceedings of the National Academy of Sciences, (2015).

[203] Q. ZHANG, Z.-F. ZHANG, J. Y. RAO, J. D. SATO, J. BROWN, D. V. MESSADI, AND A. D. LE, *Treatment with siRNA and antisense oligonucleotides targeted to HIF-1alpha induced apoptosis in human tongue squamous cell carcinomas.*, International journal of cancer. Journal international du cancer, (2004).

[204] Y. ZHANG, J. W. ZHANG, G. Y. LV, S. L. XIE, AND G. Y. WANG, *Effects of sTAT3 gene silencing and rapamycin on apoptosis in hepatocarcinoma cells*, International Journal of Medical Sciences, (2012).

[205] H. ZHONG, A. M. DE MARZO, E. LAUGHNER, M. LIM, D. A. HILTON, D. ZAGZAG, P. BUECHLER, W. B. ISAACS, G. L. SEMENZA, AND J. W. SIMONS, *Overexpression of hypoxia-inducible factor 1alpha in common human cancers and their metastases.*, Cancer research, (1999).

[206] N. ZHOU, K. B. SWAMY, J. Y. LEU, M. J. MCDONALD, S. GALAFASSI, C. COMPAGNO, AND J. PIŠKUR, *Coevolution with bacteria drives the evolution of aerobic fermentation in Lachancea kluyveri*, PLoS ONE, (2017).

[207] Y. O. ZHU, M. L. SIEGAL, D. W. HALL, AND D. A. PETROV, *Precise estimates of mutation rate and spectrum in yeast*, Proceedings of the National Academy of Sciences, (2014).

[208] A. R. ZOMORRODI AND C. D. MARANAS, *OptCom: A multi-level optimization framework for the metabolic modeling and analysis of microbial communities*, PLoS Computational Biology, (2012).